Bactericidal Potential of a Dual-Target Synthetic Amphiphile

A Thesis

Submitted in Partial Fulfillment of the Requirements for the Degree of

DOCTOR OF PHILOSOPHY

by

THIYAGARAJAN D.

Department of Biosciences and Bioengineering
Indian Institute of Technology Guwahati
Guwahati-781039, Assam, India

February 2017

Bactericidal Potential of a Dual-Target Synthetic Amphiphile

A Thesis

Submitted in Partial Fulfillment of the Requirements for the Degree of

DOCTOR OF PHILOSOPHY

by

THIYAGARAJAN D.

Department of Biosciences and Bioengineering
Indian Institute of Technology Guwahati
Guwahati-781039, Assam, India

February 2017

Dedicated to My Parents
Family members
Teachers
And
Almighty God

INDIAN INSTITUTE OF TECHNOLOGY GUWAHATI

DEPARTMENT OF BIOSCIENCES AND BIOENGINEERING

STATEMENT

I do hereby declare that the research findings of this thesis is the result of research work carried out by me in the Department of Biosciences and Bioengineering, Indian Institute of Technology Guwahati, Guwahati, India, under the supervision of Professor Aiyagari Ramesh.

As per the general norms of reporting research findings, due acknowledgements have been made, wherever the research findings of other researchers have been cited in this thesis.

Date: 27 February, 2017 **Thiyagarajan D.**

INDIAN INSTITUTE OF TECHNOLOGY GUWAHATI

DEPARTMENT OF BIOSCIENCES AND BIOENGINEERING

CERTIFICATE

It is certified that the work described in this thesis entitled "***Bactericidal Potential of a Dual-Target Synthetic Amphiphile***" by Mr. Thiyagarajan D. for the award of degree of Doctor of Philosophy is an authentic record of the results obtained from the research work carried out under my supervision in the Department of Biosciences and Bioengineering, Indian Institute of Technology Guwahati, India, and this work has not been submitted elsewhere for the award of any other degree.

CERTIFIED

Thiyagarajan D.

(Candidate)

Roll No: 11610623

Aiyagari Ramesh, Ph.D.

(Thesis Supervisor)

Date: 27 February, 2017

ACKNOWLEDGEMENT

I would like to take this opportunity to offer my heartfelt gratitude to my family and a number of people who made this journey worthwhile.

First and foremost, I would like to express my gratitude to Professor Aiyagari Ramesh, for providing me the platform to learn and accomplish this valuable experience. I wish to further thank him for inculcating in me unique perspective and intellectual thought process towards science which inspired me to retain my trust in science throughout this journey and keep myself highly motivated. His commendable dedication towards research and teaching has been my constant source of inspiration. His invaluable guidance, moral support and never ending kindness throughout my Ph.D. tenure has helped me to grow as an independent researcher, decision maker and as a contented individual.

I am thankful to my doctoral committee members, Dr. Debasish Das, Professor Kannan Pakshirajan and Professor Subrata K. Majumder for their constructive suggestions, support and motivation, which has helped me to improve the quality of my research experience.

I am extremely grateful to Professor Gopal Das, Department of Chemistry for providing me the opportunity to collaborate and learn the interdisciplinary science. I am thankful to sir for the priceless discussions and valuable suggestions that often gave new perspectives to my research work. I owe him my most sincere gratitude for giving me the opportunity to work with him and his research group.

I sincerely express my gratitude and thanks to Professor Benu Dhawan, All India Institute of Medical Sciences (AIIMS), New Delhi and Professor Kasturi Mukhopadhyay, Jawaharlal Nehru University (JNU), New Delhi for kindly providing the MRSA strain for my work.

I am grateful to Professor Siddhartha Sankar Ghosh, Professor Pranab Goswami, Dr. Biplab Bose and Professor Lingaraj Sahoo for providing an amicable environment to execute my Ph.D. work successfully.

I would like to extend my sincere gratitude towards Professor Kannan Pakshirajan, Head of the Department of Biosciences and Bioengineering, IIT Guwahati, and Professor Arun Goyal and Professor V.V. Dasu, Former Heads of the Department Biosciences and Bioengineering, IIT Guwahati for providing me the necessary facilities that helped me to pursue my research at IIT Guwahati.

I am also grateful to all faculty members and staff of the Department of Biosciences and Bioengineering for supporting me throughout the Ph.D. tenure. I would like to thank Department of Biosciences and Bioengineering for providing infrastructural facility for my research work. I would also like to thank Central Instruments Facility (CIF) of IIT Guwahati for providing ambient atmosphere of research and high-end equipments to execute my experiments.

I acknowledge the state-of-art facility at the Center for Excellence under the aegis of Program Support Grant provided by Department of Biotechnology (DBT), Government of India. I am grateful to Department of Biotechnology (DBT) and Science and Engineering Board (SERB), Department of Science & Technology (DST) for supporting my research through grants. I am also grateful to Ministry of Human Resource Department (MHRD) and IIT Guwahati for providing research fellowship. I am grateful to our collaborators Dr. Arghya Basu, Dr. Chirantan Kar, Dr. Barun Kumar Dutta, Dr. Abhijit Gogoi and Mr. Soham Samanta from the Department of Chemistry, IIT Guwahati for the scientific collaboration.

I sincerely acknowledge my M. Tech thesis supervisor Dr. Krishnan Sankaran, Center for Biotechnology, Anna University for providing me the opportunities to explore the field of protein engineering which was the stepping stone for me to venture into biotechnology. Further I sincerely thank my undergraduate faculty members Dr. Vijya Bharathi, Dr. Deattu Narayanan, Dr. Jerard Suresh, Dr. Suguna bai, Dr. Alamelu and all other faculty members of college of Pharmacy, Madras Medical College for their constant support and encouragement. I also extend my thanks to my higher secondary school teachers Mr. Karunanithi sir (Physics), Mr. Soosai sir (chemistry) and middle school teacher Mr. Stanislaus sir for their dedicated work and unconditional love and affection towards students, which in-turn helped me to develop and think about science at school level.

It is my pleasure to thank my seniors Dr. Manab Deb Adhikari and Dr. Sudeep Goswami for their helpful guidance at the initial stages of my research work. It is my pleasure to thank my current lab members Sandipan, Poulomi, Priya, Basu, Tabassum and former lab members Pallavi, Vidushi, Rajanikant, Preeti and Manik for their support and unconditional gesture of assistance in the time of need.

I wish to thank my friends Neha and Arisha for their constant support and motivation throughout the course of my Ph.D. I also wish to thank my close friends Kumaravel, Vijayan, Boopathy, Chinna, Ramakrishnan, Akil, Vignesh, Muthu, Saran, Akila, Abul and other undergraduate friends for always supporting and keeping my spirit in high level. I extend my thanks to my friends Aravinth, Baskar, Josuah, Yoganand, Sunil, Mohan, Arun, Somaiah, Himanshu, Basavraj, Santhosh, Karthikeya, Archita, Nivedita, Deepika, Aruna,

Ananya, Ruchira and all my batch mates for making my stay comfortable at IITG. I wish to thank my seniors and friends in Anna university Dr. Kumar, Arun anna, Suyavaran, Naresh, Manikandan and all other lab mates of protein engineering lab for the initial mentorship, guidance and unconditional love.

I would like to extend my appreciation for my friends at IIT Guwahati Dr. Siddique, Ravi sir, Dr.Vinoth anna, Dr.Rajesh, Siva, Dr.Radhakrishnan, Someshwaran, Dr.Vinoth, Chandru sir (Indian Air Force), Dhamu, Varma, Naren, Avinash, Tariq, Vignesh, Nitin, Rex, Prasath, Anil, Arun, Mohan, KK, Harsh, Harband, Sukjovan and all other well-wishers because of whom my stay at IIT Guwahati has become more memorable and wonderful.

I wish to thank my all seniors and friends Dr. Mohitosh, Dr. Asim Das, Dr. Amit Jaiswal, Dr. Somasekhar Reddy, Dr. Chockalingam, Dr. Pojul, Dr. Ashok, Dr. Debi Prasad, Mahesh, Poulomi, Vimal, Satendra, Kamlesh, Yashwanth, Ankana, Priyamvada, Naveen, Babina, Smita, Vinay, Devendra, Sanjeev, Muthuvel, Nishchal, Koushal, Rupam, Gavya and all other labmates for their co-operation during my work and sharing light moments with them.

Lastly, and also most importantly, I would like to thank my parents Mr. M. Durairaj and Mrs. D. Kalyani for their blessings, my sisters Thilaga and Thinesh Kumari, my brother Mani, my uncle Sekar and their respective family members for their endless and unconditional love and affection during the course of my education at every level.

Thiyagarajan D.

CONTENTS

Contents **i**

Abbreviations **xi**

List of Tables **xiii**

List of Figures **xv**

CHAPTER 1: Introduction and Literature Review

Introduction 3

Literature Review 5

1.1. Overview of Antibiotic-Resistance in Pathogenic Bacteria 5

1.2. Mechanism of Antibiotic-resistance 8

1.3. Rational in Drug Design and Bacterial Membrane as a Drug Target 10

1.4. Antimicrobial Peptides (AMPs) as Membrane-Targeting Agents 11

1.5. Synthetic Amphiphiles as AMP-Mimicking Bactericidal Agents 12

1.6. Essential Features of Synthetic Amphiphiles 12

1.7. Bactericidal Synthetic Amphiphiles 13

1.8. Factors Influencing Cytotoxicity of Synthetic Amphiphiles 16

1.9. DNA Binding Molecules: Chemistry, Activity and Antimicrobial Potential 17

1.10. Combination Therapy 19

1.11. Bacterial Biofilms 20

1.11.1. Essential Features of Biofilm 21

1.11.2. Biofilm-associated Ailments and Challenges in Anti-biofilm Therapy 21

1.12. Methicillin- Resistant *Staphylococcus aureus* (MRSA) 23

Contents

Motivation and Objective of the Present Research Work 27

CHAPTER 2: Bactericidal Spectrum and Membrane-directed Activity of C1

Abstract 33

2.1. Introduction 34

2.2. Materials and Methods

2.2.1. Growth Media and Chemicals 36

2.2.2. Synthetic Amphiphiles 36

2.2.3. Bacterial Strains and Growth Conditions 36

2.2.4. Antibacterial Spectrum of Synthetic Amphiphiles 38

2.2.5. Minimum Inhibitory Concentration (MIC) and Minimum Killing Concentration (MKC) of C1 38

2.2.6. Fluorescence-based Tracking of C1-Bacteria Interaction 39

2.2.7. Bactericidal Potency of C1 40

2.2.7.1. Time- kill Curve 40

2.2.7.2. Field Emission Scanning Electron Microscope (FESEM) Analysis 40

2.2.8. 2.2.8. Membrane-directed Activity of C1 41

2.2.8.1. cFDA-SE Leakage Assay 41

2.2.8.2. PI Uptake Assay 41

2.2.8.3. Membrane Depolarization Assay 43

2.2.9. *In Vitro* Resistance Studies 43

2.2.10. Cytotoxic Effect of C1 on Model Human Cell Line 44

2.3. Results and Discussion

2.3.1. Design Principle and Synthesis of Amphiphile 46

2.3.2. Antibacterial Spectrum, MIC and MKC of C1 47

2.3.3. Tracking Amphiphile-Bacteria Interaction 48

2.3.4. Bactericidal Potency of C1 49

2.3.5. Membrane-directed Bactericidal Activity of C1 51

2.3.6. *In Vitro* Resistance Studies with C1 54

2.3.7. Cytotoxic Potential of C1 55

2.4. Significant Findings 56

CHAPTER 3: DNA Binding and DNA Cleavage Activity of C1

Abstract 59

3.1. Introduction 60

3.2. Materials and Methods

3.2.1. Chemicals and Growth Media 61

3.2.2. UV-Visible Spectroscopy 61

3.2.3. Fluorescence Spectroscopy 61

3.2.4. Ethidium Bromide (EtBr) Displacement Assay 62

3.2.5. Plasmid DNA Cleavage Experiment 62

3.2.6. Plasmid DNA Cleavage and Ligation Studies 63

3.2.7. Uptake and Binding of C1 with Bacterial Cellular DNA 64

3.2.8. Cleavage of Intracellular Plasmid DNA by C1 64

3.3. Results and Discussion

3.3.1. DNA-binding Studies 66

3.3.2. Plasmid DNA Cleavage 68

3.3.3. Cellular DNA Binding 70

3.3.4. Intracellular Plasmid DNA Cleavage 71

3.4. Significant Findings 73

CHAPTER 4: Bactericidal Activity of C1 in Simulated Fluids and its Adjuvant Activity in Combination Therapy

Abstract 77

4.1. Introduction 78

4.2. Materials and Methods

4.2.1. Growth Media and Chemicals 80

4.2.2. Bacterial Strains and Growth Conditions 80

4.2.3. Minimum Inhibitory Concentration (MIC) of Gentamicin and Erythromycin 80

4.2.4. Antibacterial Activity of C1 in Simulated Gastric Fluid (SGF) and Simulated Intestinal Fluid (SIF) 81

4.2.5. Bactericidal Activity of C1 in Simulated Body Fluid (SBF) 81

4.2.6. Bactericidal Activity of Gentamicin and Erythromycin in Combination with C1 82

4.2.7. In Vitro Resistance Against Gentamicin in Presence of C1 83

4.2.8. Cytotoxicity of Antibiotics in Combination with C1 83

4.3. Results and Discussion

4.3.1. Bactericidal Activity of C1 in Simulated Fluids 85

4.3.2. Bactericidal Activity of Antibiotics in Combination with C1 87

4.3.3. In Vitro Resistance Development Against Gentamicin in *S. aureus* MTCC 96 in Combination with C1 91

4.3.4. Cytotoxic Potential of the Combinatorial Treatment 92

4.4. Significant Findings 93

CHAPTER 5: Biofilm eDNA-Targeting Activity of C1-loaded HSA Nanocarrier (C1-HNC)

Abstract 97

5.1. Introduction 98

5.2. Materials and Methods

5.2.1. Growth Media and Chemicals 100

5.2.2. Antibiofilm Activity of C1

5.2.2.1. Microtitre Well Assay 100

5.2.2.2. FESEM Analysis 101

5.2.2.3. Fluorescence Microscope Analysis 101

5.2.2.4. Minimum Biofilm Eradication Concentration ($MBEC_{90}$) of C1 101

5.2.3. Amphiphile-loaded Nanomaterial (C1-HNC) 102

5.2.4. Loading Capacity (LC) and Encapsulation of C1 103

5.2.5. *In Vitro* Release Kinetics of C1 from C1-HNC 103

5.2.6. Matrix-responsive Release of C1 from C1-HNC in Biofilm and Extracted EPS 104

5.2.7. Biofilm Imaging with C1-HNC 105

5.2.8. Antibiofilm Activity of C1-HNC

5.2.8.1. Microtitre Well Assay 106

5.2.8.2. FESEM Analysis 106

5.2.8.3. Fluorescence Microscope Analysis 107

5.2.9. Biofilm eDNA Cleavage Activity of C1-HNC

5.2.9.1. Time-dependent Biofilm eDNA Cleavage 107

5.2.9.2. Solution-based eDNA Cleavage Studies 108

5.2.9.3. Cleavage of eDNA in Biofilm EPS by C1-HNC 108

5.2.10. Comparison of Antibiofilm Activity of C1-HNC and DNase I by CT-DNA Supplementation Experiments 109

5.2.11. Eradication of Biofilm from Catheter Surface 110

5.2.12. Cytotoxic Effect of C1-HNC 110

5.3. Results and Discussion

5.3.1. Antibiofilm Activity of C1 112

5.3.2. C1-loaded Nanomaterial (C1-HNC) 113

5.3.3. Biofilm Matrix-responsive Release of Amphiphile 115

5.3.4. Antibiofilm Activity of C1-HNC 115

5.3.5. Biofilm eDNA Cleavage Activity of C1-HNC 118

5.3.6. Comparative Study of Biofilm eDNA Cleavage by C1-HNC and DNase I 120

5.3.7. Cytotoxic Effect and Therapeutic Potential of C1-HNC 122

5.4. Significant Findings 124

CHAPTER 6: Potential of C1-loaded PLGA Nanocarrier (C1-PNC) for Eradication of MRSA Biofilm

Abstract 127

6.1. Introduction 128

6.2. Materials and Methods

6.2.1. Compounds and Reagents 130

6.2.2. Bacterial Strain and Growth Conditions 130

6.2.3. Combinatorial Effect of C1 and Antibiotics on MRSA Planktonic Cells and Biofilm

6.2.3.1. MIC of C1, Gentamicin and Ciprofloxacin 131

6.2.3.2. Bactericidal Efficacy of Gentamicin and Ciprofloxacin in Combination with C1 131

6.2.3.3. FESEM Analysis of Planktonic Cells 132

6.2.3.4. Antibiofilm Activity of C1 and Antibiotics 132

6.2.3.5. Antibiofilm Activity of Gentamicin and Ciprofloxacin in Combination with C1 133

6.2.3.6. FESEM Analysis of Biofilm 133

6.2.4. C1-loaded PLGA Nanocarrier (C1-PNC) 134

6.2.5. Loading Capacity (LC) and Encapsulation of C1 in PLGA Nanoparticle (PNP) 134

6.2.6. Bactericidal Activity of C1-PNC 135

6.2.7. *In Vitro* Release Kinetics of C1 in Buffers 135

6.2.8. Matrix-responsive Release of C1 from C1-PNC in Biofilm and Extracted EPS 135

6.2.9. Combinatorial Effect of C1-PNC and Therapeutic Antibiotics on MRSA Planktonic Cells and Biofilm 136

6.2.10. Gentamicin Uptake in MRSA Cells in Presence of C1-PNC 137

6.2.11. Determination of Efflux Pump Inhibition by C1-PNC 137

6.2.12. Combination Effect of Ciprofloxacin and Efflux Pump Inhibitor on MRSA Planktonic Cells 138

6.2.13. Ciprofloxacin Accumulation in MRSA Cells 139

6.2.14. Homology Modelling and Molecular Docking Studies 139

6.2.15. Cytotoxicity Assay 139

6.3. Results and Discussion

6.3.1. Adjuvant Potential of Amphiphile Against MRSA Planktonic Cells and Biofilm 141

6.3.2. C1-loaded PLGA Nanocarrier (C1-PNC) 142

6.3.3. Combination Effect of C1-PNC and Therapeutic Antibiotics on MRSA Biofilm 145

6.3.4. C1-PNC Potentiates Gentamicin Uptake in MRSA Cells 147

6.3.5. Effect of C1-PNC on Efflux Activity in MRSA Cells 148

6.3.6. C1-PNC Hinders Ciprofloxacin Efflux in MRSA Cells 150

6.3.7. Plausible Mode of Efflux Inhibition in MRSA Cells 151

6.3.8. Cytotoxic Potential of Combinatorial Therapy 153

6.4. Significant Findings 155

Summary and Future Scope Perspective 159

Bibliography 165

Appendix 197

List of Publications 227

ABBREVIATIONS

µg	Microgram
µL	Microliter
µM	Micromolar
A_{600}	Absorbance at 600 nm
AMPs	Antimicrobial peptides
ANOVA	Analysis of variance
AU	Arbitrary unit
BHI	Brain-heart infusion broth
C1	Compound 1
C1-HNC	C1-loaded HSA nanocarrier
C1-PNC	C1-loaded PLGA nanoparticle
C2	Compound 2
CCCP	Carbonyl cyanide m-chlorophenylhydrazone
cFDA-SE	5(and 6)-carboxyfluorescein diacetate succinimidyl ester
CFU	Colony forming unit
cps	Counts per second
CR	Congo red
CT-DNA	Calf-thymus Deoxyribonucleic acid
CV	Crystal violet
$DiSC_35$	3,3′-dipropylthiadicarbocyanine iodide
DLS	Dynamic light scattering
DMEM	Dulbecco's modified eagles medium
DMSO	Dimethyl sulfoxide
DNA	Deoxyribonucleic Acid
DNase I	Deoxyribonuclease I
eDNA	Extracellular DNA
EDTA	Ethylene Diamine tetra Acetic Acid
EPS	Extracellular polymeric substances
EtBr	Ethidium bromide
FBS	Fetal bovine serum
FCS	Fetal calf serum

Abbreviations

FDA	Food and Drug Administration
FESEM	Field emission scanning electron microscope
FIC	Fractional inhibitory concentration
FTIR	Fourier Transform Infrared Spectroscopy
HEK	Human embryonic Kidney
HEPES	N-2-Hydroxyethyl Piperazine N-2 Ethane Sulphonic acid
HNPs	Human serum albumin (HSA)-based nanoparticles
HSA	Human serum albumin
IC	Inhibitory concentration
K_a	Association constant
K_b	Intrinsic binding constant
K_q	Quenching constant
LC	Loading capacity
LPS	Lipopolysaccharide
MBC	Minimum bactericidal concentration
$MBEC_{90}$	Minimum biofilm elimination concentration to eliminate 90% biofilm
$MBIC_{90}$	Minimum biofilm inhibition concentration to inhibit 90% biofilm
MeOH	Methanol
MIC	Minimum inhibitory concentration
mL	Milliliter
mM	Millimolar
MRGs	Metal reactive groups
MRSA	Methicillin resistant *Staphylococcus aureus*
MTCC	Microbial Type Culture Collection
MTT	3-(4,5-Dimethylthylthiazol-2-yl)-2,5-diphenyltetrazolium bromide
NB	Nutrient broth
NC	Nicked circular
nm	Nanometer
NPs	Nanoparticles
OD_{600}	Optical density at 600 nm
PBS	Phosphate buffered saline
PI	Propidium iodide
PNP	PLGA nanoparticle

Abbreviations

rpm	Rotation per minute
SBF	Simulated body fluid
SC	Supercoiled
SD	Standard deviation
SDS	Sodium dodecyl sulphate
SEM	Scanning electron microscope
SGF	Simulated gastric fluid
SRF	Spontaneous resistance frequency
SRL	Sisco research laboratories
WTA	Wall teichoic acid
λ_{Em}	Emission wavelength
λ_{Ex}	Exitation wavelength

LIST OF TABLES

CHAPTER 1		**Page No.**
Table 1.1.	Characteristic machinery of antibiotic-resistance in pathogenic bacteria	9
Table 1.2.	Overview of bactericidal synthetic amphiphiles	14
Table 1.3.	Representative examples of combination therapy used against pathogenic bacteria	20
CHAPTER 2		
Table 2.1.	MIC and MKC of C1 against target bacterial strains.	48
Table 2.2.	MIC of C1 determined against *S. aureus* MTCC 96 in a multistep *in vitro* resistance development experiment.	54
CHAPTER 3	Nil	
CHAPTER 4		
Table 4.1.	Combination effect of C1 and gentamicin on *S. aureus* MTCC 96 cells.	88
Table 4.2.	Combination effect of erythromycin and C1 on *E. coli* MTCC 433 cells	89
Table 4.3.	Combination effect of Gentamicin with C1 on *S. aureus* MTCC 96	91
CHAPTER 5	Nil	
CHAPTER 6		
Table 6.1.	MIC, $MBIC_{90}$ and $MBEC_{90}$ of C1, C1-PNC and antibiotics	141

against *S. aureus* 4s.

Table 6.2. Fold reduction in $MBIC_{90}$ of therapeutic antibiotics against biofilm of the MRSA strain *S. aureus* 4s in combination with C1-PNC. 145

Table 6.3. Fold reduction in $MBEC_{90}$ of therapeutic antibiotics against biofilm of the MRSA strain *S. aureus* 4s in combination with C1-PNC. 145

LIST OF FIGURES

CHAPTER 1 **Page No.**

Figure 1.1. The categories of pathogenic bacteria based on CDC report (2013) 6

Figure 1.2. Significant clinical implications of antibiotic-resistant pathogenic bacteria. The statistics shown in the figure is obtained from Fair and Tor, 2014 7

Figure 1.3. Challenges encountered in anti-biofilm therapy 23

CHAPTER 2

Figure 2.1. Structure of synthetic amphiphiles used in the present investigation. LogP values were determined using MarvinSketch (https://www.chemaxon.com/products/marvin/marvinsketch/). 37

Figure 2.2. Schematic representation of general steps involved in the synthesis of compound 1 (C1). (i) Dodecylamine, MeOH, reflux, (ii) $NaBH_4$, MeOH, 0^oC, (iii) R^3CH_2Cl/K_2CO_3/MeCN, reflux, 72 h, (iv) CH_3I, MeCN, 0^oC. 37

Figure 2.3. Schematic representation of the experimental protocol for determining MIC and MKC of amphiphile C1. 39

Figure 2.4. Schematic representation of the experimental protocol for (A) cFDA-SE leakage assay and (B) PI uptake assay. 42

Figure 2.5. Schematic representation of the experimental protocol to study multistep *in vitro* resistance development in presence of C1. 44

Figure 2.6. Design principle of compound 1. 46

Figure 2.7. Antibacterial activity of (A) C1 and (B) C2 against target bacterial strains. The target bacteria were interacted with the amphiphiles for 24 h. 47

Figure 2.8. (A) Fluorescence emission spectra of C1 and *S. aureus* MTCC 96 bound-C1. (B) Fluorescence microscopic image of C1-treated *S. aureus* MTCC 96. Scale bar for the images is 50 μm. 49

Figure 2.9. Time-kill curves of C1 against (A) *S. aureus* MTCC 96 and (B) *E. coli* MTCC 433. 50

Figure 2.10. FESEM analysis of target bacterial cells treated with 40 μM C1. Scale bar for the images is 300 nm. 50

Figure 2.11. cFDA-SE leakage assay in (A) *S. aureus* MTCC 96 and (B) *E. coli* MTCC 433 treated with C1. 52

Figure 2.12. Propidium iodide uptake assay in (A) *S. aureus* MTCC 96 and (B) *E. coli* MTCC 433 treated with C1. 52

Figure 2.13. $DiSC_3$5-based membrane depolarization assay in (A) *S. aureus* MTCC 96 and (B) *E. coli* MTCC 433 treated with C1. 53

Figure 2.14. MTT assay to determine the viability of HEK 293 cell lines following treatment with varying concentrations of C1. Each data point represents mean ± standard deviation from six samples. 55

CHAPTER 3

Figure 3.1. Scheme of the protocol for plasmid DNA cleavage and ligation studies. 63

Figure 3.2. Scheme of the protocol for studying uptake and binding of C1 with bacterial cellular DNA. 65

Figure 3.3. Scheme of the protocol for studying cleavage of intracellular plasmid DNA by C1. 65

Figure 3.4. (A) UV-visible absorbance spectroscopy of C1 (5.0 µM) upon addition of calf thymus DNA (0.06 µM-0.6 µM). (B) Binding isotherm of C1 with calf thymus DNA determined by UV-visible absorbance titration spectroscopy. 66

Figure 3.5. Fluorescence spectroscopy of C1 (150 nM) upon addition of calf thymus DNA (15 nM-75 nM). 67

Figure 3.6. (A) Ethidium bromide displacement assay with C1 (0.3 µM-4.5 µM). (B) Stern-Volmer plot for ethidium bromide displacement assay with C1. 67

Figure 3.7. (A) Agarose gel electrophoresis of pUC18 plasmid DNA treated with C1. Lanes 1: control (untreated plasmid DNA); 2-6: plasmid DNA treated with varying concentrations of C1 (6.0 µM - 30 µM). SC: supercoiled DNA, LC: linearised circular DNA, NC: nicked circular DNA. (B) Quantification of band intensity of the topological forms of pUC18 plasmid DNA obtained in (A) using ImageJ analysis software. 68

Figure 3.8. Agarose gel electrophoresis of pUC18 plasmid DNA treated with C1 in (A) absence of NaN3, (B) presence of NaN3, (C) absence of DMSO and (D) presence of DMSO. Lanes 1: control (untreated plasmid DNA); 2-4: plasmid DNA treated with 6.0 µM, 18 µM and 30 µM of C1, respectively. 68

Figure 3.9. (A) Agarose gel electrophoresis indicating various forms of pUC18 plasmid DNA used for transformation experiments. Lanes: (1) uncut plasmid DNA, (2) EcoRI-treated plasmid DNA, (3) C1-treated plasmid DNA. SC: supercoiled DNA, LC: linearised circular DNA, NC: nicked circular DNA. (B) Quantification of transformed *E. coli* DH5α colonies. (1-2) C1-treated pUC18 plasmid DNA, (3-4) EcoRI-treated pUC18 plasmid DNA, (5-6) untreated pUC18 plasmid DNA. The ligation negative and ligation positive samples are indicated. 70

Figure 3.10. Uptake and intracellular DNA binding by C1 in *E. coli* MTCC 433 cells. Cells were initially treated with (A) 15 µM C1 or (B) 0.5 µg/mL of polymyxin B and then stained with propidium iodide (PI). Fluorescence emission intensity of PI was measured in both (A) and (B) following 71

incremental addition of C1 (15 µM, 30 µM and 45 µM).

Figure 3.11. Agarose gel electrophoresis to study pUC18 plasmid DNA cleavage in *E. coli* DH5α cells upon interaction with C1. Lanes: (1) control pUC18 plasmid DNA, (2-3): pUC18 plasmid DNA isolated from untreated cells after 3 h and 6 h, (4-5): pUC18 plasmid DNA isolated from polymyxin B-treated cells after 3 h and 6 h, (6-7): pUC18 plasmid DNA isolated from C1-treated cells after 3 h and 6 h. SC: supercoiled DNA, NC: nicked circular DNA. 72

Figure 3.12. (A) Fluorescence emission intensity of PI measured to ascertain membrane damage in *E. coli* DH5α cells treated with either 45 µM C1 or 0.5 µg/mL polymyxin B for 3 h and 6 h. (B) Loss in viability of E. coli DH5α cells treated with either 45 µM C1 or 0.5 µg/mL polymyxin B for 3 h and 6 h. 72

CHAPTER 4

Figure 4.1. Antibacterial activity of C1 against (A) *L. monocytogenes* Scott A and (B) *E. coli* MTCC 433 cells incubated in simulated gastric fluid. Bactericidal activity of C1 against (C) *L. monocytogenes* Scott A and (D) *E. coli* MTCC 433 cells incubated in simulated intestinal fluid. 86

Figure 4.2. Antibacterial activity of C1 in combination with gentamicin against *S. aureus* MTCC 96 cells. 88

Figure 4.3. Antibacterial activity of C1 in combination with erythromycin against *E. coli* MTCC 433 cells. 90

Figure 4.4. FESEM analysis of target bacterial cells subjected to a combined treatment with C1 and antibiotics. Scale bar for the images is 500 nm. 90

Figure 4.5. MTT assay to ascertain the effect of C1 in combination with either (A) gentamicin or (B) erythromycin on HEK 293 cells. Each data point represents mean ± standard deviation from six samples. 92

CHAPTER 5

Figure 5.1. (A) Antibiofilm activity of C1 on *S. aureus* MTCC 96 biofilm ascertained by crystal violet assay. * indicates p value < 0.001 in ANOVA. (B) FESEM analysis of C1 treated *S. aureus* MTCC 96 biofilm. (C) Fluorescence microscope analysis of *S. aureus* biofilm treated with C1. Scale bar for the images is 100 µM. 112

Figure 5.2. FESEM image of (A) HSA nanoparticle (B) C1- loaded HNP (C1-HNC). Scale bar for the images is 200 nm. Characterization of C1-HNC by (C) UV-visible spectroscopy and (D) FT-IR analysis. DLS-based particle size analysis of (E) HNP and (F) C1-HNC. The particle size and percentage of the aggregated species (in parenthesis) of HNP and C1-HNC corresponding to peaks 1-3 are indicated below the plot. 114

Figure 5.3.	(A) Fluorescence emission spectra of varying concentrations of C1 upon excitation at 340 nm. Inset: Calibration plot of concentration versus emission of C1. Emission was measured at 376 nm. (B) Loading capacity (LC) and amount of encapsulated C1 in HSA nanoparticle. (C) *In vitro* release kinetics of C1 from C1-HNC in physiologically relevant fluids and HEPES buffer.	114
Figure 5.4.	(A) Release of C1 from C1-HNC in *S. aureus* MTCC 96 biofilm, extracted EPS and media. (B) Fluorescence-based imaging of the vials containing released C1 in (i) *S. aureus* biofilm and (ii) media alone. (C) Fluorescence microscopic images of HNP-treated (control) and C1-HNC-treated (corresponding to 16 µM and 128 µM of C1) *S. aureus* MTCC 96 biofilm viewed under UV, blue and green excitation. Biofilm imaging was pursued by recording the inherent fluorescence emission of C1 at various excitations. Scale bar for the images is 100 µm.	116
Figure 5.5.	(A) Eradication of *S. aureus* MTCC 96 biofilm by C1-HNC determined by MTT assay. * indicates p value < 0.001 in ANOVA. (B) FESEM images of untreated *S. aureus* MTCC 96 biofilm (control) and *S. aureus* MTCC 96 biofilm treated with C1-HNC (128 µM C1 concentration). Scale bar for the images is 1.0 µm.	117
Figure 5.6.	cFDA-SE and Congo red-based fluorescence microscopic analysis of *S. aureus* MTCC 96 biofilm following treatment with various concentrations of C1-HNC. CFDA-SE and Congo red staining indicates loss of cell viability and reduction of biofilm matrix EPS, respectively. Scale bar for the images is 100 µm.	117
Figure 5.7.	(A) Agarose gel electrophoresis of biofilm eDNA obtained from 24 h grown *S. aureus* biofilm treated with HNP, DNase I and C1-HNC for various time periods. (B) Quantification of band intensity of biofilm eDNA samples in (A) using ImageJ analysis software. (C) Fluorescence emission spectra of purified *S. aureus* biofilm eDNA-bound Hoechst 33258 dye following interaction with HNP, C1-HNC and DNase I.	118
Figure 5.8.	(A) Agarose gel electrophoresis of C1-HNC treated *S. aureus* biofilm EPS (20% v/v), pUC18 plasmid DNA (60 µM) alone and spiked in EPS (20% v/v). Lanes 1: Lamda DNA double digest, 2: Control EPS, 3: Control pUC18 DNA, 4: Control pUC18 DNA spiked in EPS, 5-8: EPS treated with 7.5 µM-30 µM C1-HNC, 9-12: pUC18 DNA treated with 7.5 µM-30 µM C1-HNC, 13-16: pUC18 DNA spiked in EPS and treated with 7.5 µM-30 µM C1-HNC. eDNA: Extracellular DNA, NC: Nicked circular DNA, SC: Supercoiled DNA. (B) Band intensity of eDNA (lane 2 and lanes 5-8 in panel A). (C) Band intensity of the topological forms of pUC18 plasmid DNA and eDNA obtained from pUC18 plasmid DNA spiked *S. aureus* MTCC 96 biofilm EPS treated with varying concentrations of C1-HNC (lane 4 and lanes 13-16 in panel A). The band intensities were quantified using ImageJ analysis software.	119
Figure 5.9.	Effect of CT-DNA supplementation on (A) C1-HNC-treated and (B) DNAse I-treated *S. aureus* MTCC 96 biofilm. (C) Fluorescence microscope analysis to study the effect of CT-DNA supplementation on C1-HNC-treated and DNAse I-treated *S. aureus* MTCC 96 biofilm. Biofilm was	121

stained with the DNA binding Hoechst 33258 dye. Scale bar for the images is 100 µm.

Figure 5.10. (A) MTT assay to evaluate the effect of C1-HNC on the viability of HEK 293 cells. (B) Fluorescence microscope images of HNP-treated (control) and C1-HNC-treated HEK 293 cells. Scale bar for the images is 100 µm. 122

Figure 5.11. (A) MTT assay to ascertain the effect of C1-HNC on *S. aureus* MTCC 96 biofilm grown on Foley's urinary catheter. (B) FESEM images of Foley's urinary catheter segments indicating (i) bare catheter surface, (ii) untreated *S. aureus* MTCC 96 biofilm, (iii) C1 treated *S. aureus* MTCC 96 biofilm and (iv) *S. aureus* MTCC 96 biofilm treated with C1-HNC (corresponding to 128 µM C1). Scale bar for the images is 2.0 µm. 123

CHAPTER 6

Figure 6.1. Combination effect of (A) C1 and gentamicin and (B) C1 and ciprofloxacin on *S. aureus* 4s biofilm. (C) FESEM analysis of the combination effect of C1 with either gentamicin or ciprofloxacin on pre-formed MRSA biofilm. Scale bar for the images is 2.0 µm. 142

Figure 6.2. FESEM image of (A) PLGA nanoparticle (PNP), (B) C1-loaded PLGA nanoparticle (C1-PNC). Scale bar for the images is 200 nm. Characterization of C1-PNC using (C) UV-visible spectroscopy and (D) FT-IR analysis. Dynamic light scattering (DLS) based particle size analysis of (E) PNP and (F) C1-PNC. The particle size and percentage of aggregated species of C1-PNC (in parentheses) corresponding to peaks 1-3 are indicated below the plot. 143

Figure 6.3. (A) Estimation of C1 loading in PLGA nanoparticle. (B) Release of C1 from C1-PNC in buffers and in *S. aureus* 4s biofilm and EPS. 144

Figure 6.4. Combination effect of (A) C1-PNC and gentamicin and (B) C1-PNC and ciprofloxacin on *S. aureus* 4s biofilm. (C) cFDA-SE based fluorescence microscopic analysis of MRSA biofilm following treatment with C1-PNC in combination with either gentamicin or ciprofloxacin. Scale bar for the images is 100 µm. 146

Figure 6.5. (A) Uptake of gentamicin in C1-PNC-treated MRSA cells. The concentration of gentamicin was 256 µM. (B) Partitioning of gentamicin in C1-PNC treated MRSA cells. The concentration of gentamicin used was 256 µM. 148

Figure 6.6. (A) Effect of C1-PNC on EtBr efflux in *S. aureus* 4s planktonic cells. (B) EtBr accumulation in S. aureus 4s cells subjected to treatment with C1-PNC and C1. 149

List of Figures

Figure 6.7. Measurement of *S. aureus* 4s cell-associated ciprofloxacin. Cells were incubated in 50 mM phosphate buffer (pH 7.0) with 32 µM ciprofloxacin for the first five minutes. Following addition of either C1 or C1-PNC (indicated by an arrow) in separate sets, the cells were incubated for another five minutes. Subsequently the cells were washed with ice cold phosphate buffer and incubated in 0.1 M glycine buffer (pH 3.0) for 15 h and then the cells were pelleted and ciprofloxacin in the supernatant was measured. 151

Figure 6.8. MTT assay to ascertain the effect of C1-PNC in combination with gentamicin and ciprofloxacin on HEK 293 cells. Each data point represents mean ± standard deviation from six samples. 153

Chapter 1

Introduction and Literature Review

Introduction and Literature Review

Introduction

The menace of drug-resistant pathogenic bacteria is a burgeoning issue in contemporary healthcare. Pathogenic bacteria can acquire drug-resistance trait through a number of inherent mechanisms such as enzyme-catalyzed target modification, presence of an outer membrane barrier, drug inactivation, presence of efflux pump and others. There is an acute dearth in the turnover of new antibiotics that can counter the challenge of drug-resistant pathogenic bacteria and this has exacerbated the healthcare crisis worldwide. This predicament has also bolstered the need for an aggressive drug discovery program, which is focusssed towards the generation of potent antimicrobial agents. It is envisaged that such an endeavor should be essentially based on astute medicinal chemistry and drug design principles in order to develop bactericidal agents that can act on profound cellular targets and are counterproductive to resistance development.

In this context, membrane-targeting antibacterials such as antimicrobial peptides (AMPs) hold special interest. Notwithstanding their promise, therapeutic application of AMPs is plagued by high production cost, poor pharmacokinetics and protease sensitivity. In order to address this concern, AMP-mimicking synthetic bactericidal amphiphiles have emerged as promising candidates and gained prominence based on their facile synthesis and the potential to generate a plethora of membrane-acting bactericidal scaffolds through rational structural design. Membrane-acting synthetic amphiphiles have been extensively reported as antibacterial agents. However, in the context of drug-resistant pathogens, the ability of an antibacterial agent to directly target the genetic basis of antibiotic-resistance and disarm the resistance mechanism thereof is critical. Thus, a dual-target synthetic amphiphile that can be tailored to breach the membrane barrier, gain access and then cleave intracellular DNA could render significant therapeutic benefit, since drug-resistant pathogens are known to have plasmids that can harbor and disseminate antibiotic-resistance traits through gene transfer mechanism. It is also possible that membrane-targeting synthetic amphiphiles can be explored in combination with antibiotics so as to ward off the drug- resistant pathogens. It is envisaged that such a combinatorial therapeutic

approach is likely to render elimination of pathogenic bacteria in presence of low concentrations of antibiotics, thereby reducing drug overuse and its consequent toxic effects.

Bacterial biofilm is a formidable healthcare challenge as it is implicated in a number of clinical infections. A major crux in the elimination of biofilm is the presence of a complex and heterogeneous matrix, which can afford protection to the underlying cells against host-mediated immunity and therapeutic antibiotics. Based on literature reports, it is now evident that the biofilm extracellular DNA (eDNA) plays a germane role in the initiation and establishment of biofilm. The presence of eDNA in the biofilm matrix can also lead to transmission of resistance-traits and therefore targeting the biofilm eDNA is an appealing therapeutic avenue for mitigation of biofilm-mediated infections. In this context, it is conceived that a synthetic antibacterial that can readily invade the biofilm matrix, disrupt the eDNA scaffold and concurrently abolish the underlying cells or restore susceptibility of the cells to therapeutic antibiotics could be a viable antibiofilm agent.

Based on the aforementioned premise and recognizing the prospect of developing bi-functional synthetic amphiphile as a novel and potent bactericidal agent, the present investigation ascertains the bactericidal potential of a rationally designed dual-target synthetic amphiphile tailored to disrupt the bacterial membrane and cleave cellular DNA. The investigation also demonstrates how the dual-target activity of the synthetic amphiphile translates into enhanced capabilities and provides a unique therapeutic leverage in combating the menace of bacterial biofilm. The following section provides a detailed literature review pertinent to the research area of the present investigation.

Literature Review

1.1. Overview of Antibiotic-Resistance in Pathogenic Bacteria

The emergence of antibiotic-resistant pathogenic bacteria is a contemporary healthcare problem. Antibiotic-resistant pathogenic bacteria are known to adopt a plethora of strategies in order to develop resistance against commonly used therapeutic agents. Further, the arbitrary use of antibiotics in the therapeutic regime has, in turn, triggered the evolution of drug-resistant strains. A number of seminal review articles discuss the emergence and healthcare implications of antibiotic-resistant pathogenic bacteria (Brown and Wright 2016; Fair and Tor 2014; Gootz 2010; Nikaido 2009; Fischbach and Walsh 2009). As discussed in the review article of Fischbach and Walsh (2009), the prevalent antibiotic-resistant pathogenic bacteria can be categorized as:

(a) Methicillin-resistant *Staphylococcus aureus* (MRSA), which is implicated in a number of nosocomial and life-threatening infections.
(b) Multidrug-resistant (MDR) Gram-negative pathogenic bacteria such as *Acinetobacter baumannii, Escherichia coli, Klebsiella pneumoniae* and *Pseudomonas aeruginosa*, which are known to possess an outer membrane drug permeability barrier and efflux pumps to expel out antimicrobial agents.
(c) Multidrug-resistant (MDR) and extensively-drug-resistant (XDR) strains of *Mycobacterium tuberculosis* (MDR-TB and XDR-TB), which is a cause of serious concern in the developing countries.

In the report published by the Centre for Disease Control and Prevention (CDC) in 2013, pathogenic bacteria have been categorized into various threat levels. A schematic representation of the categorization and representative examples of the pathogenic bacteria is indicated in Figure 1.1. The World Health Organization (WHO) in its report in 2014 has highlighted the concern regarding the common infections caused by drug-resistant bacteria and according to the report, in certain cases, the risk of death is doubled owing to drug resistant-bacteria as compared to a non-resistant pathogen.

Figure 1.1. The categories of pathogenic bacteria based on CDC report (2013).

On the basis of literature reports, the clinically relevant drug-resistant pathogenic bacteria include β-lactam resistant *Pneumococci*, penicillin and chloramphenicol resistant *Neisseria meningitides,* vancomycin-resistant enterococci (VRE), vancomycin-resistant *Staphylococcus aureus* (VRSA) (Kaye and Kaye 2000; Yang et al. 2007; Alekshun and Levy 2007; Chang et al. 2015), methicillin-resistant *Staphylococcus aureus* (MRSA) and penicillin-resistant *Streptococcus pneumoniae* (Chambers and DeLeo 2009; Deresinski 2005; Stryjewski and Corey 2014; Alekshun and Levy 2007; Chang et al. 2015; Lowy 2003); multidrug-resistant *Salmonella Typhimurium* (MRST) (Mather et al. 2013), multidrug-resistant *Acinetobacter*, carbapenem-resistant Enterobacteriaceae (CRE) and several others (Fair and Tor 2014). In recent times, the prevalence of *Klebsiella pneumonia* NDM-1 is a cause of great concern, as by virtue of a metallo-β-lactamase-resistance gene

(blaNDM.1), the pathogen exhibits resistance against penicillin, cephalosporins and other antimicrobial agents (Hawkey and Jones 2009; Nordmann et al. 2011; Barantsevich et al. 2013; Brink et al. 2012; Jin et al. 2015; Arpin et al. 2012). According to the Center for Disease Control and Prevention's 2013 report, out of nearly 2.0 million people who get affected by pathogenic bacteria, the number of annual deaths is 23,000 in United States

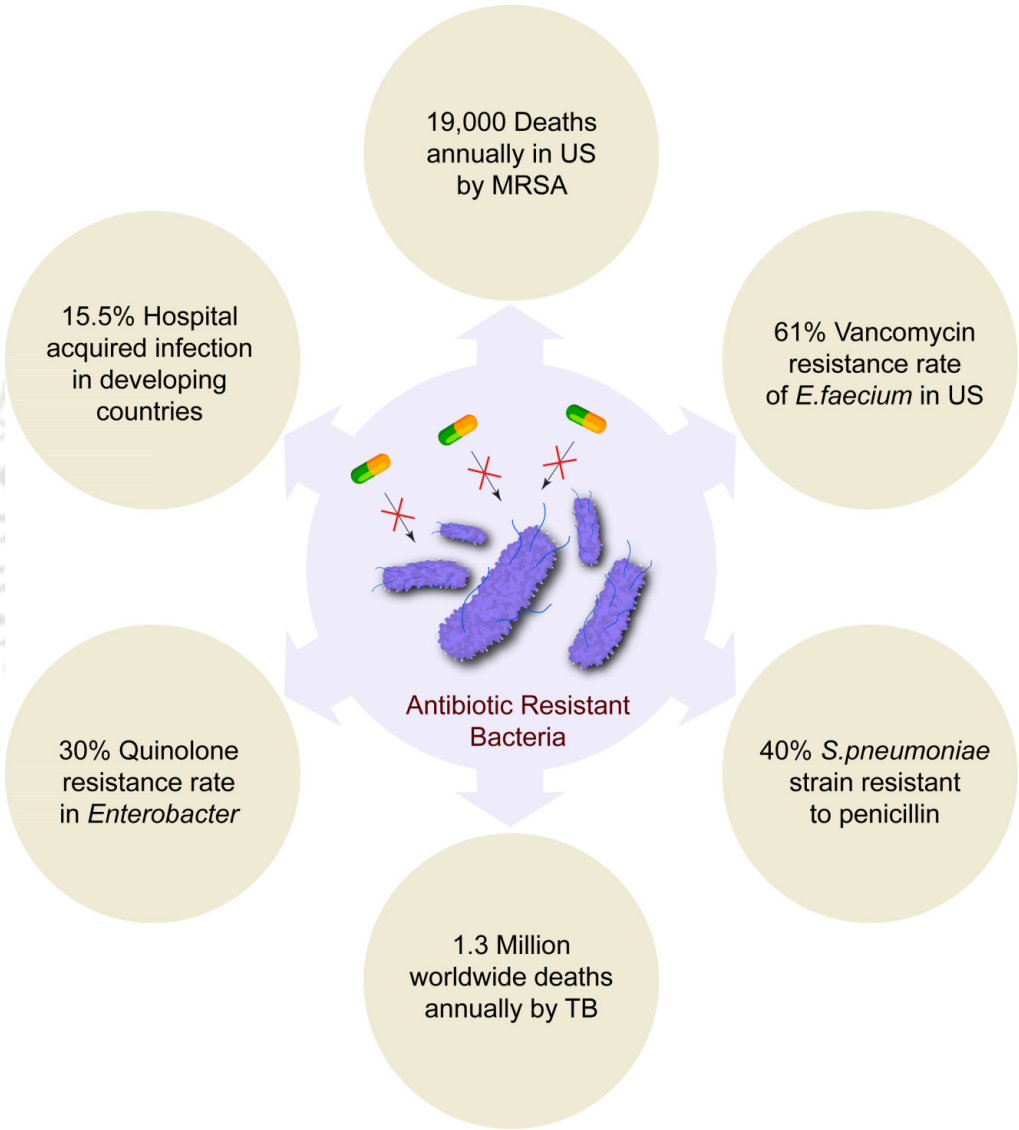

Figure 1.2. Significant clinical implications of antibiotic-resistant pathogenic bacteria. The statistics shown in the figure is obtained from Fair and Tor, 2014.

alone due to infections caused by drug-resistant bacteria. A schematic illustrating the significant implications of antibiotic-resistant pathogenic bacteria is indicated in Figure 1.2. It is quite evident from the statistics presented in Figure 1.2, that there is a critical need to discover novel classes of antibacterial drugs in order to tackle the global problem of drug resistance.

All major groups of antibiotics were essentially discovered between 1930s-1960s and since then very few new classes of antibiotics have been introduced, which reflects the innovation gap and the slow pace in drug discovery research (Fischbach and Walsh 2009; Silver 2011). A review by Brown and Wright (2016), demarcates 100 years of the antimicrobial drug discovery into four major periods on the basis of the level of screening and spectrum of antimicrobial activity. Accordingly, the major era's include the golden era, medicinal chemistry era, resistance era and narrow-spectrum era.

1.2. Mechanism of Antibiotic-Resistance

Antibiotic-resistant pathogenic bacteria are bestowed with effective countermeasures that enable the bacteria to evade the action of most therapeutic antibiotics (Blair et al., 2015; Fernandes 2006; Wright 2011). Most of the therapeutic antibiotics impede fundamental physiological processes in cells such as DNA synthesis (Collin et al. 2011; Kohanski et al. 2010), cell wall synthesis (Hurdle et al. 2011; Lewis 2013), protein synthesis (McCoy et al. 2011; Wilson 2014) and folate synthesis (Lange et al. 2007; Palmer and Kishony 2014). However, to evade the host defense mechanism and foil the action of antibiotics, drug-resistant bacteria exhibit a number of attributes such as (a) the presence of a permeability barrier that prevents drug diffusion, (b) an efflux pump that exports certain drugs from the cell and thus diminishes its availability at target sites, (c) alterations in molecular targets, (d) presence of a metabolic bypass that renders the cell insensitive to the drug, (e) presence of antibiotic-altering and antibiotic-degrading enzymes (Nikaido 2009; Wright 2011). Further, it is acknowledged that excessive use of antibiotics may promote or favor the growth of resistant cells and transmission of the resistance trait can then be facilitated through horizontal gene transfer (Davies and Davies 2010; Fair and Tor 2014; Toprak et al. 2012). A overview of various antibiotic-resistance mechanisms is represented in Table 1.1.

Table 1.1. Characteristic machinery of antibiotic-resistance in pathogenic bacteria.

Inherent Strategy	Cellular Component	Nature of Resistance Determinant	Specific Outcome	Reference
Mechanisms affecting the maintenance of intracellular concentration of drug	Membrane lipids and porins	Physical barrier of lipopolysaccharide (LPS) in outer membrane	Drug-resistance in Gram-negative bacteria	Delcour 2009; Lavigne et al. 2012
		Physical barrier of Peptidoglycan and wall teichoic acid (WTA) in cell wall	Drug-resistance in Gram-positive bacteria	Kohler et al. 2009; Weidenmaier and Peschel 2008
		Modified porin proteins (Opr and Omp)	Diminished drug entry	Fernandez and Hancock 2012
	Multidrug efflux pumps	ATP-binding cassette (ABC) Major facilitator superfamily (MFS) Multidrug and toxic compound extrusion (MATE) Small multidrug resistance (SMR)	Efflux out the drug molecule from bacterial cell	Fernández Fuentes et al. 2014; Li and Nikaido 2009; Sun et al. 2014; Chambers and DeLeo 2009; Deresinski 2005; Stryjewski and Corey 2014
Altering the enzymatic activity to deactivate or de-recognize the drug molecule	Drug degrading and modifying enzymes	Enzymatic hydrolysis, phosphorylation, acetylation, etc.	Negates β-lactams (β-lactamases), macrolides (esterases), aminoglycosides and choramphenicol (acetyl & methyl) transferase	Gootz 2010; Kumar and Varela 2013; Wright 2005
	Target modifying enzymes	LPS reconstitution by L-Arap4N Modifying gyrase and DNA polymerase binding rRNA methylation Mutation in penicillin binding protein (PBP)	Decreased electro-negativity of LPS and resistance development against cationic antibiotics Quinolones, Rifamycin, Macrolides and β-lactam resistance	Gutsmann and Seydel 2010; Kaye and Kaye 2000

Inherent Strategy	Cellular Component	Nature of Resistance Determinant	Specific Outcome	Reference
Transfer of genetic traits	Plasmid carrying drug-resistance genes and mutated genes	Mutations in *kat*G, *inh*A, *ahp*C, *kas*A and *ndh*	Multidrug-resistant TB	Almeida Da Silva and Palomino 2011
		bla_{CTX-M} *mec*A operon	Beta-lactamase, Methicillin-resistant *S. aureus* (MRSA)	Chambers and Deleo 2009; Hawkey and Jones 2009
		*acr*B, *efr, qep, msrA, cml,*	Macrolide and chloramphenicol efflux	Fernández Fuentes et al. 2014
		qac genes	Resistance against quaternary ammonium compounds	Wassenaar et al. 2015
		*tet*A gene *nor* genes, *aph,*and *aadA1* genes	Resistance against tetracycline, norfloxacin, quinolone and aminoglycoside	Blair et al. 2015; Nikaido, 2009
		*msr*A/B, *mph*A, and *mef*A	Resistance against macrolide	Fernández Fuentes et al. 2014
Over expression and modification of target molecule	Target protein	Dihydropteroate synthase	Resistance against sulfonamide and trimethoprim	Alekshun and Levy 2007; Palmer and Kishony 2014
	Modified target site	Amino acid substitution	Resistance against vancomycin	Wright 2011

1.3. Rational in Drug Design and Bacterial Membrane as a Drug Target

In the endeavor towards drug discovery against antibiotic-resistant bacterial strains, the following cardinal elements are acknowledged to be critical (a) identification of profound cellular targets, which are likely to play a critical role in the survival and virulence of the target strain (Murima et al. 2014; Johnston et al. 2016) (b) prudent selection of targets that lack structural homologs in the mammalian host, (c) generate candidate molecules, which possess optimum pharmacodynamic and pharmacokinetic criteria (Craig 1998; Craig 2003; Mueller et al. 2004; Silver, 2011; Onufrak et al. 2016),

(d) develop candidate molecules that are non-toxic to host cells, even when administered at concentrations higher than their MIC (Wispelwey 2005), (e) develop candidate molecules that display high antibacterial activity but are not liable to induce resistance development.

Bactericidal agents that can target the bacterial membrane are considered as promising therapeutic agents against antibiotic-resistant pathogens. In contrast to antibiotics that are known to target specific physiological processes and are thus liable to resistance development, the likelihood of developing resistance against membrane-targeting agents demands large scale restoration of membrane components, which is physiologically demanding for the bacteria (Chen et al. 2010; Van Bambeke et al. 2008; Hurdle et al. 2011). Further, membrane acting agents are also effective against infections caused by dormant bacterial cells such as biofilm or slow-growing bacteria like *Mycobacterium tuberculosis*, unlike β-lactam antibiotics, which are known to act on only growing cells (Hurdle et al. 2011). Cationic membrane acting agents are particularly appealing and possess high antibacterial selectivity, as bacterial membranes have a higher content of anionic phospholipids as opposed to mammalian cytoplasmic membranes (van Meer and de Kroon 2011; Zasloff 2002).

1.4. Antimicrobial Peptides (AMPs) as Membrane-Targeting Agents

Antimicrobial peptides (AMPs) are archetypical membrane acting agents, which are ubiquitous and possess a broad-spectrum antibacterial activity (Hancock and Sahl 2006; Shai 2002; Zasloff 2002; Kosikowska and Lesner 2016, Zhang and Gallo 2016). On the basis of a large number of studies, it is well established that the cationic charge of AMPs are involved in interactions with anionic bacterial cells, while the hydrophobic scaffold of AMPs penetrate and disrupt membrane integrity (Wimley 2010, Brogden 2005, Yeaman and Yount 2003, Chen et al., 2010; Kosikowska and Lesner 2016, Zhang and Gallo 2016, Lombardi et al. 2015). The models that describe AMP-mediated membrane permeabilization are the barrel-stave, toroidal pore and carpet model (Hurdle et al., 2011, Wimley 2010; Mahlapuu et al. 2016). In spite of their strong antibacterial activity, the therapeutic potential of AMPs is hampered by several factors such as: (a) high manufacturing cost (Marr et al. 2006), (b) challenges in drug formulations (Findlay et al.

2010), (c) propensity to lose activity in presence of mono and divalent cations (Bowdish et al. 2005) and (d) proteolytic inactivation (Marr et al., 2006; Yeaman and Yount 2003).

1.5. Synthetic Amphiphiles as AMP-Mimicking Bactericidal Agents

Owing to the bottlenecks in the exploration of AMPs as bactericidal agents, extensive research in the area of medicinal chemistry has led to the generation of AMP-mimicking synthetic amphiphiles. In contrast to AMPs, synthetic amphiphiles offer several advantages such as (a) facile and inexpensive large scale synthesis, (b) membrane-directed activity, which augers well to combat antibiotic-resistant pathogens, (c) structural tailoring introduced through synthesis, which generates a library of scaffolds that can be characterized through structure-function studies, (d) resistance to proteolytic degradation, (e) amenable to functionalization with a fluorophore that would enable to tracking interactions with target cell and (f) high therapeutic index achieved through judicious choice of functional groups in the amphiphile.

The central theme of the present investigation is to explore rationally designed synthetic amphiphile as a bactericidal agent. In the following sections, a brief review on the essential features of synthetic amphiphiles, their bactericidal activity, factors contributing to their cytotoxicity and the adjuvant potential of amphiphiles in combination therapy with antibiotics is presented.

1.6. Essential Features of Synthetic Amphiphiles

Synthetic amphiphiles essentially consist of a hydrophilic/polar head group e.g. phosphates, heterocyclic aromatic/non-aromatic rings, amines, hydroxyl or acidic groups and a hydrophobic moiety, which is generally a hydrocarbon chain. Based on the nature of the charge on the head group, amphiphiles can be classified as cationic, anionic, zwitterionic or nonionic (Ramanathan et al. 2013). On the basis of the number and type of connection of polar head(s)/hydrophobic tail(s), amphiphiles can be categorized as: single head/single tail amphiphiles, bolaamphiphiles having two hydrophilic heads, gemini amphiphiles consisting of two hydrocarbon tails and two ionic groups linked by a spacer, a double or triple chain amphiphiles and catanionic amphiphiles, which encompasses oppositely charged surfactants (Sorrenti et al. 2013). Apart from the conventional

amphiphiles, supra-amphiphiles, which are essentially based on noncovalent interactions have come to the forefront (Kang et al. 2014).

1.7. Bactericidal Synthetic Amphiphiles

Membrane-targeting synthetic amphiphile are promising therapeutic agents against antibiotic-resistant pathogenic bacteria (Findlay et al. 2010; Gokel and Negin 2012; Jennings et al. 2014). A large number of reports have highlighted the structure-activity correlation of synthetic amphiphiles. For instance, aminoglycoside antibiotics-derived amphiphiles were generated based on neomycin B, kanamycin A, amikacin, and neamine with polycarbamates and polyethers, wherein neomycin B-derived heptaphenyl carbamate displayed superior activity against MRSA as compared to native neomycin B (Bera et al. 2010). In case of quinoline-based synthetic amphiphiles, the antimicrobial activity had been shown to be governed by cationic charge and increasing alkyl chain length (Vudumula et al. 2012). Amongst a group of low molecular weight random methacrylamide copolymers, it was demonstrated that the bactericidal activity was boosted manifold as the length of the alkyl side chain was increased (Palermo et al. 2009). In another structure-activity study, it was demonstrated that the antibacterial activity of cationic amphiphilic polymethacrylate derivatives can be influenced by charge, hydrophobicity and molecular weight (Kuroda and DeGrado 2005). Multiple cationic head groups and the structure of the head group have also been shown to influence the antibacterial activity of synthetic amphiphiles (Haldar et al. 2005; Mitra et al. 2009). In another study, modulation of bactericidal activity by chain length and relative positioning of the head groups on the aromatic core has been described (LaDow et al. 2011).

Literature reports have indicated that an increase in hydrophobicity of the amphiphile may lead to cytotoxic effect (Goswami et al., 2013). Hence a judicious balance between hydrophilic and hydrophobic moieties is recommended for amphiphiles meant for therapeutic applications (Brahmachari et al. 2010; Hoque et al., 2012). In case of low molecular weight random methacrylamide copolymers, the alkyl chain length and mole fraction of alkyl chain could effect haemolysis and membrane-directed activity (Palermo et al. 2009). For hydrocarbon polymers having cationic and hydrophobic groups, the balance of spacer distance, hydrophobicity, and charge was critical to attain higher

biocompatibility and membrane-targeting antimicrobial activity (Song et al. 2011). In another study, it has been demonstrated that pyridinium-based amphiphiles can be explored to form complexes with metals such as zinc. The high affinity of the metal-amphiphile complex towards anionic metal reactive groups (MRGs) present in bacterial cell surface can then be leveraged for high antibacterial selectivity of the molecule (Goswami et al. 2015). Based on available literature reports, a representative information on bactericidal synthetic amphiphiles is shown in Table 1.2.

Table 1.2. Overview of bactericidal synthetic amphiphiles.

Sl. No.	Amphiphile	Bactericidal Spectrum	MIC Range	Cytotoxic Potential	Reference
1.	Triple-headed, double-tailed amphiphiles	*S. aureus, E. coli P. aeruginosa*	1.0-16 µM	Not determined	Marafino et al. 2015
2.	Polyamine derived amphiphiles	*S.aureus, E. faecalis, E. coli, P. aeruginosa*	0.5-125 µM	Not determined	Paniak et al. 2014
3.	Quinoline-based amphiphiles	*S. aureus*, *E. coli*	5.0-20 µM	Non cytotoxic	Vudumula et al. 2012
4.	Cationic dimeric amphiphiles	*E. coli, S. aureus*	10-13 µM	Non-toxic	Hoque et al. 2012
5.	Bicephalic amphiphile	*S. aureus*, *E. coli*	4.0-31 µM	Not determined	LaDow et al. 2011
6.	Hydrogelating amphiphiles	*B. subtilis, S. aureus, E. coli*	1.0-12.5 µg/mL	Cytotoxic above 20 µg/mL	Dutta et al. 2011
7.	Methacrylate amphiphile	*S. mutans*	1.0-25 µg/ml	Not determined	He et al. 2011
8.	Random and uniform side chain polymers	*P. aeruginosa, E. coli, B. cereus, S. aureus*	8.0- 256 µg/ml	Hemolytic	Song et al. 2011

Sl. No.	Amphiphile	Bactericidal Spectrum	MIC Range	Cytotoxic Potential	Reference
9.	Amphiphilic Neamine derivatives	*S. aureus, P. aeruginosa E. coli*	4.0-32 µg/ml	Not determined	Baussanne et al. 2010
10.	Aminoglycoside antibiotic-derived amphiphiles	*S. aureus, E. faecalis, E. coli*	0.25 µg/ml - 1.0 µg/ml	Not determined	Bera et al. 2010
11.	Dipeptide-based cationic amphiphiles	*B. subtilis, S. aureus, E. coli, P. aeruginosa*	0.1-150 µg/mL	Cytotoxic at higher concentration	Mitra et al. 2009
12.	Random methacrylamide copolymers	*E. coli, S. aureus*	14 µM -340 µM	HC_{50} = 5.0-100	Palermo et al. 2009
13.	Anionic amphiphilic dendrimers	*B. subtilis*	EC_{50} = 40-60 µM	EC_{50} =130-1500 µM	Meyers et al. 2008
14.	Random and sequence-specific copolymers	*E. coli, B.subtilis, S. aureus*	3-25 µg/mL	Hemolytic (MHC=100 µg/mL)	Mowery et al. 2007
15.	Antimicrobial oligomers	*E. coli*, *B. subtilis*, MRSA	0.8-100 µg/mL	Hemolytic (3.2-100 µg/ml)	Yang et al. 2007
16.	Homologous dendritic amphiphile	*Mycobacterium smegmatis*	0.35 µM	Not determined	Sugandhi et al. 2007
17.	Amphiphilic Polymethacrylate	*E. coli*	16 µM	HC_{50} < 1 µg/mL	Kuroda and DeGrado 2005
18.	Multiple pyridinium headgroup amphiphile	*E. coli, S. aureus, E. faecalis*	4.9-11.3 µM	Not determined	Haldar et al. 2005
19.	Synthetic hydraphile	*E. coli, B. subtilis,*	0.6-175 µM	Cytotoxic	Leevy et al. 2005
20.	Amphiphilic neomycin and neosamine derivatives	*S. aureus P. aeruginosa,*	0.5-8 µM	Majorly non-toxic	Zimmermann et al. 2016

Sl. No.	Amphiphile	Bactericidal Spectrum	MIC Range	Cytotoxic Potential	Reference
21.	Biscationic tartaric acid-based amphiphiles	*S. aureus, L. monocytogenes, E. coli, P. aeruginosa*	12.5-125 µM	Not determined	Faig et al. 2015
22.	Lysine norspermidine conjugates	*S. aureus, E. faecium, MRSA, VREF, β-lactam resistant K. pneumoniae*	1.2 -250 µM	HC_{50} 108-< 1000 µM	Konai and Halder 2015
23.	Quartenary ammonium compound-based amphiphile	MRSA and MSSA	1.2 -250 µM	$Lysis_{20}$ 2.0 -125 µM	Jennings et al. 2015
24.	Amphiphilic Helical Peptides	*E. coli, MRSA, Salmonella, L. monocytogenes, M. luteus, Bacillus, Shigella, P. fluorescens*	0.21-142.3 µM	Moderate Toxic	Ma et al. 2016
25.	Cationic multi-domain peptide amphiphiles	*S. aureus, S. epidermidis, E. coli, P. aeruginosa*	5.0 - >80 µM	Non toxic	Xu et al. 2015

1.8. Factors Influencing Cytotoxicity of Synthetic Amphiphiles

Literature reports have indicated that an increase in hydrophobicity of the amphiphile may lead to cytotoxic effect (Dymond and Attard 2008; Goswami et al., 2013). A rational balance between hydrophilic and hydrophobic moieties is thus recommended for amphiphiles meant for therapeutic applications (Brahmachari et al., 2010; Hoque et al., 2012). In case of anionic amphiphilic dendrimers, which can form supramolecular assemblies, a high bactericidal activity was recorded with minimal cytotoxic effect against mammalian cell lines (Meyers et al. 2008). In another study, it was observed that amino acid-based hydrogelating amphiphiles prepared with hydrophobic anionic counterions and

a nanocomposite formed by AgNP-amphiphile interaction could enhance the antimicrobial activity and biocompatibility (Dutta et al. 2011). In case of low molecular weight random methacrylamide copolymers, haemolysis and membrane-directed activity was effected by alkyl chain length and mole fraction of alkyl chain (Palermo et al., 2009). For hydrocarbon polymers having cationic and hydrophobic groups, the balance of spacer distance, hydrophobicity, and charge was emphasized to attain higher biocompatibility and membrane-targeting antimicrobial activity (Song et al., 2011). In case of polymeric amphiphiles it has been suggested that biocompatibility is governed by molecular weight, charge density, cationic nature, structure, sequence and conformational flexibility of the molecule (Fischer et al., 2003). In a structure-activity study, it was observed that the structure of the macromolecular amphiphilic copolymer, especially the presence of block copolymers is critical to impart selectivity against bacterial cells over human cells (Oda et al. 2011). It has also been demonstrated that metal binding amphiphiles such as pyridinium-based amphiphiles can be explored to form complexes with metals such as zinc, to form bactericidal agents which display reduced cytotoxicity. The high affinity for the metal-amphiphile complex towards anionic metal reactive groups (MRGs) present in bacterial cell surface leads to high antibacterial selectivity of the molecule (Goswami et al., 2015).

1.9. DNA Binding Molecules: Chemistry, Activity and Antimicrobial Potential

Drug-resistant pathogens are known to have plasmids that can harbor and disseminate antibiotic-resistance traits through gene transfer mechanism. Hence, there is considerable interest in designing DNA binding and cleaving agents in order to target the genetic basis of antibiotic-resistance and disarm the resistance mechanism. The DNA binding ability of a molecule is essentially based on the structure and polarity of the molecule. In general, cationic molecules tend to bind with DNA owing to the negative charge of DNA. The DNA binding molecules can be essentially categorized into two groups: (a) intercalators and (b) groove binders. Many aromatic molecules are known to bind to DNA through intercalation. Common examples of such molecules are pyrene, quinoline and anthracene derivatives, ethidium bromide, propidium iodide, acridine orange and others. Some poly amides are known to be minor groove binders. For instance, Hoechst dye can bind with

DNA through minor grooves, which results in an enhancement of the fluorescence of the dye. A planar structure of the molecules generally facilitates intercalation with DNA and this interaction can be tracked by spectroscopy. In one such study, pyrene based fluorophores were used, which could discriminate single stranded DNA (ssDNA) and double stranded DNA (dsDNA) based on the change in fluorescence upon binding with the DNA molecule (Okamoto et al. 2005). In another study, spectroscopic analysis indicated that synthetic copper complexes exhibited a $\pi \rightarrow \pi^*$ interaction with DNA and that these compounds were toxic to human skin cancer cells (Raja et al. 2011). In another study, DNA sequence specific binders were developed which can inhibit topoisomerase IB activity (Vekhoff et al. 2011). Structure function studies on heterocyclic carboxamide with various substituents were shown to bind with DNA minor groove and display bactericidal and fungicidal activity (Burli et al. 2002). Some of the DNA binding polyamides have shown specific DNA binding and antifungal activity (Marini et al. 2003). Many compounds, which bear cationic charge have shown DNA binding activity including certain antibiotics. But the DNA cleavage activity was dependent on many criteria and it follows various mechanisms. In general, the DNA cleavage activity follows either a hydrolytic or oxidative cleavage pathway. Copper (II) complexes of the pyridine-pyrazole-containing ligands have been shown to cleave the φX174 DNA and the cleavage was found to be oxidative (Maheswari et al. 2007). In another study the dipeptide compounds having thiazole orange was conjugated with either tyrosin or tryptophan or glycine. The compounds with aromatic amino acids showed DNA cleavage but with glycine it failed to show any DNA cleavage activity. The DNA cleavage was found to be oxidative (Mahon et al. 2003). Further the binuclear iron complexes with N,N-bis (2-pyridylmethyl)-N-bis(2-pyridyl)methylamine were shown to render cleavage of DNA by oxidative mechanism (van den Berg et al. 2007). N,N-bis (2-pyridylmethyl) methylamine based Zn complex were also shown to render hydrolytic double strand DNA cleavage by Zn metal center (Qian et al. 2011). Additional studies have also highlighted the DNA intercalation and DNA cleavage activity of metal complexes (Ramakrishnan et al. 2011; Kawade et al. 2011).

Cationic amphiphiles have been reported to bind strongly with DNA and hence have been used as transfection agents. (Banerjee et al.1999). Conceivably, cationic

amphiphiles can bind to DNA through electrostatic interaction and the hydrophobic part of the molecule triggers compaction (Banerjee et al. 1999, Izumrudov et al. 2002). Amongst antibiotics, neomycin is an aminoglycoside antibiotic that has high propensity to bind with DNA. Neomycin-pyrylene conjugate has been shown to bind with human telomeric DNA (Xue et al. 2011). Further neomycin-neomycin dimer has shown high affinity towards AT-rich DNA duplexes (Kumar et al. 2011). Distamycin is a prototype groove binder and various derivatives of distamycin have been reported as antimicrobials (Khalaf et al. 2004, Burli et al. 2002, Burli et al. 2004, Vooturi et al. 2009).

1.10. Combination Therapy

As the use of single antibiotics is becoming futile in combating the challenge of drug-resistant strains, combination therapy is emerging as an attractive option. Combination therapy is likely to enhance the bactericidal efficacy, restore susceptibility of the target cells, render synergism between drugs and hinder the emergence of resistance during therapy leading to better clinical outcome (Fischbach 2011; Worthington and Melander 2013; Ejim et al. 2011; Thangamani et al. 2016). AMPs have been shown to synergistically enhance the activity of conventional antibiotics (Yeaman and Yount 2003, Marr et al. 2006). Antimicrobial polymers such as the muco-adhesive amphiphilic polymer pDMAEMA has been shown to disrupt the outer membrane of the Gram-negative bacteria and potentiate the activity of erythromycin (Rawlinson et al. 2010). Studies have revealed that synthetic crown ether-based pore forming hydraphiles could pre-dispose microbes towards the action of antibiotics such as erythromycin, kanamycin, rifampicin, and tetracycline (Atkins et al. 2010). Several cationic-membrane permeabilizing agents including amphiphilic molecules have been shown to synergistically enhance the bactericidal activity of conventional antibiotics like erythromycin (Naghmouchi et al. 2010; Matsuzaki et al. 1998; Westerhoff et al. 1995; Yeaman and Yount 2003; Saha et al. 2008; Goswami et al. 2013; Uday et al. 2014). Based on literature reports, additional representative examples of combination therapy are collated in Table 1.3.

Table 1.3. Representative examples of combination therapy used against pathogenic bacteria.

Sl. No.	Combinations	Target Bacteria	Nature of Interaction	Reference
1.	20-hydroxyecdysone with ampicillin and gentamicin	MRSA	Mostly synergy	Sook et al. 2009
2.	Pentadecenyl Tetrazole and gentamicin	MRSA biofilm	Synergy	Olson et al. 2011
3.	Minocycline with non-antibiotics (benserazide and loperamide)	*S. aureus, E. coli, P. aeruginosa, Salmonella infection model*	Synergy	Ejim et al. 2011
4.	Auranofin with polymixin B nonapeptide	*P. aeruginosa, E. coli, K. pneumoniae, S. typhimurium, A. baumannii*	Additive	Thangamani et al. 2015
5.	Glycolipids with β-lactams	MRSA	Synergy	Hu et al. 2015
6.	Ceftobiprole and daptomycin	*S. aureus*	Synergy	Barber et al. 2014
7.	Tricyclic indoline and β-lactam	MRSA	Synergy	Podoll et al. 2013
8.	Gentamicin and piperine	MRSA	Synergy	Khameneh et al. 2014

1.11. Bacterial Biofilms

In the present study, the prospect of a dual-target synthetic amphiphile as an antibiofilm agent was also investigated. Hence, in the following section, an overview of the salient features of biofilm, infections caused by biofilms and therapeutic challenges in the elimination of biofilm are highlighted.

1.11.1. Essential Features of Biofilm

Bacterial biofilms consist of surface-adherent cells enveloped in a self-secreted extracellular polymeric substance (EPS) or matrix, which is critical for the attachment process (Archer et al. 2011; Flemming and Wingender 2010; Kostakioti et al. 2013). The structural components of the biofilm matrix include cells, water, enzymes, lipids (LPS, phospholipids surfactin, viscosin and emulsan), and other cellular metabolic products such as slimy exopolysaccharide and proteinaceous adhesins. In addition, extracellular DNA (eDNA) is a critical component of the biofilm matrix (Flemming and Wingender, 2010). The presence of eDNA is considered to render structural stability to biofilm matrix and supports cell-to-cell and cell-surface interactions (Allesen-Holm et al. 2006, Whitchurch et al. 2002). Biofilm formation is a lifestyle adaptation in microorganisms in order to tide over unfavorable or harsh conditions such as shortage of nutrition, exposure to antibiotics, host-directed immune response and desiccation (Bordi and de Bentzmann 2011; Hall-Stoodley et al. 2004). *In vitro* experimental models have deciphered the typical stages in the formation of biofilm as follows: (a) initially, a reversible interaction of planktonic cells with a substratum sets off, governed by hydrophobic, van der Waals and electrostatic interactions followed by adhesion promoted by proteinaceous ligands (Arciola et al. 2012; Danhorn and Fuqua 2007), (b) in the second step, Microbial Surface Components Recognizing Adhesive Matrix Molecules (MSCRAMMs) play a critical role leading to formation of micro-colony (Speziale et al. 2009; (Parsek and Tolker-Nielsen 2008), (c) In the next stage, the micro-colony mature and cell-cell communication is established (Bordi and de Bentzmann 2011), (d) in the final step, cell dispersion leads to release of the planktonic cells, which can then initiate invasion and colonization of a new substratum (Molin and Tolker-Nielsen 2003; Kaplan et al. 2004; Otto 2008).

1.11.2. Biofilm-associated Ailments and Challenges in Anti-biofilm Therapy

Bacterial strains, which are commonly implicated in forming biofilms are *S. aureus*, *S. epidermidis*, *P. aeruginosa*, *E. faecalis*, *S. viridans, E. coli, K. pneumoniae* and *P. mirabilis* (Donlan 2001). Chronic and occasionally life-threatening ailments are caused by biofilms formed either on implants or in host-tissues. A large number of implant-related infections are caused by staphylococci and enterococci species (Arciola et al. 2012;

Hetrick and Schoenfisch 2006; Noimark et al. 2009; Otto 2008). Biofilm-forming *S. aureus* and *S. epidermidis* have also been detected in cardiovascular devices (Otto 2008, 2009). *S. aureus* and *P. aeruginosa* have been implicated in formation of biofilms on the surface of Foley's urinary catheter and can thus cause urinary tract infections (Muder et al. 2006, Singh et al. 2012). Biofilm-forming pathogenic bacteria are also known as causative agents of respiratory infections (Govan and Deretic 1996; Koch and Hoiby 1993).

Biofilms are highly resistance to therapeutic antibiotics (Burton et al. 2006; Hogan and Kolter 2002; Kostakioti et al. 2013). The clinical implications of biofilm is profound as approximately 80% of all microbial infections are caused by biofilms, which leads to a huge healthcare burden (Chambers and Deleo 2009; Stone 2009). The extracellular matrix can act as a barrier for diffusion of antibiotics and there are reports that highlight the role of biofilm matrix in developing resistance towards antibiotics (Tseng et al. 2013; Stewart and Costerton 2001; Singh et al. 2010; Bordi and de Bentzmann, 2011; Flemming and Wingender, 2010; Kostakioti et al. 2013). Literature reports also indicate that persister cells in the core of the biofilm display an inherent resistance towards antibiotics, which target metabolically active cells (Lewis 2008; Stewart and Costerton 2001). Biofilm extracellular DNA (eDNA) can sequester cationic aminoglycosides such as tobramycin and reduce their efficacy (Purdy Drew et al. 2009). In addition, high levels of metal ions and low pH associated with the biofilm matrix can also inactivate antibiotics (Jones et al. 2001; Kostakioti et al. 2013). It has also been suggested that the drug-resistance trait can be acquired through horizontal gene transfer of resistance determinants in biofilm (Madsen et al. 2012). A cartoon depicting the major challenges in anti-biofilm therapy is indicated in Figure 1.3.

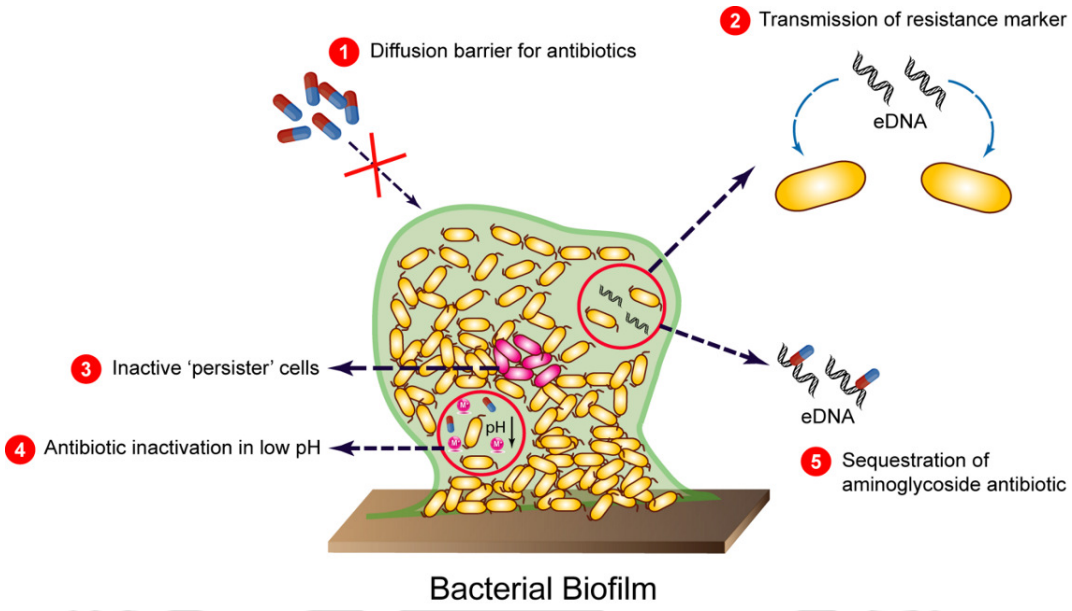

Figure 1.3. Challenges encountered in anti-biofilm therapy.

1.12. Methicillin- Resistant Staphylococcus aureus (MRSA)

In the present investigation, the potential of the generated amphiphile as a bactericidal agent against a clinical strain of MRSA was also tested. Hence in the following section, a brief overview on the antibiotic-resistance and the problems and pointers in anti-MRSA therapy is discussed.

MRSA is considered to be a serious threat, as it is not only prevalent in hospital-acquired infections, but is also implicated in community-acquired infections (Deresinki 2005; Stryjewski and Corey 2014). MRSA has evolved as multi-drug resistant strain and with therapeutic antibiotics becoming ineffective in eliminating clinical strains of MRSA, the challenge in the mitigation of MRSA is overwhelming. For instance, MRSA strains resistant to a critical therapeutic antibiotic such as vancomycin have been reported (Deresinski 2009; Rehm and Tice 2010), thus limiting the scope of the antibiotic. Similarly, MRSA strains, which are resistant to daptomycin have also been reported (Hayden et al. 2005; Marty et al. 2006). Clearly, there is a critical need to develop alternative and effective therapeutic approaches to counter the menace of MRSA infections.

In the context of multi-drug resistance in MRSA, efflux pump activity has been shown to be centrally involved (Li and Nikaido 2009; Poole 2005; Jang 2016). Several review articles and research papers have highlighted that a gamut of efflux pumps in MRSA can contribute to resistance against biocides and therapeutic antibiotics (Kaatz et al. 1993; Floyd et al. 2010; Kaatz et al. 2005). Thus, given the established role of drug efflux in imparting resistance to MRSA, targeting the efflux pump is thought to be a feasible therapeutic avenue.

MOTIVATION AND OBJECTIVES OF THE PRESENT INVESTIGATION

MOTIVATION AND OBJECTIVES OF THE PRESENT INVESTIGATION

The growing menace of drug-resistant pathogenic bacteria is a global problem in modern healthcare and to combat this daunting challenge, discovery of efficient bactericidal scaffolds that can act on irrefutable targets and defy the resistance mechanism is critical. Based on the fundamental understanding that a membrane-targeting bactericidal agent can offer considerable therapeutic leverage, there is an enormous scope to generate novel and rationally designed synthetic membrane-acting amphiphiles as next generation antibacterial agents. The present research investigation is essentially based on the following motivating factors:

(1) In an age of unrestrained antibiotic-resistance fraught with a dwindling drug armory to combat life-threatening infections, a rational target selection in a drug discovery program is pivotal. The bacterial membrane is conceived as an Achilles heel, given its significant physiological role and thus membrane-targeting antibacterials are perceived to likely thwart resistance development.

(2) Synthetic amphiphiles, which can mimic membrane-acting antimicrobial peptides (AMPs) are viable antibacterials owing to their facile synthesis, the potential to generate a library of bactericidal scaffolds through rational structural design and their resistance to proteolysis.

(3) The activity of synthetic amphiphiles can be manipulated through a rational tweaking of their structures. In particular, amphiphiles that can be tailored to cleave cellular DNA, in addition to their intrinsic membrane-targeting activity are envisaged to render therapeutic leverage, given that cellular plasmid DNA is often implicated in harboring and dissemination of resistance traits in pathogenic bacteria.

(4) A cationic head group in synthetic amphiphile holds the key to set-off strong interactions with anionic bacterial cells. However, it is imperative that the head group is biocompatible in order to curb unwarranted host cell toxicity. Further, tethering a fluorescent group to a synthetic bactericidal amphiphile can provide a sensing handle for

probing interactions with cell or macromolecules and be exploited as an imaging tool in *in vitro* and *in vivo* infection models.

(5) The devastating infections associated with *Staphylococcus aureus* biofilm calls for a novel paradigm in antibiofilm therapeutics. Given that the *S. aureus* biofilm extracellular DNA (eDNA) largely underpins its defiance against therapeutic interventions, a DNA and membrane-targeting amphiphile can perhaps reap dividends by breaching the eDNA scaffold and mounting a concurrent attack on underlying cells. To this end, development of a biocompatible nanocarrier that can render a biofilm matrix-responsive release of the dual-target amphiphile would render significant therapeutic benefit.

(6) The profound healthcare burden imposed by methicillin-resistant *S. aureus* (MRSA) biofilm demands new drugs or alternative effective therapies. The use of a bactericidal amphiphile as an adjuvant in order to restore antibiotic sensitivity, reduce the minimum effective dose and toxicity of therapeutic antibiotics is a particularly appealing approach against MRSA. Such a combinatorial regime, wherein the amphiphile can be used to counter the core resistance mechanism and render synergistic elimination of MRSA with antibiotics is likely to result in effective mitigation of MRSA in the clinical setting.

In the light of the enormous scope of exploring synthetic amphiphiles as potential antibacterial therapeutics, the essential objectives of the Ph.D. thesis encompassed the following:

1. Evaluation of the bactericidal spectrum, membrane-directed activity and *in vitro* cytotoxic effect of a rationally designed pyridinium-based dual-target synthetic amphiphile referred as compound 1 (C1).

2. Determination of the DNA binding activity and DNA cleavage activity of C1.

3. Evaluation of the bactericidal activity of C1 in physiologically relevant fluids and the prospect of C1 as an adjuvant to potentiate the activity of antibiotics against target bacteria.

4. Evaluation of biofilm extracellular DNA (eDNA)-targeting activity of C1 and eradication of *Staphylococcus aureus* by C1-loaded human serum albumin (HSA)-based nanocarrier.

5. Evaluation of the potential of C1-loaded poly (lactic-co-glycolic acid) (PLGA)-based nanocarrier in potentiating antibiotic-mediated eradication of biofilm formed by a clinical strain of methicillin-resistant *Staphylococcus aureus* (MRSA).

Chapter 2

Bactericidal Spectrum and Membrane-directed Activity of C1

This chapter essentially describes the bactericidal potential of a rationally designed dual-target amphiphile C1. Fluorescence-based studies could establish the membrane-targeting activity of the bactericidal amphiphile.

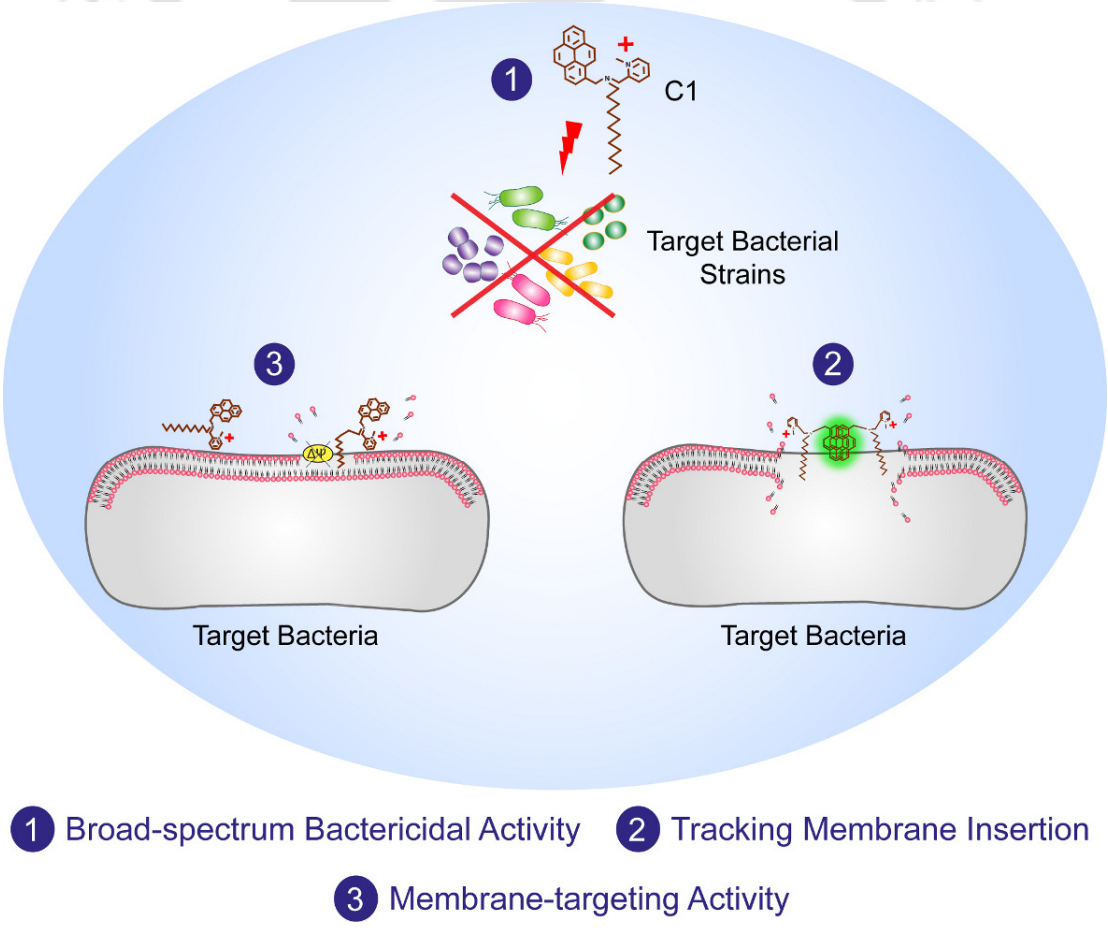

ABSTRACT

In this chapter, the bactericidal activity of a pyridinium-based synthetic amphiphile referred to as compound 1 (C1) is described. The dual-target amphiphile C1 was synthesized through incorporation of (i) a cationic pyridinium head group to initiate electrostatic interactions with anionic bacterial cells and DNA, (ii) a hydrophobic tail (12 carbon chain length) for membrane insertion and (iii) a fluorogenic pyrene group to facilitate intercalation with DNA and spectroscopic probing of interactions. Antibacterial screening experiments indicated that C1 exhibited broad-spectrum bactericidal activity and was more potent against Gram-positive bacteria as compared to Gram-negative counterparts. The presence of a fluorogenic pyrene in C1 enabled probing of amphiphile-bacteria interactions and membrane-insertion, as evidenced in the reduction of the pyrene monomer emission at 340 nm and a concomitant emergence of a broad red-shifted emission at around 480 nm. Interestingly, fluorescence microscope analysis indicated that C1-treated bacterial cells exhibited strong fluorescence in a wide range of excitation, reiterating the merit of the fluorogenic amphiphile in probing interactions with bacterial cells. The membrane-directed activity of C1 was captured in a cFDA-SE leakage assay as well as PI uptake assay, which suggested a dose-dependent bactericidal activity. The amphiphile C1 could also induce collapse of the transmembrane potential (Ψ) in target bacterial cells. Interestingly, an *in vitro* study revealed that the target bacteria *S. aureus* MTCC 96 failed to develop resistance against the amphiphile C1. Cytotoxicity assays indicated that the amphiphile C1 was non-toxic to cultured human cells (HEK 293 cells) even at concentrations higher than the MIC of the amphiphile against the target bacteria *S. aureus* MTCC 96.

2.1. Introduction

The prevalence of drug-resistant pathogenic bacteria in conjunction with a diminishing antibiotic armory has spurred the need for a radical approach in the discovery of antibacterials. Drug-resistant pathogenic bacteria are armed with a plethora of inherent attributes, which empower them to either evade or thwart the action of common therapeutic antibiotics (Nikaido 2009; Fischbach and Walsh 2009; Gootz 2010; Morar and Wright 2010). In order to assuage this crisis, it is paramount to develop new bactericidal agents that act on compelling targets. The bacterial membrane can be conceived as a viable target, given its fundamental physiological role in the survival of bacteria. Membrane-targeting antibacterials are thus perceived to be effective therapeutic agents as they are likely to contravene resistance development (Hurdle et al. 2011; Van Bambeke et al. 2008; Adhikari et al. 2013; Goswami et al. 2015). Amongst various membrane-acting bactericidal agents, antimicrobial peptides (AMPs) hold special interest. The cationic and amphiphilic nature of AMPs enable them to interact and insert in the negatively charged bacterial cell membrane through electrostatic and hydrophobic interactions resulting in membrane damage (Zasloff 2002; Wimley 2010; Brogden 2005). A number of models that describe AMP-triggered pore formation and cell death, host-directed toxicity and synergistic action with therapeutic antibiotics have been reported (Brogden 2005; Hancock 1999; Ulvatne et al. 2001). Although AMPs are potent bactericidal agents, their large scale therapeutic application is hindered owing to their high cost of production, inferior pharmacokinetics, susceptibility to proteolytic inactivation and also perhaps due to a knowledge gap in acquiring a nuanced understanding on the mechanism of action and therapeutic implications of AMPs (Marr et al. 2006; Wimley and Hristova 2011).

Given the limitations of using AMPs as bactericidal agents, AMP-mimicking synthetic amphiphiles have emerged as promising antibacterials owing to their ease in synthesis and the possibility to generate a plethora of membrane-targeting bactericidal molecules based on rational structural design (Findlay et al. 2010; Gokel and Negin 2012). There are reports on synthetic cationic peptide- and polymer-based amphiphiles as potent antimicrobial agents (Palermo et al. 2009; Kuroda and DeGrado 2005; Haldar et al. 2005). Cationic quinoline-based amphiphiles and amphiphilic neamine derivatives have been shown to display broad-spectrum bactericidal activity (Vudumula et al. 2012; Baussanne et

al. 2010). Further, the potential of amphiphilic hydrogelators and structurally diverse cationic amphiphiles with multiple head groups as therapeutic antibacterial agents has also been highlighted in previous studies (Song et al. 2011; Debnath et al. 2010; LaDow et al. 2011; Goswami et al. 2013). With regard to the mechanism of action on bacterial cells, it is now well established that the cationic nature of the synthetic amphiphile enables initial electrostatic interaction with the negatively charged bacterial cell surface, while the hydrophobic tail renders insertion into the core of the membrane, which results in membrane disruption culminating in cell death (Findlay et al. 2010; Vudumula et al. 2012; Song et al. 2011; Goswami et al. 2013).

In the context of developing potent bactericidal agents that can act on compelling cellular targets, deployment of dual-target bactericidal agents that act on distinct and irrefutable targets is conceived as a viable and effective therapeutic approach against drug-resistant pathogens, as compared to a single-target pharmacophore (Silver 2011; O'Connell et al. 2013). In this context, antibacterials that target cellular DNA in addition to displaying a membrane-directed activity could bear significant therapeutic prospect, given that drug-resistant pathogenic bacteria acquire genes encoding for resistance and that cellular plasmid DNA is often involved in harboring and dissemination of such resistance traits (Nikaido 2009; Davies and Davies, 2010). In line with this rationale, the present chapter describes the bactericidal activity of a dual-target pyridinium synthetic amphiphile referred to as compound 1 (C1). Mechanistic studies provide evidence for the membrane-directed bactericidal activity of the amphiphile on target bacteria. This chapter also describes the results pertaining to testing the cytotoxic potential of the amphiphile on human embryonic kidney cell line (HEK 293).

2.2. Materials and Methods

2.2.1. Growth Media and Chemicals

1-Pyrenecarboxaldehyde and 2- (Chloromethyl) pyridine hydrochloride were purchased from Sigma Aldrich (USA). Dodecylamine was purchased from Fluka (Sweden) and Iodomethane was purchased from Merck (Germany). 5 (and 6)-carboxyfluorescein diacetate succinimidyl ester (cFDA-SE), propidium iodide (PI), $DiSC_35$, valinomycin, Dulbecco's Modified Eagle Medium (DMEM), trypsin-EDTA and 3-(4,5-dimethyl-2-thiazolyl)-2,5-diphenyl-2H-tetrazolium bromide (MTT) were procured from Sigma-Aldrich (USA). Penicillin-Streptomycin solution, Nutrient Broth (NB), Brain-Heart Infusion (BHI) broth and Luria-Bertani (LB) broth were procured from HiMedia, Mumbai, India. Dimethyl sulfoxide (DMSO) was obtained from Merck, India. N-2-hydroxyethyl piperazine N-2 ethane sulphonic acid (HEPES buffer) was procured from Sisco Research Laboratories SRL, Mumbai, India. Fetal bovine serum (FBS) was procured from PAA Laboratories, USA.

2.2.2. Synthetic Amphiphiles

The general structure of the synthetic amphiphiles compound 1 (C1) and compound 2 (C2) used in the present study is shown in Figure. 2.1. Representative steps involved in the synthesis of C1 is illustrated in Figure. 2.2. Detailed information regarding synthesis and characterization of the amphiphiles is provided in the Appendix of Chapter 2. Stock solutions of the amphiphiles were prepared in DMSO and stored at room temperature in dark condition.

2.2.3. Bacterial Strains and Growth Conditions

The target bacterial strains consisted of *Staphylococcus aureus* MTCC 96 (*S. aureus*), *Listeria monocytogenes* Scott A (*L. monocytogenes*), *Bacillus subtilis* MTCC 441 (*B. subtilis*), *Micrococcus luteus* NCIM 2379 (*M. luteus*), *Escherichia coli* MTCC 433 (*E. coli*), *Enterobacter aerogenes* MTCC 2822 (*E. aerogenes*), *Pseudomonas aeruginosa* MTCC 2488 (*P. aeruginosa*) and *Yersinia enterocolitica* MTCC 859 (*Y. enterocolitica*).

B. subtilis MTCC 441, *E. coli* MTCC 433, *P. aeruginosa* MTCC 2488 and *E. aerogenes* MTCC 2822 were grown in NB medium at 37^{o}C and 180 rpm for 12 h whereas *S. aureus*

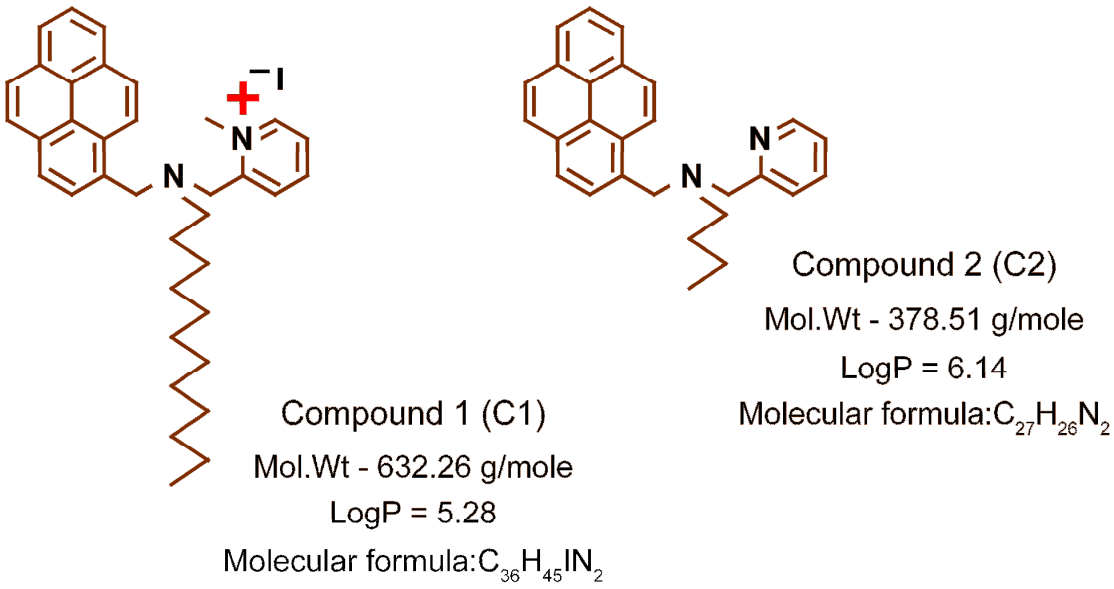

Figure 2.1. Structure of synthetic amphiphiles used in the present investigation. LogP values were determined using MarvinSketch (https://www.chemaxon.com/products/marvin/marvinsketch/)

.

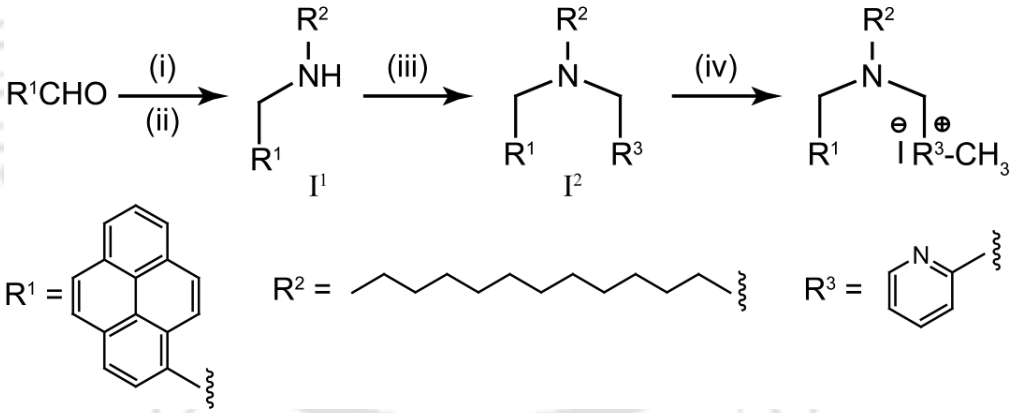

Figure 2.2. Schematic representation of general steps involved in the synthesis of compound 1 (C1). (i) Dodecylamine, MeOH, reflux, (ii) $NaBH_4$, MeOH, 0°C, (iii) R^3CH_2Cl /K_2CO_3/MeCN, reflux, 72 h, (iv) CH_3I, MeCN, 0°C.

MTCC 96, *L. monocytogenes* Scott A, *M. luteus* NCIM 2379 and *Y. enterocolitica* MTCC 859 were propagated in BHI broth at 37°C and 180 rpm for 12 h.

2.2.4. Antibacterial Spectrum of Synthetic Amphiphiles

The bactericidal activity of the amphiphiles was determined against a group of Gram-positive and Gram-negative bacteria. The target bacterial strains were grown in requisite growth media in presence of varying concentrations of either C1 or C2 (50 µg/mL and 100 µg/mL each) for 24 h. The growth of amphiphile-treated bacterial cells was determined by recording the absorbance at 600 nm from replica samples in a spectrophotometer (CARY 300 Bio, Varian) and was expressed as percentage growth compared to control (untreated cells).

2.2.5. Minimum Inhibitory Concentration (MIC) and Minimum Killing Concentration (MKC) of C1

MIC and MKC of C1 was ascertained against Gram-positive bacteria *L. monocytogenes* Scott A and *S. aureus* MTCC 96 and Gram-negative bacteria *E. coli* MTCC 433 and *E. aerogenes* MTCC 2822. The bacterial cultures were inoculated at 1% level in microtitre wells (approximately 5×10^5 CFU/well) having 100 µL of the specific growth medium and propagated overnight at 37°C and 180 rpm in presence of varying concentrations of C1. The growth of the bacterial strains was assessed by measuring absorbance at 600 nm in a microtitre plate reader (Infinite M200, TECAN, Switzerland). MIC of C1 was defined as the minimum amphiphile concentration that resulted in growth inhibition of the target bacteria (A_{600}<0.1). An aliquot (1% v/v) from all the wells that indicated a lack of cell growth (A_{600}<0.1) was re-inoculated into separate microtitre wells with fresh growth medium in the absence of amphiphile and incubated overnight at 37°C and 180 rpm. MKC of C1 was defined as the lowest amphiphile concentration that inhibited the growth of the target bacterial cells following re-inoculation (A_{600}<0.1). MIC and MKC values were determined from six independent experiments and expressed as average values. A schematic of the protocol used to determine MIC and MKC of C1 is indicated in Figure 2.3.

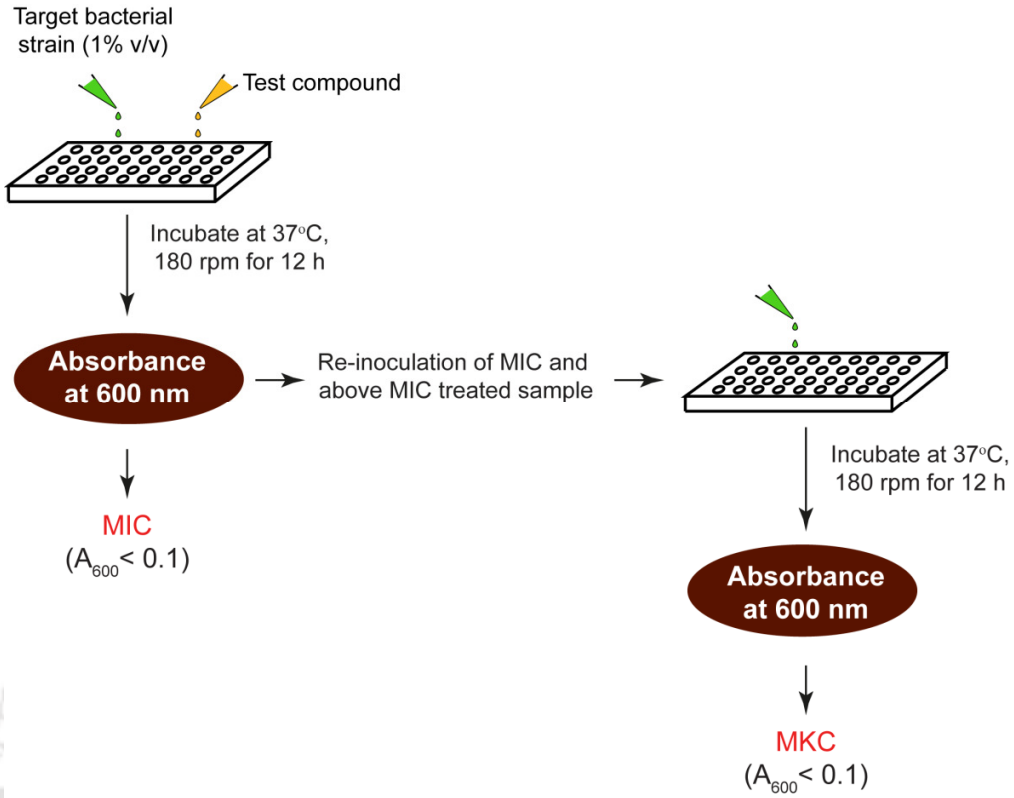

Figure 2.3. Schematic representation of the experimental protocol for determining MIC and MKC of amphiphile C1.

2.2.6. Fluorescence-based Tracking of C1-Bacteria Interaction

Cells of *S. aureus* MTCC 96 were suspended in sterile phosphate buffered saline (PBS) in separate sets (10^6 CFU/mL in each set) and incubated with various concentrations of C1 (1.5 µM, 3.0 µM, 4.5 µM and 6.0 µM) at 37°C for 3 h in a shaking incubator. Subsequently the cells were collected by centrifugation at 8000 rpm for 5 minutes. The cell pellet representing cell-bound C1 was resuspended in 1.0 mL sterile PBS and the supernatant representing unbound C1 was collected in a sterile tube. The fluorescence spectra of all the samples (C1 alone, cell-bound C1 and unbound C1) was recorded by exciting at 340 nm and measuring the emission from 360-600 nm.

For fluorescence microscope analysis, cells of *S. aureus* MTCC 96 were suspended in 1.0 mL sterile PBS (10^6 CFU/mL) and incubated with 4.5 µM of C1 at 37°C for 3 h in a shaking incubator. The cells were then separated by centrifugation at 8000 rpm for 5

minutes. The supernatant was discarded and the cell pellet was resuspended in PBS. An aliquot of the resuspended cells was then smeared on a clean glass slide, dried and observed under a fluorescence microscope (Eclipse Ti-U, Nikon, USA) in UV, blue, green and white light. Images of the cells under each excitation were recorded.

2.2.7. Bactericidal Potency of C1

The following experiments were performed to ascertain the antibacterial potency of C1:

2.2.7.1. Time- kill Curve

Target cells of *S. aureus* MTCC 96 and *E. coli* MTCC 433 (approximately 10^6 CFU/mL each, suspended in sterile PBS) were treated in separate sets with varying concentration of C1 (3.0 µM - 15 µM) at 37^{o}C and 180 rpm. Samples were withdrawn at regular intervals of 3 h, 6 h, 12 h and 24 h and subjected to serial dilution and plating to ascertain the viable cell number (Log_{10} CFU/mL). The viability of cells suspended in sterile PBS as well as cells treated with DMSO alone (solvent control) was also determined.

2.2.7.2 Field Emission Scanning Electron Microscope (FESEM) Analysis

Overnight grown cells of *S. aureus* MTCC 96 and *E. coli* MTCC 433 were collected by centrifugation, washed twice with sterile PBS and resuspended in the same. The cells were then treated with 40 µM C1 for 6 h at 37°C. Untreated cells were also incubated in sterile PBS under the same incubation conditions as control samples. Following 6 h incubation, untreated as well as treated cells were collected by centrifugation, washed with sterile PBS and sterile MilliQ water and finally suspended in sterile MilliQ water. A 10 µL aliquot of each sample was spotted on separate aluminium foil covered glass FESEM grid and air dried in the laminar hood. The samples were then mounted on a carbon tape covered metal grid and gold (Au) coating was done twice. Finally, the samples were analyzed in a field emission scanning electron microscope (Zeiss Sigma, USA) at 1.5-3.0 kV and their images were recorded.

2.2.8. Membrane-directed Activity of C1

The following experiments were performed to verify the membrane-targeting activity of C1:

2.2.8.1. cFDA-SE Leakage Assay

A stock solution of cFDA-SE (500 µM) was prepared in ethanol and stored at -20°C. Cells of *S. aureus* MTCC 96 and *E. coli* MTCC 433 were harvested from overnight grown cultures by centrifugation at 8000 rpm for 5 min. The cell pellet was washed twice with sterile PBS, resuspended in the same to achieve a cell concentration of 10^6 CFU/mL and labelled with cFDA-SE (final concentration of 50 µM) for 20 min at 37°C. The cells were then centrifuged, washed twice with sterile PBS to remove excess cFDA-SE and resuspended in 1.0 mL of sterile PBS. Varying concentrations of C1 (4.0 µM, 8.0 µM, 12 µM and 16 µM) was then added to separate sets of cFDA-SE labelled *S. aureus* MTCC 96 and *E. coli* MTCC 433 cells and incubated at 37°C and 180 rpm. As a control sample, only DMSO solution devoid of C1 (solvent control) was also added to cFDA-SE labelled cells and incubated under the same conditions. At intermittent periods of incubation (1 h, 2 h and 3 h), cells were harvested by centrifugation and leakage of carboxyfluorescein from the cells was determined by measuring fluorescence of the cell free supernatant at an excitation wavelength of 488 nm and emission wavelength of 518 nm in a spectrofluorimeter (FluoroMax-3, HORIBA). The fluorescence measurements were recorded after subtracting the fluorescence of effluxed dye from control samples. Fluorescence measurements were recorded from three independent experimental samples for every amphiphile concentration and control sample. A schematic of the protocol for cFDA-SE leakage assay is indicated in Figure 2.4A.

2.2.8.2. PI Uptake Assay

A stock solution of PI (1.5 mM) was prepared in sterile MilliQ water and stored at 4°C. Overnight grown cells of *S. aureus* MTCC 96 and *E. coli* MTCC 433 were harvested by centrifugation, washed twice with sterile PBS and resuspended in the same to achieve a cell concentration of 10^6 CFU/mL. In separate sets, the cells were then incubated with varying concentrations of C1 (4.0 µM, 8,0 µM, 12 µM and 16 µM) at 37°C and 180 rpm

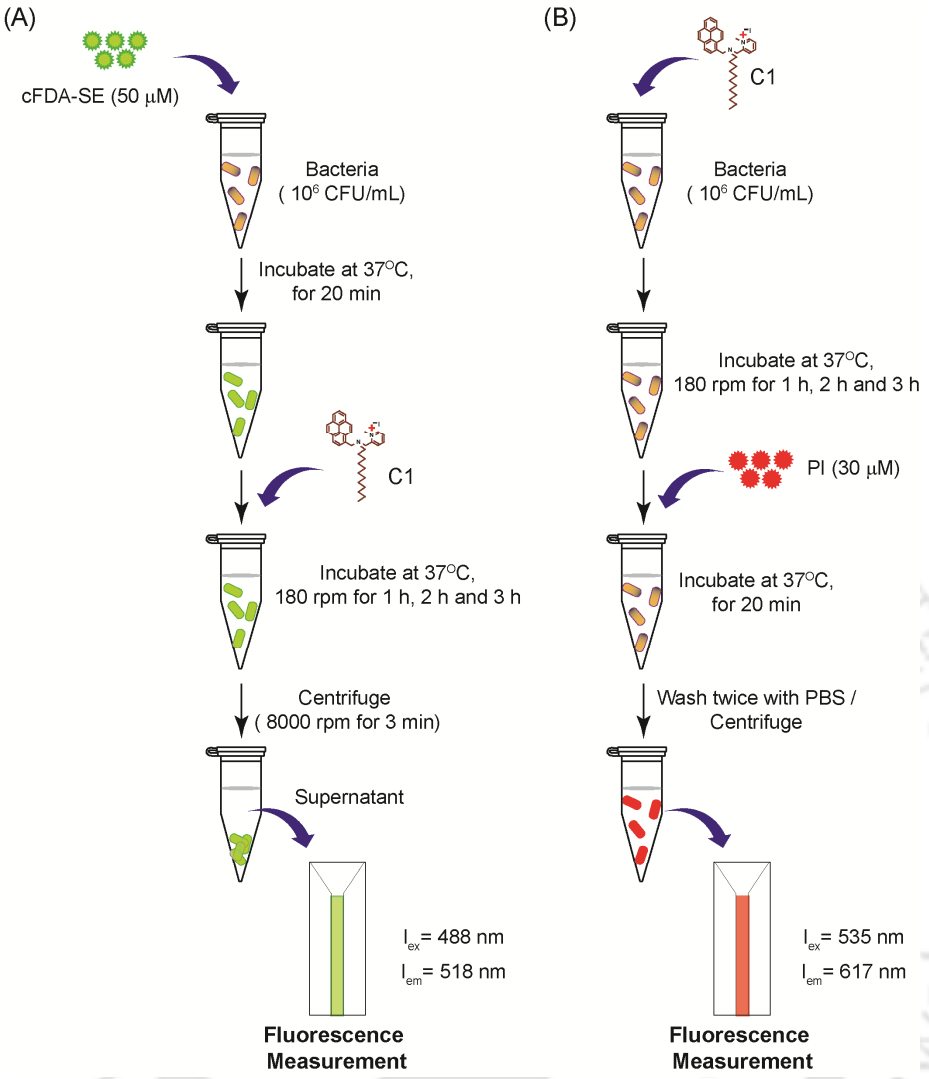

Figure 2.4. Schematic representation of the experimental protocol for (A) cFDA-SE leakage assay and (B) PI uptake assay.

for 1 h, 2 h and 3 h. In case of solvent control sample, only DMSO was added to the cells and incubated under the same conditions. Following incubation, cells from all the samples were washed with sterile PBS, resuspended in the same and incubated with PI (final concentration of 30 µM) for 30 min at 37°C in a circulating water bath incubator (Amersham, USA). Subsequently, the cells were centrifuged, washed with sterile PBS to remove excess dye and resuspended in the same. The fluorescence emission spectra of the samples was then measured in a spectrofluorimeter (FluoroMax-3, HORIBA) at an

excitation wavelength of 535 nm and emission wavelength of 617 nm. Fluorescence measurements were acquired from three independent experimental samples. A schematic of the protocol for PI uptake assay is indicated in Figure 2.4B.

2.2.8.3. Membrane Depolarization Assay

S. aureus MTCC 96 and *E. coli* MTCC 433 cells were grown till mid-logarithmic phase (A_{600} = 0.4-0.5), harvested by centrifugation, washed and resuspended in HEPES buffer (5.0 mM HEPES, 20 mM glucose, pH 7.2). The cell suspensions (A_{600} of 0.05) were then incubated with 0.4 µM $DiSC_35$ for 1 h at 37°C followed by the addition of KCl (final concentration of 100 mM) and further incubated for 15 min (Vooturi et al. 2009). The cell suspension was then placed in a quartz cuvette to which varying concentrations of C1 (4.0 µM, 8.0 µM, 12 µM and 16 µM) was added and the fluorescence emission spectra (λ_{Ex} = 622 nm and λ_{Em} = 670 nm) was recorded in short time intervals in a spectrofluorimeter (FluoroMax-3, HORIBA) with excitation and emission slit width set at 10 nm each. In a parallel set, cells treated with valinomycin (30 µM) were used as positive control. All fluorescence measurements were taken for three independent experimental samples.

2.2.9. In Vitro Resistance Studies

The *in vitro* resistance of *S. aureus* MTCC 96 against C1 was determined in a multistep experiment following a method described earlier (Locher et al. 2014). The concentrations of C1 used in these experiments corresponded to 2 × MIC - 16 × MIC against the target bacteria. Enumeration of *S. aureus* MTCC 96 colonies was accomplished on BHI-agar plates following an incubation period of 48 h at 37°C. For the samples treated with various MIC levels of C1, a viable colony appearing in the plate having the highest level of the amphiphile was selected and used to prepare the inoculum for the subsequent resistance selection step and this procedure was repeated for three independent steps. For every step a single colony from the sample treated with the highest concentration of C1 was isolated and purified by three passages in C1-free media and then the MIC of C1 was determined using a standard method as described in section 2.2.5. All experiments were performed in triplicates. Data analysis and calculation of standard deviation was performed with Microsoft Excel 2010 (Microsoft Corporation, USA). A schematic illustration of the

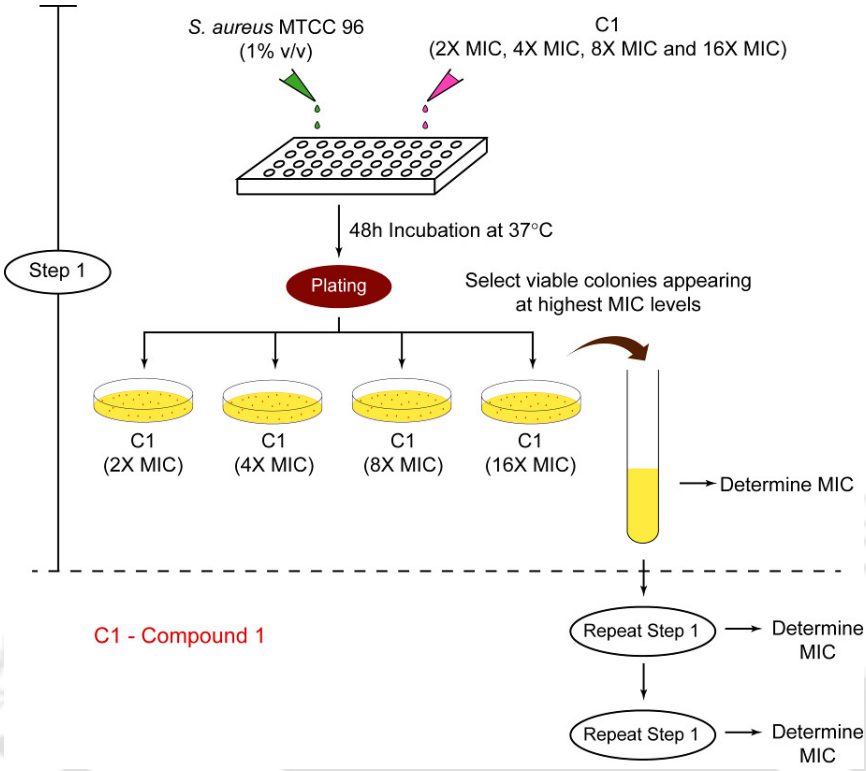

Figure 2.5. Schematic representation of the experimental protocol to study multistep *in vitro* resistance development in presence of C1.

experimental steps to determine *in vitro* resistance development against C1 is shown in Figure 2.5.

2.2.10. Cytotoxic Effect of C1 on Model Human Cell Line

The cytotoxic effect of C1 was assessed against cultured human embryonic kidney (HEK 293) cell line by a standard MTT-based assay following the manufacturer's instructions (Sigma-Aldrich, USA). HEK 293 cells were initially grown in a 25 cm^2 tissue culture flask in Dulbecco's Modified Eagle Medium (DMEM) supplemented with 10% (v/v) fetal bovine serum (FBS), penicillin (100 µg/mL) and streptomycin (100 µg/mL) at 37°C under a humidified atmosphere of 5% CO_2 in an incubator. The cells were subsequently seeded onto 96-well tissue culture plates at a density of 10^4 cells per well and incubated in separate sets with varying concentrations of C1 (6.0 µM, 12 µM, 24 µM) made in DMEM

for a period of 24 h. Control samples (cells treated with DMSO alone) were also included in parallel sets and incubated under the same conditions. Following incubation, the media was carefully aspirated and fresh DMEM medium containing MTT solution was added to the wells and the plates were incubated for 4 h at 37°C. Subsequently, the supernatant was aspirated and the insoluble formazan product was solubilized in DMSO and its absorbance was measured in a microtiter plate reader (Infinite M200, TECAN, Switzerland) at 550 nm. MTT assays were performed in three independent sets and every set consisted of six replicates. Data analysis and determination of standard deviation was performed with Microsoft Excel 2007 (Microsoft Corporation, USA). The absorbance obtained for solvent control samples (cells treated with DMSO alone) was considered to represent 100% cell viability, whereas the absorbance for C1-treated cells were compared to the solvent control cells to determine % cell viability.

2.3. Results and Discussion

2.3.1. Design Principle and Synthesis of Amphiphile

In the present investigation, the key motivation driving the design of the bactericidal synthetic amphiphile was the incorporation of dual features that would enable the amphiphile to act on indispensable targets such as the bacterial membrane and cellular DNA and thereby diminish the possibility of resistance development in pathogenic bacteria. To accomplish this goal, the amphiphilic compound 1 was synthesized through tethering of (i) a cationic pyridinium head group to initiate electrostatic interactions with both anionic bacterial cell surface and DNA, (ii) a hydrophobic tail (12 carbon chain length) to promote membrane insertion and (iii) a planar fluorogenic pyrene group to enable intercalation with DNA as well as spectroscopic tracking of interactions (Figure 2.6). Compound 1 was synthesized following a previously reported procedure (Kar et al. 2012) with an additional step of N-alkylation to the pyridine ring. For comparative studies, a control compound 2 (Figure 2.1), which was uncharged and having a short hydrophobic tail (four carbon chain length) was also synthesized.

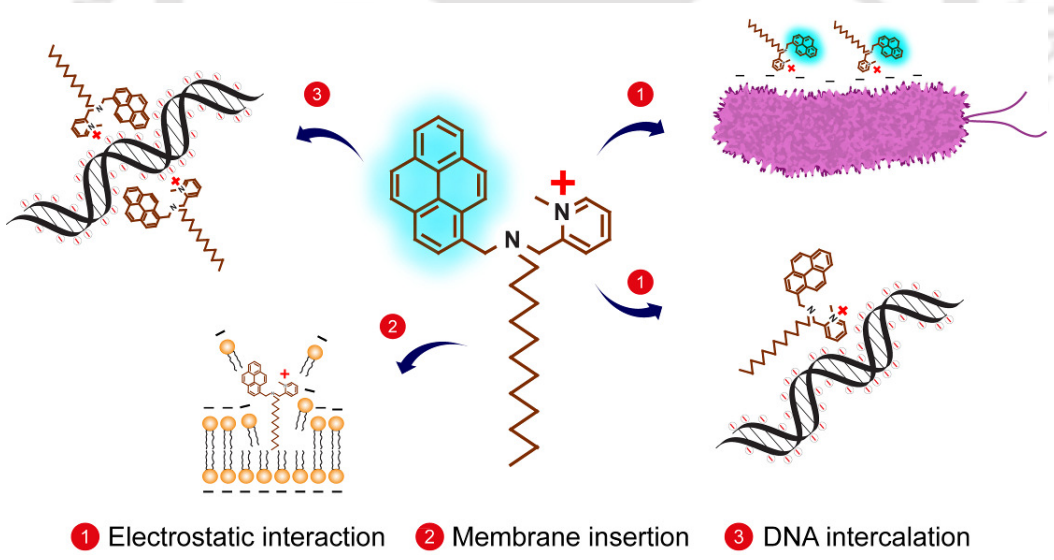

Figure 2.6. Design principle of compound 1**.**

2.3.2. Antibacterial Spectrum, MIC and MKC of C1

The antibacterial screening experiments revealed that at the tested concentrations, C1 displayed potent activity against a panel of Gram-positive and Gram-negative bacteria, except *Pseudomonas aeruginosa* MTCC 2488 (Figure 2.7A), which can perhaps be attributed to the inherent low permeability of its cell wall (Lambert 2002). On the contrary, C2 failed to display any antibacterial activity against the tested bacterial strains (Figure 2.7 B), reiterating the notion that a cationic charge and a long chain hydrophobic tail in a synthetic amphiphile are critical determinants of its antibacterial activity (Findlay et al. 2010; Vudumula et al. 2012; Goswami et al. 2013).

The MIC and MKC of C1 indicated that the amphiphile C1 displayed a higher bactericidal activity against Gram-positive bacteria like *S. aureus* MTCC 96 and *L. monocytogenes* Scott A, in contrast to the Gram-negative counterparts *E. coli* MTCC 433 and *E. aerogenes* MTCC 2822 (Table 2.1). This phenomenon perhaps originates from the presence of an outer membrane permeability barrier in Gram-negative bacteria (Bolla et al. 2011; Nikaido 2003). The potent activity of C1 against *S. aureus* MTCC 96 is encouraging as this strain is a putative MRSA strain (Vudumula et al. 2012).

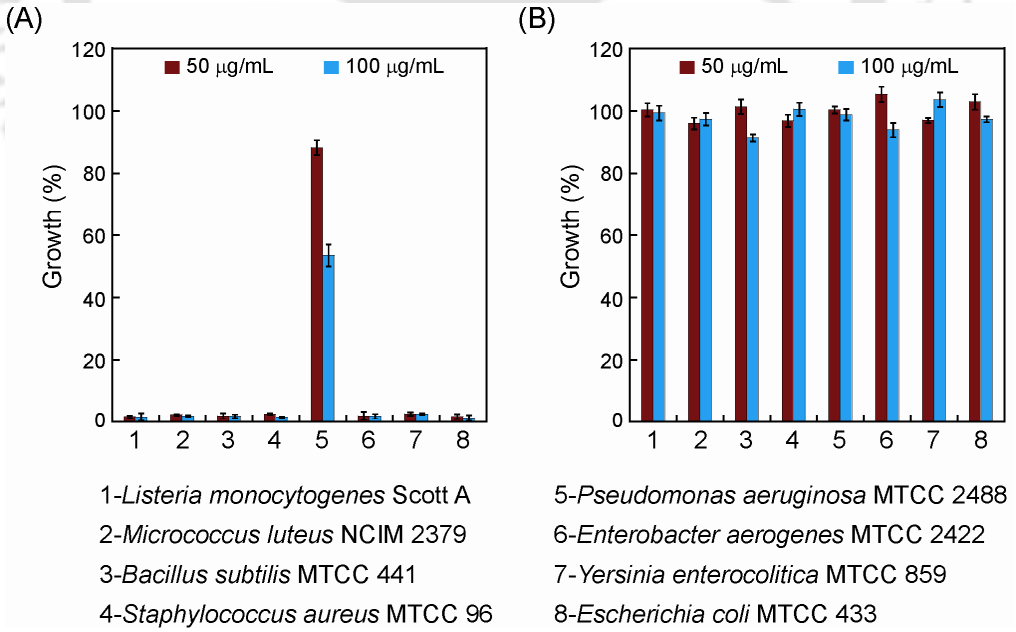

Figure 2.7. Antibacterial activity of (A) C1 and (B) C2 against target bacterial strains. The target bacteria were interacted with the amphiphiles for 24 h.

Table 2.1. MIC and MKC of C1 against target bacterial strains.

Synthetic Amphiphile	*S. aureus* MTCC 96		*L. monocytogenes* Scott A		*E .coli* MTCC 433		*E. aerogenes* MTCC 2822	
	MIC (µM/ µg/mL)	MKC (µM/ µg/mL)	MIC (µM/ µg/mL)	MKC (µM/ µg/mL)	MIC (µM/ µg/mL)	MKC (µM/ µg/mL)	MIC (µM/ µg/mL)	MKC (µM/ µg/mL)
C1	12 / 7.9	40 / 26.5	12 /7.9	40 / 26.5	32 / 21.2	48 / 31.8	40 / 26.5	64 / 42.4

2.3.3. Tracking Amphiphile-Bacteria Interaction

Apart from the cationic charge and the hydrophobic tail, which are characteristic features of a bactericidal amphiphile, an important design rationale for C1 was to incorporate a planar fluorogenic pyrene group, which can perhaps be exploited for spectroscopic probing of interactions with cellular entities. At an excitation wavelength of 340 nm, C1 exhibited fluorescence emission peaks at 376 nm and 395 nm (Figure 2.8A), which are the typical emission peaks of pyrene monomers (Winnik 1993). In case of cell-bound C1, a reduction in the monomer emission was accompanied by a simultaneous emergence of a broad red-shifted emission at around 480 nm (Figure 2.8A), which is characteristic of pyrene excimer formation (Winnik 1993; Xu et al. 2010). This phenomenon was also captured using varying concentrations of C1 (refer to Appendix, Figure A2.5). Upon interaction with bacterial cells, membrane insertion of the amphiphile likely renders a favorable geometry for pyrene excimer formation, analogous to earlier findings, which suggest excimer formation of pyrene-derivated lipids in the membrane bilayer (Winnik 1993; Repakova et al. 2006). Thus, in the present study, the design of a pyrene-tethered bactericidal amphiphile was beneficial as it provided a spectroscopic handle to evaluate amphiphile-bacteria interactions and subsequent membrane-insertion. Interestingly, fluorescence microscope analysis revealed that C1-treated bacterial cells displayed significant fluorescence in various excitation range including UV, blue, green and white light excitation (Figure 2.8B), validating the merit of the fluorogenic amphiphile in probing interactions with bacterial cells in a wide range of excitation. This feature could be especially beneficial in a complex light absorbing system.

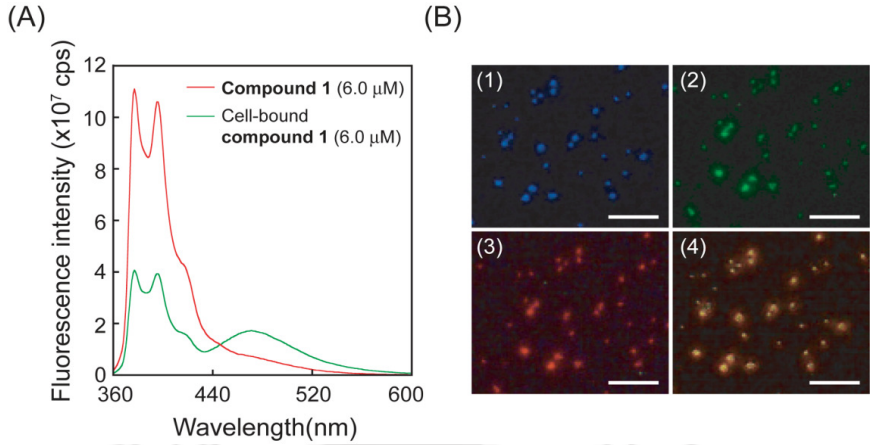

Figure 2.8. (A) Fluorescence emission spectra of C1 and *S. aureus* MTCC 96 bound-C1. Samples were excited at 340 nm and emission spectra was recorded from 360 nm to 600 nm. (B) Fluorescence microscopic image of C1-treated *S. aureus* MTCC 96 upon various excitations. 1. UV excitation / blue emission, 2. Blue excitation / green emission, 3. Green excitation / red emission, 4. White light excitation / no filter. Scale bar for the images is 50 μm.

2.3.4. Bactericidal Potency of C1

In order to verify the bactericidal activity of C1, its activity was tested against *S. aureus* MTCC 96 and *E. coli* MTCC 433 cells suspended in sterile PBS (10^6 CFU/mL each). Based on the MIC of C1 against the target strains *S. aureus* MTCC 96 and *E. coli* MTCC 433, the concentration of C1 chosen in these experiments varied for the respective target bacteria. A general feature, which emerged from these experiments was that there was a prominent decrease in the viability of the treated cells, which could be correlated with increasing amphiphile concentration and incubation time, as evident in the steep slopes of the time-kill curves (Figure 2.9). Given that the MIC of C1 was lower against *S. aureus* as compared to Gram-negative *E. coli* (Table 2.1), the time-kill curve analysis also suggested that upon treatment with C1, the loss of cell viability was more prominent in Gram-positive *S. aureus* as compared to Gram-negative *E. coli* (Figure 2.9). In FESEM analysis, untreated cells of *S. aureus* MTCC 96 and *E. coli* MTCC 433 exhibited a morphology characteristically associated with the respective bacteria (Figure 2.10). In contrast, cells treated with 40 μM of C1 appeared shriveled and lost their typical morphology, which suggested membrane damage (Figure 2.10).

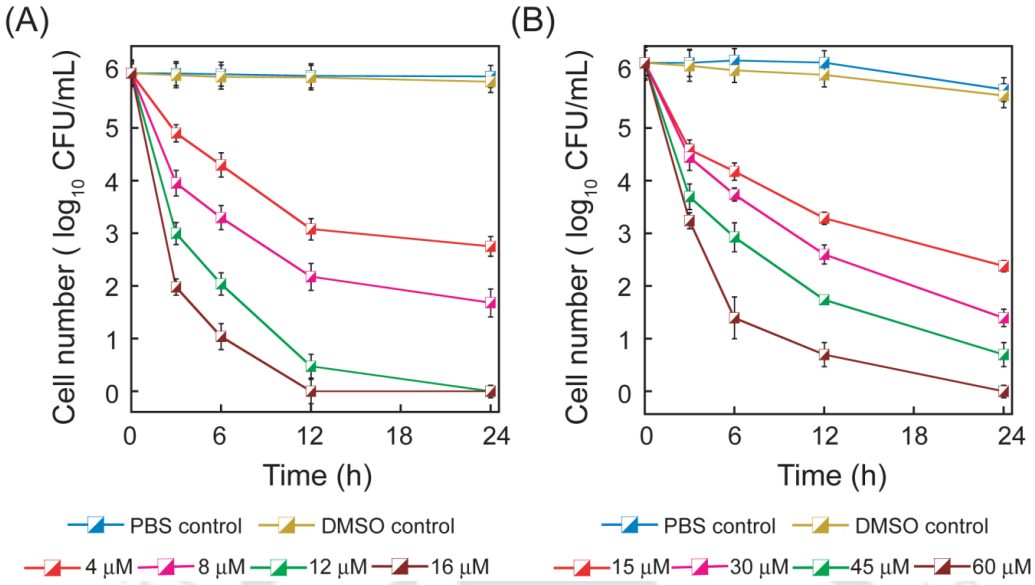

Figure 2.9. Time-kill curves of C1 against (A) *S. aureus* MTCC 96 and (B) *E. coli* MTCC 433.

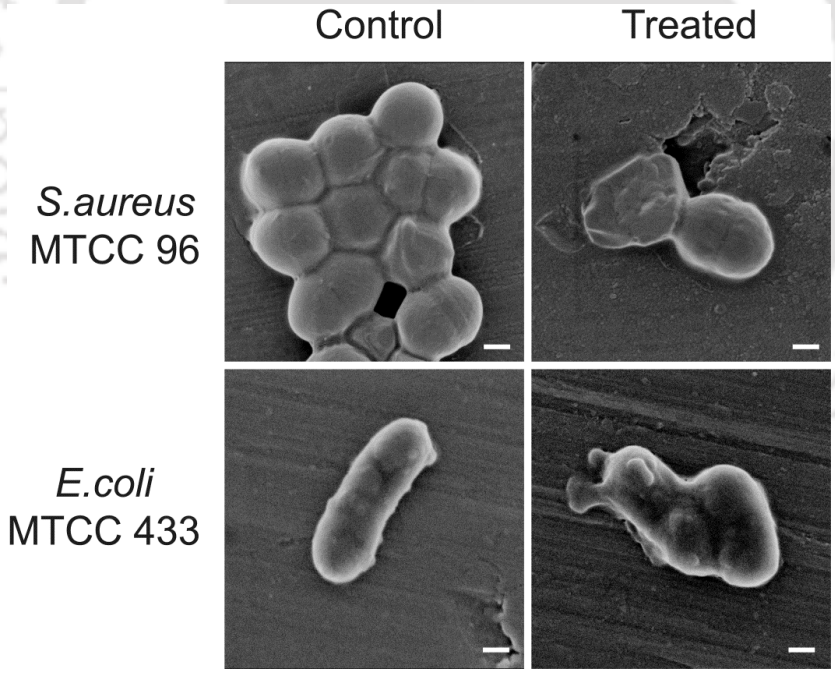

Figure 2.10. FESEM analysis of target bacterial cells treated with 40 µM C1. Scale bar for the images is 300 nm.

2.3.5. Membrane-directed Bactericidal Activity of C1

Apart from morphological examination, fluorescence based assays were also pursued to ascertain the membrane directed activity of the C1. Cells of *S. aureus* MTCC 96 and *E. coli* MTCC 433 were labeled with cFDA-SE and then treated with varying concentrations of the C1 (4.0 μM, 8.0 μM, 12 μM and 16 μM) for various time periods (1 h, 2 h and 3 h). cFDA-SE is a non-fluorescent membrane permeable dye, which accrues readily in viable bacterial cells. Subsequently, the ester bond of the dye is cleaved owing to intracellular esterase activity associated with viable cells. This results in accumulation of a highly fluorescent form of the dye in the cell (Hoefel et al. 2003). These fluorescently labelled cells are especially suitable in antibacterial assays, as the amine reactive fluorophore conjugates with intracellular proteins and thereby reduces passive leakage of the dye from viable cells. The potency of a membrane-targeting antibacterial agent can thus be determined quantitatively by measuring the leakage of the dye from the target cells owing to membrane damage (Singh et al. 2012). In the current study, it was observed that the cFDA-SE leakage in the treated bacteria increased significantly and this phenomenon was unequivocally observed for both the target bacteria and could be correlated with the dose of amphiphile (Figure 2.11A-B). The cFDA-SE leakage assay also indicated that the membrane-directed bactericidal activity of C1 was superior against Gram-positive *S. aureus* MTCC 96 as compared to the Gram-negative *E. coli* MTCC 433 (Figure 2.11A-B), which was consistent with the MIC and MKC results (Table 2.1). The outer membrane permeability barrier present in Gram-negative bacteria (Bolla et al. 2011; Nikaido 2003) likely impedes uptake of the amphiphile, resulting in lower levels of cFDA-SE leakage. Membrane damage in C1-treated target cells was also evident in PI uptake assay. PI is a cell-impermeant dye, which can only be internalized in cells with compromised membrane. Following uptake, PI intercalates with cellular nucleic acids, resulting in the manifestation of a characteristic red fluorescence emission (Virto et al. 2005). Results of the PI uptake assay also revealed higher membrane damage in C1-treated *S. aureus* MTCC 96 cells as opposed to *E. coli* MTCC 433 cells (Figure 2.12A-B), which corroborated the results obtained in cFDA-SE leakage assay (Figure 2.11A-B).

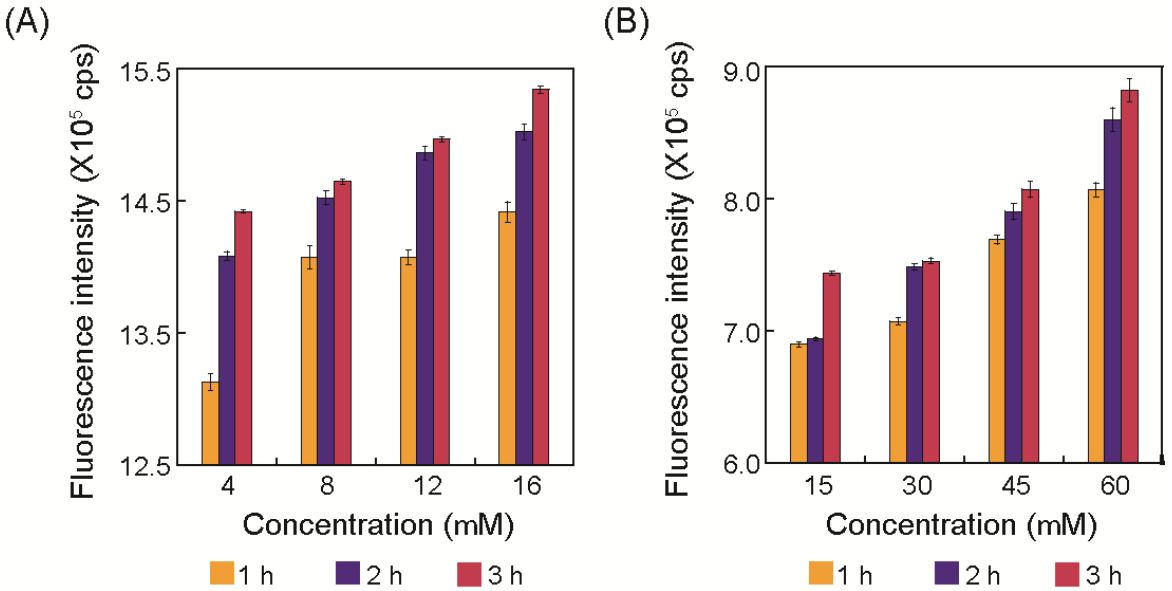

Figure 2.11. cFDA-SE leakage assay in (A) *S. aureus* MTCC 96 and (B) *E. coli* MTCC 433 treated with C1.

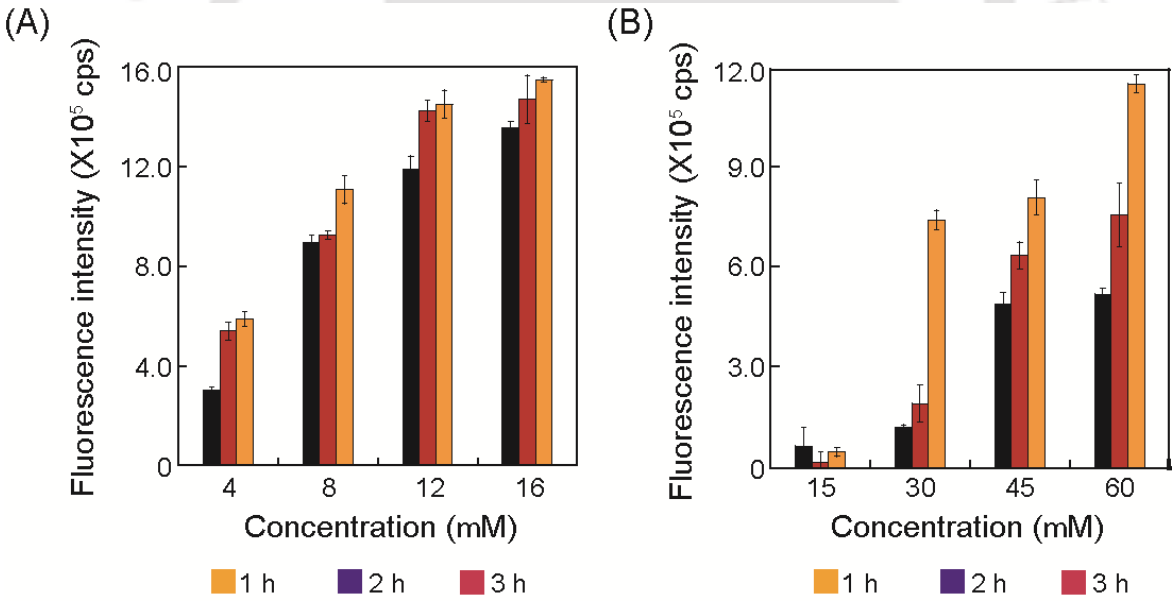

Figure 2.12. Propidium iodide uptake assay in (A) *S. aureus* MTCC 96 and (B) *E. coli* MTCC 433 treated with C1.

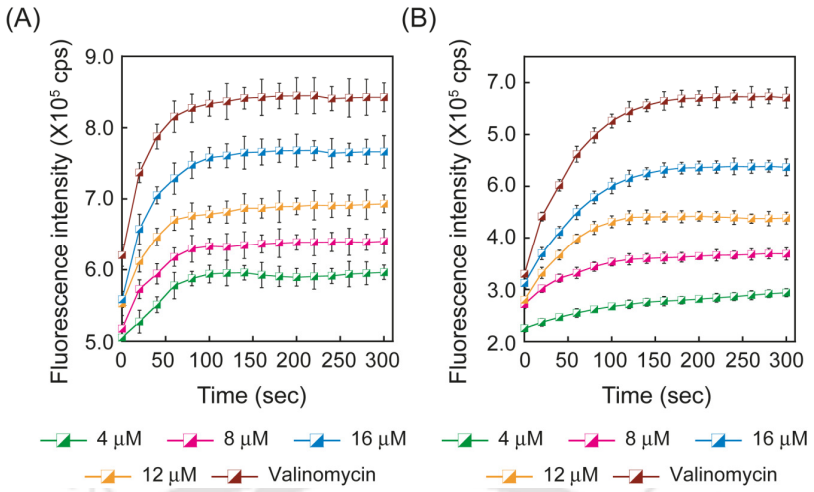

Figure 2.13. $DiSC_3$5-based membrane depolarization assay in (A) *S. aureus* MTCC 96 and (B) *E. coli* MTCC 433 treated with C1. The samples were excited at 622 nm and the fluorescence emission spectra was recorded at 670 nm.

It has been shown in previous studies that the loss in cell viability following treatment with membrane-acting bactericidal agents can be attributed to membrane depolarization (Song et al. 2011; Adhikari et al. 2012). Based on this tenet, the subsequent objective of the current study was to probe whether the amphiphile C1 could depolarize the membrane of the target bacteria. To this end, a fluorescence-based assay was employed using the membrane potential sensitive probe $DiSC_3$5. Interestingly, treatment of *S. aureus* MTCC 96 and *E. coli* MTCC 433 with C1 resulted in an increase in $DiSC_3$5 fluorescence (Figure 2.13), which suggested that the amphiphile could dispel the transmembrane potential (Ψ) in target cells. The membrane depolarization effect rendered by C1 was more prominent in case of Gram-positive *S. aureus* MTCC 96 as compared to Gram-negative *E. coli* MTCC 433 (Figure 2.13), corroborating the earlier observation that C1 displayed a higher membrane-directed activity against Gram-positive bacteria as opposed to the Gram-negative counterpart (Figures 2.11-2.12). These results are consistent with earlier studies, which revealed membrane depolarization in target bacteria treated with bactericidal synthetic amphiphiles (Vudumula et al. 2012; Goswami et al. 2013). Further, it was observed that the extent of membrane depolarization in the target bacteria could be correlated with the dose of C1 (Figure 2.13). It is significant to mention here that the

amphiphile C1 could render membrane depolarization even at concentrations below its MIC against the respective target bacteria (Figure 2.13).

2.3.6. In Vitro Resistance Studies with C1

Drug-resistance is unbridled and an inherent phenomenon associated with many pathogenic bacteria (Bush et al. 2011, Fair and Tor 2014, Nikaido 2009). Bacterial strains can develop a proclivity to exhibit resistance against antimicrobial agents and a continuous exposure to such agents is likely to enhance the chances of resistance development. Staphylococcal strains are highly prevalent in hospitals and are regarded as nosocomial pathogens that impose a significant healthcare burden (Lowy 1998; Naber 2009). With the emergence of drug-resistant staphylococci, this predicament bears serious healthcare implications (Chambers and DeLeo 2009; Stryjewski and Corey 2014). Based on the notion that membrane-targeting agents can be counterproductive to resistance development, it was pertinent to determine whether the target bacterial strain could develop resistance against the membrane-targeting C1. To this end, a well-established multiple step experiment was performed in order to ascertain *in vitro* resistance development in *S. aureus* MTCC 96 cells against C1. The cells were treated with the amphiphile for approximately 100 generations (in three steps). Importantly, in every step, the MIC of C1 against *S. aureus* MTCC 96 was observed to be conserved and there was only a minimal and non-significant change in the spontaneous resistance frequency (Table 2.2). Collectively, these observations strongly suggested a lack of resistance development in the target bacteria against the amphiphile.

Table 2.2. MIC of C1 determined against *S. aureus* MTCC 96 in a multistep *in vitro* resistance development experiment.

Test compound	Selection step/Medium	MIC (μM) / OD_{600} ± standard deviation	Spontaneous Resistance Frequency (SRF) #
C1	Step 1/ Agar	12/0.041 ± 0.005	2.50×10^{-10}
C1	Step 2/ Agar	12/0.017 ± 0.003	1.71×10^{-10}
C1	Step 3/ Agar	12/0.033 ± 0.007	1.20×10^{-10}

SRF was calculated following the method described by Locher et al. 2014

2.3.7. Cytotoxic Potential of C1

In order to evaluate the therapeutic prospect of C1, it was critical to ascertain the cytotoxic effect of the amphiphile. To pursue this objective, a standard MTT assay was pursued on cultured human embryonic kidney cells (HEK 293 cells). The cytotoxic assays revealed that C1 did not render any detrimental effect on HEK 293 cells even at concentrations as high as 32 μM, with the viability of the cultured HEK 293 cells being nearly 80% (Figure 2.14). It may be mentioned here that 32 μM of C1 represents a working concentration, which was considerably higher than the MIC of the amphiphile against *S. aureus* MTCC 96. The antibacterial selectivity of the cationic C1 can perhaps be attributed to the presence of a significantly higher content of negatively charged phospholipids in bacterial membrane as compared to mammalian cell membranes, which essentially consist of zwitterionic lipids and cholesterol (Nikaido 2009).

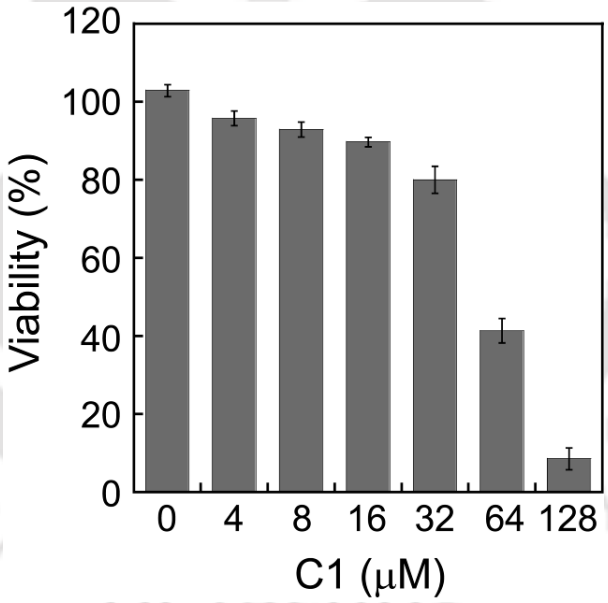

Figure 2.14. MTT assay to determine the viability of HEK 293 cell lines following treatment with varying concentrations of C1. Each data point represents mean ± standard deviation from six samples.

2.4. Significant Findings

The salient findings of the present study can be enlisted as follows:

1. A rationally designed dual-target amphiphile C1 exhibited broad-spectrum antibacterial activity against common pathogenic bacteria. The amphiphile displayed superior bactericidal activity against Gram-positive bacteria as compared to Gram-negative bacterial strains.
2. Presence of a pyrene group in the amphiphile enabled efficient tracking of the interactions with bacterial cells through both solution-based fluorescence spectroscopy as well as fluorescence microscope analysis.
3. Fluorescence-based assays established the membrane-targeting activity of C1 against target bacteria.
4. In an *in vitro* study, it was observed that the target bacteria *S. aureus* MTCC 96 failed to display resistance against C1.
5. The cytotoxic assays indicated that the amphiphile C1 was non-toxic to model human cells even at concentrations much higher than the MIC against the target bacteria *S. aureus* MTCC 96.

Based on the leads obtained in the study, it was evident that the bactericidal amphiphile C1 could act on a compelling target such as the membrane, its activity was not compromised by resistance development and the therapeutic prospect of the molecule was enhanced owing to its non-toxic nature in the bactericidal window. In order to fortify the scope of the amphiphile C1 as a potentially therapeutic antibacterial, its design principle also entailed a functionalization that would render interaction of the molecule with DNA. In this context, the next chapter highlights the detailed study on the DNA binding and cleavage activity of C1.

Chapter 3

DNA Binding and DNA Cleavage Activity of C1

This chapter essentially describes the DNA binding and cleaving activity of C1. The mechanism of DNA cleavage and the intracellular DNA binding and cleavage activity of C1 are illustrated in detail.

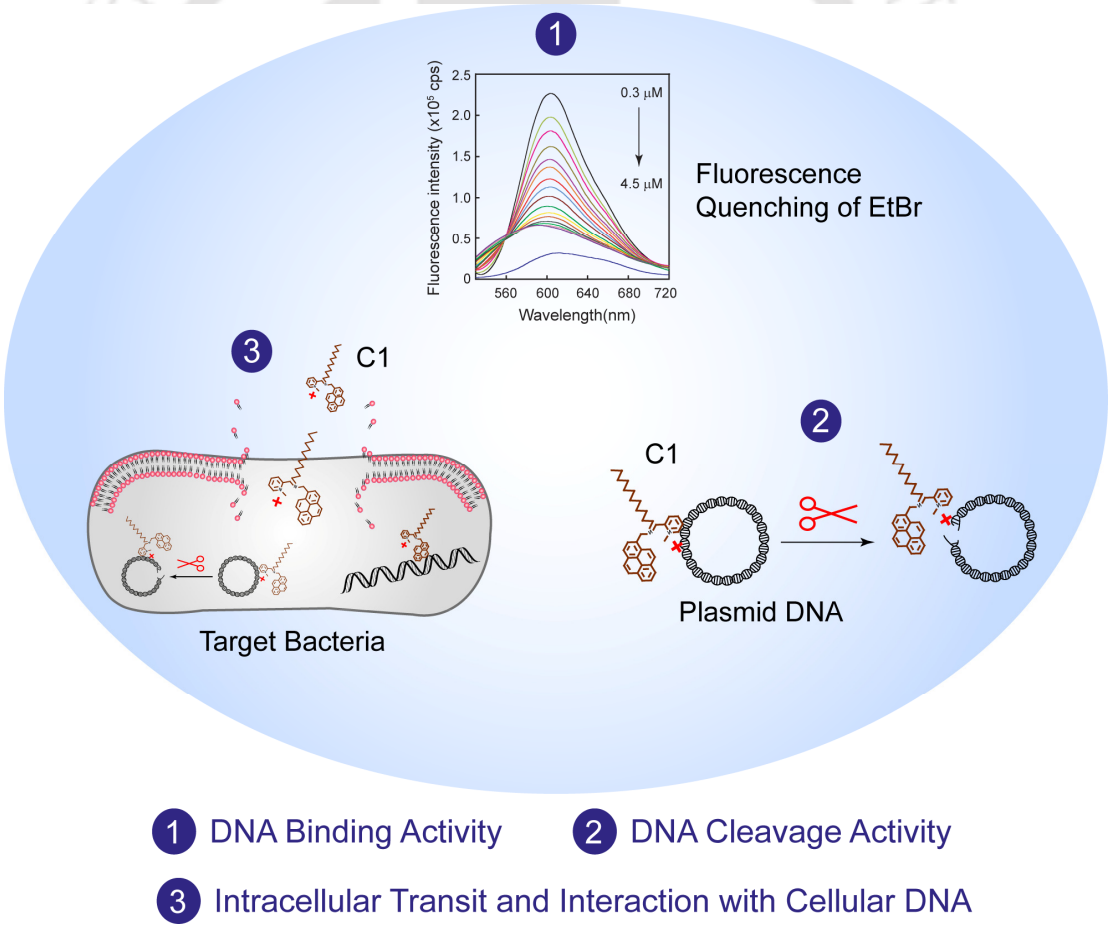

ABSTRACT

This chapter illustrates the DNA binding and DNA cleavage property of the amphiphile C1. UV-visible titration experiments with calf-thymus DNA (CT-DNA) indicated a hypochromic shift in the absorbance bands of C1, which suggested intercalation with DNA. An ethidium bromide (EtBr) displacement assay indicated a systematic reduction in the fluorescence of DNA-bound EtBr upon addition of C1, which was consistent with the intercalation mode of binding of the amphiphile with DNA. Interaction of pUC18 plasmid DNA with C1 resulted in to plasmid DNA cleavage, which was captured in a dose-dependent manifestation of the nicked circular (NC) form of plasmid DNA relative to supercoiled (SC) form. Interestingly, C1 cleaved plasmid DNA at low concentrations and in physiological conditions in the absence of any additives or photo-activation, suggesting a hydrolytic mode of DNA cleavage. The cationic pyridinium nitrogen and tertiary bridgehead nitrogen group in C1 perhaps promoted hydrolytic cleavage of DNA. This notion was corroborated by the fact that the amphiphile C2, which was devoid of the cationic charge failed to display any DNA cleavage activity. Ligation of both C1-treated as well as *Eco*RI-treated pUC18 plasmid DNA prior to transformation could restore DNA damage and enhance transformation efficiency, which also supported that C1-mediated DNA cleavage was hydrolytic. A dose-dependent reduction of PI fluorescence in *E. coli* MTCC 433 cells upon incremental addition of C1 indicated intracellular transit and binding of C1 with cellular DNA, while treatment of *E. coli* DH5α cells with C1 resulted in a progressive cleavage of intracellular pUC18 plasmid DNA. Considering that plasmid DNA harbor and disseminate drug-resistance encoding genes, by virtue of its DNA cleavage activity, C1 can potentially disarm the resistance mechanism and thereby restrain the dissemination of drug-resistance trait in pathogenic bacteria.

3.1. Introduction

Prevalence of antibiotic-resistant pathogenic bacteria continues to be a scourge in modern healthcare. Given this predicament, the challenge in medicinal chemistry is to develop antibacterials that act on compelling targets and are not compromised by resistance development. In this context, in lieu of a single-target pharmacophore, it is conceived that the use of bi-functional bactericidal agents that have multiple targets can be a promising therapeutic approach to mitigate the challenge of drug-resistant pathogens (Silver 2011; O'Connell et al. 2013). Especially, antibacterial agents that have an inherent propensity to target cellular DNA could bear therapeutic prospects, as drug-resistant pathogenic bacteria are known to acquire genes encoding for resistance traits and the cellular plasmid DNA is often involved in housing these genetic determinants as well as in dissemination of such resistance traits (Nikaido 2009). Amongst therapeutic antibiotics, distamycin is a prototype DNA groove binder and various derivatives of distamycin have been reported as antimicrobials (Khalaf et al. 2004; Burli et al. 2004). Recognizing the promise of DNA targeting agents, a library of DNA binding molecules have been synthesized and characterized for their DNA binding affinity and antibacterial activity against drug-resistant pathogens (Dyatkina et al. 2002; Burli et al. 2002; Kaizerman et al. 2003).

Cationic amphiphiles have strong DNA binding property and hence they have been extensively used as vehicles in DNA transfection (Walker et al. 1998; Banerjee et al. 1999). Cationic amphiphiles bind to DNA through electrostatic interaction and their lipophilic moiety assists to form a compact structure (Banerjee et al. 1999; Izumrudov et al. 2002), which presumably enhances transfection efficiency. The design principle and synthetic chemistry involved in the generation of membrane-acting synthetic amphiphilic scaffolds or a DNA binding synthetic amphiphile is well established and validated in the literature. In the present investigation, it was envisaged that a membrane-acting synthetic amphiphile endowed with an add-on feature of DNA binding and DNA cleavage activity could be a promising and potentially therapeutic dual-target pharmacophore especially against antibiotic-resistant pathogens. Based on the aforementioned rationale, a pyridinium based dual-target amphiphile C1 was generated. In the previous chapter, the bactericidal potential and the membrane-directed activity of C1 were highlighted. The present chapter describes the DNA binding and DNA cleavage activity of C1.

3.2. Materials and Methods

3.2.1. Chemicals and Growth Media

Ethidium bromide (EtBr), propidium iodide (PI) and GenElute plasmid DNA miniprep kit, polymyxin B were procured from Sigma-Aldrich (USA). Calf thymus DNA (CT-DNA) and cesium chloride purified pUC18 plasmid DNA was procured from Bangalore Genei, India. Nutrient Broth (NB), Brain-Heart Infusion (BHI) broth and Luria-Bertani (LB) broth were procured from HiMedia, Mumbai, India. Dimethyl sulfoxide (DMSO) was obtained from Merck, India. N-2-hydroxyethyl piperazine N-2 ethane sulphonic acid (HEPES buffer) was procured from Sisco Research Laboratories SRL, Mumbai, India.

3.2.2. UV-Visible Spectroscopy

A stock solution of CT-DNA was prepared in sterile nuclease-free MilliQ water and the molar extinction coefficient value of 6600 M^{-1} cm^{-1} at 260 nm was used to calculate the molarity of DNA (Raja et al. 2011). In separate sets of experiments, varying concentrations of CT-DNA (0.06 µM-0.6 µM) was added drop-wise to either C1 or C2 (5.0 µM each), mixed gently and then the absorbance of the solution was recorded in a spectrophotometer (CARY 300 Bio, Varian) in scanning mode from 235 nm to 600 nm. Control samples consisted of only DNA or amphiphile. The absorbance measurements were acquired from three independent experimental samples. The binding constants (K_b) for C1 and C2 were ascertained by monitoring the change in absorbance at 260 nm with increasing concentration of DNA and calculating the ratio of the slope to the y intercept in the plots of [DNA] / ($\varepsilon_a - \varepsilon_f$) versus [DNA] (Basu et al. 2013).

3.2.3. Fluorescence Spectroscopy

Varying concentrations of CT-DNA (15 nM-75 nM) prepared in sterile nuclease-free MilliQ water was added drop-wise to separate sets of C1 or C2 (150 nM each). The contents of the tubes were gently mixed and the fluorescence emission spectra of the samples were recorded in a spectrofluorometer (FluoroMax-3, HORIBA) in a scanning mode from 360 nm to 600 nm by setting the excitation wavelength at 340 nm. The scan rate was set at 1 s / nm and the excitation and emission slit width were kept as 1 nm and

5 nm, respectively. Control samples consisted of only DNA or amphiphile solution. Fluorescence measurements were obtained from three independent experimental samples.

3.2.4. Ethidium Bromide (EtBr) Displacement Assay

Multiple sets of CT-DNA solution (0.75 µM each) were incubated with 0.15 µM EtBr solution for 30 min in an amber color microcentrifuge tube. The fluorescence emission spectra of the solution was measured in a spectrofluorometer (FluoroMax-3, HORIBA) in scanning mode from 530 nm to 720 nm (scan rate of 1s/nm, slit width 1/5) by exciting at 515 nm. Subsequently, varying concentrations of C1 or C2 (0.3 µM-4.5 µM each) were gradually dispensed into separate sets of the solution, incubated for 5 min at room temperature and the fluorescence emission spectra of the samples were again recorded in scanning mode from 530 nm to 720 nm by setting the excitation wavelength at 515 nm. The emission spectra for DNA-bound EtBr alone was also recorded in the absence of the amphiphiles. Fluorescence measurements were obtained from three independent experimental samples. The quenching constant (K_q) for C1 and C2 was determined from a standard Stern-Volmer plot (Basu et al. 2013).

3.2.5. Plasmid DNA Cleavage Experiment

E. coli DH5α cells harboring pUC18 plasmid DNA was grown overnight at 37^{o}C in LB broth in presence of 100 µg/mL ampicillin and pUC18 plasmid DNA was isolated from the cells using a plasmid DNA isolation kit (Sigma-Aldrich, USA). The concentration of plasmid DNA was determined by measuring the absorbance at 260 nm. To ascertain DNA cleavage activity of the amphiphiles, purified pUC18 plasmid DNA (60 µM) was taken in sterile nuclease-free MilliQ water and incubated with varying concentrations of C1 or C2 in separate sets (6.0 µM, 12 µM, 18 µM, 24 µM and 30 µM of each amphiphile) for 1 h at 37^{o}C. Cleavage reactions were also performed in the presence of NaN_3 and DMSO (Maheswari et al. 2007). Following incubation, the cleavage reactions were terminated by adding loading dye (0.05% bromophenol blue, 50% glycerol, 2.0 mM EDTA) and the samples were analyzed by agarose gel (0.8%) electrophoresis followed by staining the gel with EtBr solution. The DNA bands were visualized in a gel documentation system (Gel

Doc XR + System, Bio-Rad). Quantification of band intensity was accomplished by ImageJ analysis (http://rsb.info.nih.gov/ij/).

3.2.6. Plasmid DNA Cleavage and Ligation Studies

Cesium chloride purified pUC18 plasmid DNA (1.0 µg) was incubated in separate sets with either *Eco*RI enzyme (Fermentas, Lithuana) or C1 (30 µM) at 37°C for 1 h. A negative control sample consisting of pUC18 plasmid DNA alone was also included. The reaction mixtures were then purified using a PCR purification kit (Sigma-Aldrich, USA). Cleavage of pUC18 plasmid DNA by *Eco*RI enzyme and C1 was verified by agarose gel electrophoresis of the samples. Subsequently, ligation reactions were performed with C1-treated plasmid DNA, *Eco*RI-treated plasmid DNA and untreated plasmid DNA (50 ng of plasmid DNA in each) using T4 DNA ligase (New England Biolabs) at 16°C for 16 h. Negative control experiments in the absence of T4 DNA ligase enzyme were also set up in parallel. The ligation reaction mixtures were used to transform *E. coli* DH5α cells following a standard protocol (Chung et al. 1989). The transformed colonies were enumerated to determine the transformation efficiency. A schematic representation of the protocol for plasmid DNA cleavage and ligation studies is indicated in Figure 3.1.

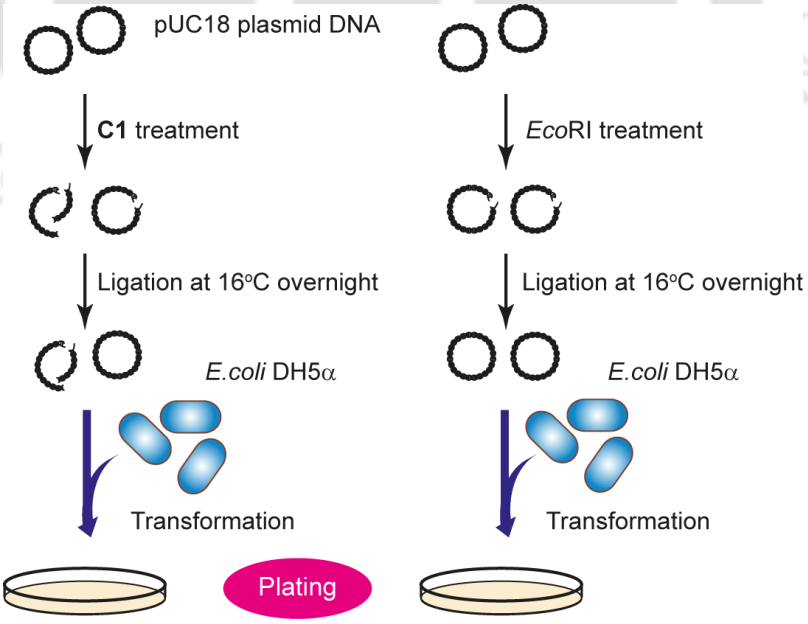

Figure 3.1. Scheme of the protocol for plasmid DNA cleavage and ligation studies.

3.2.7. Uptake and Binding of C1 with Bacterial Cellular DNA

Overnight grown cells of *E. coli* MTCC 433 were harvested by centrifugation, washed twice with sterile PBS and resuspended in the same (10^6 CFU/mL). In separate sets, the cells were incubated with 15 µM C1 or 0.5 µg/mL polymyxin B for 3 h to induce membrane damage. The cells were then washed twice with sterile PBS, resuspended in 1.0 mL of the same and stained with PI following the method described earlier in section 2.2.8.2. To ascertain membrane damage caused by either C1 or polymyxin B treatment, uptake and intercalation of PI with bacterial cellular DNA was measured by recording the fluorescence emission spectra of the cell suspensions in a spectrofluorometer (FluoroMax-3, HORIBA) at an excitation wavelength of 535 nm and emission wavelength of 617 nm. Subsequently, varying concentrations of C1 (15 µM, 30 µM and 45 µM) was further added separately to either C1- or polymyxin B-treated and PI stained cell suspensions and the change in the fluorescence emission intensity was measured intermittently over a period of 20 min, at an excitation wavelength of 535 nm and emission wavelength of 617 nm. Fluorescence measurements were acquired from three independent experimental samples. A schematic representation of the protocol for studying uptake and binding of C1 with bacterial cellular DNA is shown in Figure 3.2.

3.2.8. Cleavage of Intracellular Plasmid DNA by C1

Overnight grown cells of *E. coli* DH5α harboring pUC18 plasmid DNA were harvested by centrifugation, washed twice with sterile PBS and resuspended in the same. In two separate sets, either polymyxin B (0.5 µg/mL) or C1 (45 µM) was added to the cell suspensions. At two different time periods (3 h and 6 h), the cells were centrifuged, washed twice with sterile PBS and then pUC18 plasmid DNA was isolated from the cells using the plasmid DNA isolation kit (Sigma-Aldrich, USA). A control sample consisting of *E. coli* DH5α cells alone was also subjected to the same experimental conditions. pUC18 plasmid DNA isolated from all the samples were analyzed by agarose gel electrophoresis. A schematic representation of the protocol for cleavage of intracellular plasmid DNA by C1 is depicted in Figure 3.3.

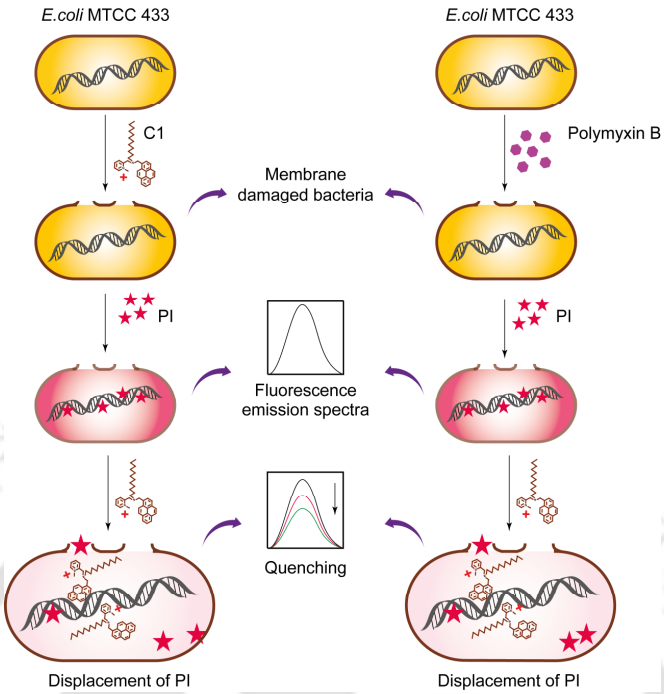

Figure 3.2. Scheme of the protocol for studying uptake and binding of C1 with bacterial cellular DNA.

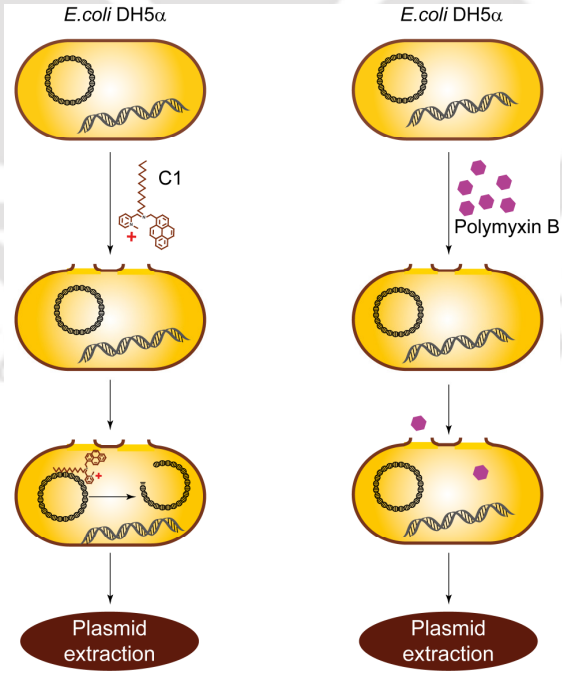

Figure 3.3. Scheme of the protocol for studying cleavage of intracellular plasmid DNA by C1.

3.3. Results and Discussion

3.3.1. DNA-binding Studies

In UV-visible titration experiments with calf-thymus DNA (CT-DNA), the absorbance bands of C1 and C2 revealed a hypochromic shift (Figure 3.4A, Appendix Figure A3.1A), which indicated an intercalation mode of binding to DNA (Liu et al. 2009; Basu et al. 2013). The binding constant (K_b) for C1 and C2 was determined from the binding isotherm (Figure 3.4B, Appendix Figure A3.1B) and was found to be 2.87 x 10^6 M^{-1} and 2.11 x 10^6 M^{-1}, respectively.

A concentration-dependent quenching of the fluorescence emission spectra of C1 and C2 was observed upon addition of CT-DNA (Figure 3.5, Appendix Figure A3.1C). This reduction in the fluorescence emission intensity of C1 upon interaction with DNA was distinctive from the pyrene-excimer observed earlier in case of C1-bacterial cell interaction (Figure 2.8A). Based on this observation, it was evident that C1 provided unique spectroscopic signatures to probe interactions with bacterial cell and DNA.

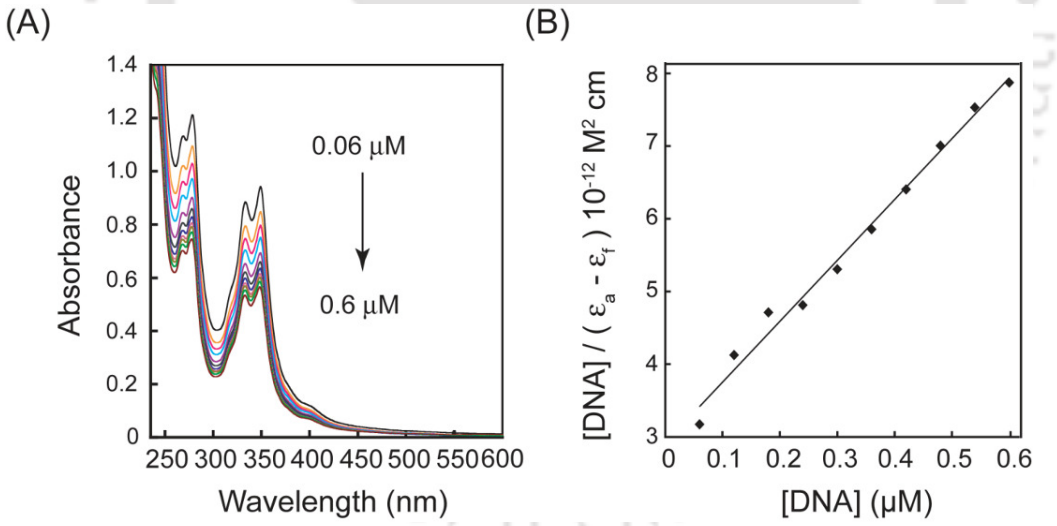

Figure 3.4. (A) UV-visible absorbance spectroscopy of C1 (5.0 µM) upon addition of calf thymus DNA (0.06 µM-0.6 µM). (B) Binding isotherm of C1 with calf thymus DNA determined by UV-visible absorbance titration spectroscopy.

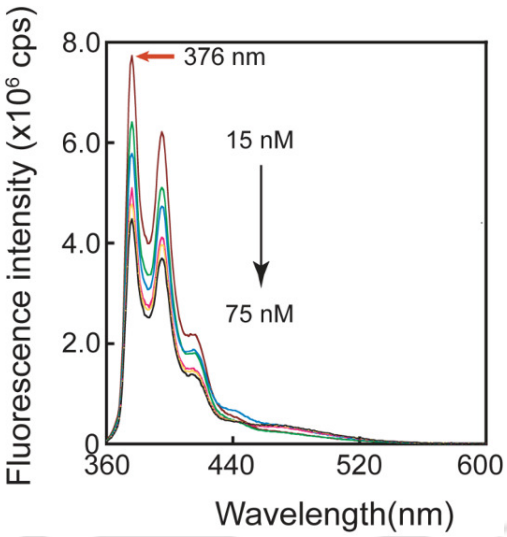

Figure 3.5. Fluorescence spectroscopy of C1 (150 nM) upon addition of calf thymus DNA (15 nM-75 nM).

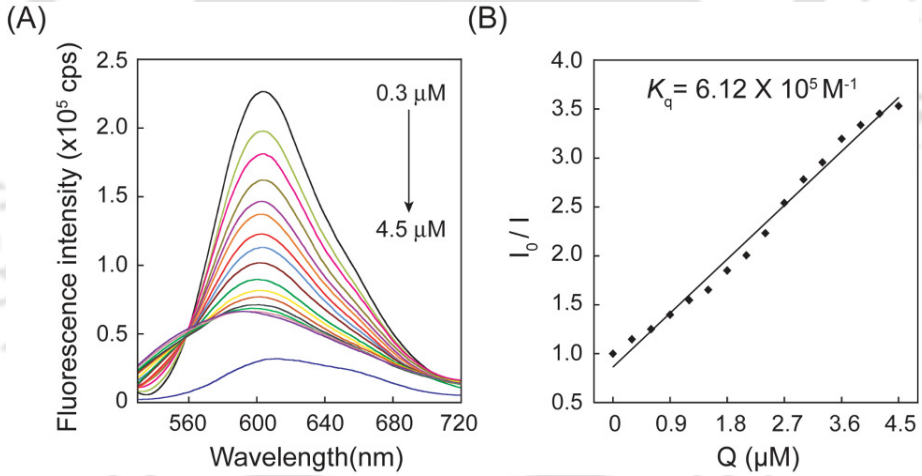

Figure 3.6. (A) Ethidium bromide displacement assay with C1 (0.3 µM-4.5 µM). (B) Stern-Volmer plot for ethidium bromide displacement assay with C1.

An EtBr displacement assay indicated a systematic reduction in the fluorescence of DNA-bound EtBr upon addition of C1 or C2, which again corroborated the intercalation mode of DNA binding (Figure 3.6A, Appendix Figure A3.1D). Based on a Stern-Volmer plot (Figure 3.6B, Appendix Figure A3.1E), the quenching constant (K_q) for C1 and C2

were observed to be 6.12 x 10^5 M^{-1} and 1.3 x 10^5 M^{-1}, respectively. The similar pattern of DNA binding exhibited by C1 and C2 observed in these experiments indicated that the planar pyrene molecule, which was present in both the amphiphiles perhaps plays an important role in promoting interactions with DNA.

3.3.2. Plasmid DNA Cleavage

Interaction of pUC18 plasmid DNA with C1 resulted in a dose-dependent manifestation of the nicked circular (NC) form of plasmid DNA relative to supercoiled (SC) form (Figure 3.7), suggesting a single-strand DNA cleavage activity of C1. It may be mentioned here that pUC18 plasmid DNA used in these experiments was isolated using a plasmid DNA purification kit, which predominantly yielded high content of SC plasmid in comparison to the other topological forms of the plasmid (Figure 3.7A, lane 1).

Interestingly, C1 cleaved plasmid DNA at low concentrations (micromolar range) and in physiological conditions in the absence of any additives or photo-activation, suggesting the possibility of a hydrolytic mechanism of DNA cleavage. Plasmid DNA cleavage was unaffected in presence of known radical scavengers such as NaN_3 and DMSO, which also suggested a hydrolytic mode of DNA strand scission by C1 (Figure 3.8)

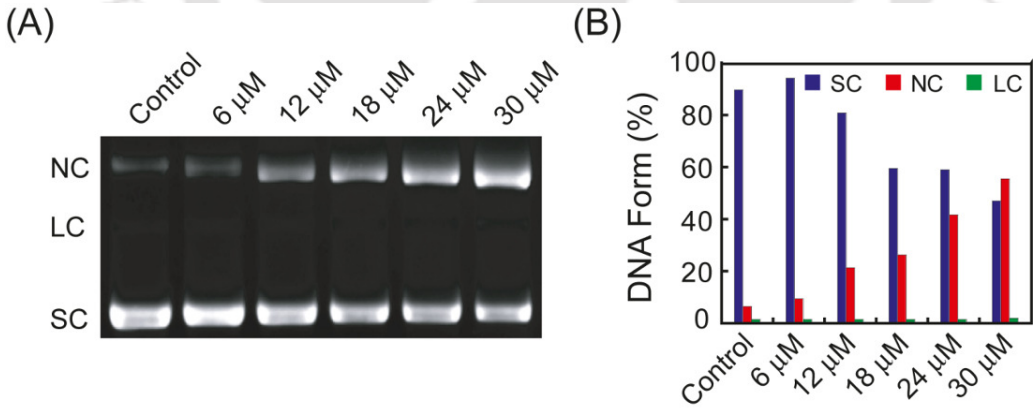

Figure 3.7. (A) Agarose gel electrophoresis of pUC18 plasmid DNA treated with C1. Lanes 1: control (untreated plasmid DNA); 2-6: plasmid DNA treated with varying concentrations of C1 (6.0 μM - 30 μM). SC: supercoiled DNA, LC: linearised circular DNA, NC: nicked circular DNA. (B) Quantification of band intensity of the topological forms of pUC18 plasmid DNA obtained in (A) using ImageJ analysis software.

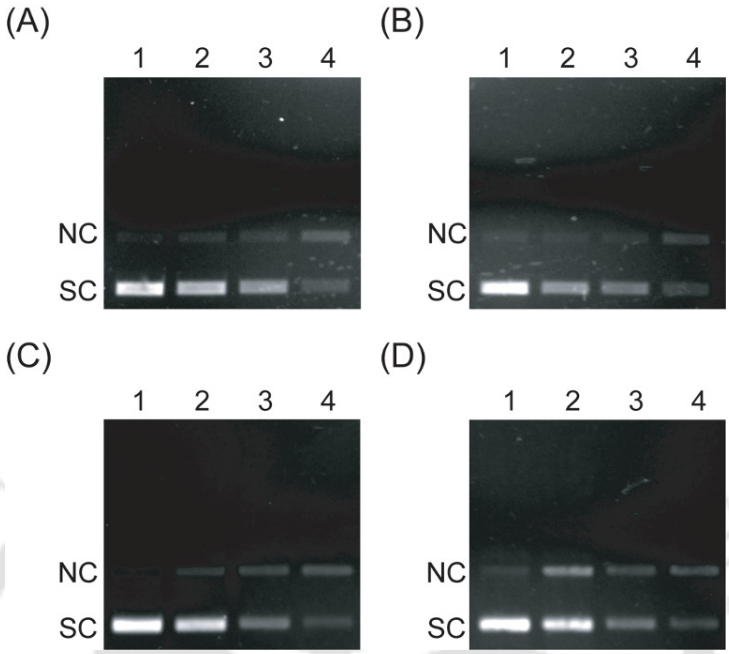

Figure 3.8. Agarose gel electrophoresis of pUC18 plasmid DNA treated with C1 in (A) absence of NaN_3, (B) presence of NaN_3, (C) absence of DMSO and (D) presence of DMSO. Lanes 1: control (untreated plasmid DNA); 2-4: plasmid DNA treated with 6.0 µM, 18 µM and 30 µM of C1, respectively.

Perhaps the combination of cationic pyridinium nitrogen and tertiary bridgehead nitrogen group in C1 promotes hydrolytic cleavage of DNA, as observed in earlier studies (Scheffer et al. 2005; Hernandez-Gil et al. 2013). The possible involvement of the cationic pyridinium nitrogen in promoting hydrolytic cleavage of DNA is supported by the fact that the control C2, which is devoid of the positive charge failed to exhibit any plasmid DNA cleavage activity (Appendix Figure A3.2).

To further probe the mechanism of DNA cleavage, CsCl-purified pUC18 plasmid DNA (SC form) was treated with C1 as well as the restriction enzyme *Eco*RI (control sample) to induce cleavage (Figure 3.9A) and then used to transform *E. coli* DH5α cells. The transformation efficiency obtained with both C1- as well as *Eco*RI-treated pUC18 plasmid DNA was low in the absence of ligation (Figure 3.9B). However, ligation of both

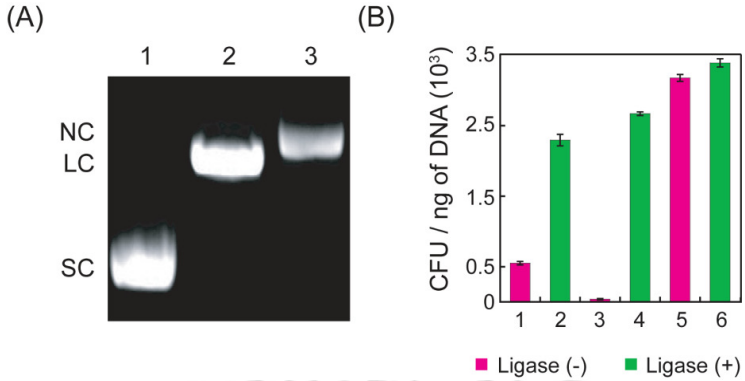

Figure 3.9. (A) Agarose gel electrophoresis indicating various forms of pUC18 plasmid DNA used for transformation experiments. Lanes: (1) uncut plasmid DNA, (2) *Eco*RI-treated plasmid DNA, (3) C1-treated plasmid DNA. SC: supercoiled DNA, LC: linearised circular DNA, NC: nicked circular DNA. (B) Quantification of transformed *E. coli* DH5α colonies. (1-2) C1-treated pUC18 plasmid DNA, (3-4) *Eco*RI-treated pUC18 plasmid DNA, (5-6) untreated pUC18 plasmid DNA. The ligation negative and ligation positive samples are indicated.

C1-treated as well as *Eco*RI-treated pUC18 plasmid DNA prior to transformation yielded high numbers of transformed colonies (Figure 3.9B). Given that ligation could redress DNA damage and enhance transformation efficiency also supported the premise that C1-mediated DNA cleavage was hydrolytic.

3.3.3. Cellular DNA Binding

Considering the potent membrane-directed bactericidal activity and DNA binding attribute of C1, it was conceived that upon interaction with bacterial cells, C1 would likely breach the membrane barrier by pore formation, which in turn, would facilitate intracellular transit of C1 and its subsequent binding to cellular DNA. To verify this possibility, cells of *E. coli* MTCC 433 were initially treated with either C1 (15 µM) or polymyxin B (0.5 µg/mL) to induce membrane damage. Polymyxin B was chosen as a membrane acting agent known to induce pore formation in cells (Yeaman and Yount, 2003). A high PI fluorescence obtained for cells treated with either C1 or polymyxin B (Figure 3.10A-B) indicated membrane disruption, uptake and intercalation of PI with cellular DNA. Interestingly, upon further addition of C1 to both these samples, PI fluorescence declined in a dose-dependent manner (Figure 3.10A-B), suggesting competitive displacement of PI bound to cellular DNA by

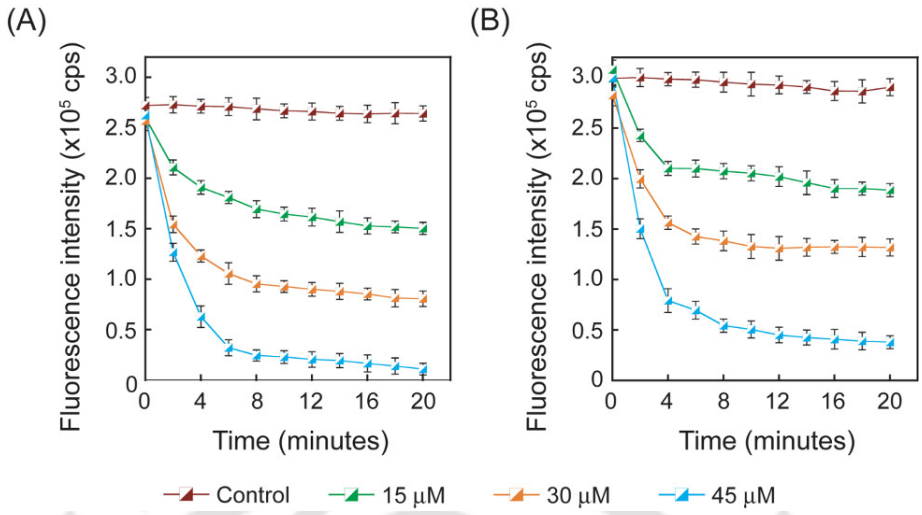

Figure 3.10. Uptake and intracellular DNA binding by C1 in *E.coli* MTCC 433 cells. Cells were initially treated with (A) 15 µM C1 or (B) 0.5 µg/mL of polymyxin B and then stained with propidium iodide (PI). Fluorescence emission intensity of PI was measured in both (A) and (B) following incremental addition of C1 (15 µM, 30 µM and 45 µM).

C1 owing to intracellular transit and an intercalative mode of binding of the amphiphile with cellular DNA.

3.3.4. Intracellular Plasmid DNA Cleavage

Given that C1 exploits a membrane-directed activity to promote its intracellular transit and binds with intracellular DNA (Figure 3.10) and can also cleave plasmid DNA (Figure 3.7A) in solution, it was envisioned that the amphiphile may hold interesting prospect as a therapeutic antibacterial since plasmid DNA is involved in harboring and transfer of resistance traits in drug-resistant pathogenic bacteria (Nikaido 2009). To validate this rationale, model experiments were conducted with *E. coli* DH5α cells harboring pUC18 plasmid DNA. In case of both untreated as well as polymyxin B-treated *E. coli* DH5α cells, the relative content of SC and NC forms of pUC18 plasmid DNA was retained (Figure 3.11, lanes 2-5), which suggested lack of DNA cleavage in these samples. However, treatment of *E. coli* DH5α cells with C1 resulted in cleavage of intracellular pUC18

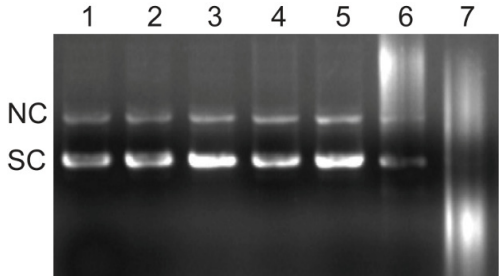

Figure 3.11. Agarose gel electrophoresis to study pUC18 plasmid DNA cleavage in *E. coli* DH5α cells upon interaction with C1. Lanes: (1) control pUC18 plasmid DNA, (2-3): pUC18 plasmid DNA isolated from untreated cells after 3 h and 6 h, (4-5): pUC18 plasmid DNA isolated from polymyxin B-treated cells after 3 h and 6 h, (6-7): pUC18 plasmid DNA isolated from C1-treated cells after 3 h and 6 h. SC: supercoiled DNA, NC: nicked circular DNA.

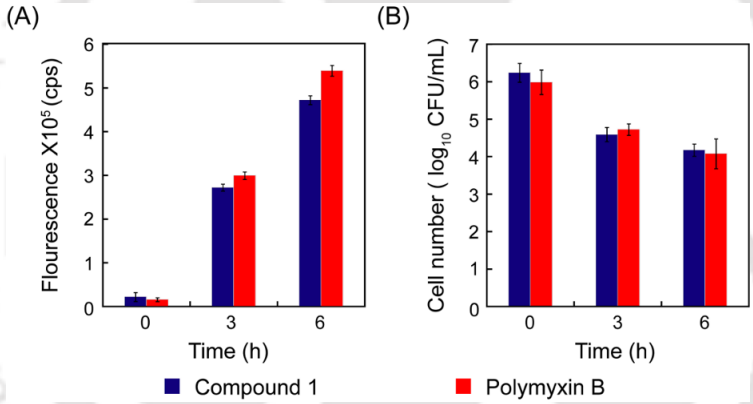

Figure 3.12. (A) Fluorescence emission intensity of PI measured to ascertain membrane damage in *E. coli* DH5α cells treated with either 45 µM C1 or 0.5 µg/mL polymyxin B for 3 h and 6 h. (B) Loss in viability of *E. coli* DH5α cells treated with either 45 µM C1 or 0.5 µg/mL polymyxin B for 3 h and 6 h.

plasmid DNA after 3 h (Figure 3.11, lane 6) and this effect was manifested as large scale degradation of plasmid DNA in case of 6 h treatment (Figure 3.11, lane 7). As membrane damage and loss in cell viability was commonly observed for polymyxin B as well as C1-treated cells of *E. coli* DH5α (Figure 3.12), degradation of intracellular pUC18 plasmid DNA in C1-treated cells could perhaps be attributed to the uptake followed by the intrinsic DNA cleavage activity of the amphiphile and not to a mere loss in cell viability.

3.4. Significant Findings

The salient findings of the present study are as follows:

1. UV-Visible spectroscopy and fluorescence spectroscopy suggested an intercalation mode of binding of C1 with DNA.
2. The DNA cleavage activity of C1 was demonstrated against plasmid DNA. DNA cleavage by C1 occurred in the absence of any additives and the mechanism of DNA cleavage was found to be hydrolytic based on the ligation experiments.
3. The PI displacement experiment with bacterial cells revealed intracellular transit and binding of C1 with cellular DNA.
4. Plasmid DNA analysis in C1-treated bacterial cells revealed the ability of the amphiphile to render plasmid DNA cleavage in bacterial cells.

The results obtained in this chapter in conjunction with the results obtained in the previous chapter established the dual-target nature of the bactericidal amphiphile C1. Bestowed with an ability to cleave cellular plasmid DNA, which is known to harbor and disseminate drug-resistance encoding genes, the dual arsenal C1 emerges as a potential therapeutic that is likely to disarm the resistance mechanism and thereby curtail the spread of drug-resistance trait in pathogenic bacteria. Further, given the potent membrane-directed activity of C1 even at concentrations below its MIC, it was envisaged that the amphiphile can perhaps be used as an adjuvant to breach the bacterial membrane and enhance the uptake and efficacy of therapeutic antibiotics. In line with this rational, the next chapter describes the adjuvant potential and the therapeutic prospect of the bactericidal amphiphile C1.

Chapter 4

Bactericidal Activity of C1 in Simulated Fluids and its Adjuvant Activity in Combination Therapy

This chapter highlights the bactericidal activity of C1 in various physiologically relevant fluids and the adjuvant potential of C1 in enhancing antibiotic-mediated killing of target bacteria.

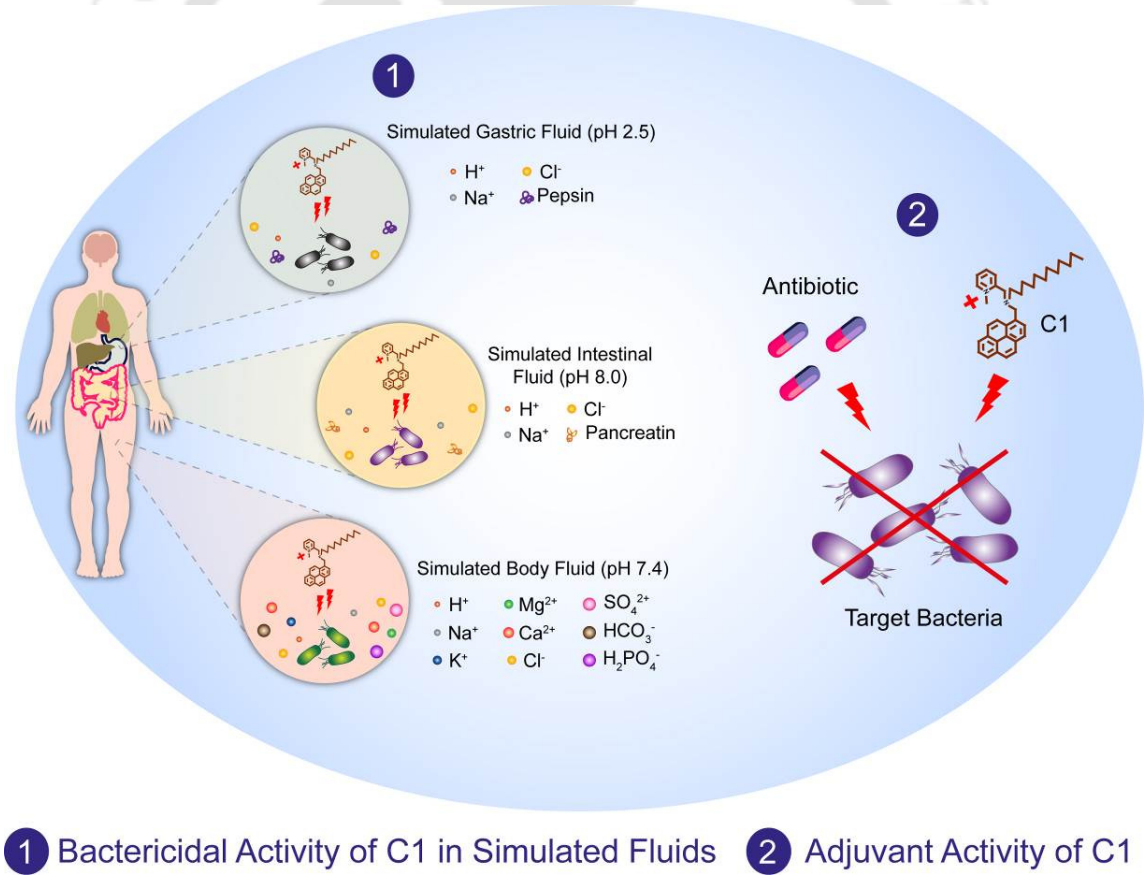

ABSTRACT

The investigation describes the retention of the bactericidal activity of the amphiphile C1 in physiologically relevant fluids and its adjuvant activity in combinatorial treatment with antibiotics. The bactericidal activity of C1 was retained in simulated gastric fluid (SGF), wherein a dose-dependent reduction in the viability of the target bacteria was recorded. Interestingly, when subjected to treatment with C1, the viability of the target bacterial cells was also reduced in other niches such as simulated intestinal fluid (SIF) and simulated body fluid (SBF). In the combination experiments with C1 and gentamicin, a prominent growth inhibition of *S. aureus* MTCC 96 cells could be readily observed, accompanied by an eightfold reduction in the MIC of gentamicin and a synergistic interaction between C1 and gentamicin. Superior growth inhibition of *E. coli* MTCC 433 cells was observed in case of combination therapy with C1 and erythromycin. Akin to the results obtained with gentamicin, a substantial decrease in the MIC of erythromycin and a synergistic interaction between C1 and the antibiotic was captured in the combination experiments. Interestingly, in the combination experiments, C1 could reduce the development of gentamicin-resistance in *S. aureus* MTCC 96 cells. Cytotoxicity assays on HEK 293 cells indicated that the combinatorial use of the amphiphile C1 and the antibiotics was non-toxic, highlighting the potential of C1 as an adjuvant in antibacterial therapy.

4.1. Introduction

The dearth in the turnover of effective bactericidal agents that are capable of countering the challenge of rapidly evolving drug-resistant strains has aggravated the burden of the healthcare crisis (Silver 2011; Fischbach and Walsh 2009; Nolte 2014; Fair and Tor 2014). The alarming prevalence of drug-resistant bacteria is also envisaged to be the outcome of their remarkable robustness and adaptability to various niches. In addition, the indiscriminate and arbitrary use of therapeutic antibiotics has also contributed to the spread of drug-resistance amongst pathogenic bacteria. Based on a large body of literature, it is now widely acknowledged that the outer membrane of Gram-negative bacteria can act as a formidable barrier that can prevent the intracellular transit of antibacterial agents. This phenomenon enables the bacteria to evade the action of therapeutic antibiotics (Delcour 2009, Nikaido 2003, Bolla et al. 2011). In case of Gram-positive bacteria, the thick cell wall, which is essentially made of peptidoglycan, may yield a protective barrier (Weidenmaier and Peschel 2008, Kohler et al. 2009), which can contribute to the inherent drug resistance exhibited by pathogenic bacteria.

In the context of a defiant membrane barrier present in pathogenic bacteria, it is conceivable that deployment of a membrane-targeting agent may be particularly beneficial as perturbation of the membrane of target bacteria is likely to result in efficient uptake of a therapeutic antibiotic and enhanced killing of the target bacteria. Previous studies with membrane-targeting agents support this notion (Saha et al. 2008; Goswami et al. 2013; Uday et al. 2014; Goswami et al. 2015). The deployment of a membrane-acting agent in combinatorial therapy with antibiotics is further vindicated by the fact that the adjuvant activity of the membrane-targeting agent is expected to reduce the dose of antibiotics required to eliminate the target bacteria. This outcome is significant in two aspects. Firstly, it is thought that the use of therapeutic antibiotics at a low dose is likely to curtail the evolution of drug-resistance (Yeh et al. 2009; Ejim et al. 2011). Secondly, the toxicity associated with certain therapeutic antibiotics can also be addressed in a combinatorial therapy regime.

As the menace of the life-threatening infections caused by drug-resistant pathogenic bacteria assumes an alarming proportion and the use of a single antibiotic to combat the pathogens is becoming less effective, combination therapy is emerging as a

promising option. The use of a combinatorial treatment regimen seems to be particularly credible as the synergy between the drugs is likely to heighten the overall bactericidal effect, reinstate susceptibility of the target cells and perhaps even hinder the emergence of resistance during therapy (Fischbach 2011; Worthington and Melander 2013; Ejim et al. 2011; Tamma et al. 2012; Gill et al. 2015; Thangamani et al. 2016). In the context of combination therapy, the potential of small synthetic molecules as adjuvants has also been recognized (Hess et al. 2014; Hu et al. 2015; Harris et al. 2012). Based on the aforementioned rationale and given the potent membrane-directed activity of the synthetic amphiphile C1, in this chapter the adjuvant activity of C1 is ascertained by determining the ability of the amphiphile to potentiate the activity of model therapeutic antibiotics gentamicin and erythromycin against target bacterial strains. The potential of C1 to curtail *in vitro* resistance development of the antibiotic gentamicin in *S. aureus* cells and the cytotoxicity of a combinatorial treatment regimen of C1 and antibiotics on cultured human cells is also reported in this chapter.

4.2. Materials and Methods

4.2.1. Growth Media and Chemicals

5 (and 6)-carboxyfluorescein diacetate succinimidyl ester (cFDA-SE), Erythromycin, Dulbecco's Modified Eagle Medium (DMEM), trypsin-EDTA, 3-(4,5-dimethyl-2-thiazolyl)-2,5-diphenyl-2H-tetrazolium bromide (MTT), human serum albumin (HSA, Fraction V and Human serum albumin), pepsin and pancreatin were procured from Sigma-Aldrich (USA). Brain-Heart Infusion (BHI) broth and gentamicin was procured from HiMedia, Mumbai, India. Dimethyl sulfoxide (DMSO) was obtained from Merck, India. N-2- hydroxyethyl piperazine N-2 ethane sulphonic acid (HEPES buffer) was procured from Sisco Research Laboratories SRL, Mumbai, India. Fetal bovine serum (FBS) was procured from PAA Laboratories, USA

4.2.2. Bacterial Strains and Growth Conditions

In the present investigation, Gram-positive *S. aureus* MTCC 96, *Listeria monocytogenes* Scott A and Gram-negative *E. coli* MTCC 433 were chosen as target bacteria. The growth condition of these bacterial strains are mentioned before in section 2.2.3.

4.2.3. Minimum Inhibitory Concentration (MIC) of Gentamicin and Erythromycin

MIC of gentamicin and erythromycin was determined against *S. aureus* MTCC 96 and *E. coli* MTCC 433, respectively. A standard protocol was followed for determining MIC of the antibiotics as described in section 2.2.5. Briefly, the target bacterial strains were inoculated at 1% level in microtitre wells having the specific growth medium and grown overnight at 37^{o}C and 180 rpm in presence of varying concentrations of either gentamicin (0.5 µM - 128 µM) or erythromycin (1.25 µM - 320 µM). The growth of the bacterial strains was monitored by measuring absorbance at 600 nm in a microtitre plate reader (Infinite M200, TECAN, Switzerland). MIC of the antibiotics was recorded as the lowest concentration, which resulted in an absorbance reading of <0.1 at 600 nm (A_{600} = <0.1). The MIC values for gentamicin and erythromycin were calculated from three independent experiments, each having three replicas. Data analysis and calculation of standard deviation was performed with Microsoft Excel 2010 (Microsoft Corporation, USA).

4.2.4. Antibacterial Activity of C1 in Simulated Gastric Fluid (SGF) and Simulated Intestinal Fluid (SIF)

Simulated gastric fluid (SGF) was prepared according to the method described earlier (Charteris et al. 1998). The pH of SGF was adjusted to 2.5 with 1.0 N HCl. Simulated intestinal fluid (SIF) was prepared as per the composition mentioned in US Pharmacopeia and consisted of 6.8 g/L of monobasic potassium phosphate and 10 g/L of pancreatin in sterile water. Pancreatin was used as an ingredient of SIF based on a previous report (Charteris et al. 1998). The pH of SIF was adjusted to 8.0. The target bacterial strains *E. coli* MTCC 433 and *L. monocytogenes* Scott A were grown in the respective growth medium overnight. The cells were harvested by centrifugation from a 1.0 mL aliquot of the overnight grown culture, washed twice in sterile 0.85% saline to remove media ingredients and finally resuspended (10^6 CFU) in separate sets in either SGF or SIG. The cells were treated with varying concentrations of C1 (4.0 µM, 8.0 µM, 12 µM and 16 µM for *L. monocytogenes* Scott A and 15 µM, 30 µM, 45 µM and 60 µM for *E. coli* MTCC 433) at 37°C for 2 h in case of SGF and 6 h in case of SIF. During incubation, the samples were withdrawn periodically and plated to determine the percentage of viable cells as compared to control (cells suspended in either SGF or SIF alone). Triplicate samples were analyzed for both SGF and SIF, Data analysis and calculation of standard deviation was performed with Microsoft Excel 2010 (Microsoft Corporation, USA).

4.2.5. Bactericidal Activity of C1 in Simulated Body Fluid (SBF)

Simulated body fluid (SBF) was prepared as described earlier (Kukubo et al. 1990). *S. aureus* MTCC 96 and *E. coli* MTCC 433 were grown in the respective growth medium overnight. The cells were harvested by centrifugation from a 1.0 mL aliquot of the overnight grown culture, washed twice in sterile 0.85% saline to remove media ingredients and finally resuspended (10^6 CFU) in separate sets in SBF and were treated with varying concentrations of C1 (4.0 µM, 8.0 µM, 12 µM and 16 µM for *S. aureus* MTCC 96 and 15 µM, 30 µM, 45 µM and 60 µM for *E. coli* MTCC 433) at 37°C for 24 h. During incubation, the samples were withdrawn periodically and plated to determine the percentage of viable cells as compared to control (cells suspended in SBF). Triplicate

samples were analyzed for both the cases. Data analysis and calculation of standard deviation was performed with Microsoft Excel 2010 (Microsoft Corporation, USA).

4.2.6. Bactericidal Activity of Gentamicin and Erythromycin in Combination with C1

To determine the potential of C1 as a therapeutic adjuvant, the bactericidal activity of gentamicin and erythromycin in combination with the amphiphile was ascertained against *S. aureus* MTCC 96 and *E. coli* MTCC 433, respectively. Initially a 10 µL aliquot of bacterial cell suspension (10^6 CFU of the respective target bacteria suspended in sterile PBS) were inoculated in separate sets into sterile microtitre plate wells having requisite growth media (100 µL) incorporated with a serial two-fold dilution of either gentamicin (1.0 µM - 4.0 µM) or erythromycin (7.5 µM - 30 µM). The concentrations of the antibiotics used in these experiments were manifold below the MICs against the respective target bacteria. For every concentration of gentamicin or erythromycin, varying concentrations of C1 was used in combination, depending upon the MIC of the amphiphile for the respective target bacterial strains. In the combination experiments, the concentrations of C1 used were 1.0 µM and 2.0 µM in case of *S. aureus* MTCC 96, whereas in case of *E. coli* MTCC 433 the concentrations of C1 were 5.0 µM and 10 µM. The cells were incubated at 37°C and 180 rpm for 12 h. Bacterial growth was estimated by measuring absorbance at 600 nm in a microtitre plate reader (Infinite M200, TECAN, Switzerland) and expressed as percentage growth inhibition compared to untreated cells (cells grown in the absence of antibiotics and C1). In separate sets, the effect of varying concentrations of the antibiotics or C1 alone on the growth of target bacteria was also ascertained. For every sample, three independent experiments were performed, each having three replicas. Fold decrease in the MIC of gentamicin and erythromycin in presence of C1 were compared with that obtained in the absence of the amphiphile. Data analysis and calculation of standard deviation was performed with Microsoft Excel 2007 (Microsoft Corporation, USA). The interaction of C1 and the antibiotics was quantified and expressed as the fractional inhibitory concentration (FIC) index.

FIC index was determined using the following expression:

$$FIC = \frac{[A]}{MIC_A} + \frac{[B]}{MIC_B}$$

where MIC_A and MIC_B represent the MIC of drug A (gentamicin or erythromycin) and drug B (C1), respectively. [A] and [B] are the MIC of drug A and drug B when used in combination. The interaction was interpreted as synergy (FIC ≤ 0.5), addition (FIC > 0.5 to 1.0), indifference (FIC >1.0 to <4.0) and antagonism (FIC ≥ 4.0) following the method described earlier (Giacometti et al. 2000).

4.2.7. In Vitro Resistance Against Gentamicin in Presence of C1

Development of spontaneous *in vitro* resistance in *S. aureus* MTCC 96 against gentamicin alone or gentamicin in presence of C1 were essentially determined by following a standard method described earlier (Locher et al. 2014). In case of gentamicin alone, *S. aureus* MTCC 96 was treated with various levels of the antibiotic, which corresponded to 2 × MIC - 16 × MIC (32 µM-256 µM) and the *in vitro* resistance against the antibiotic was ascertained in a multi-step experiment as described earlier in section 2.2.9. In case of the combination experiment, the concentration of the amphiphile C1 was 2.0 µM, whereas gentamicin was used at levels, which corresponded to 2 × MIC - 16 × MIC of the antibiotic in combination (8.0 µM-64 µM). Subsequently, the *in vitro* resistance of *S. aureus* MTCC 96 cells against gentamicin in presence of C1 was determined in a multi-step experiment as described earlier in section 2.2.9. The spontaneous resistance frequency (SRF) was calculated using the following expression:

$$\text{Spontaneous Resistance Frequency (SRF)} = \frac{\text{No. of colonies from compound treated sample}}{\text{No. of colonies from untreated sample}}$$

4.2.8. Cytotoxicity of Antibiotics in Combination with C1

The cytotoxic effect of C1 in combination with common antibiotics was determined on human embryonic kidney cells line (HEK 293 cells) by a standard MTT assay. Prior to the MTT assay, the cells were grown in a 25 cm^2 tissue culture ask in Dulbecco's modified

Eagle medium (DMEM) supplemented with 10% (v/v) fetal bovine serum (FBS), penicillin (100 mg/mL) and streptomycin (100 mg/mL) at 37°C in a CO_2 incubator under a humidified atmosphere of 5% CO_2. Cells were subsequently seeded onto 96-well tissue culture plates at a density of 10^4 cells per well and incubated with varying concentrations of C1 (1.0 µM or 2.0 µM) in combination with gentamicin (1.0 µM, 2.0 µM, 4.0 µM) or C1 (5.0 µM or 10 µM) in combination with erythromycin (5.0 µM, 10 µM, 20 µM) in DMEM, for a period of 24 h in a CO_2 incubator under 5% CO_2. Untreated cells as well as cells treated with the antibiotics singularly were also incubated in parallel sets. Following incubation, the medium was aspirated and fresh DMEM containing MTT solution was added to the wells. The plates were further incubated for 4 h at 37°C. Subsequently, the supernatant was carefully aspirated and the insoluble formazan product was solubilized in DMSO and its absorbance was measured with a microtitre plate reader (Infinite M200, TECAN, Switzerland) at 550 nm. The MTT assay was performed in six sets for each sample. Data analysis and determination of standard deviation were performed with Microsoft Excel 2007 (Microsoft Corporation, USA). In the MTT assay, the absorbance obtained for untreated cells was assumed to represent 100% cell viability, and the absorbance for other samples was compared to that obtained for untreated cells in order to determine % cell viability.

4.3. Results and Discussion

4.3.1. Bactericidal Activity of C1 in Simulated Fluids

Pathogenic bacteria are highly robust and are known to endure various harsh environment. This tenet is validated by gastrointestinal pathogens, which display a remarkable adaptation and are capable of surviving in the harsh niche prevalent in the stomach and the intestine. Owing to the highly acidic pH, the human gastric fluid is thought to be a defense barrier against enteric pathogens (Tamplin 2005). However, many enteric pathogens are empowered to prevail in the acidic milieu of the stomach and subsequently colonize the intestine (Foster, 1999; Foster, 2004; Cotter et al., 2000; Bavaro, 2009; Richard and Foster, 2004). In addition, the challenge in the elimination of acid-resistant pathogenic bacteria lies in the fact that therapeutic agents including certain antibiotics are liable to become inactive in the acidic milieu (Lamp et al. 1992; Mercier et al. 2002; Merrell and Camilli 2002). Given the potent bactericidal activity of C1 and in order to strengthen the scope of the amphiphile as a therapeutic antibacterial, it was pertinent to ascertain its bactericidal efficacy in physiologically relevant fluids such as SGF and SIF. To this end, cells of *E. coli* MTCC 433 and *L. monocytogenes* Scott A were suspended in SGF (pH 2.0) and subjected to treatment varying concentrations of C1 for 2 h. An assay period of 2 h was relevant in the context of gastric transit (Gordon et al., 1993). The essential observation in these experiments was that there was a decrease in the cell viability for both the target bacteria (Figure 4.1A-B). In SGF, a time-dependent decrease in cell viability was also observed upon treatment with C1 (Figure 4.1A-B). It may be mentioned here that when the target bacterial cells were incubated in SGF alone for 2 h, there was only a one log reduction in the cell viability (Figure 4.1A-B), which indicated that the reduced viability of C1-treated target bacteria in SGF could not be attributed to the acidic pH of SGF per se. Interestingly, the potent bactericidal activity of the amphiphile C1 was observed to be retained even in simulated intestinal fluid. However, the reduction in the viability of the target bacteria treated with C1 was comparatively marked in SIF as compared to SGF (Figure 4.1C-D). For instance, at the highest tested concentration of the amphiphile, the viable cell numbers for *L. monocytogenes* Scott A as well as *E. coli* MTCC 433 reduced dramatically and was observed to be around 2.0 log CFU following 6 h of incubation in SIF. It may be mentioned here that the antibacterial activity of the amphiphile C1 was also conserved in a

simulated body fluid (SBF) (Appendix Figure A4.1). Collectively, retention of the antibacterial activity of C1 in various simulated and physiologically relevant fluids enhances the therapeutic potential of the amphiphilic material. In future, it would perhaps be pertinent to consolidate these findings in *in vivo* infection models.

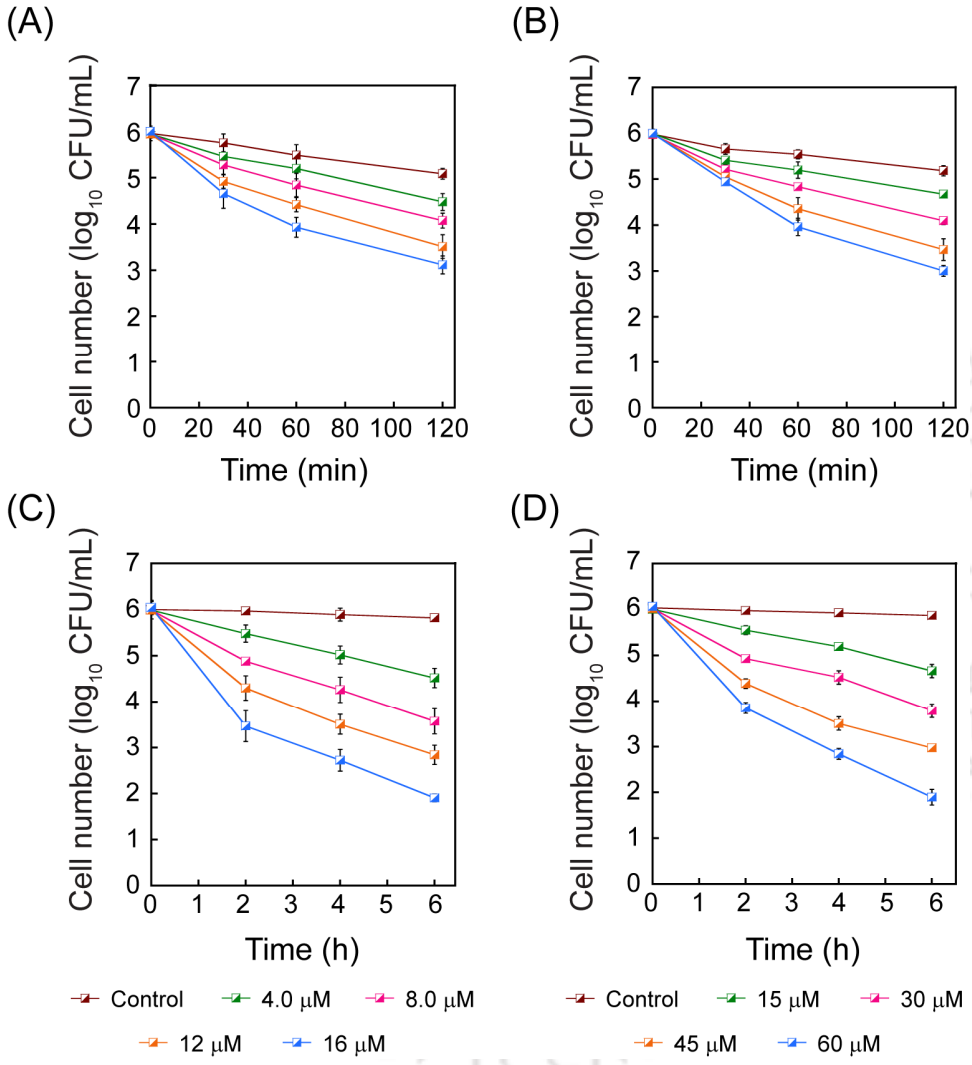

Figure 4.1. Antibacterial activity of C1 against (A) *L. monocytogenes* Scott A and (B) *E. coli* MTCC 433 cells incubated in simulated gastric fluid. Bactericidal activity of C1 against (C) *L. monocytogenes* Scott A and (D) *E. coli* MTCC 433 cells incubated in simulated intestinal fluid.

4.3.2. Bactericidal Activity of Antibiotics in Combination with C1

The presence of an outer membrane permeability barrier in case of Gram-negative bacteria (Bolla et al. 2011; Nikaido 2003; Delcour 2009) or a thick cell wall in Gram-positive bacteria, may constitute a protective barrier (Weidenmaier and Peschel 2008; Kohler et al. 2009), which may contribute to the inherent drug resistance exhibited by pathogenic bacteria. In this regard, it has been demonstrated earlier that synthetic antibacterial agents that can breach the bacterial membrane can promote the antibiotic uptake and thereby enhance antibiotic-mediated elimination of the target bacteria (Saha et al. 2008; Goswami et al. 2013; Uday et al. 2014; Goswami et al. 2015). The initial studies conducted with the amphiphile C1 (Chapter 2) clearly indicated that the amphiphile could render extensive membrane disruption in target bacteria. This observation suggested that C1 can perhaps be exploited to breach the membrane barrier in target bacteria and render the cells susceptible to the action of therapeutic antibiotics. In order to explore this possibility, gentamicin and erythromycin were chosen as model therapeutic antibiotics and experiments were conducted to ascertain the adjuvant potential of the amphiphile C1 in order to enhance the bactericidal efficacy of these antibiotics.

Gentamicin is an aminoglycoside, which holds significant potential in the mitigation of staphylococcal infections. To this end, there are literature reports on the synergism between gentamicin and other therapeutic antibiotics such as daptomycin and vancomycin for alleviation of staphylococci mediated infections (LaPlante and Woodmansee 2009; Houlihan et al. 1997; Tsuji and Rybak 2005; Hess et al. 2014). However, gentamicin is also known to be toxic to host cells (Cosgrove et al. 2009) and hence a synergistic combination that reduces the effective killing dose of the antibiotic is desirable. Based on this rational, combinatorial treatment of *S. aureus* MTCC 96 with C1 and gentamicin was pursued. Initially, the MIC of gentamicin against *S. aureus* MTCC 96 was determined and was observed to be 16 μM. In the combinatorial assay, the growth of the target bacteria *S. aureus* MTCC 96 was only marginally inhibited upon treatment with varying concentrations of gentamicin (1.0 - 4.0 μM) in conjunction 1.0 μM C1, as opposed to treatment with the antibiotic or amphiphile alone (Figure 4.2A). However, when varying concentrations of gentamicin was combined with 2.0 μM of C1, a remarkable suppression of *S. aureus* MTCC 96 cell growth was observed, as compared to the growth observed

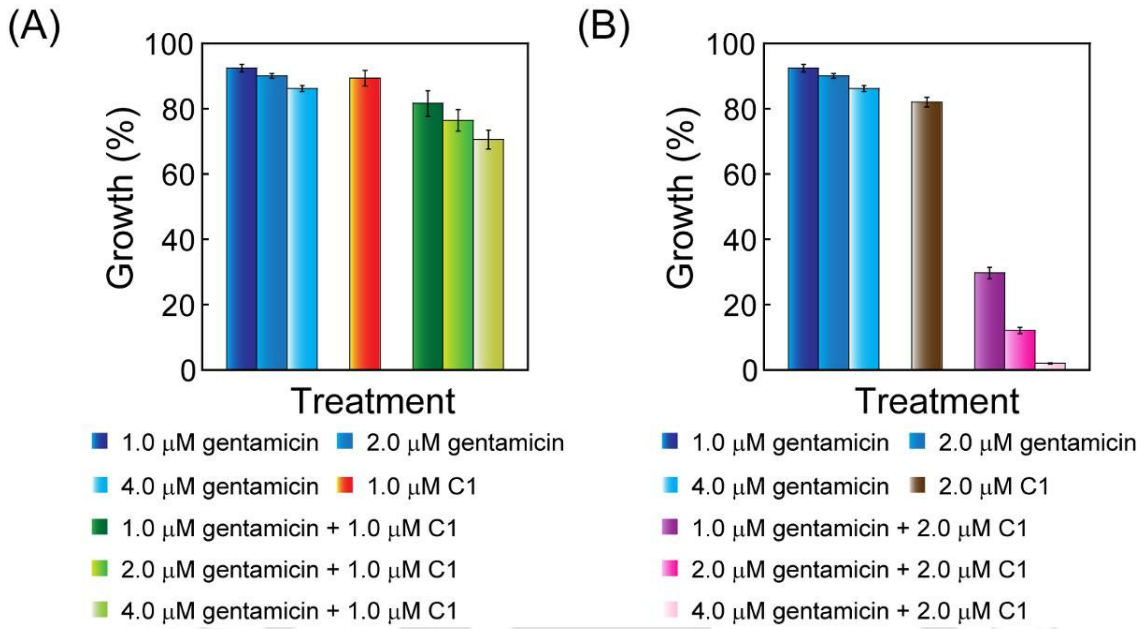

Figure 4.2. Antibacterial activity of C1 in combination with gentamicin against *S. aureus* MTCC 96 cells.

Table 4.1. Combination effect of C1 and gentamicin on *S. aureus* MTCC 96 cells.

S.No.	C1 (μM)	Gentamicin (μM)	Fold Reduction in MIC of Gentamicin	FIC Index*	Effect
1	2.0	2.0	8 ×	0.29	SYN
2	2.0	4.0	4 ×	0.416	SYN

* FIC index calculated according to Giacometti et al. 2000. SYN: Synergism.

when the cells were treated with either the antibiotic or amphiphile singularly (Figure 4.2B). This observation strongly suggested that a higher concentration of the amphiphile could significantly potentiate the activity of gentamicin against the target bacteria. It may be mentioned here that the concentration of C1 used in the combination experiments (1.0 μM or 2.0 μM) was lower than the MIC of the amphiphile for *S. aureus* MTCC 96. It was also noteworthy that in the presence of 2.0 μM of C1, the MIC of gentamicin was reduced eight-fold and a synergistic interaction was manifested between C1 and gentamicin (Table

4.1). In the backdrop of increasing concerns regarding excessive use of antibiotics and their toxic implications, it is noteworthy that in a combination therapy, C1 could significantly reduce the MIC of gentamicin and thereby facilitate elimination of *S. aureus* cells at low antibiotic concentration.

The adjuvant potential of C1 was also tested in additional experiments, wherein the amphiphile was used in combination with erythromycin against the Gram-negative *E. coli* MTCC 433. In case of erythromycin, it is acknowledged that the uptake of the antibiotic in target cells may be hampered due to the presence of an outer membrane permeability barrier in Gram-negative bacteria (Saha et al. 2008; Rawlinson et al. 2010; Choi and Lee 2012: Ulvatne et al. 2001). Hence, it was conceived that the membrane-targeting activity of C1 can perhaps be leveraged to potentiate the uptake of erythromycin and subsequent annihilation of the target *E. coli* cells. The combinatorial assays indicated that treatment with varying concentrations of erythromycin (7.5 μM - 30 μM) singularly resulted in only a marginal growth inhibition, while treatment of the target cells with erythromycin in combination with 5.0 μM C1 resulted in a higher degree of growth inhibition of *E. coli* MTCC 433 cells (Figure 4.3A). Interestingly, when a higher concentration of C1 (10 μM) was used in combination with erythromycin, a remarkable growth inhibition of *E. coli* MTCC 433 cells was manifested as opposed to treatment with either the antibiotic or amphiphile alone (Figure 4.3B). It may be mentioned here that the concentration of both C1 and erythromycin used in the combination experiments were lower than their respective MICs against *E. coli* MTCC 433. In the combination experiments, it was also noted that in the presence of 10 μM of C1, the MIC of erythromycin was reduced eight-fold and a synergistic interaction ensued between C1 and erythromycin (Table 4.2).

Table 4.2. Combination effect of erythromycin and C1 on *E. coli* MTCC 433 cells

S.No.	C1 (μM)	Erythromycin (μM)	Fold Reduction in MIC of Erythromycin	FIC Index*	Effect
1	10	15	8 ×	0.375	SYN
2	10	30	4 ×	0.5	SYN

* FIC index calculated according to Giacometti et al. 2000. SYN: Synergism

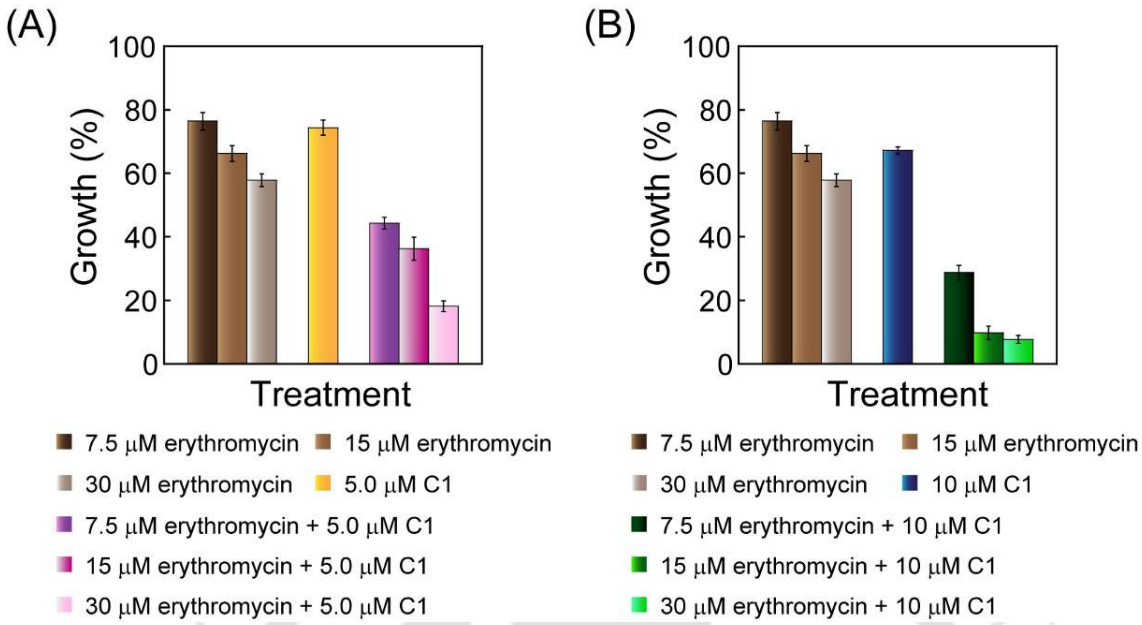

Figure 4.3. Antibacterial activity of C1 in combination with erythromycin against *E. coli* MTCC 433 cells.

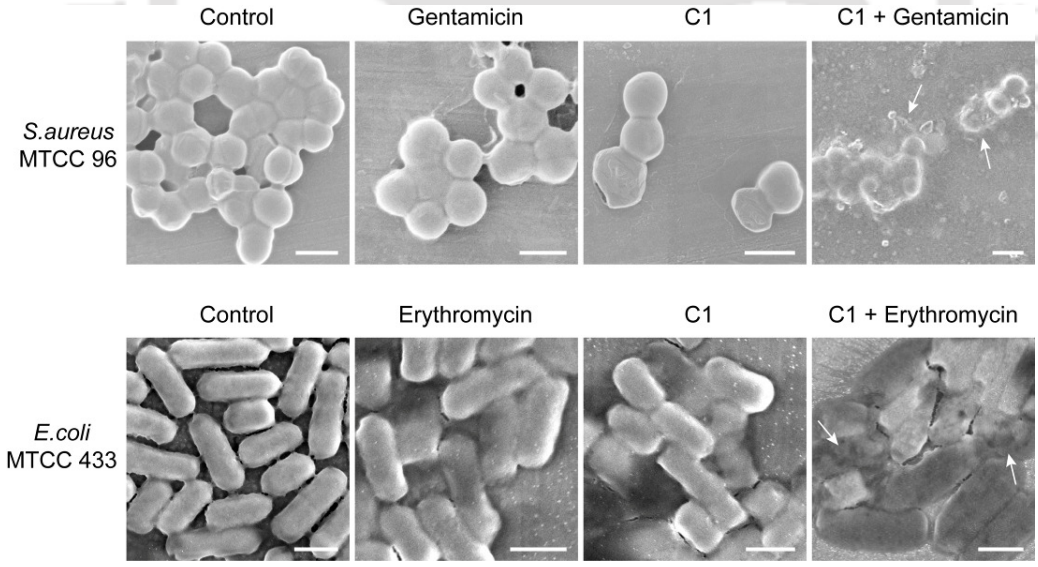

Figure 4.4. FESEM analysis of target bacterial cells subjected to a combined treatment with C1 and antibiotics. Scale bar for the images is 500 nm.

The adjuvant potential of C1 and its ability to enhance antibiotic-mediated killing of target bacterial cells could also be captured in FESEM analysis, wherein the loss of the characteristic cell morphology and the degree of cell disruption were distinctly prominent in target cells following the combinatorial treatment as compared to treatment with either the antibiotic or amphiphile alone (Figure 4.4).

4.3.3. In Vitro Resistance Development Against Gentamicin in S. aureus MTCC 96 in Combination with C1

Given that membrane-targeting agents can flout resistance development in target bacteria (Van Bambeke et al. 2008), it was pertinent to assess whether the amphiphile C1 could prevent resistance development in *S. aureus* MTCC 96 against the antibiotic gentamicin, when used in combination. To this end, a multiple step experiment was pursued to probe *in vitro* resistance development in *S. aureus* MTCC 96 cells against gentamicin. When used singularly, the MIC of gentamicin against *S. aureus* MTCC 96 was observed to be conserved (Table 4.3). However, the spontaneous resistance frequency against the antibiotic increased in every step. On the contrary, in the combination experiment, the MIC of gentamicin as well as the spontaneous resistance frequency against the antibiotic was conserved, indicating a lack of resistance development in the target bacteria against gentamicin in presence of C1.

Table 4.3. Combination effect of Gentamicin with C1 on *S. aureus* MTCC 96

Test compound	Selection step / medium	MIC (μM) / OD_{600} ± standard deviation	Spontaneous Resistance Frequency
GEN	Step 1 / agar	16 / 0.053 ± 0.004	7.14×10^{-10}
	Step 2 / agar	16 / 0.047± 0.006	3.55×10^{-8}
	Step 3 / agar	16 / 0.061 ± 0.003	8.33×10^{-8}
GEN*	Step 1 / agar	4 / 0.029 ± 0.003	5.48×10^{-10}
	Step 2 / agar	4 / 0.044 ± 0.006	5.68×10^{-10}
	Step 3 / agar	4 / 0.038 ± 0.005	1.07×10^{-10}

GEN*- gentamicin in presence of 2.0 μM of C1.

4.3.4. Cytotoxic Potential of the Combinatorial Treatment

In the context of the therapeutic potential of the combinatorial deployment of the amphiphile C1 and antibiotics for mitigation of pathogenic bacteria, it is critical that the amphiphile used in conjunction with the antibiotics should not lead to any cytotoxic effect against human cells. Hence, to evaluate the therapeutic prospect of the combinatorial regime, the cytotoxic effect of the combination of C1 and the antibiotics (at concentrations leading to bactericidal effect in combination) was determined against HEK 293 cells by a standard MTT assay. It was observed that the viability of cultured HEK 293 cells was nearly 95% in the presence of 2.0 μM C1 in conjunction with 4.0 μM gentamicin and about 89% in the presence of 10 μM C1 and 30 μM erythromycin (Figure 4.5). The cytotoxicity assay thus clearly revealed that at the tested concentrations of the amphiphile and the antibiotics, the combinatorial treatment regimen against the target bacteria was non-toxic. This observation highlighted the merit of deploying the amphiphilic molecule C1 as an adjuvant for antibacterial therapy.

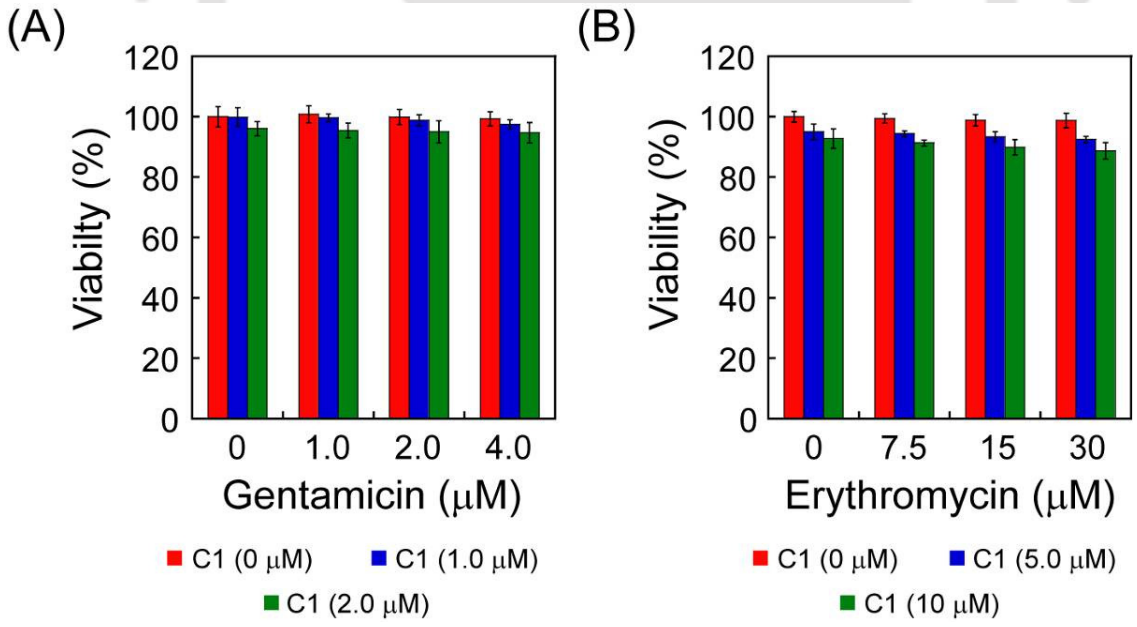

Figure 4.5. MTT assay to ascertain the effect of C1 in combination with either (A) gentamicin or (B) erythromycin on HEK 293 cells. Each data point represents mean ± standard deviation from six samples.

4.4. Significant Findings

The salient findings of this chapter are as follows:

1. The bactericidal activity of the synthetic amphiphile C1 was retained even in the complex milieu of the tested simulated fluids such as SGF, SIF and SBF, which suggested that the amphiphile was stable in physiologically relevant fluids and thus holds potential in mitigation of *in vivo* bacterial infection.

2. In the combinatorial treatment assays, the amphiphile at low concentrations could bring about a significant reduction in the MIC of model therapeutic antibiotics against target bacteria and a synergistic interaction was evident between the amphiphile and the antibiotics.

3. The beneficial adjuvant effect of C1 and the remarkable enhancement in the bactericidal activity of antibiotics in presence of C1 was also evident in FESEM analysis.

4. The multistep *in vitro* resistance development studies indicated that in the combinatorial mode, the amphiphile C1 prevented resistance development against the antibiotic gentamicin as evident from the conserved MIC of the antibiotic as well as a lack of increase in the spontaneous resistance frequency (SRF) for gentamicin in *S. aureus* MTCC 96 cells.

5. The combination of the amphiphile C1 and the antibiotics, which rendered elimination of the target bacteria was found to be non-toxic in nature.

The high incidence of serious bacterial biofilm-associated infections has triggered a critical demand for anti-biofilm therapeutics. Based on the potent membrane and DNA targeting activity of C1, its adjuvant potential and retention of bactericidal activity in physiological conditions, it was conceived that the amphiphile could perhaps be explored as an antibiofilm agent. In the following chapter, the generation of C1-loaded HSA nanocarrier and its antibiofilm potential is discussed.

Chapter 5

Biofilm eDNA-Targeting Activity of C1-loaded HSA Nanocarrier (C1-HNC)

This chapter describes the development of an amphiphile-loaded HSA Nanocarrier (C1-HNC) that renders release of the amphiphilic payload in the biofilm matrix, cleaves the biofilm eDNA and concurrently targets the underlying cells resulting in irrevocable annihilation of biofilm.

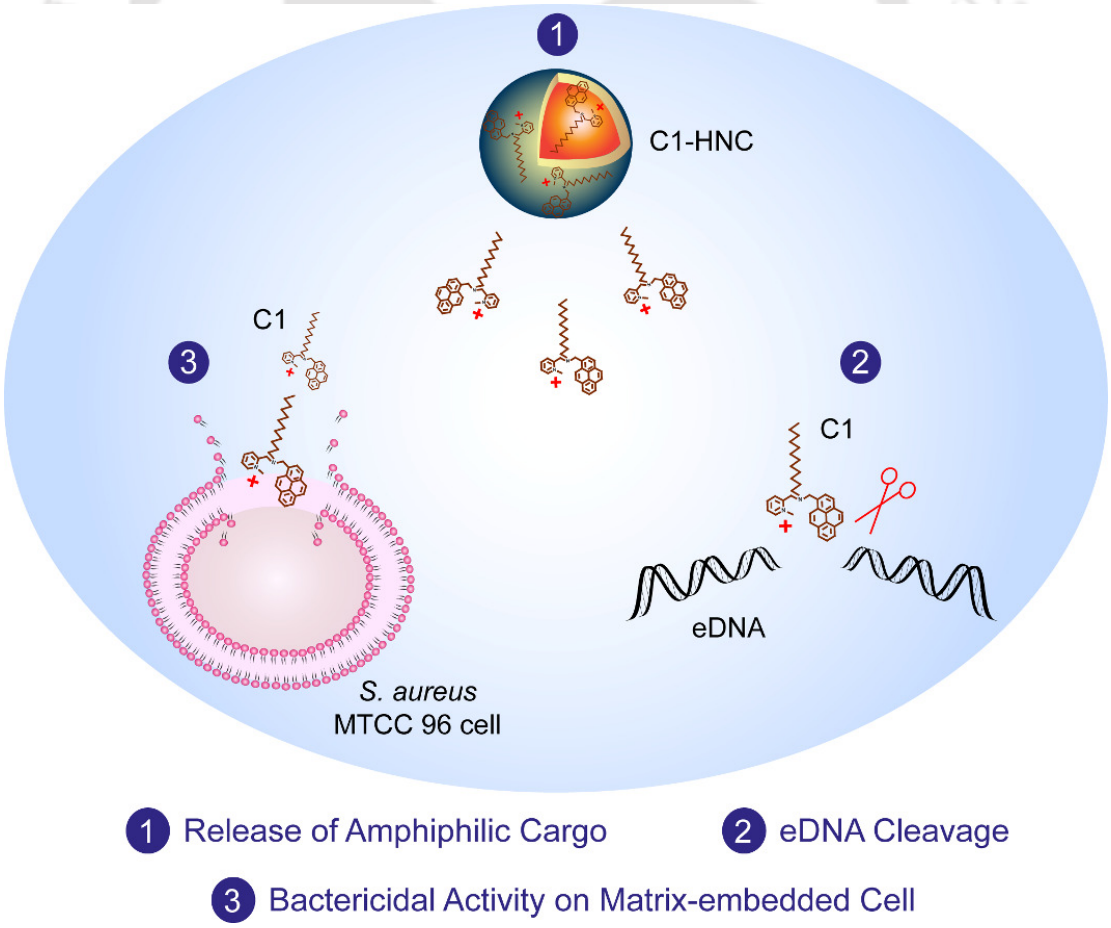

ABSTRACT

The present chapter describes the generation of a human serum albumin (HSA)-based nanocarrier loaded with the amphiphile C1 (C1-HNC) that could cleave the extracellular DNA (eDNA) of *S. aureus* MTCC 96 biofilm and annihilate the underlying cells. FESEM analysis revealed that C1-HNC was aggregated, whereas DLS analysis indicated that the major aggregated species in solution was around 156 nm in size. The loading capacity (LC) and the amount of encapsulated C1 was estimated to be nearly 12% and 184 μM, respectively, at the highest loading concentration of 400 μM. The release of C1 in *S. aureus* biofilm was higher as compared to extracted biofilm extra-polymeric substance (EPS) or media, which suggested a biofilm matrix-responsive release of the amphiphile from the nanocarrier. Interestingly, the pyrene group present in C1 facilitated a non-invasive fluorescence-based imaging of *S. aureus* biofilm niche and provided evidence for a dose-dependent elimination of biofilm by C1-HNC, which was also supported by measuring the biofilm cell metabolic activity by an MTT assay. A notable reduction of eDNA in C1-HNC treated *S. aureus* biofilm could be observed with time, analogous to the results obtained in DNase I-treated biofilm. The *S. aureus* biofilm eDNA cleavage activity of C1-HNC was also captured in a solution-based fluorescence assay using the DNA binding Hoechst dye. CT-DNA supplementation experiments could unequivocally demonstrate that recovery of *S. aureus* biofilm could not be achieved in case of treatment with C1-HNC as opposed to DNase I treatment, which indicated the superior potential of C1-HNC as an antibiofilm agent. C1-HNC could also render eradication of *S. aureus* biofilm from the surface of a model catheter and was non-toxic to HEK 293 cells in an *in vitro* MTT assay, which indicated the potential of the nanomaterial as a therapeutic antibiofilm agent.

5.1. Introduction

The prevalence of *Staphylococcus aureus* biofilm in chronic and device-associated infections in conjunction with its remarkable ability to resist the action of therapeutic antibiotics is a serious healthcare problem (Costerton et al. 1999; Otto 2008; Archer et al. 2011; Bordi and Bentzmann 2011; McCarthy et al. 2015). This crisis underscores the need for antibiofilm agents that can act on key targets and eliminate *S. aureus* biofilm. Alleviation of biofilm infection is particularly challenging, the crux being the presence of a heterogeneous matrix, which protects the underlying cells against host-mediated immunity and therapeutic antibiotics (Cue et al. 2012; Foster et al. 2014; Scherr et al. 2014). The biofilm matrix is generally a complex niche consisting of host derived factors, polysaccharide, proteins, and extracellular DNA (eDNA) (Cue et al. 2012; Foster et al. 2014; Flemming and Wingender, 2010). Based on emerging reports, it is now apparent that eDNA is a key matrix component, which is critical to bacterial biofilm formation (Whitchurch et al. 2002; Jakubovics et al. 2013; Clare and Patrick, 2010). Some of the vital functions ascribed to eDNA include cell aggregation and coordination of cell movement during biofilm formation (Das et al. 2010; Das et al. 2011; Gloag et al. 2013), resistance against antibiotics (Mulcahy et al. 2009; Chiang et al. 2013) and dissemination of genetic trait (Molin and Tolker-Nielsen 2003). In line with the view that eDNA is vital for bacterial biofilm formation and resistance development against antibiotics, the fundamental role of eDNA in *S. aureus* biofilm has also been highlighted (Izano et al. 2008; Rice et al. 2007; Mann et al. 2009).

Given that eradication of biofilm by therapeutic antibiotics is becoming difficult, the prospect of targeting eDNA is an appealing option (Okshevsky et al. 2015). In this regard, the use of the enzyme DNase for disrupting biofilm and sensitizing the matrix-embedded cells to antibiotics has gained importance (Kaplan et al. 2012). However, there are bottlenecks associated with DNase-based antibiofilm therapy. Dispersal of biofilm cells by DNase may promote acute infection if the released cells are not annihilated. To this end, the use of antibiotics in conjunction with DNase-based therapy could be a viable option. However, sub-inhibitory concentration of antibiotics in combination with a dispersal agent like DNase may promote eDNA release and biofilm formation in *S. aureus* (Kaplan et al.

2012). This calls for a novel therapeutic intervention for effective elimination of *S. aureus* biofilm.

Conceivably, a bactericidal agent that can readily invade *S. aureus* biofilm matrix, disrupt the eDNA shield, gain access and abolish the underlying cells could be an effective approach for eradication of biofilm. However, delivery of such antibacterials in the biofilm matrix at sufficiently high concentrations would be paramount. To this end, nanomaterials could be employed as delivery agents as their sub-cellular size and superior pharmacological attributes can lead to high antibiofilm activity and reduction of unwarranted side effects (Forier et al. 2014; Adhikari et al. 2013; Slomberg et al. 2013; Wang et al. 2016; Duncan et al. 2015). In addition, biodegradable nanocarriers that can invade the biofilm matrix and render a matrix-responsive sustained delivery of the antibacterial agent is desirable. In this regard, proteinaceous nanomaterials can be a rational choice, based on their proven utility as delivery agents (Shimanovich et al. 2014; Elzoghby et al. 2012; Elzoghby et al. 2012). It is also likely that such nanomaterials could render a matrix-responsive release of the antibiofilm agent, triggered by the presence of extracellular proteases in *S. aureus* biofilm matrix.

Based on the above mentioned notion, the present chapter describes the generation of a human serum albumin (HSA)-based nanoparticle loaded with the membrane and DNA-targeting amphiphile C1 and evaluates the potential of the payload nanomaterial (C1-HNC) as an antibiofilm agent.

5.2. Materials and Methods

5.2.1. Growth Media and Chemicals

Penicillin-Streptomycin solution, Brain-Heart Infusion (BHI) broth and crystal violet (CV) were purchased from HiMedia, Mumbai, India. Dimethyl sulfoxide (DMSO) and absolute ethanol were procured from Merck, Mumbai, India. N-2-hydroxyethyl piperazine N-2 ethane sulphonic acid (HEPES Buffer), calf thymus DNA (CT-DNA) and Deoxyribonuclease I (DNase I) ex Bovine Pancreas were procured from Sisco Research Laboratories SRL, Mumbai, India. Human serum albumin (HSA, Fraction V), pepsin, pancreatin, 5 (and 6)-carboxyfluorescein diacetate succinimidyl ester (cFDA-SE), propidium iodide (PI), congo red (CR), Hoechst 33258 dye, ethidium bromide (EtBr), 3-(4,5-dimethyl-2-thiazolyl)-2,5-diphenyl-2H-tetrazolium bromide (MTT), Dulbecco's Modified Eagle Medium (DMEM), trypsin–EDTA, valinomycin and bacterial genomic DNA isolation kit were procured from Sigma Aldrich Chemicals, USA. Cesium chloride purified pUC18 DNA was procured from Bangalore Genei, India. Fetal bovine serum (FBS) was procured from PAA Laboratories, USA

5.2.2. Antibiofilm Activity of C1

5.2.2.1. Microtitre Well Assay

S. aureus MTCC 96 biofilm was grown in BHI media supplemented with 0.25% glucose in sterile 96 well microtitre plate by essentially following a standard protocol described earlier (Goswami et al. 2014). Following 24 h of biofilm growth in static and humid condition at 37°C, the spent media from the microtitre plate wells was gently aspirated and the established biofilms were exposed to fresh growth media having varying concentrations of C1 (4.0 μM - 128 μM) and incubated for 24 h in a static and humid chamber at 37^{o}C. Untreated biofilms were also incubated under the same conditions as control. Subsequently the antibiofilm activity of C1 was ascertained by crystal violet binding assay, MTT assay and Congo red binding assay by following the method described previously (Goswami et al. 2014). All the experiments were performed in three independent sets and every set consisted of three replicates. Data analysis and calculation of standard deviation was performed with Microsoft Excel 2010 (Microsoft Corporation, USA).

5.2.2.2. FESEM Analysis

Glass cover slips (18 mm x 18 mm) were sterilized by immersion in sodium hypochlorite solution (0.5%) for 2 h and rinsed thoroughly with sterile MilliQ grade water. Biofilm growth on the sterilized glass cover slips was initiated by immersing them in BHI medium supplemented with 0.25% glucose taken in separate sterile 35 mm petriplate. An inoculum of *S. aureus* MTCC 96 cell suspension (A_{600} = 0.02) was added separately to each set and incubated for 24 h at 37^{o}C in a humid chamber. The glass cover slips with grown *S. aureus* biofilm was transferred to fresh requisite medium (BHI medium supplemented with 0.25% glucose) incorporated with C1 (corresponding to 128 µM C1) and incubated at 37^{o}C in a humid chamber for 24 h. The C1-treated samples as well as control samples (48 h grown untreated biofilm) were washed twice with sterile PBS to remove spent media and finally with sterile MilliQ grade water. The samples were then air-dried in laminar hood and examined in a field emission scanning electron microscope (Zeiss Sigma, USA) at 1.5-3.0 kV and their images were recorded.

5.2.2.3. Fluorescence Microscope Analysis

S. aureus MTCC 96 biofilm was grown in sterile 96 well microtitre plate as mentioned earlier (Goswami et al. 2014). The biofilm samples were then treated in separate sets with varying concentrations of C1 (16 µM, 64 µM and 128 µM C1) for 24 h. Subsequently, untreated biofilm samples (control) as well as C1-treated biofilm samples were subjected separately to cFDA-SE and Congo red staining by following a standard procedure described previously (Goswami et al. 2014). The stained biofilms were then observed under a fluorescence microscope (Eclipse Ti-U, Nikon) with a filter that allowed blue light excitation for cFDA-SE and green light excitation for Congo red stained biofilm. Images of the treated and control biofilms were recorded. Biofilm imaging experiments were performed in three independent sets wherein each set comprised of three replicates. For every sample, images were recorded from three different fields

5.2.2.4. Minimum Biofilm Eradication Concentration ($MBEC_{90}$) of C1

S. aureus MTCC 96 biofilm was grown in BHI media supplemented with 0.25% glucose in sterile 96 well microtitre plate by essentially following a standard protocol described

earlier (Goswami et al. 2014). After 24 h of biofilm growth in static and humid condition at 37°C, the spent media from the microtitre plate wells was gently aspirated and the established biofilms were exposed to fresh growth media having varying concentrations of C1 (4.0 µM - 128 µM) and incubated for 24 h in a static and humid chamber at 37°C. Untreated biofilms were also incubated under the same conditions as control. Subsequently the media was removed and wells were washed with 200 µL sterile phosphate buffered saline (PBS) to remove non-adherent bacterial cells. The wells were air dried and 1% (v/v) crystal violet solution (150 µL) was added to each well and incubated for 45 min to stain the biofilm. The crystal violet stain incorporated by biofilms was solubilized with 95% ethanol (200 µL) and the biofilm biomass was estimated by transferring the ethanol-solubilized dye solution from each well into fresh well and measuring absorbance at 590 nm in a microtiter plate reader (Infinite M200, TECAN, Switzerland). The minimum biofilm eradication concentration ($MBEC_{90}$) for C1 was determined as the concentration, which resulted in 90% reduction in biofilm biomass as compared to untreated control sample. All the experiments were performed in three independent sets and every set consisted of three replicates. Data analysis and calculation of standard deviation was performed with Microsoft Excel 2010 (Microsoft Corporation, USA).

5.2.3. Amphiphile-loaded Nanomaterial (C1-HNC)

HSA nanoparticles (HNPs) were initially generated by following a previously described desolvation method (Goswami et al, 2014). For generation of C1-loaded HSA nanocarrier (C1-HNC), HNPs (1.0 mg/mL in sterile MilliQ water, pH titrated to 8.2) were interacted overnight with varying concentrations of C1 (10 µM - 400 µM) on a rocker at room temperature. Following incubation, the solution was centrifuged at 7,000 × g for 3 min. The pellet representing C1-HNC was resuspended in sterile MilliQ water (pH titrated to 8.2). Aliquots of HNP and C1-HNC were added separately onto clean sterile cover slip, air-dried in a laminar hood and examined in a field emission scanning electron microscope (Zeiss Sigma, USA). For estimation of particle size, C1-HNC loaded with 175 µM of C1 (1.0 mg/mL HNPs having a final concentration of 175 µM C1) was dispersed in 1.0 mL of sterile MilliQ water. A 0.1 mL aliquot of this solution was further diluted to 1.0 mL in sterile MilliQ water and subjected to particle size estimation by DLS (Zeta Sizer, Malvern,

U.K.). In a separate set, HNPs (1.0 mg/mL in sterile MilliQ water) and C1 (175 μM) were also diluted ten-fold in sterile MilliQ water and subjected to DLS analysis. All the experiments were performed in three independent sets and every set consisted of three replicate. UV-visible spectra of HSA, HNPs, C1 and C1-HNC were recorded in a spectrophotometer (CARY 300 Bio, Varian). FT-IR spectra of HSA, C1, HNPs and C1-HNC were also recorded in KBr pellets at 4.0 cm^{-1} resolution in an infrared spectrometer (Spectrum One, Perkin-Elmer). Eight scans were performed for every sample in the range of 4000 cm^{-1} to 500 cm^{-1}. A background spectrum for pure KBr was also measured.

5.2.4. Loading Capacity (LC) and Encapsulation of C1

Initially the fluorescence emission spectra of varying concentrations of C1 (0.2 μM - 3.0 μM) was recorded in a spectrofluorometer (FluoroMax-4, HORIBA) at an excitation wavelength of 340 nm. The fluorescence emission intensity of C1 at 376 nm was recorded to generate a standard curve, which was subsequently used for estimation of loading capacity (LC) and encapsulated C1. For estimation of LC, HNPs (1.0 mg/mL in sterile MilliQ water) were interacted with varying concentrations of C1 (10.0 μM - 400 μM) for 12 h on a rocker at room temperature. Following incubation, the solution was centrifuged at 7,000 × g for 3 min. The pellet, which represents C1-HNC was resuspended in sterile MilliQ water. The concentration of free C1 in the supernatant was determined using the previously generated calibration curve for the amphiphile. The loading capacity (LC) was determined using a standard calculation and was expressed in percentage (Goswami et al. 2014). All the experiments were performed in three independent sets and every set consisted of three replicates. Data analysis and calculation of standard deviation was performed with Microsoft Excel 2010 (Microsoft Corporation, USA).

5.2.5. In Vitro Release Kinetics of C1 from C1-HNC

C1-HNC having a final concentration of 175 μM C1 (1.0 mg/mL HNPs loaded with a final concentration of 175 μM C1) was dispersed in separate sets in 1.0 mL each of 10 mM HEPES buffer (pH 7.4), simulated gastric fluid (SGF), simulated intestinal fluid (SIF) and simulated body fluid (SBF). The composition of SGF, SIF and SBF were as described previously (Mukherjee et al. 2013; Kokubo et al. 1990). The samples were incubated in an

orbital shaker at 120 rpm and 37°C. At specific time intervals (3 h, 6 h, 12 h, 24 h, 48 h, and 72 h) the samples were withdrawn and centrifuged at 7,000 × g for 3 min. The supernatant from various samples were transferred into a fresh microcentrifuge tube and fluorescence emission spectra of the solutions were measured in a spectrofluorometer (FluoroMax-4, HORIBA) at an excitation wavelength of 340 nm. The emission intensity of the samples at 376 nm and a previously generated calibration curve for C1 was used to measure the quantity of C1 released from C1-HNC at specific time periods and expressed as % cumulative release. A cumulative release of 100% corresponds to 175 µM of released C1 (equivalent to initial loading concentration of C1 in C1-HNC). All the experiments were performed in three independent sets and every set consisted of three replicates.

5.2.6. Matrix-responsive Release of C1 from C1-HNC in Biofilm and Extracted EPS

To estimate the release of the amphiphile in biofilm, C1-HNC having a final concentration of 175 µM C1 (1.0 mg/mL HNPs loaded with a final concentration of 175 µM C1) was added to 24 h pre-grown *S. aureus* MTCC 96 biofilm in fresh BHI media supplemented with 0.25% glucose. The samples were incubated in static and humid condition at 37°C. At specific time intervals (3 h, 6 h, 12 h, 24 h, 48 h, and 72 h) the spent media was carefully aspirated without disturbing the biofilm samples and centrifuged at 7,000 × g for 3 min. Subsequently the supernatant was diluted with MilliQ water and fluorescence emission spectra of the solutions were measured in a spectrofluorometer (FluoroMax-4, HORIBA) at an excitation wavelength of 340 nm. Considering the background emission from the media, the corrected emission intensity of the samples at 376 nm and a previously generated calibration curve for C1 was used to measure the quantity of C1 released from C1-HNC at specific time periods and expressed as % cumulative release. To ascertain the matrix-responsive release of C1, the experiments were performed in three independent sets and every set consisted of three replicates.

In a separate set of experiment, *S. aureus* MTCC 96 biofilm was grown in BHI media supplemented with 0.25% glucose in sterile 96 well microtitre plate by essentially following a standard protocol described earlier (Goswami et al. 2014). After 24 h of biofilm growth in static and humid condition at 37°C, the spent media from the microtitre plate wells was gently aspirated without disturbing the biofilm. The biofilm samples in the

well were washed with sterile PBS by gentle pipetting, and then biofilm samples in each well were resuspended in 200 µL sterile PBS solution by scraping the bottom and wall of the wells by the pipette tip. Multiple samples from different wells were processed as mentioned and pooled together for EPS extraction. The pooled samples were filtered through 0.22 µm filter (Pall Corporation, USA) and the filtrate was considered as biofilm EPS. To estimate the release of the amphiphile in biofilm EPS, C1-HNC having a final concentration of 175 µM C1 (1.0 mg/mL HNPs loaded with a final concentration of 175 µM C1) was added to extracted biofilm EPS. The samples were incubated in static and humid condition at 37^{o}C. At specific time intervals (3 h, 6 h, 12 h, 24 h, 48 h, and 72 h) samples were withdrawn and centrifuged at 7,000 × g for 3 min. Subsequently the supernatant was diluted with MilliQ water and fluorescence emission spectra of the solutions were measured in a spectrofluorometer (FluoroMax-4, HORIBA) at an excitation wavelength of 340 nm. Considering the background emission from the media, the corrected emission intensity of the samples at 376 nm and a previously generated calibration curve for C1 was used to measure the quantity of C1 released from C1-HNC at specific time periods and expressed as % cumulative release. Likewise, release of the amphiphile from C1-HNC incubated in biofilm media alone was estimated. In order to measure the release of C1 in biofilm EPS and media, the experiments were performed in three independent sets and every set consisted of three replicates. Fluorescence-based images of the vials containing released C1 in biofilm and media alone were also captured under UV illumination.

5.2.7. Biofilm Imaging with C1-HNC

S. aureus MTCC 96 biofilm was grown in BHI media supplemented with 0.25% glucose in sterile 96 well microtitre plate by essentially following a standard protocol described earlier (Goswami et al. 2014). After 24 h of biofilm growth in static and humid condition at 37^{o}C, the spent media from the microtitre plate wells was gently aspirated. In separate sets of the established biofilms, fresh growth media were added having varying concentrations of C1-HNC (corresponding to 16 µM and 128 µM C1, respectively) and incubated for 24 h in a static and humid chamber at 37^{o}C. Subsequently the media was removed and wells were washed with 200 µL sterile PBS to remove non-adherent bacterial

cells. The samples were then observed under a fluorescence microscope (Eclipse Ti-U, Nikon, USA) under UV, blue and green excitation. Images of the treated biofilm were recorded under each excitation. Biofilm imaging experiments were performed in three independent sets wherein each set comprised of three replicates. For every sample, images were recorded from three different fields.

5.2.8. Antibiofilm Activity of C1-HNC

5.2.8.1. Microtitre Well Assay

S. aureus MTCC 96 biofilm was grown in BHI media supplemented with 0.25% glucose in sterile 96 well microtitre plate by essentially following a standard protocol (Goswami et al. 2014). After 24 h of biofilm growth in static and humid condition at 37^{o}C, the spent media from the microtitre plate wells was gently aspirated and the established biofilms were exposed to fresh growth media having varying concentrations of C1-HNC (corresponding to 4.0 µM, 8.0 µM, 16 µM, 32 µM, 64 µM and 128 µM of C1) and incubated for 24 h in a static and humid chamber at 37^{o}C. Untreated biofilm as well as HNP-treated biofilm were also incubated under the same conditions as control. Subsequently the media was removed and the wells were washed with 200 µL sterile phosphate buffered saline (PBS) to remove non-adherent bacterial cells. The wells were air dried and then the metabolic activity of biofilm cells and estimation of the biofilm biomass were pursued in separate sets by performing an MTT assay and crystal violet binding assay, respectively (Goswami et al., 2014). All the experiments were performed in three independent sets and every set consisted of three replicates. Data analysis and calculation of standard deviation was performed with Microsoft Excel 2010 (Microsoft Corporation, USA) and a one way analysis of variance (ANOVA) was performed using Sigma Plot.

5.2.8.2. FESEM Analysis

S. aureus MTCC 96 biofilm was grown on cover slips as mentioned before in section 5.2.2.2. The glass cover slips with established *S. aureus* biofilm was transferred to fresh requisite medium (BHI medium supplemented with 0.25% glucose) incorporated with C1-HNC (corresponding to 128 µM C1) and incubated at 37^{o}C in a humid chamber for 24 h. The C1-HNC-treated samples as well as control samples (48 h grown untreated biofilm)

were washed twice with sterile PBS to remove spent media and finally with sterile MilliQ grade water. The samples were then air-dried in laminar hood and examined in a field emission scanning electron microscope (Zeiss Sigma, USA) at 1.5-3.0 kV and their images were recorded.

5.2.8.3. Fluorescence Microscope Analysis

S. aureus MTCC 96 biofilm was grown in sterile 96 well microtitre plate following a standard procedure (Goswami et al. 2014). The biofilm samples were then treated in separate sets with varying concentrations of C1-HNC (corresponding to 16 µM, 64 µM and 128 µM C1) for 24 h. Subsequently, untreated biofilm samples (control) as well as C1-HNC-treated biofilm samples were subjected separately to cFDA-SE and Congo red staining by following a standard procedure described previously (Goswami et al. 2014). The images of the treated and control biofilms were recorded in fluorescence microscope using the conditions described in section 5.2.2.3. Biofilm imaging experiments were performed in three independent sets, each set consisting of three replicates. For every sample, images were recorded from three different fields.

5.2.9. Biofilm eDNA Cleavage Activity of C1-HNC

5.2.9.1. Time-dependent Biofilm eDNA Cleavage

S. aureus MTCC 96 biofilm was grown for 24 h in sterile 96 well microtitre plate following a standard procedure (Goswami et al. 2014). Subsequently the spent media was carefully aspirated and the biofilm was treated with C1-HNC (corresponding to a C1 concentration of 128 µM), DNase I (16 µg /mL) or HNPs (700 µg /mL) in separate sets. Following incubation of the samples for various time periods (3 h, 6 h, 12 h, 18 h and 24 h), the spent media from the microtitre plate wells of the treated samples was gently aspirated. The biofilm samples in the well were then washed with sterile PBS by gentle pipetting, and then biofilm samples in each well were resuspended in 200 µL sterile PBS solution by gently scraping the bottom and wall of the wells by the pipette tip. Multiple samples from different wells were processed as mentioned, pooled together and treated with Proteinase K (5.0 µg /mL) for 30 minutes under shaking condition at 37°C. The sample was then filtered through 0.22 µm filter (Pall Corporation, USA). Biofilm eDNA

present in the filtrate was then purified by loading onto a DNA extraction column provided with the bacterial genomic DNA isolation kit (Sigma-Aldrich, USA) and following the manufacturer instruction. The purity of biofilm eDNA was ascertained by A_{260}/ A_{280} ratio. The extracted pure biofilm eDNA from all the treated samples were then subjected to agarose gel electrophoresis. Following electrophoresis, the gel was stained with EtBr solution and the DNA bands were visualized in a gel documentation system (Gel Doc XR + System, Bio-Rad). To ascertain eDNA cleavage, quantification of band intensity was accomplished by ImageJ analysis (http://rsb.info.nih.gov/ij/).

5.2.9.2. Solution-based eDNA Cleavage Studies

Biofilm eDNA from a 24 h grown *S. aureus* MTCC 96 biofilm was initially purified using the method described previously. Subsequently, 0.5 µM of purified eDNA was incubated with 25 nM of Hoechst 33258 dye in DNAse I buffer (50 mM Tris.HCl, pH 7.5 supplemented with 10 mM $MgCl_2$) under shaking conditions at 37°C for 30 min. To this solution, C1-HNC (corresponding to 25 nM of C1) was added and fluorescence emission spectra of the mixture was measured at 455 nm in scan mode for every 3 min for a period of 1 h at an excitation wavelength of 350 nm. The fluorescence emission intensity of 25 nM C1-HNC alone under the same conditions was also measured and used to calculate the corrected fluorescence emission intensity. In an analogous control experiment, *S. aureus* MTCC 96 biofilm eDNA cleavage in solution by DNase I (1.0 µg /mL) was also determined. All the experiments were performed in three independent sets and every set consisted of three replicates.

5.2.9.3. Cleavage of eDNA in Biofilm EPS by C1-HNC

S. aureus MTCC 96 biofilm EPS was initially extracted by following the procedure described in section 5.2.6. Subsequently, 20 % v/v of *S. aureus* biofilm EPS was interacted in separate sets with C1-HNC (corresponding to 7.5 µM, 15 µM, 22.5 µM and 30 µM of C1) for 1 h and analyzed by agarose gel electrophoresis. In parallel sets, 60 µM of pUC18 plasmid DNA alone or 60 µM of pUC18 plasmid DNA spiked into 20% v/v of *S. aureus* MTCC 96 biofilm EPS was also treated with the same concentrations of C1-HNC and analyzed by agarose gel electrophoresis. Following electrophoresis, the gel was stained

with EtBr solution and the DNA bands were visualized in a gel documentation system (Gel Doc XR + System, Bio-Rad). To determine DNA cleavage by C1-HNC, quantification of band intensity was accomplished by ImageJ analysis (http://rsb.info.nih.gov/ij/)d

5.2.10. Comparison of Antibiofilm Activity of C1-HNC and DNase I by CT-DNA Supplementation Experiments

S. aureus MTCC 96 biofilm grown in microtitre well plate was treated in separate sets with varying concentrations of C1-HNC (corresponding to 4.0 µM, 8.0 µM, 16 µM, 32 µM, 64 µM and 128 µM of C1) for 24 h. Following treatment, the spent media was gently aspirated from the wells and in one set fresh BHI medium having 0.25% glucose was added while in the other set CT-DNA solution (10 µg /mL) made in fresh BHI medium having 0.25% glucose was added to each well. Following 24 h incubation at 37°C in a static humid chamber the biofilm cell metabolic activity in all the samples was quantified using MTT assay as described previously. Biofilm cell metabolic activity was expressed with respect to untreated biofilm. In an analogous experiment, the effect of CT-DNA supplementation on *S. aureus* MTCC 96 biofilm treated with varying concentrations of DNase I (0.5 µg /mL, 1.0 µg /mL, 2.0 µg /mL, 4.0 µg /mL, 8.0 µg /mL and 16 µg /mL) was also ascertained. All the experiments were performed in three independent sets and every set consisted of three replicates.

The effect of CT-DNA supplementation on the viability of C1-HNC or DNase I-treated *S. aureus* MTCC 96 biofilm was also evaluated by fluorescence microscopic analysis using Hoechst 33258 dye as well as cFDA-SE staining. Following treatment of the samples with either C1-HNC or DNase I, the media was gently removed and wells were washed with 200 µL sterile PBS to remove non-adherent bacterial cells. Finally the samples were either incubated with Hoechst 33258 dye prepared in sterile PBS (final concentration 10 µg/mL) for 20 min at 37°C or cFDA-SE (final concentration of 50 µM) for 20 min at 37°C. The samples were then observed in a fluorescence microscope (Eclipse Ti-U, Nikon, USA) either under UV excitation for Hoechst staining or blue excitation for cFDA-SE staining and the images of the biofilm samples were recorded. Fluorescence-based biofilm imaging experiments were performed in three independent sets wherein each

set comprised of three replicates. For every sample, images were recorded from three different fields.

5.2.11. Eradication of Biofilm from Catheter Surface

Biofilm of *S. aureus* MTCC 96 was grown over Foley's urinary catheter as described in an earlier study (Goswami et al. 2014). The catheter segments colonized with *S. aureus* biofilm were transferred to separate sterile tissue culture petridish containing fresh media incorporated with varying concentrations of C1-HNC (corresponding to 4.0 µM, 8.0 µM, 16 µM, 32 µM, 64 µM and 128 µM of C1) and incubated for 24 h. The catheter segments were then harvested, gently rinsed in sterile PBS and subjected to MTT assay as described previously (Goswami et al. 2014). Each assay was performed in three independent sets and every set included three replicates. For FESEM analysis, catheter segments with pre-grown *S. aureus* MTCC 96 biofilm were incubated in separate sets in fresh requisite media incorporated with C1-HNC (corresponding to 128 µM C1) for 24 h. Following treatment, the catheter segments were gently removed, rinsed with sterile MilliQ water, and fixed with 2.5% glutaraldehyde for 1 h at room temperature followed by further rinsing with sterile MilliQ water and drying. Bare catheter segment (devoid of any biofilm growth) and the untreated catheter segment with established *S. aureus* biofilm were also fixed similarly. Subsequently, all the processed catheter segments were examined in a field emission scanning electron microscope (Zeiss Sigma) and their images were recorded.

5.2.12. Cytotoxic Effect of C1-HNC

The cytotoxic effect of C1-HNC was assessed against cultured human embryonic kidney (HEK 293) cell line by a standard MTT-based assay following the manufacturer's instructions (Sigma-Aldrich, USA). HEK 293 cells were initially cultured in a 25 cm^2 tissue culture flask in Dulbecco's Modified Eagle Medium (DMEM) supplemented with 10% (v/v) fetal bovine serum (FBS), penicillin (100 µg /mL), and streptomycin (100 µg /mL) at 37°C under a humidified atmosphere of 5% CO_2 in an incubator. The cells were subsequently seeded onto 96-well tissue culture plates at a density of 10^4 cells per well and incubated in separate sets with either C1-HNC or C1 (corresponding to 4.0 µM, 8 µM, 16 µM, 32 µM, 64 µM and 128 µM of C1) for a period of 24 h. Untreated cells were also

incubated in parallel sets. Following incubation, the media was carefully aspirated and fresh DMEM medium containing MTT solution was added to the wells and the plates were incubated for 4 h at 37°C. Subsequently, the supernatant was aspirated and the insoluble formazan product was solubilized in DMSO and its absorbance was measured in plate reader (Infinite M200, TECAN, Switzerland) at 550 nm. The absorbance obtained for untreated cells was assumed to represent 100% cell viability, and the absorbance for other samples was compared to that obtained for untreated cells in order to determine % cell viability. In order to ascertain the cytotoxic effect, MTT assays were performed in three independent sets and every set consisted of three replicates. Data analysis and determination of standard deviation were performed with Microsoft Excel 2010 (Microsoft Corporation).

For fluorescence microscope analysis, HEK 293 cells were seeded onto 96 well tissue culture plates (approximately 10^4 cells per well) and grown till 80% confluency. Subsequently, the cells were incubated with 128 µM of C1-HNC made in DMEM, for a period of 24 h. Control samples (untreated HEK 293 cells) were also incubated in separate wells. Cells belonging to all the experimental samples were thoroughly washed with sterile PBS and labelled with 50 µM cFDA-SE for 15 min. The cells were subsequently washed with sterile PBS and images of the cells were captured using a fluorescence microscope (Eclipse Ti-U, Nikon, USA) with a filter that allowed blue light excitation. Fluorescence-based imaging experiments were performed in three independent sets wherein each set comprised of three replicates. For every sample, images were recorded from three different fields.

5.3. Results and Discussion:

5.3.1. Antibiofilm Activity of C1

A dose-dependent eradication of *S. aureus* MTCC 96 biofilm by C1 (Figure 5.1A, Appendix Figure A5.1A-B) suggested that the amphiphile was antagonistic in the complex niche of the biofilm matrix and the minimum biofilm eradication concentration ($MBEC_{90}$) of C1 against *S. aureus* MTCC 96 biofilm was observed to be 128 µM. FESEM analysis revealed significant disintegration of *S. aureus* biofilm architecture upon treatment with C1 in comparison to untreated biofilm (Figure 5.1B). The antibiofilm activity of C1 was substantiated by cFDA-SE and Congo red-based fluorescence microscopy, which revealed a dose-dependent depletion of biofilm network and loss of cell viability accompanied by reduction of biofilm matrix (Figure 5.1C).

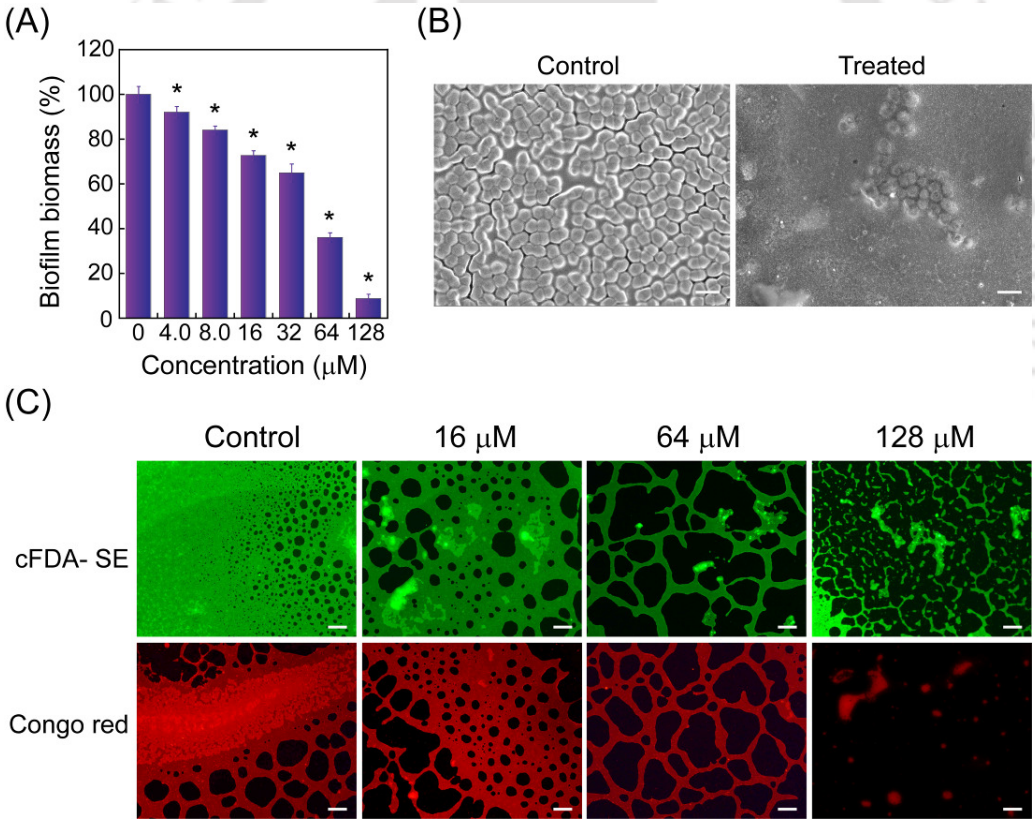

Figure 5.1. (A) Antibiofilm activity of C1 on *S. aureus* MTCC 96 biofilm ascertained by crystal violet assay. * indicates *p* value < 0.001 in ANOVA. (B) FESEM analysis of C1 treated *S. aureus* MTCC 96 biofilm. Scale bar for the image is 2 µm. (C) Fluorescence microscope analysis of *S. aureus* MTCC 96 biofilm treated with C1. Scale bar for the images is 100 µm.

5.3.2. C1-loaded Nanomaterial (C1-HNC)

In order to leverage the antibiofilm activity of C1 for potential therapeutic intervention, a critical criterion is the development of a biocompatible delivery system that enables a biofilm niche-responsive sustained delivery, ensures adequate bioavailability of the payload for effective biofilm eradication and is non-toxic to host cell. In this context, it was envisaged that a human serum albumin (HSA)-based nanoparticles (HNPs) loaded with C1 could be explored as an effective antibiofilm agent. Upon interaction with the biofilm, the proteinaceous nanomaterial (C1-HNC) is likely to render facile release of the payload, triggered by matrix-specific extracellular proteases in *S. aureus* biofilm (Speziale et al. 2014). Subsequently, the biofilm-associated eDNA shield would be disrupted owing to the DNA cleavage activity of the released C1, leading to enhanced accessibility of the underlying target cell. The membrane-targeting activity of the amphiphile against the exposed biofilm cells could then be simultaneously leveraged for effective annihilation of *S. aureus* biofilm. Based on this tenet, C1-HNC was generated by incubating HSA nanoparticles (HNPs) (Figure 5.2A) obtained by desolvation (Langer et al. 2003) with varying concentrations of the amphiphile C1. FESEM analysis indicated that C1-HNC was aggregated (Figure 5.2B). Retention of the salient absorption bands and stretching frequencies of HSA and C1 evidenced by UV-visible spectroscopy and FTIR analysis, respectively, suggested loading of C1 in HNPs (Figure 5.2C- D), while DLS analysis suggested that the particle size of the major aggregated species of HNPs, C1-HNC and C1 alone in solution was around 176 nm, 156 nm and 118 nm, respectively (Figure 5.2E-F, Appendix Figure A5.2).

Based on the emission spectra of C1 and a calibration plot (Figure 5.3A), a dose-dependent loading was apparent upto 200 µM of C1 (Figure 5.3B), while the loading capacity (LC) and amount of encapsulated C1 was estimated to be nearly 12% and 184 µM, respectively, at the highest loading concentration of 400 µM (Figure 5.3B). C1-HNC displayed a sustained release profile in a physiologically relevant milieu of HEPES buffer, simulated body fluid (SBF) and simulated intestinal fluid (SIF) (Figure 5.3C). Interestingly, in acidic pH and in presence of pepsin in simulated gastric fluid (SGF), the release of C1 was several folds higher amounting to nearly 88% or 154 µM C1 in 24 h (Figure 5.3C), which surpassed the $MBEC_{90}$ of C1 against *S. aureus* MTCC 96 biofilm.

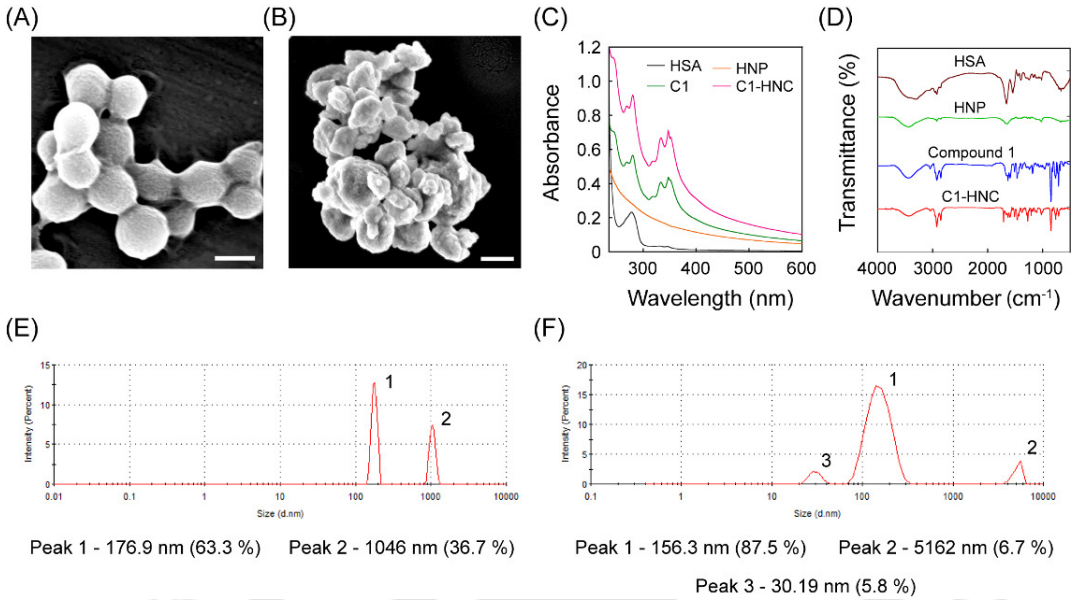

Figure 5.2. FESEM image of (A) HSA nanoparticle (B) C1- loaded HNP (C1-HNC). Scale bar for the images is 200 nm. Characterization of C1-HNC by (C) UV-visible spectroscopy and (D) FT-IR analysis. DLS-based particle size analysis of (E) HNP and (F) C1-HNC. The particle size and percentage of the aggregated species (in parenthesis) of HNP and C1-HNC corresponding to peaks 1-3 are indicated below the plot.

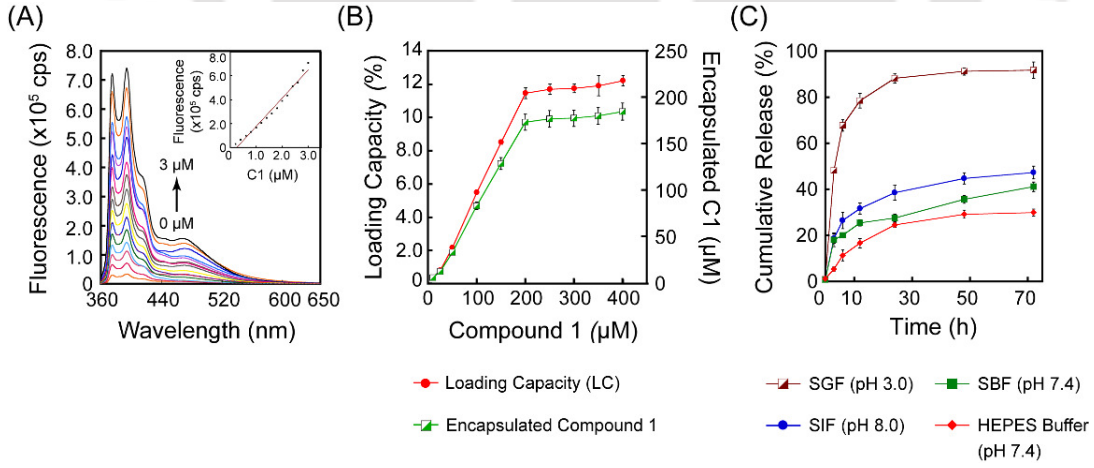

Figure 5.3. (A) Fluorescence emission spectra of varying concentrations of C1 upon excitation at 340 nm. Inset: Calibration plot of concentration versus emission of C1. Emission was measured at 376 nm. (B) Loading capacity (LC) and amount of encapsulated C1 in HSA nanoparticle. (C) *In vitro* release kinetics of C1 from C1-HNC in physiologically relevant fluids and HEPES buffer.

This observation is significant as it enhances the prospect of C1-HNC as an antibiofilm nanomaterial, given the acidic nature and the prevalence of extracellular proteases in *S. aureus* biofilm matrix (Speziale et al. 2014; Foulston et al. 2014).

5.3.3. Biofilm Matrix-responsive Release of Amphiphile

Delivery of antibacterials into the biofilm matrix at sufficiently high concentrations is critical for effective antibiofilm therapy. To this end, delivery vehicles, which can render a niche-responsive release of the payload are desirable. The release of the amphiphilic C1 in *S. aureus* biofilm matrix after 24 h as measured by the inherent pyrene-based fluorescence of the amphiphile (C1) amounted to around 75% release or 131 μM C1 (Figure 5.4A), which was noteworthy as it exceeded the $MBEC_{90}$ of C1 against *S. aureus* MTCC 96 biofilm. The higher levels of release of C1 in *S. aureus* biofilm as compared to extracted biofilm extra-polymeric substance (EPS) or media alone suggested a biofilm matrix-responsive release of the amphiphile from the nanocarrier (Figure 5.4A-B) and reiterated the merit of using the proteinaceous HNP as a vehicle to deliver C1 into the biofilm matrix. It may be mentioned here that at the time of addition of C1-HNC to a 24 h pre-grown *S. aureus* biofilm, the pH of the biofilm spent media was ~3.0. Perhaps the acidic pH and prevalence of extracellular proteases in mature *S. aureus* biofilm matrix (Speziale et al. 2014; Foulston et al. 2014) likely triggers dissolution of the albumin-based proteinaceous nanomaterial leading to a niche-responsive release of C1. Tracking the release of an antibacterial in the biofilm matrix can be impeded by the inherent complexity of the matrix. Interestingly, the pyrene group tethered in C1 rendered a non-invasive fluorescence-based imaging handle in the complex *S. aureus* biofilm niche as it provided evidence for a dose-dependent annihilation of *S. aureus* biofilm (Figure 5.4C) and thus avoided the need for any externally added sensing probe to determine the antibiofilm activity of C1-HNC.

5.3.4. Antibiofilm Activity of C1-HNC

Assessment of biofilm cell viability by an MTT assay revealed a dose-dependent elimination of *S. aureus* biofilm upon treatment with C1-HNC (Figure 5.5A), akin to the earlier observation with C1 alone (Appendix Figure A5.1A), albeit of a slightly lesser

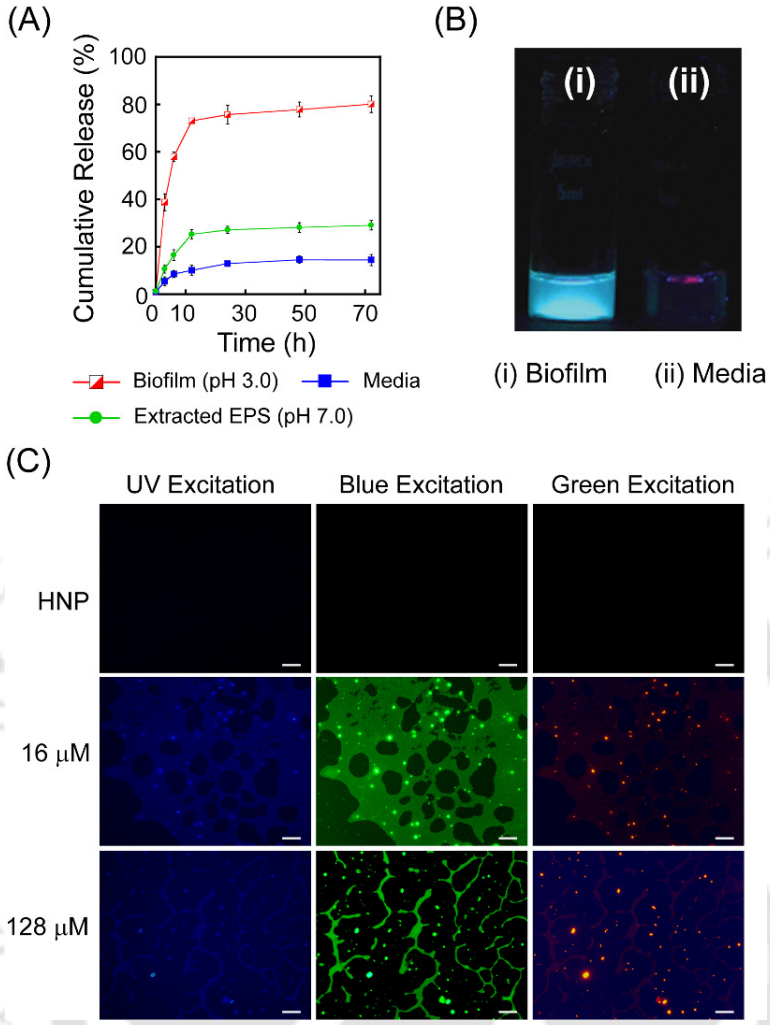

Figure 5.4. (A) Release of C1 from C1-HNC in *S. aureus* MTCC 96 biofilm, extracted EPS and media. (B) Fluorescence-based imaging of the vials containing released C1 in (i) *S. aureus* biofilm and (ii) media alone. (C) Fluorescence microscopic images of HNP-treated (control) and C1-HNC-treated (corresponding to 16 μM and 128 μM of C1) *S. aureus* MTCC 96 biofilm viewed under UV, blue and green excitation. Biofilm imaging was pursued by recording the inherent fluorescence emission of C1 at various excitations. Scale bar for the images is 100 μm.

magnitude. Evidence for antibiofilm activity of C1-HNC was also captured in a crystal violet assay, which suggested a dose-dependent reduction in biofilm biomass following treatment with C1-HNC (Appendix Figure A5.3). FESEM analysis of C1-HNC-treated *S. aureus* biofilm indicated distortion of cell morphology and a breach of cell-cell

adhesion, in contrast to untreated biofilm (Figure 5.5B). Effective elimination of *S. aureus* biofilm by C1-HNC was also supported by cFDA-SE and Congo red staining, which suggested loss in cell viability and reduction of biofilm matrix, respectively (Figure 5.6).

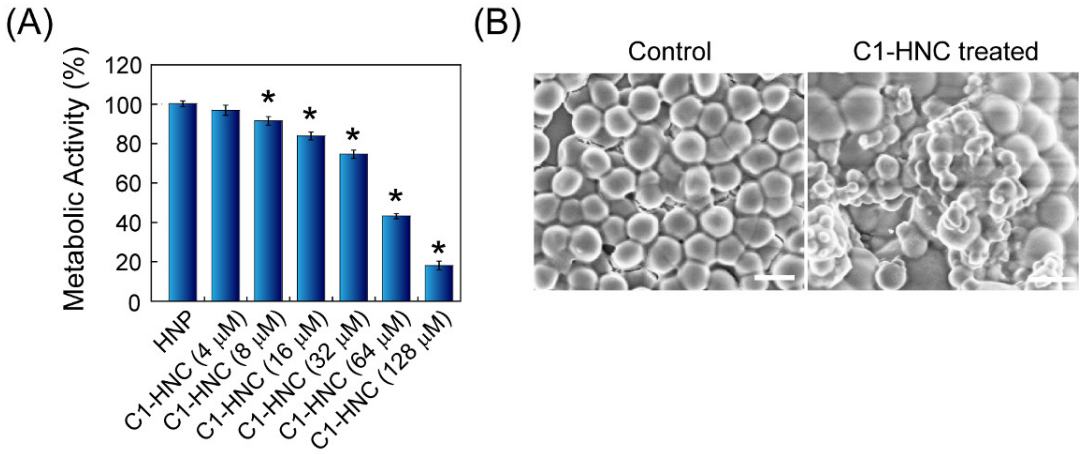

Figure 5.5. (A) Eradication of *S. aureus* MTCC 96 biofilm by C1-HNC determined by MTT assay. * indicates p value < 0.001 in ANOVA. (B) FESEM images of untreated *S. aureus* MTCC 96 biofilm (control) and *S. aureus* MTCC 96 biofilm treated with C1-HNC (128 μM C1 concentration). Scale bar for the images is 1.0 μm.

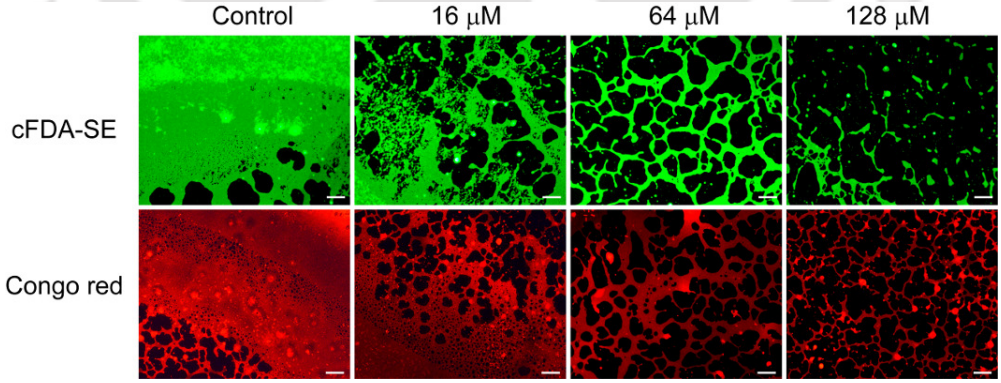

Figure 5.6. cFDA-SE and Congo red-based fluorescence microscopic analysis of *S. aureus* MTCC 96 biofilm following treatment with various concentrations of C1-HNC. CFDA-SE and Congo red staining indicates loss of cell viability and reduction of biofilm matrix EPS, respectively. Scale bar for the images is 100 μm.

5.3.5. Biofilm eDNA Cleavage Activity of C1-HNC

Based on the inherent DNA cleavage activity of C1, the antibiofilm activity of C1-HNC can perhaps be attributed to biofilm eDNA cleavage by C1-HNC, which triggers matrix disruption and facilitates exposure of the underlying cells to the bactericidal action of the amphiphile. To ascertain eDNA cleavage by C1-HNC, pre-grown *S. aureus* biofilm was treated with C1-HNC and the extracted eDNA from the treated samples were analyzed at various time periods. Electrophoresis in conjunction with image analysis revealed a distinct depletion of eDNA with time in C1-HNC treated *S. aureus* biofilm as evidenced in the progressive reduction of eDNA, which was also captured in a parallel experiment with DNase I-treated samples, while HNPs alone failed to render cleavage of biofilm eDNA (Figure 5.7A-5.7B). In solution-based experiments, a systematic decrease in *S. aureus* biofilm eDNA-bound Hoechst fluorescence upon treatment with C1-HNC was evident, albeit at a lesser rate than DNase I treatment (Figure 5.7C). This observation reiterated the eDNA cleavage activity of the payload nanomaterial.

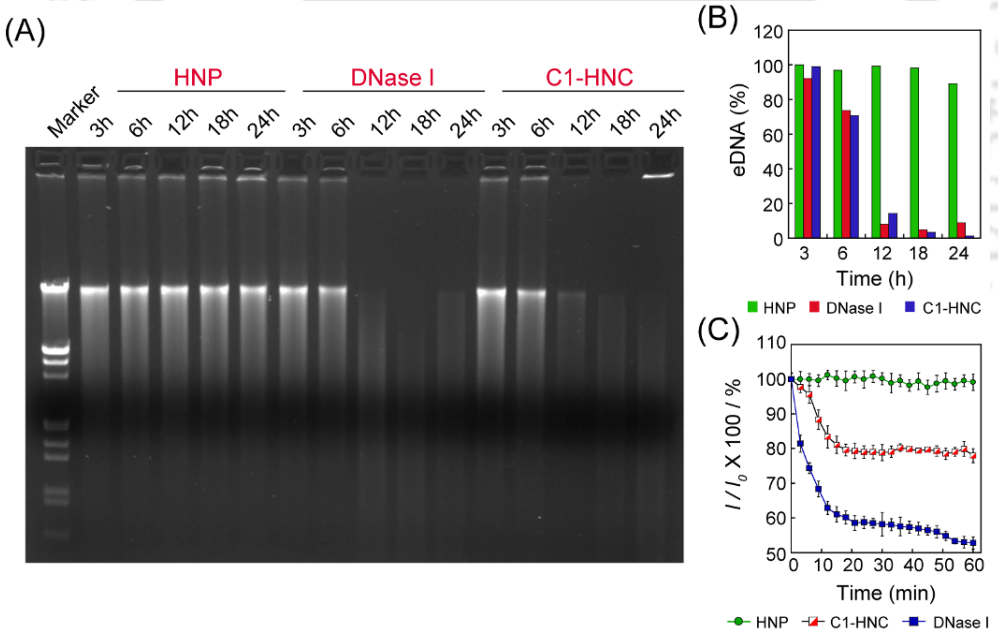

Figure 5.7. (A) Agarose gel electrophoresis of biofilm eDNA obtained from 24 h grown *S. aureus* biofilm treated with HNP, DNase I and C1-HNC for various time periods. (B) Quantification of band intensity of biofilm eDNA samples in (A) using ImageJ analysis software. (C) Fluorescence emission spectra of purified *S. aureus* biofilm eDNA-bound Hoechst 33258 dye following interaction with HNP, C1-HNC and DNase I.

The ability of C1-HNC to cleave eDNA even in the presence of a complex EPS milieu in *S. aureus* biofilm was further substantiated by treating extracted biofilm EPS with C1-HNC. Electrophoresis followed by image analysis indicated that eDNA present in extracted *S. aureus* biofilm EPS as well as pUC18 plasmid DNA present singularly or spiked in extracted biofilm EPS were readily cleaved by C1-HNC as manifested in the degradation of eDNA and emergence of nicked circular (NC) form of plasmid DNA in presence of increasing concentration of C1-HNC (Figure 5.8A-5.8C). It may be mentioned

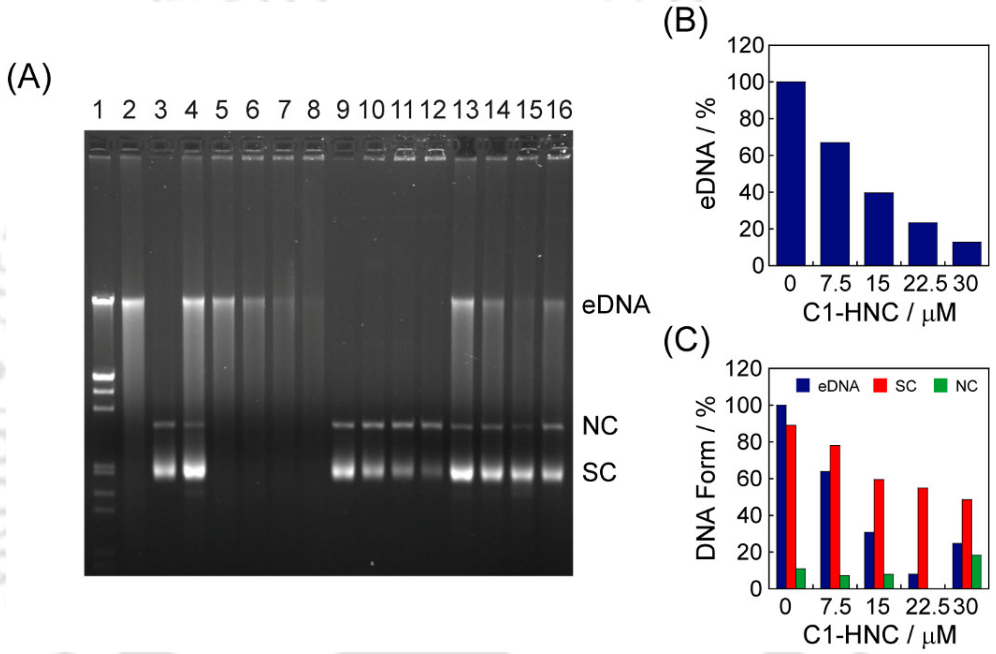

Figure 5.8. (A) Agarose gel electrophoresis of C1-HNC treated *S. aureus* biofilm EPS (20% v/v), pUC18 plasmid DNA (60 μM) alone and spiked in EPS (20% v/v). Lanes 1: Lamda DNA double digest, 2: Control EPS, 3: Control pUC18 DNA, 4: Control pUC18 DNA spiked in EPS, 5-8: EPS treated with 7.5 μM-30 μM C1-HNC, 9-12: pUC18 DNA treated with 7.5 μM-30 μM C1-HNC, 13-16: pUC18 DNA spiked in EPS and treated with 7.5 μM-30 μM C1-HNC. eDNA: Extracellular DNA, NC: Nicked circular DNA, SC: Supercoiled DNA. (B) Band intensity of eDNA (lane 2 and lanes 5-8 in panel A). (C) Band intensity of the topological forms of pUC18 plasmid DNA and eDNA obtained from pUC18 plasmid DNA spiked *S. aureus* MTCC 96 biofilm EPS treated with varying concentrations of C1-HNC (lane 4 and lanes 13-16 in panel A). The band intensities were quantified using ImageJ analysis software.

mentioned here that in these experiments, pUC18 plasmid DNA was spiked as an internal control in biofilm EPS in order to verify the characteristic DNA cleavage activity of the amphiphile C1. Given that the biofilm matrix and eDNA in particular is implicated in resistance of biofilms (Mulcahy et al. 2009; Chiang et al. 2013), the antibiofilm nanomaterial C1-HNC that clearly disrupts *S. aureus* biofilm eDNA provides a significant therapeutic leverage as eDNA cleavage by the nanomaterial would not only induce matrix destruction but would also curb any eDNA-mediated dissemination of resistant traits.

5.3.6. Comparative Study of Biofilm eDNA Cleavage by C1-HNC and DNase I

Disruption of eDNA by DNase coupled with antibiotic treatment is conceived as a viable antibiofilm therapy (Kaplan et al. 2012). However, a major crux in such combinatorial therapy is that certain antibiotics at sub-inhibitory concentration may activate virulence gene, induce eDNA release and biofilm formation in *S. aureus* (Kaplan et al. 2012; Joo et al. 2010). In this context, deployment of C1-HNC for disrupting *S. aureus* biofilm eDNA perhaps holds superior therapeutic prospect than the convention of using the enzyme DNase. As evident from previous experiments, C1-HNC could breach *S. aureus* biofilm eDNA barrier and eradicate the underlying matrix-embedded cells (Figures 5.5-5.8 and Appendix Figure A5.3). This is contrary to the action of DNase, which is thought to cause dispersal of cells without killing them and hence requires co-administration of an antibiotic. In order to corroborate the aforementioned premise, *S. aureus* biofilm was initially treated with C1-HNC and then the biofilm recovery was ascertained following supplementation of calf thymus DNA (CT-DNA), which was used as an additive in these experiments to emulate the effect of high molecular weight eDNA as a matrix material (Izano et al. 2008). The potent eDNA as well as cell-targeting activity of C1-HNC was apparent in these experiments, which clearly indicated that recovery of *S. aureus* biofilm by CT-DNA supplementation could not be achieved in case of treatment with C1-HNC as compared to DNase I treatment (Figure 5.9A-5.9B), indicating the limitations of DNase I-based antibiofilm therapy. The superior antibiofilm potential of C1-HNC was also evident in Hoechst- and cFDA-SE- based fluorescence microscope analysis, which revealed significant reduction of eDNA and concomitant loss of cell viability and this marked effect could not be reversed by CT-DNA supplementation, in contrast to samples treated with

DNase I (Figure 5.9C, Appendix Figure A5.4). Based on these results, the amphiphile-loaded nanomaterial C1-HNC offers a promising therapeutic intervention for effective and irrevocable elimination of *S. aureus* biofilm as it overcomes the limitations associated with DNase-based therapy. By virtue of its eDNA-targeting activity, C1-HNC likely destroys the structural barrier of *S. aureus* biofilm and renders superior target cell accessibility leading to enhanced eradication of biofilm.

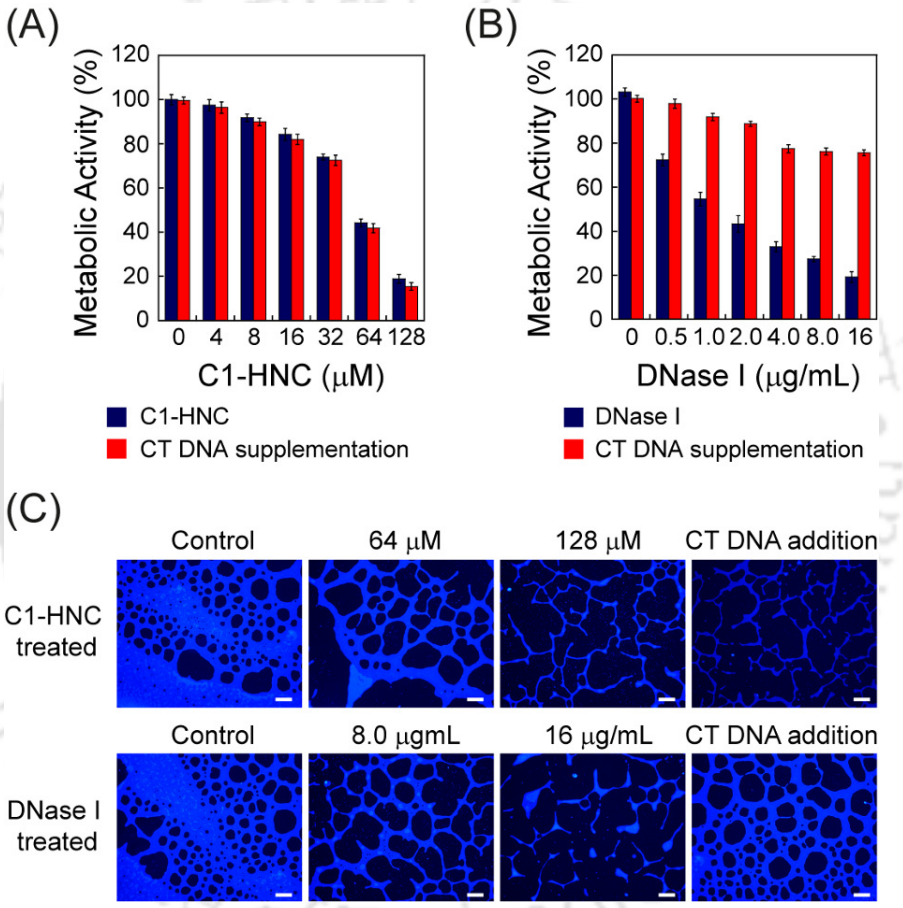

Figure 5.9. Effect of CT-DNA supplementation on (A) C1-HNC-treated and (B) DNAse I-treated *S. aureus* MTCC 96 biofilm. (C) Fluorescence microscope analysis to study the effect of CT-DNA supplementation on C1-HNC-treated and DNAse I-treated *S. aureus* MTCC 96 biofilm. Biofilm was stained with the DNA binding Hoechst 33258 dye. Scale bar for the images is 100 μm.

5.3.7. Cytotoxic Effect and Therapeutic Potential of C1-HNC

To ascertain the therapeutic prospect of C1-HNC as an antibiofilm agent, cytotoxic effect of the payload nanocarrier was determined on cultured human embryonic kidney (HEK 293) cells. Interestingly, the viability of HEK 293 cells treated with C1-HNC loaded with 128 μM amphiphile (equivalent to $MBEC_{90}$ against *S. aureus* MTCC 96 biofilm) was as high as ~80% (Figure 5.10A). It may be mentioned here that when C1 alone was used at an equivalent concentration (128 μM), a remarkable loss in the viability of HEK 293 cells was observed (Chapter 2, Figure 2.14), which suggested that deployment of C1 alone in solution perhaps resulted in high local concentration of the amphiphile, which subsequently lead to host cell toxicity. Collectively, the results of the cytotoxicity assay highlighted the benefit of developing the nanomaterial C1-HNC and indicated that loading of C1 in a biocompatible nanomaterial such as HNP likely leads to a slow and sustained release of the amphiphile in physiological pH, which in turn, reduces unwarranted host-directed toxicity. Fluorescence microscopic analysis also indicated a significant number of viable cFDA-SE stained HEK 293 cells in case of treatment with C1-HNC, which again emphasized the non-toxic nature of C1-HNC and reiterated the promise of the payload nanocarrier in antibiofilm therapy (Figure 5.10B).

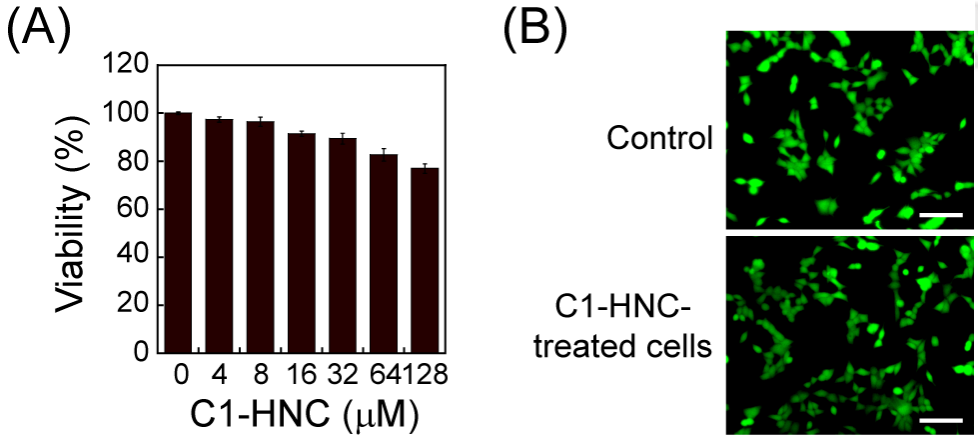

Figure 5.10. (A) MTT assay to evaluate the effect of C1-HNC on the viability of HEK 293 cells. (B) Fluorescence microscope images of HNP-treated (control) and C1-HNC-treated HEK 293 cells. Scale bar for the images is 100 μm.

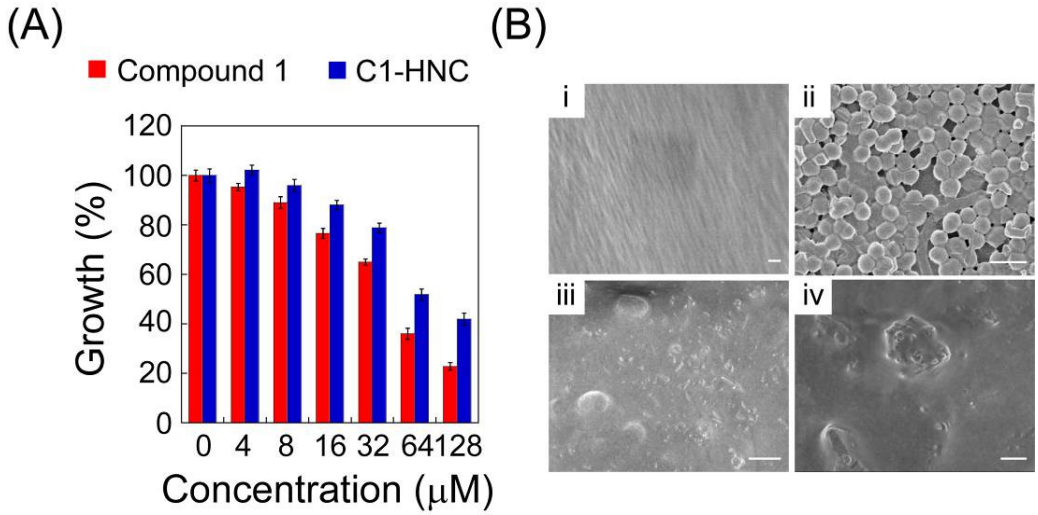

Figure 5.11. (A) MTT assay to ascertain the effect of C1-HNC on *S. aureus* MTCC 96 biofilm grown on Foley's urinary catheter. (B) FESEM images of Foley's urinary catheter segments indicating (i) bare catheter surface, (ii) untreated *S. aureus* MTCC 96 biofilm, (iii) C1 treated *S. aureus* MTCC 96 biofilm and (iv) *S. aureus* MTCC 96 biofilm treated with C1-HNC (corresponding to 128 μM C1). Scale bar for the images is 2.0 μm.

Further, it was also interesting to observe that C1-HNC could render elimination of *S. aureus* biofilm from the surface of a model catheter (Figure 5.11), which validated its prospect as a therapeutic antibiofilm nanomaterial and highlighted the potential of the developed nanocarrier in device-associated antibiofilm therapy.

5.4. Significant Findings

The salient findings of this chapter are as follows:

1. Amphiphile C1-loaded human serum albumin (HSA)-based nanocarrier was generated and characterized. At the highest concentration of C1 (400 μM), the loading capacity of HNPs and the amount of encapsulated C1 was observed to be around 12% and 184 μM, respectively.

2. At physiological pH, sustained release of the bactericidal payload (C1) from C1-HNC was observed, whereas in acidic pH (pH 3.0), release of C1 from the nanocarrier was higher, as compared to physiological pH.

3. C1-HNC displayed a biofilm matrix-responsive release of the bactericidal payload (C1) and eradication of *S. aureus* MTCC 96 biofilm could be captured microscopically by exploiting the inherent fluorescence of C1 in imaging studies.

4. C1-HNC could disrupt *S. aureus* biofilm eDNA even in the complex milieu of the biofilm matrix and is thus expected to provide therapeutic benefit as eDNA cleavage would not only lead to matrix disruption but would also curb any eDNA-mediated transmission of resistant traits.

5. CT-DNA supplementation experiments revealed that C1-HNC was superior to DNase as it triggered eDNA cleavage and concurrently eliminated the matrix-encased *S. aureus* biofilm cells.

6. Interestingly, C1-HNC was non-toxic to cultured HEK 293 cells and could also eradicate *S. aureus* MTCC 96 biofilm from the surface of a model catheter.

In times when the current therapeutic antibiotics are becoming ineffective against biofilm-mediated infections, the present study demonstrates the generation of a non-toxic nanomaterial that can provide a potent conduit for abolition of biofilm. Encouraged by these results, in the subsequent and final chapter of the thesis, the bactericidal potential of the dual-target amphiphile C1 against a clinical strain of methicillin-resistant *Staphylococcus aureus* (MRSA) is reported.

Chapter 6

Potential of C1-loaded PLGA Nanocarrier (C1-PNC) for Eradication of MRSA Biofilm

This chapter describes the development of C1-loaded PLGA nanocarrier (C1-PNC) and its application in eradication of MRSA biofilm in combination with therapeutic antibiotics.

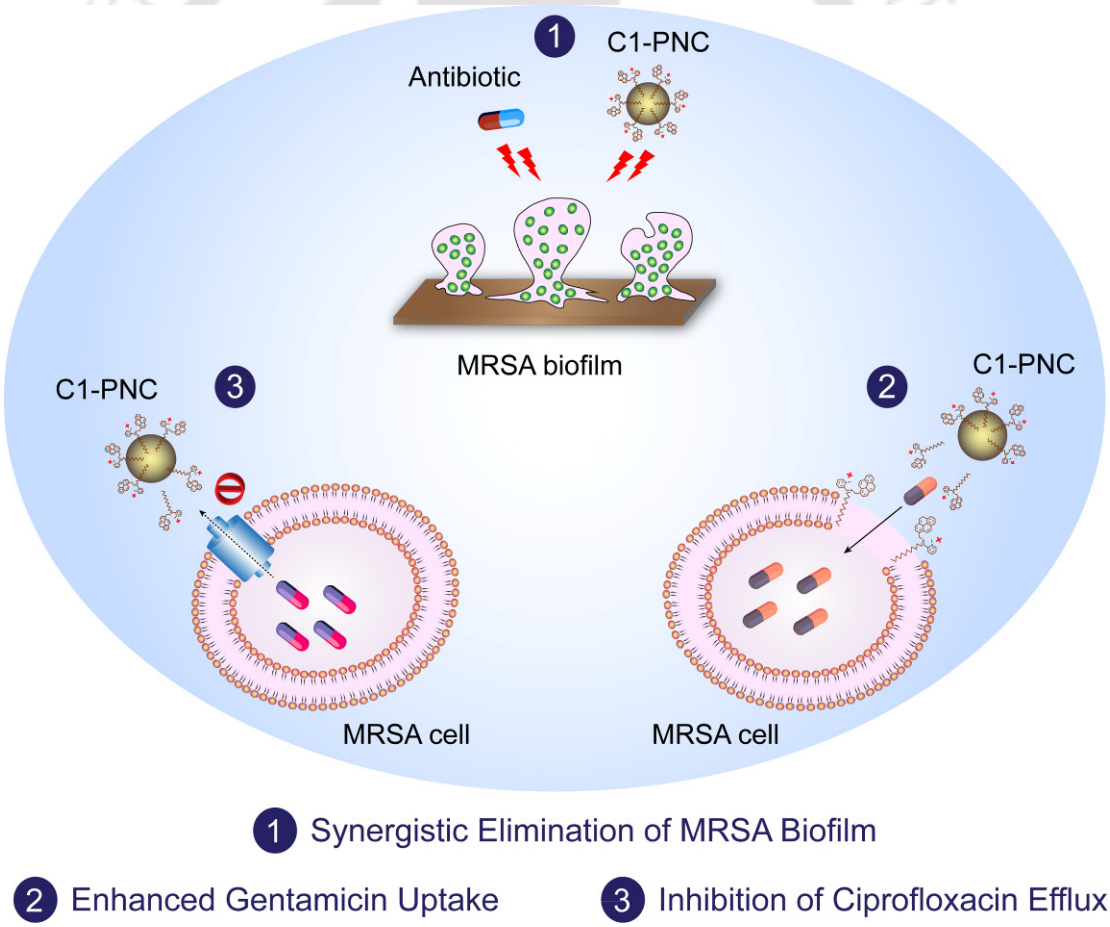

ABSTRACT

The ominous rise of methicillin-resistant *Staphylococcus aureus* (MRSA) in conjunction with a dwindling arsenal of therapeutic antibiotics has triggered an urgent need for alternate therapies. The use of a membrane-targeting small molecule as an adjuvant in order to break the resistance and restore susceptibility of target cells to therapeutic antibiotics is conceived to be a viable approach for effective mitigation of MRSA. To this end, the dual-target bactericidal amphiphile C1 was explored as an adjuvant and the potential of C1-loaded PLGA nanocarrier (C1-PNC) in the eradication of biofilm formed by the MRSA *S. aureus* 4s in combination with the antibiotics gentamicin and ciprofloxacin was ascertained. In combinatorial assays, C1-PNC could significantly abolish MRSA biofilm and render 8 × and 6 × reduction of the minimum biofilm eradication concentration ($MBEC_{90}$) of gentamicin and ciprofloxacin, respectively. Mechanistic studies on *S. aureus* 4s planktonic cells revealed that in case of gentamicin, C1-PNC promoted enhanced cellular uptake of the antibiotic, while the propensity of C1-PNC to inhibit efflux pump activity could be leveraged to enhance cellular accumulation of ciprofloxacin leading to effective killing of the MRSA cells. Interestingly, the combinatorial dosing regime of C1-PNC and the antibiotics was non-toxic to cultured HEK 293 cells. It is conceived that the non-toxic amphiphile-loaded nanomaterial holds considerable prospect as an adjuvant for antibiotic-mediated alleviation of MRSA biofilm.

6.1. Introduction

The prevalence of life threatening infections caused by methicillin-resistant *S. aureus* (MRSA) in conjunction with the emergence of MRSA strains exhibiting resistance to therapeutic antibiotics is becoming a significant healthcare burden (Chambers and DeLeo 2009; Deresinski 2005; Stryjewski and Corey 2014). The problem is further compounded by the fact that MRSA strains are known to form robust biofilms (McCarthy et al. 2015). MRSA is known to exhibit multi-drug resistance and as therapeutic antibiotics are becoming ineffective, alleviation of MRSA infections is emerging as a daunting challenge. For instance, with reports emerging on MRSA strains becoming resistant to a potent antibiotic such as vancomycin (Deresinski 2009; Rehm and Tice 2010), there is a growing concern with regard to the feasibility of using this antibiotic for anti-MRSA therapy. Likewise, there are reports on the prevalence of daptomycin-resistant MRSA strains (Hayden et al. 2005; Marty et al. 2006). In the light of these reports, there is an overwhelming need to develop alternative and effective therapeutic interventions to combat the menace of MRSA infections.

Combination therapy can be considered as a viable option for mitigation of severe MRSA infections. It has been recognized that combination therapy can be beneficial as the synergy between drugs may enhance the overall bactericidal effect, restore susceptibility of the target cells and prevent the emergence of resistance during therapy (Fischbach 2011; Worthington and Melander 2013; Ejim et al. 2011; Thangamani et al. 2016). Synergism between an aminoglycoside such as gentamicin and other therapeutic antibiotics like daptomycin and vancomycin has been reported for mitigation of *Staphylococcus*-mediated infections (LaPlante et al. 2009; Houlihan et al. 1997; Tsuji and Rybak 2005). In addition, the promise of non-antibiotics or small molecules in combination with antibiotics for anti-staphylococcal intervention is also evident from previous studies (Hess et al. 2014; Hu et al. 2015; Harris et al. 2012). A synergistic combination that lowers the effective killing dose of a therapeutic antibiotic also reduces the risk of host-directed toxicity. In this context, the use of a combinatorial regime against MRSA is particularly relevant for aminoglycoside, fluoroquinolone and glycopeptide-based antibiotics, which are known to have toxic implications (Cosgrove et al. 2009; Owens and Ambrose 2005; Finch and Eliopoulos 2005).

With regard to staphylococci-mediated infections, efflux pump activity in the pathogen has been shown to be implicated in rendering high levels of resistance and a gamut of efflux pumps contribute to resistance against biocides and therapeutic antibiotics (Li and Nikaido 2009; Poole 2005; Jang 2016; Kaatz et al.1993; Floyd et al. 2010; Kaatz et al. 2005). Hence, targeting the efflux pump in *S. aureus* can be a rational therapeutic approach. To this end, the potential of small molecules as synthetic efflux pump inhibitor (EPI) against *S. aureus* has been reported (Pieroni et al. 2010; Sabatini et al. 2011; Holler et al. 2012; Ganesan et al. 2016). Further, the structural determinants of effective EPIs and the prospect of combining EPIs with antibiotics for elimination of *S. aureus* has been demonstrated (Brincat et al. 2012; Sabatini et al. 2013; Lepri et al. 2016; Sabatini et al. 2008; Sabatini et al. 2012).

Owing to the limitations of antibiotic monotherapy and the scarcity of new and effective antibiotics, the use of adjuvants brings forth new opportunities for effective combinatorial treatment regime against MRSA infections. To this end, an adjuvant molecule, which can contravene the core resistance mechanism and thereby enhance the bactericidal efficacy of a therapeutic antibiotic will be largely beneficial. In a previous investigation, the adjuvant potential of C1 was established (Chapter 4). However, given the remarkable drug-resistance of clinical MRSA strains, it was envisaged that C1 can be explored in combination therapy to potentiate antibiotic activity against clinical MRSA strain. To this end, the potential of C1-loaded PLGA nanocarrier (C1-PNC) to restore susceptibility of MRSA biofilm to antibiotics is demonstrated. Mechanistic studies indicated that the adjuvant nanomaterial promoted gentamicin uptake in MRSA cells, while in case of ciprofloxacin, the nanomaterial impeded efflux of the antibiotic leading to significant elimination of MRSA cells. Interestingly, the synergistic combination of the nanomaterial and the antibiotics was non-toxic to model human cells, highlighting the potential of the amphiphile-loaded adjuvant nanomaterial in anti-MRSA therapy.

6.2. Materials and Methods

6.2.1. Compounds and Reagents

5 (and 6)-carboxyfluorescein diacetate succinimidyl ester (cFDA-SE), ethidium bromide (EtBr), 3,3′-Dipropylthiadicarbocyanine iodide ($DiSC_35$), carbonyl cyanide m-chlorophenylhydrazone (CCCP), Poly(D,L-lactide-co-glycolide) lactide:glycolide (50:50), molecular weight 30,000-60,000 (PLGA) , Poly(vinyl alcohol) average molecular weight 85,000-124,000, 87-89% hydrolyzed (PVA), ciprofloxacin, reserpine, Dulbecco's Modified Eagle Medium (DMEM), trypsin-EDTA and 3-(4,5-dimethyl-2-thiazolyl)-2,5-diphenyl-2H-tetrazolium bromide (MTT) were procured from Sigma-Aldrich (USA). Brain-Heart Infusion (BHI) broth, gentamicin sulphate, ready to use methicillin and oxacillin discs was procured from HiMedia, Mumbai, India. Dimethyl sulfoxide (DMSO) was obtained from Merck, India. Fetal bovine serum (FBS) was procured from PAA Laboratories, USA. N-2-hydroxyethyl piperazine N-2 ethane sulphonic acid (HEPES buffer) was procured from Sisco Research Laboratories SRL, Mumbai, India.

6.2.2. Bacterial Strain and Growth Conditions

Staphylococcus aureus 4s, a clinical MRSA strain was used as the target bacterial strain in the present investigation. The strain was kindly provided by Prof. Benu Dhawan, All India Institute of Medical Sciences (AIIMS), New Delhi and Prof. Kasturi Mukhopadhyay, Jawaharlal Nehru University (JNU), New Delhi. *S. aureus* 4s was propagated in BHI broth at 37°C and 180 rpm for 12 h. In order to ascertain the methicillin-resistant trait in *S. aureus* 4s, a disc diffusion assay was performed with ready to use discs of methicillin (5.0 µg) and oxacillin (1.0 µg), following the recommended protocol (CLSI 2007). For PCR-based detection of *mecA* gene in *S. aureus* 4s, template DNA was extracted from the strain by following a previous method (Singh and Ramesh 2009) and PCR was performed using the *mecA* gene specific primers (Jaffe et al. 2000). The template DNA was initially subjected to denaturation at 94°C for 5 min followed by a total of 35 amplification cycles. Each cycle included denaturation for 1 min at 94°C, primer annealing for 45 seconds at 57°C and extension for 1 min at 72°C. A final extension at 72°C for 10 min followed the last cycle. The PCR products were subjected to agarose (1%) gel electrophoresis.

6.2.3. Combinatorial Effect of C1 and Antibiotics on MRSA Planktonic Cells and Biofilm

6.2.3.1. MIC of C1, Gentamicin and Ciprofloxacin

MIC of C1, gentamicin and ciprofloxacin was determined against *S. aureus* 4s by a microtiter broth dilution method. Briefly, the target bacterial strain was inoculated at 1% level in microtitre wells having the specific growth medium and grown overnight at 37^{o}C and 180 rpm in separate sets in presence of varying concentrations of C1 (2.0 µM - 128 µM) or gentamicin (2.0 µM - 2048 µM) or ciprofloxacin (2.0 µM - 128 µM). MIC of C1 and the antibiotics was ascertained by measuring the absorbance of the samples at 600 nm as mentioned previously in section 2.2.5. The MIC values for C1 and the antibiotics was calculated from three independent experiments, each having three replicas. Data analysis and calculation of standard deviation was performed with Microsoft Excel 2010 (Microsoft Corporation, USA).

6.2.3.2. Bactericidal Efficacy of Gentamicin and Ciprofloxacin in Combination with C1

Initially a 10 µL aliquot of *S. aureus* 4s cell suspension (10^6 CFU suspended in sterile PBS) was inoculated in separate sets into sterile microtitre plate wells having requisite growth media (100 µL) incorporated with a serial two-fold dilution of either gentamicin (64 µM - 512 µM) or ciprofloxacin (1.0 µM - 8.0 µM). In another set, the same concentrations of the antibiotics were used in combination with 2.0 µM of C1. The cells were incubated at 37^{o}C and 180 rpm for 12 h. Bacterial growth was estimated by measuring absorbance at 600 nm in a microtitre plate reader (Infinite M200, TECAN, Switzerland) and expressed as percentage growth inhibition compared to untreated cells (cells grown in the absence of antibiotics and C1). In separate sets, the effect of varying concentrations of the antibiotic or C1 alone on the growth of target bacteria was also ascertained. The fold decrease in the MIC of gentamicin and ciprofloxacin in presence of C1 was determined and the fractional inhibitory concentration (FIC) index and the nature of interaction was assessed following the method described earlier (Giacometti et al. 2000). For every sample, three independent experiments were performed, each having three replicas. Data analysis and calculation of standard deviation was performed with Microsoft Excel 2010 (Microsoft Corporation, USA).

6.2.3.3. FESEM Analysis of Planktonic Cells

Overnight grown cells of *S. aureus* 4s were collected by centrifugation, washed twice with sterile phosphate buffered saline (PBS) and resuspended in the same. Approximately 10^6 CFU/mL cells were treated in separate sets with C1 (2.0 µM) or gentamicin (512 µM) or ciprofloxacin (8.0 µM) for 6 h at 37°C. In a separate set, cells were also treated with either a combination of C1 (2.0 µM) and gentamicin (512 µM) or a combination of C1 (2.0 µM) and ciprofloxacin (8.0 µM). Untreated cells were incubated in PBS for the same period as control sample. Following incubation, all the samples were washed twice with sterile PBS and fixed in 2.5% glutaraldehyde for 90 min at 4°C. Following fixation, cells were washed and resuspended in sterile MilliQ grade water. A 10 µL aliquot of each sample was processed for FESEM analysis by following the method described earlier in section 2.2.7.2.

6.2.3.4. Antibiofilm Activity of C1 and Antibiotics

Biofilm of *S. aureus* 4s was grown in sterile 96 well microtitre plate by following a standard protocol (Goswami et al. 2014). Following 24 h of biofilm growth in static and humid condition at 37°C, the spent media from the microtitre plate wells was gently aspirated and the wells were washed thrice with sterile MilliQ water (200 µl) to remove non-adherent bacteria. The pre-grown biofilm was then treated in separate sets with a serial two-fold dilution of either C1 (16 µM - 512 µM) or gentamicin (16 µM - 8192 µM) or ciprofloxacin (16 µM - 1024 µM) for 24 h. Untreated biofilm was also incubated under the same conditions as control. Following incubation for 24 h, media from the wells was removed, the wells were washed with sterile PBS to remove non-adherent bacterial cells and air dried. Subsequently, the biofilm biomass and metabolic activity of biofilm cells was estimated in separate sets of experiments by performing a crystal violet binding assay and an MTT assay, respectively (Goswami et al. 2014). From the crystal violet assay, the minimum biofilm eradication concentration ($MBEC_{90}$) for C1 and the antibiotics was determined as the concentration, which resulted in 90% reduction in biofilm biomass as compared to untreated control sample. All the experiments were performed in three independent sets and every set consisted of three replicates. Data analysis and calculation

of standard deviation was performed with Microsoft Excel 2010 (Microsoft Corporation, USA).

In another experiment, biofilm of *S. aureus* 4s was grown in sterile 96 well microtitre plate in BHI medium incorporated with 0.25% glucose and varying concentrations of either C1 (16 µM - 512 µM) or gentamicin (16 µM - 8192 µM) or ciprofloxacin (16 µM - 1024 µM) for 24 h. Following biofilm growth, biomass and metabolic activity of biofilm was estimated by crystal violet and MTT assay as mentioned before. From the crystal violet assay, the minimum biofilm inhibition concentration ($MBIC_{90}$) of C1 and the antibiotics was defined as the concentration, which resulted in 90% decrease of the biofilm biomass. All experiments were performed in three independent sets and every set consisted of three replicates. Data analysis and calculation of standard deviation were performed with Microsoft Excel 2010 (Microsoft Corporation, USA).

6.2.3.5. Antibiofilm Activity of Gentamicin and Ciprofloxacin in Combination with C1

S. aureus 4s biofilm was treated with either a serial two-fold dilution of gentamicin (16 µM - 1024 µM) or ciprofloxacin (16 µM - 256 µM), both in combination with either 16 µM C1 or 32 µM C1. The combinatorial effect on biofilm was determined by crystal violet and MTT assay and the $MBEC_{90}$ and $MBIC_{90}$ of the antibiotics in combination with C1 was ascertained as mentioned before.

6.2.3.6. FESEM Analysis of Biofilm

S. aureus 4s biofilm was grown on cover slips as mentioned before in section 5.2.2.2. The glass cover slips with established *S. aureus* 4s biofilm was transferred to fresh requisite medium (BHI medium supplemented with 0.25% glucose) incorporated with either gentamicin (1024 µM) or ciprofloxacin (256 µM) singularly or in combination with C1 (32 µM) and incubated at 37^{o}C in a humid chamber for 24 h. The treated samples as well as control samples (48 h grown untreated biofilm) were washed twice with sterile PBS to remove spent media and finally with sterile MilliQ grade water. The samples were then air-dried in laminar hood and examined in a field emission scanning electron microscope (Zeiss Sigma, USA) at 1.5-3.0 kV and their images were recorded.

6.2.4. C1-loaded PLGA Nanocarrier (C1-PNC)

Synthesis of PLGA nanoparticle (PNP) was accomplished by following a single emulsion technique (Cartiera et al. 2009). C1-loaded PLGA nanocarrier (C1-PNC) was generated by incubating PNPs (1.0 mg/mL in sterile MilliQ water) overnight with varying concentrations of C1 (10 µM-500 µM) on a rocker at room temperature. Subsequently, the solution was centrifuged at 10,000 × g for 5 minutes and the pellet representing C1-PNC was resuspended in sterile MilliQ water. Aliquots of PNP and C1-PNC were added separately onto clean sterile cover slip, air-dried in a laminar hood, examined in a field emission scanning electron microscope (Zeiss Sigma, USA) and their images were recorded. For particle size estimation, C1-PNC loaded with 184 µM C1 (1.0 mg/mL PNPs having a final concentration of 184 µM C1) was dispersed in sterile MilliQ water (1.0 mL). A 0.1 mL aliquot of this solution was further diluted to 1.0 mL in sterile MilliQ water and subjected to particle size estimation by DLS (Zeta Sizer, Malvern, UK). In a separate set of experiments, PNPs (1.0 mg/mL in sterile MilliQ water) were also diluted tenfold in sterile MilliQ water and subjected to DLS analysis. The DLS experiments were performed in three independent sets and every set consisted of three replicates. For further characterization, UV-visible spectra of PNPs, C1 and C1-PNC were measured in a spectrophotometer (CARY 300 Bio, Varian). FT-IR spectra of PNPs, C1 and C1-PNC were also recorded in KBr pellets at 4.0 cm^{-1} resolution in an infrared spectrometer (Spectrum One, Perkin-Elmer). For every sample, eight scans were performed in the range of 4000 cm^{-1} to 400 cm^{-1}. A background spectrum for pure KBr was also measured.

6.2.5. Loading Capacity (LC) and Encapsulation of C1 in PLGA Nanoparticle (PNP)

Initially a calibration plot was generated with varying concentrations of C1 by measuring the fluorescence emission spectra of the amphiphile at 376 nm in a spectrofluorometer (FluoroMax-4, HORIBA) at an excitation wavelength of 340 nm. For estimation of LC, PNPs (1.0 mg / mL in sterile MilliQ water) were interacted in separate sets with varying concentrations of C1 (10.0 µM - 500 µM) for 12 h on a rocker at room temperature. Subsequently, the solution was centrifuged at 10,000 × g for 5 min. The pellet, which represents C1-PNC was resuspended in sterile MilliQ water. The concentration of free C1 in the supernatant was determined using the previously generated calibration plot and the

loading capacity (LC) in percentage was determined using a standard calculation (Goswami et al. 2014). All the experiments were performed in three independent sets and every set consisted of three replicates. Data analysis and calculation of standard deviation was performed with Microsoft Excel 2010 (Microsoft Corporation, USA).

6.2.6. Bactericidal Activity of C1-PNC

Cells of *S. aureus* 4s suspended in sterile PBS (approximately 10^6 CFU/mL) were treated with C1-PNC (24 µM C1 concentration) at 37°C and 180 rpm for 6 h. In case of control sample, the cells were incubated with PNPs under the same conditions. Subsequently, cells were washed twice with sterile PBS and labelled with cFDA-SE and PI in separate sets and subjected to fluorescence microscope analysis as described earlier (Goswami et al. 2015).

6.2.7. In Vitro Release Kinetics of C1 in Buffers

C1-PNC (1.0 mg/mL PNPs loaded with a final concentration of 200 µM C1) was dispersed in separate sets in 1.0 mL each of 10 mM HEPES buffer (pH 7.4) and 10 mM citrate buffer (pH 3.0). The samples were incubated in an orbital shaker at 120 rpm and 37°C. Samples were withdrawn at regular intervals (3 h, 6 h, 12 h, 24 h, 48 h, and 72 h) and centrifuged at 7,000 × g for 3 min. The supernatant from the samples were transferred into a fresh micro centrifuge tube and fluorescence emission spectra of the solutions were measured at 376 nm in a spectrofluorometer (FluoroMax-4, HORIBA) at an excitation wavelength of 340 nm. A previously generated calibration curve for C1 was used to quantify the release of C1 from C1-PNC at various time periods and expressed as % cumulative release. A cumulative release of 100% corresponds to 200 µM of released C1 (equivalent to initial loading concentration of C1 in C1-HNC). All the experiments were performed in three independent sets and every set consisted of three replicates.

6.2.8. Matrix-responsive Release of C1 from C1-PNC in Biofilm and Extracted EPS

To estimate the release of C1 in biofilm, C1-PNC loaded with 200 µM of C1 was added to 24 h pre-grown *S. aureus* 4s biofilm in fresh BHI media. The samples were incubated in static and humid condition at 37°C. At specific time intervals (3 h, 6 h, 12 h, 24 h, 48 h, and 72 h) the spent media was carefully aspirated without disturbing the biofilm samples

and the quantity of C1 released from C1-PNC at specific time periods was quantified by fluorescence emission spectroscopy and expressed as % cumulative release as described in section 5.2.6.

In a separate set of experiment, *S. aureus* 4s biofilm EPS was extracted by following a method described earlier in section 5.2.6. To estimate the release of C1 in biofilm EPS, C1-PNC loaded with 200 µM of C1 was added to extracted biofilm EPS. The samples were incubated in static and humid condition at 37°C. At specific time intervals (3 h, 6 h, 12 h, 24 h, 48 h, and 72 h) samples were withdrawn and the quantity of C1 released at various time periods were estimated by fluorescence emission spectroscopy and expressed as % cumulative release as mentioned before. Likewise, release of the amphiphile from C1-PNC incubated in biofilm media alone was also estimated. All the experiments were performed in three independent sets and every set consisted of three replicates.

6.2.9. Combinatorial Effect of C1-PNC and Therapeutic Antibiotics on MRSA Planktonic Cells and Biofilm

Initially the MIC, $MBEC_{90}$ and $MBIC_{90}$ of C1-PNC against planktonic cells and biofilm of *S. aureus* 4s was determined by following the microtitre well assay method described earlier for C1. In order to ascertain the bactericidal effect of antibiotics in combination with C1-PNC, the planktonic cells of *S. aureus* 4s were treated with a serial two-fold dilution of either gentamicin (64 µM - 512 µM) or ciprofloxacin (1.0 µM - 8.0 µM) in combination with 4.0 µM of C1-PNC. The FIC index and nature of interaction between C1-PNC and the antibiotics was determined as mentioned before.

The antibiofilm activity of gentamicin or ciprofloxacin in combination with C1-PNC was also ascertained against *S. aureus* 4s. In these experiments, *S. aureus* 4s biofilm was treated with either a serial two-fold dilution of gentamicin (16 µM - 1024 µM) or ciprofloxacin (16 µM - 256 µM), both in combination with either 32 µM or 64 µM C1-PNC. The combinatorial effect on biofilm was determined by crystal violet and MTT assay and the $MBEC_{90}$ and $MBIC_{90}$ of the antibiotics in combination with C1-PNC was determined as mentioned before.

The antibiofilm activity of gentamicin or ciprofloxacin in combination with C1-PNC was also determined by fluorescence microscope analysis. *S. aureus* 4s biofilm was grown in sterile 96 well microtitre plate and treated with either gentamicin (1024 µM) or ciprofloxacin (256 µM) singularly or in combination with C1-PNC (64 µM) at 37^{o}C in a humid chamber for 24 h. Subsequently, untreated biofilm samples (control) as well as treated biofilm samples were subjected separately to cFDA-SE staining and observed under a fluorescence microscope (Eclipse Ti-U, Nikon) by following a standard procedure (Goswami et al. 2014). Biofilm imaging experiments were performed in three independent sets wherein each set comprised of three replicates. For every sample, images were recorded from three different fields.

6.2.10. Gentamicin Uptake in MRSA Cells in Presence of C1-PNC

S. aureus 4s cells were grown till mid-logarithmic state and collected by centrifugation at 8,000 rpm for 3 minutes. The cells were washed thrice with sterile PBS, resuspended in the same (approximately 10^7 CFU/mL) and treated in separate sets with either 256 µM or 512 µM of gentamicin in combination with 4.0 µM of C1-PNC for 2h 37°C at 180 rpm. Following incubation, the samples were centrifuged at 8000 rpm for 5.0 min and the supernatant was subjected to quantification of gentamicin as described in an earlier method (Gubernator et al. 2006). The gentamicin concentration in the supernatant was calculated using a calibration plot generated with varying concentrations of the antibiotic (1.0 µM - 10 µM). Gentamicin uptake in MRSA cells either in the absence of C1-PNC or in presence of 2.0 µM C1 was also ascertained.

6.2.11. Determination of Efflux Pump Inhibition by C1-PNC

The ability of C1-PNC to inhibit efflux pump activity in *S. aureus* 4s planktonic cells was ascertained by the well-established ethidium bromide (EtBr) efflux assay and EtBr accumulation assay. *S. aureus* 4s cells were grown (A_{600} = 0.6), washed with sterile PBS and resuspended in the same. Subsequently, the cell suspension (A_{600} = 0.3) was incubated in separate sets with 5.0 mg/mL of ethidium bromide (EtBr) for 1 h at 25°C and 180 rpm in presence of either C1-PNC (1.0 µM, 2.0 µM and 4.0 µM) or PNP (1.0 mg/mL) or C1 (0.5 µM, 1.0 µM and 2.0 µM) or the known efflux pump inhibitors reserpine (20 µg/mL) or

CCCP (8.0 µM). The excess EtBr was removed by centrifugation at 10,000 rpm for 3.0 minutes and the cells were washed twice with sterile PBS. Finally, the cells were resuspended in sterile PBS containing 0.4 % glucose and the loss of fluorescence emission of the samples was intermittently recorded for a period of 30 min at 600 nm by exciting the samples at 515 nm. The fluorescence emission of control cells without exposure to glucose was also measured in the same way.

In a separate experiment, EtBr accumulation assay was also performed with *S. aureus* 4s planktonic cells. Cells of the MRSA strain were grown (A_{600} = 0.6), washed with sterile PBS and resuspended in the same. To the cell suspension (A_{600} = 0.3), 0.4 % glucose and 5.0 mg/mL EtBr was then added in separate sets and the samples were incubated with either C1-PNC or C1 (0.5 µM, 1.0 µM and 2.0 µM each) or reserpine (20 µg/mL) or CCCP (8.0 µM) at 25°C and 180 rpm for 1 h. Subsequently, fluorescence emission of the samples was recorded at 600 nm by exciting the samples at 515 nm. The fluorescence emission of control cells (untreated) and control cells without glucose treatment was also measured in the same way.

6.2.12. Combination Effect of Ciprofloxacin and Efflux Pump Inhibitor on MRSA Planktonic Cells

The bactericidal activity of ciprofloxacin in combination with known efflux pump inhibitors (EPIs) reserpine or CCCP was ascertained against *S. aureus* MRSA 4s. Initially a 10 µL aliquot of bacterial cell suspension (10^6 CFU of *S. aureus* 4s cells suspended in sterile PBS) was inoculated in separate sets into sterile microtitre plate wells having requisite growth media (100 µL) incorporated with a serial two-fold dilution of ciprofloxacin (1.0 µM - 8.0 µM) in combination with either 20 µg/mL of reserpine or 4.0 µM of CCCP. The cells were incubated at 37°C and 180 rpm for 12 h. Bacterial cell growth was estimated by measuring absorbance at 600 nm in a microtitre plate reader (Infinite M200, TECAN, Switzerland) and expressed as percentage growth inhibition compared to untreated cells (cells grown in the absence of antibiotic and EPIs). For every sample, three independent experiments were performed, each having three replicas. Data analysis and calculation of standard deviation was performed with Microsoft Excel 2010 (Microsoft Corporation, USA).

6.2.13. Ciprofloxacin Accumulation in MRSA Cells

The accumulation of ciprofloxacin in *S. aureus* 4s cells in presence of EPIs was measured by essentially following a previously described method (Giraud et al. 2000). *S. aureus* 4s cells were grown to late logarithmic phase at 37°C in BHI medium, harvested by centrifugation, washed thrice with 50 mM sodium phosphate buffer (pH 7.0) and resuspended in the same buffer (A_{600} = 1.0). The cells were further equilibrated in the same buffer at 37°C for 10 minutes. Ciprofloxacin (32 µM) was added to the cells and around 0.5 mL sample was removed intermittently over a period of 5.0 min. Following 5.0 min exposure to ciprofloxacin, the cells were incubated in separate sets with either C1-PNC (4.0 µM) or C1 (2.0 µM) or CCCP (4.0 µM) or reserpine (20 µg/mL) and the samples were again collected periodically (every minute) over a period of 5.0 min. The collected samples were diluted in ice cold 50 mM sodium phosphate buffer (pH 7.0) and centrifuged at 8000 rpm for 5 min. The supernatant was removed and the cell pellet was washed twice with ice cold sodium phosphate buffer. Then the cells were resuspended in 1.0 mL of 0.1 M glycine hydrochloride (pH 3.0) and incubated for 15 h at room temperature. Following incubation, the samples were centrifuged at 8000 rpm for 5 min and the fluorescence emission of the supernatant was measured at 447 nm using a microtitre plate reader (Infinite M200, TECAN, Switzerland) by exciting the sample at 279 nm. The concentration of ciprofloxacin present in the supernatant was determined from a calibration plot of the antibiotic (0.5 µM to 10 µM) and expressed as micromolar of ciprofloxacin per milligram (dry weight) of cells.

6.2.14. Homology Modelling and Molecular Docking Studies

Homology modelling of *S. aureus* NorA protein and molecular docking studies to predict interaction of C1 with the modelled NorA protein was pursued as described in the Appendix of Chapter 6.

6.2.15. Cytotoxicity Assay

The cytotoxic effect of C1 and C1-PNC in combination with either gentamicin or ciprofloxacin was assessed against cultured human embryonic kidney (HEK 293) cell line by a standard MTT-based assay following the manufacturer's instructions (Sigma-Aldrich,

USA). HEK 293 cells were initially cultured in a 25 cm^2 tissue culture flask in Dulbecco's Modified Eagle Medium (DMEM) supplemented with 10% (v/v) fetal bovine serum (FBS), penicillin (100 µg/mL), and streptomycin (100 µg/mL) at 37°C under a humidified atmosphere of 5% CO_2 in an incubator. The cells were subsequently seeded onto 96-well tissue culture plates at a density of 10^4 cells per well and incubated in separate sets with either C1-PNC (corresponding to 32 µM and 64 µM of C1) or C1 (32 µM and 64 µM) in combination with either gentamicin (128 µM, 256 µM, 512 µM and 1024 µM) or ciprofloxacin (32 µM, 64 µM, 128 µM and 256 µM) for a period of 24 h. Untreated cells were also incubated in parallel sets. Following incubation, the media was carefully aspirated and fresh DMEM medium containing MTT solution was added to the wells and the plates were incubated for 4 h at 37°C. Subsequently, the supernatant was aspirated and the insoluble formazan product was solubilized in DMSO and its absorbance was measured in a microtiter plate reader (Infinite M200, TECAN, Switzerland) at 550 nm. The absorbance obtained for untreated cells was assumed to represent 100% cell viability, and the absorbance for other samples was compared to that obtained for untreated cells in order to determine % cell viability. In order to ascertain the cytotoxic effect, MTT assays were performed in six independent sets and every set consisted of three replicates. Data analysis and determination of standard deviation were performed with Microsoft Excel 2010 (Microsoft Corporation).

6.3. Results and Discussion

6.3.1. Adjuvant Potential of Amphiphile Against MRSA Planktonic Cells and Biofilm

The bactericidal effect of gentamicin and ciprofloxacin in combination with C1 on planktonic cells and biofilm of a clinical MRSA strain *S. aureus* 4s was ascertained. Detection of methicillin-resistance trait in *S. aureus* 4s was accomplished by a standard disc assay and PCR-mediated amplification of *mecA* gene (Appendix Figure A6.1). For the combination experiments, gentamicin and ciprofloxacin were chosen as prototype aminoglycoside and fluoroquinolone antibiotics, respectively. Gentamicin holds considerable prospect in anti-MRSA therapy, while the efficacy of ciprofloxacin is hampered by the efflux mechanism in *S. aureus* (LaPlante et al. 2009; Jang 2016; Tsuji and Rybak 2005; Costa et al. 2015). The choice of C1 as an adjuvant was based on the fact that the amphiphile can breach the bacterial membrane barrier and likely predispose the cells to the action of therapeutic antibiotics. Further, the prospect of using C1 in conjunction with the antibiotics gentamicin or ciprofloxacin is appealing as the targets for the antimicrobial combinations are different. Initially, the MIC, $MBIC_{90}$ and $MBEC_{90}$ of C1 and the selected antibiotics was determined against planktonic cells and biofilm of *S. aureus* 4s (Table 6.1). In the combinatorial assay, a systematic reduction in the growth of MRSA planktonic cells was observed upon treatment with 2.0 µM C1 in combination with increasing concentration of the antibiotics (Appendix Figure A6.2A-B) and this enhanced bactericidal effect was also apparent in FESEM analysis (Appendix Figure 6.2. C). Akin to the results obtained against planktonic cells, determination of the metabolic activity of biofilm cells by an MTT assay suggested that the elimination of *S. aureus* 4s

Table 6.1. MIC, $MBIC_{90}$ and $MBEC_{90}$ of C1, C1-PNC and antibiotics against *S. aureus* 4s.

Bactericidal Agents	MIC (µM)	$MBIC_{90}$ (µM)	$MBEC_{90}$ (µM)
C1	12	128	192
Gentamicin	2048	4096	8192
Ciprofloxacin	32	64	1536
C1-PNC	20	256	384

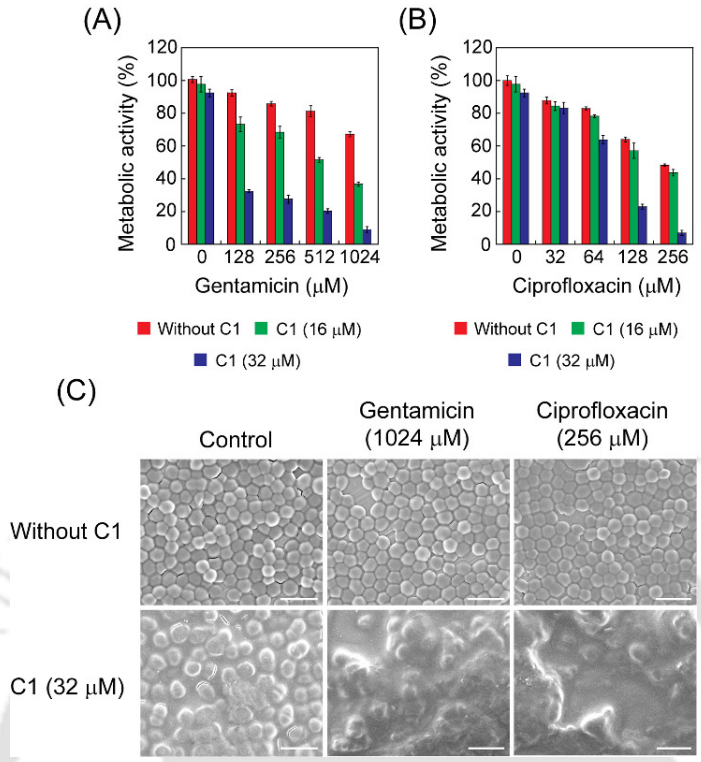

Figure 6.1. Combination effect of (A) C1 and gentamicin and (B) C1 and ciprofloxacin on *S. aureus* 4s biofilm. (C) FESEM analysis of the combination effect of C1 with either gentamicin or ciprofloxacin on pre-formed MRSA biofilm. Scale bar for the images is 2.0 μm.

biofilm was higher in the combinatorial treatment as compared to treatment with either the antibiotics or C1 alone (Figure 6.1A-B). Evidence for superior eradication of MRSA biofilm in the combination treatment was also captured in FESEM analysis, wherein significant disruption of cell-cell adhesion and disintegration of the cells was manifested (Figure 6.1C).

6.3.2. C1-loaded PLGA Nanocarrier (C1-PNC)

To harness the adjuvant potential of C1 in antibiofilm therapy, it was pertinent to develop a robust and non-toxic delivery system that can afford sustained release of the amphiphilic payload and retain its activity in the complex biofilm matrix. In this regard, deployment of nanoscale carriers can be regarded as a viable option, based on their beneficial attributes and well documented use in bactericidal and antibiofilm applications (Huh and Kwon

2011; Wang et al. 2014; Adhikari et al. 2013; Goswami et al. 2014; Duncan et al. 2015). In the present study, PLGA nanoparticles (PNPs) were employed for the delivery of C1 into MRSA biofilm matrix, given the biocompatibility and biodegradable property of PNPs and their ability to support sustained release of a bioactive payload (Danhier et al. 2012). PNPs were synthesized by a single-emulsion method, while C1-loaded PLGA nanocarrier (C1-PNC) was generated by incubating PNPs with varying concentration of C1. FESEM analysis indicated that PNPs as well as C1-PNC were spherical in shape (Figure 6.2A-B). UV-visible spectroscopy and FTIR analysis revealed that the characteristic absorption bands and stretching frequencies of PNP and C1 were conserved in C1-PNC, which indicated loading of the amphiphile in PNPs (Figure 6.2C-D). DLS analysis indicated that the primary species in solution for PNPs was around 174 nm in size (Figure 6.2E), while that of C1-PNC was around 293 nm (Figure 6.2F), which suggested that loading of the amphiphile in PNPs resulted in the formation of larger aggregates in solution.

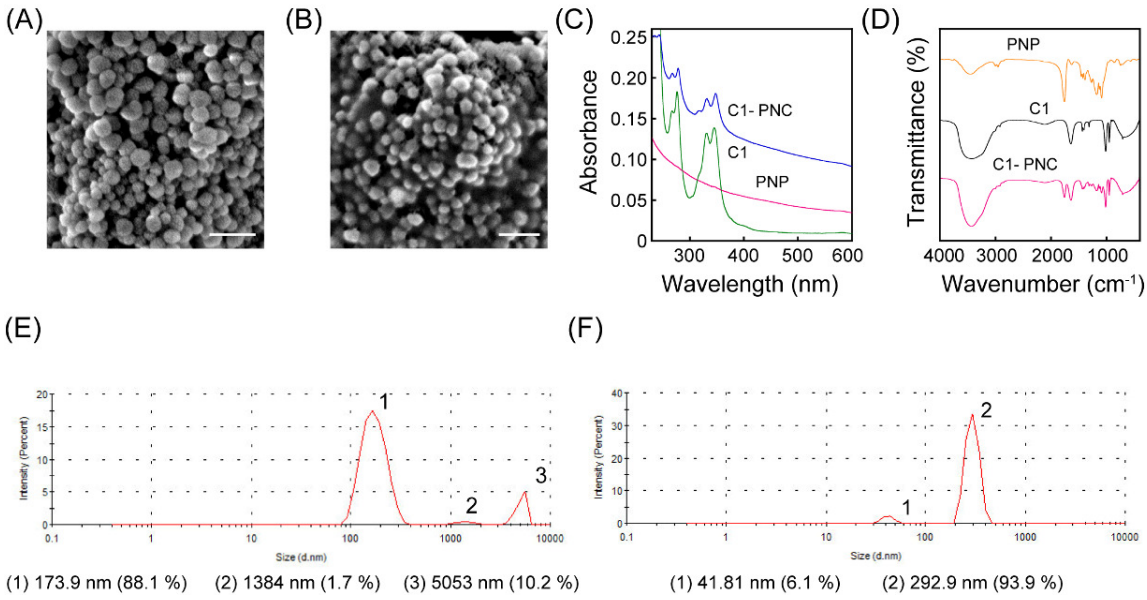

Figure 6.2. FESEM image of (A) PLGA nanoparticle (PNP), (B) C1-loaded PLGA nanoparticle (C1-PNC). Scale bar for the images is 200 nm. Characterization of C1-PNC using (C) UV-visible spectroscopy and (D) FT-IR analysis. Dynamic light scattering (DLS) based particle size analysis of (E) PNP and (F) C1-PNC. The particle size and percentage of aggregated species of C1-PNC (in parentheses) corresponding to peaks 1-3 are indicated below the plot.

Quantitative estimation of amphiphile loading in PNPs revealed that at an amphiphile loading concentration of 400 µM, the loading capacity (LC) and the amount of encapsulated C1 in PNPs was around 15% and 226 µM, respectively (Figure 6.3A). Fluorescence microscopy based live-dead assay with the dyes cFDA-SE and PI indicated that C1-PNC displayed bactericidal activity against the tested MRSA strain (Appendix Figure A6.3), which also suggested that the membrane-directed activity of C1 was retained in the amphiphile-loaded nanocarrier. The *in vitro* release kinetics experiments with C1-PNC (loaded with of 200 µM C1) revealed that at physiological pH, a slow release of the amphiphile from C1-PNC was observed in both HEPES buffer and *S. aureus* biofilm EPS and after 72 h of incubation, the cumulative release of C1 in HEPES buffer and biofilm EPS was around 27% and 20%, respectively (Figure 6.3B). In acidic pH (citrate buffer, pH 3.0), the cumulative release of C1 was relatively high and estimated as nearly 55% after 72 h of incubation (Figure 6.3B). Interestingly, the release of C1 in MRSA biofilm (the pH of MRSA biofilm spent media was ~3.0) was manifold higher and estimated to be nearly 73% in 72 h (Figure 6.3B). Perhaps the acidic nature of *S. aureus* biofilm matrix (Foulston et al. 2014) in conjunction with the soluble smaller constituents of the MRSA biofilm matrix account for a biofilm matrix-responsive of C1 as the corresponding release from the matrix-associated EPS at pH 7.0 was relatively less (Figure 6.3B).

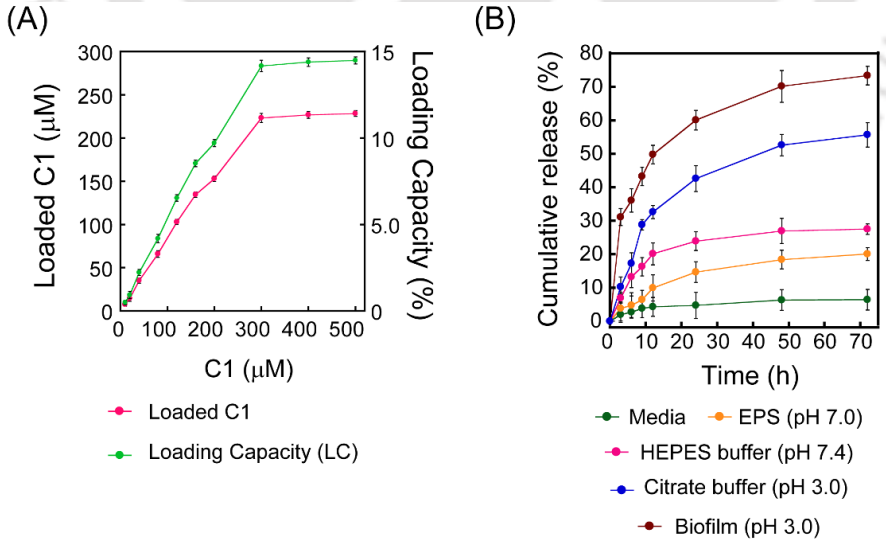

Figure 6.3. (A) Estimation of C1 loading in PLGA nanoparticle. (B) Release of C1 from C1-PNC in buffers and in *S. aureus* 4s biofilm and EPS.

6.3.3. Combination Effect of C1-PNC and Therapeutic Antibiotics on MRSA Biofilm

The MIC, $MBIC_{90}$ and $MBEC_{90}$ of C1-PNC against planktonic cells and biofilm of *S. aureus* 4s was initially determined and was observed to be 20 µM, 256 µM and 384 µM, respectively (Table 6.1). In the combination experiments, the concentration of C1-PNC and the antibiotics was lower than their respective $MBIC_{90}$ and $MBEC_{90}$ against the target MRSA. Estimation of biofilm cell metabolic activity by an MTT assay clearly indicated that C1-PNC could potentiate the efficacy of the antibiotics and render eradication of MRSA biofilm and the magnitude of biofilm elimination could be correlated with the dose of C1-PNC and the antibiotics (Figure 6.4A-B). It may be mentioned here that C1-PNC could also enhance the efficacy of the antibiotics and prevent biofilm formation by the MRSA strain as evident in the biofilm inhibition assays (Figure A6.4). The adjuvant potential of C1-PNC was further substantiated by a marked decrease in the $MBIC_{90}$ and

Table 6.2. Fold reduction in $MBIC_{90}$ of therapeutic antibiotics against biofilm of the MRSA strain *S. aureus* 4s in combination with C1-PNC.

Antibiotic (µM)	C1-PNC (µM)	Fold reduction in $MBIC_{90}$ of antibiotic
Gentamicin (1024 µM)	32	4.0
Ciprofloxacin (16 µM)	32	4.0

Table 6.3. Fold reduction in $MBEC_{90}$ of therapeutic antibiotics against biofilm of the MRSA strain *S. aureus* 4s in combination with C1-PNC.

Antibiotic (µM)	C1-PNC (µM)	Fold reduction in $MBEC_{90}$ of antibiotic
Gentamicin (1024 µM)	64	8.0
Ciprofloxacin (256 µM)	64	6.0

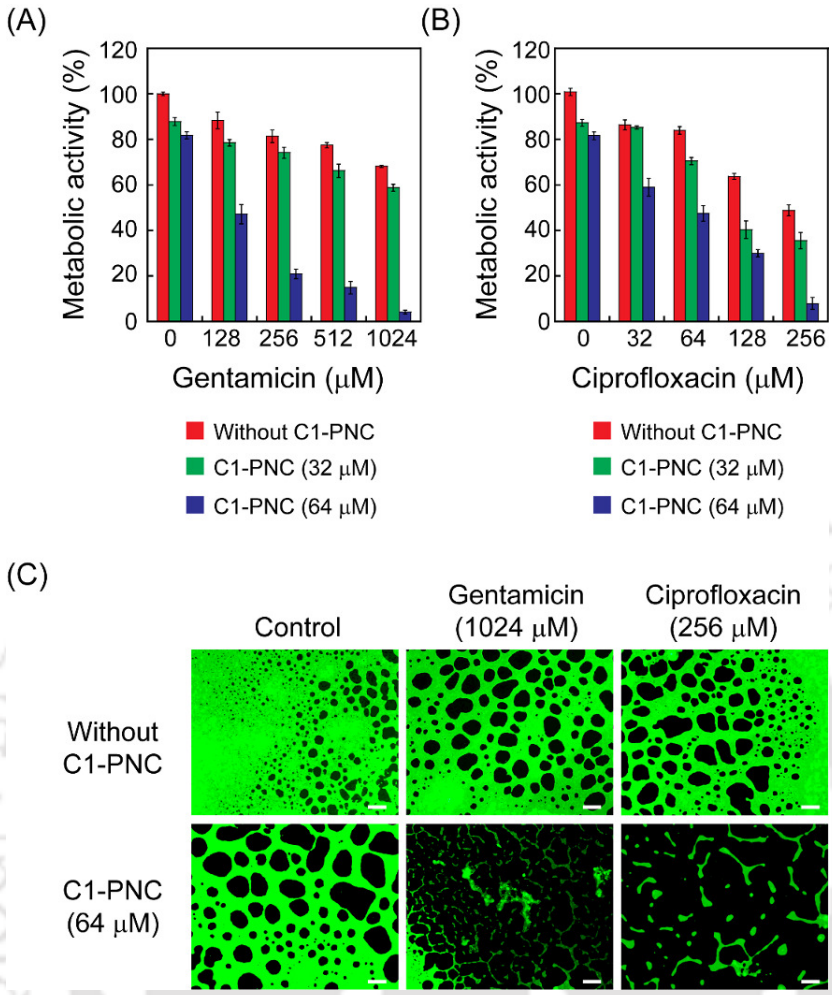

Figure 6.4. Combination effect of (A) C1-PNC and gentamicin and (B) C1-PNC and ciprofloxacin on *S. aureus* 4s biofilm. (C) cFDA-SE based fluorescence microscopic analysis of MRSA biofilm following treatment with C1-PNC in combination with either gentamicin or ciprofloxacin. Scale bar for the images is 100 μm.

$MBEC_{90}$ of the antibiotics in the combinatorial assays against the tested MRSA biofilm (Table 6.2-6.3). The enhanced bactericidal effect is perhaps a consequence of an increased uptake and superior access to internal targets for the chosen antibiotics. The significant enhancement in MRSA biofilm eradication by the combination of C1-PNC and the therapeutic antibiotics was also apparent in fluorescence microscopic analysis using the dye cFDA-SE, which indicated superior disruption of biofilm network in the combinatorial

assay in comparison to treatment with either the amphiphile or antibiotics alone (Figure 6.4C).

6.3.4. C1-PNC Potentiates Gentamicin Uptake in MRSA Cells

The biofilm experiments demonstrated the potential benefits of the combination between C1-PNC and gentamicin against MRSA biofilm. A plausible mechanism to explain this effect is that the membrane-targeting C1-PNC may increase cell permeability, facilitate higher uptake of gentamicin in MRSA cells and render the cells more susceptible to antibiotic-mediated killing. In order to corroborate the findings of the biofilm experiments, the combination effect of C1-PNC and gentamicin on the growth of MRSA planktonic cells was assessed. A significant decline in the growth of MRSA planktonic cells was observed upon treatment with 4.0 μM C1-PNC in combination with an increasing concentration of gentamicin and the combination resulted in a fourfold reduction in the MIC of gentamicin against the MRSA strain and a synergistic interaction was observed (Appendix Table A6.1). In order to ascertain whether the enhanced bactericidal efficacy of gentamicin in the combination studies is an outcome of increased cellular uptake of the antibiotic, a fluorescence-based assay was pursued to measure the cellular accumulation of gentamicin (Gubernator et al. 2006) in MRSA planktonic cells. Based on a calibration plot (Appendix Figure A6.5B), it was evident that when the initial gentamicin concentration was 256 μM, the uptake of the antibiotic in MRSA cells increased with time and was manifold higher in presence of 4.0 μM C1-PNC as compared to that observed when the antibiotic was used singularly (Figure 6.5A). Enhanced uptake of gentamicin in MRSA cells in presence of C1-PNC was also evident in the combination studies when a higher antibiotic concentration (512 μM) was used (Appendix Figure A6.5C). Further, enhanced uptake of gentamicin in MRSA cells was also evident in a control experiment, where the free form of the amphiphile (2.0 μM) was used in combination (Appendix Figure A6.5D). In order to gain further insight into antibiotic uptake in the combination experiments, the partitioning of gentamicin in MRSA cells was ascertained by measuring the ratio of the percentage of intracellular (I_{gen}) versus extracellular gentamicin (E_{gen}) as a function of time. When gentamicin was used singularly (256 μM), the relative gentamicin level in MRSA cells (I_{gen}/E_{gen}) exhibited an increasing trend, which was linear (Figure 6.5B).

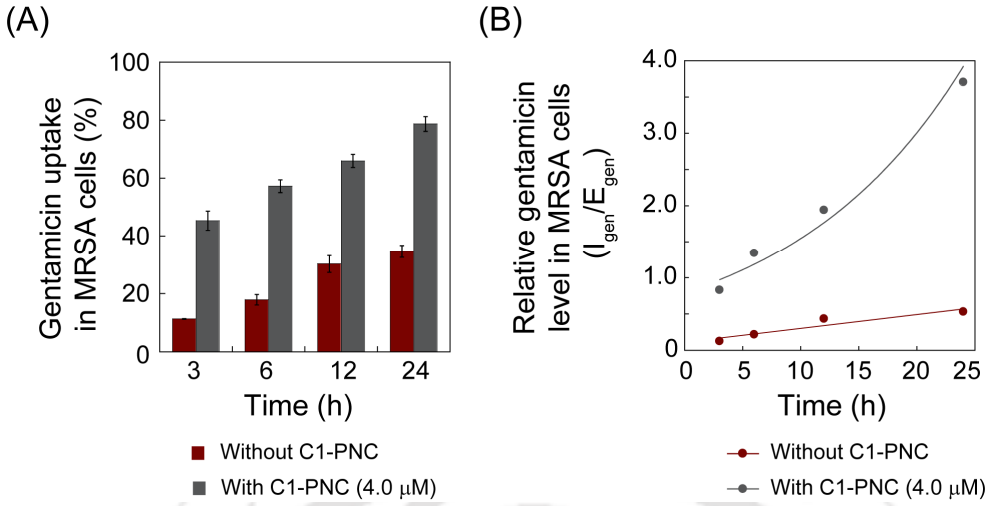

Figure 6.5. (A) Uptake of gentamicin in C1-PNC-treated MRSA cells. The concentration of gentamicin was 256 μM. (B) Partitioning of gentamicin in C1-PNC treated MRSA cells. The concentration of gentamicin used was 256 μM.

In contrast, gentamicin accretion in MRSA cells subjected to the combination treatment was distinctly higher and observed to increase exponentially with time (Figure 6.5B), clearly indicating the beneficial outcome of the combination treatment against MRSA cells. A similar trend was also observed when a higher concentration of gentamicin (512 μM) was used in combination with C1-PNC. Collectively, these experiments suggested that owing to the membrane targeting activity, C1- PNC could perhaps permeabilize the cells and augment the rate of gentamicin uptake, which led to higher accrual of antibiotic in cells and superior killing of MRSA cells.

6.3.5. Effect of C1-PNC on Efflux Activity in MRSA Cells

The combinatorial assays clearly indicated that superior eradication of MRSA biofilm was achieved when ciprofloxacin was used in combination with C1-PNC (Figure 6.4B-C), which suggested that the amphiphile-loaded nanocomposite could perhaps counter the resistance of MRSA against ciprofloxacin, resulting in enhanced elimination of the target pathogen. The phenomenon of efflux pump-mediated resistance against ciprofloxacin in *S. aureus* strains, including MRSA is well documented (Jang 2016; Costa et al. 2015).

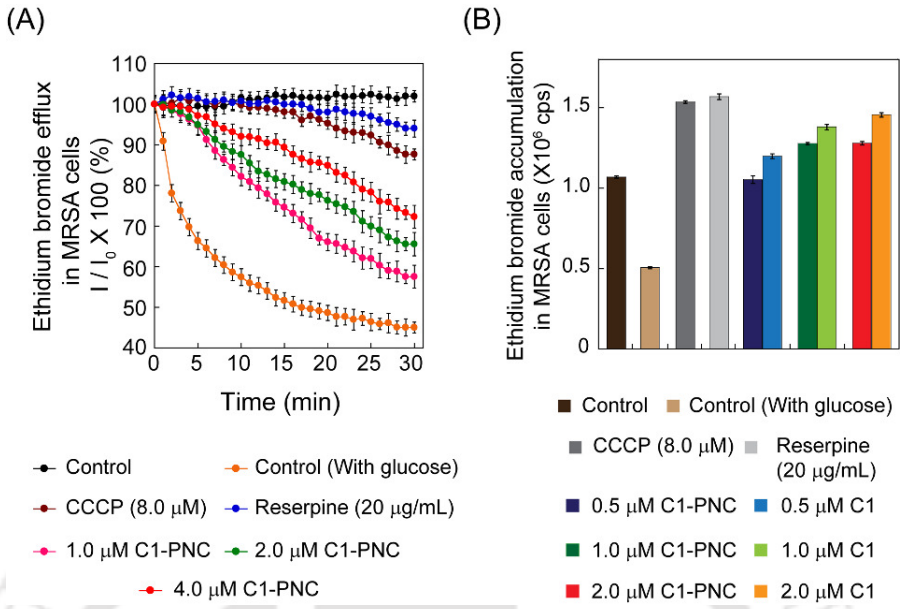

Figure 6.6. (A) Effect of C1-PNC on EtBr efflux in *S. aureus* 4s planktonic cells. (B) EtBr accumulation in *S. aureus* 4s cells subjected to treatment with C1-PNC and C1.

Based on the fact that C1-PNC could enhance the efficacy of ciprofloxacin against the MRSA strain *S. aureus* 4s, it was envisaged that the amphiphile-loaded nanocomposite perhaps hindered efflux activity in the MRSA strain. To probe this tenet, the presence of efflux activity in *S. aureus* 4s strain was ascertained by using the broad range efflux pump substrate, ethidium bromide (EtBr) in a fluorescence-based assay. In presence of glucose, MRSA cells displayed active efflux of EtBr as evident from the rapid decline in the relative fluorescence emission of the dye over an assay period of 30 min (Figure 6.6A). This observation is in agreement with the established notion that efflux of EtBr is induced in energized cells in presence of glucose (Viveiros et al. 2008) and it provided an indication of the presence of efflux activity in the tested MRSA strain. Further, the lack of EtBr efflux activity in MRSA cells incubated in the absence of glucose in conjunction with a strong inhibition of EtBr efflux in presence of the known EPIs CCCP and reserpine provided additional evidence of the presence of efflux activity in the tested MRSA strain. It may be mentioned here that the concentration of CCCP used in the assay was 8.0 µM. In the present study, it was observed that the MIC of CCCP against *S. aureus* 4s was 16 µM. Hence, CCCP was used in the EtBr efflux assay at sub-MIC levels. Susceptibility of

S. aureus strains to CCCP may vary and the use of low levels of CCCP in efflux assay has been reported earlier (Couto et al. 2008). Interestingly, a dose-dependent reduction in the efflux of EtBr was observed in MRSA cells upon exposure to C1-PNC (Figure 6.6A), which suggested that the amphiphile-loaded nanocarrier displayed efflux pump inhibitory activity. A control experiment indicated that bare PLGA nanoparticles (PNPs) failed to inhibit EtBr efflux activity in cells, while C1 in its free form rendered considerable inhibition of EtBr efflux (Appendix Figure A6.6), thereby indicating that efflux inhibition by C1-PNC could be attributed to the amphiphile and not the nanoparticle per se. Evidence for efflux pump inhibition by C1-PNC was further consolidated through an EtBr accumulation assay, which clearly indicated the propensity of *S. aureus* 4s cells to accrue EtBr in presence of the amphiphile-loaded nanocomposite, akin to the results obtained with the known EPIs CCCP and reserpine (Figure 6.6B).

6.3.6. C1-PNC Hinders Ciprofloxacin Efflux in MRSA Cells

The effective elimination of MRSA biofilm observed in the combinatorial assays using C1-PNC and ciprofloxacin (Figure 6.4B-C) was further verified in experiments with MRSA planktonic cells, which revealed enhanced ciprofloxacin-mediated killing of *S. aureus* 4s cells (Appendix Figure A6.7A), an eightfold reduction in the MIC of the ciprofloxacin and a synergistic interaction between the adjuvant nanomaterial and the antibiotic (Appendix Table A6.1). A similar trend of enhanced killing of MRSA cells was apparent when ciprofloxacin was employed in combination with the EPIs CCCP and reserpine (Appendix Figure A6.7B-C). Given that C1-PNC could impede EtBr efflux in the MRSA strain *S. aureus* 4s and EtBr is known to be a surrogate substrate for efflux pumps implicated in extrusion of fluoroquinolones such as ciprofloxacin in MRSA (Jang 2016; Patel et al. 2010) it was pertinent to ascertain whether the potentiating activity of C1-PNC observed in the combinatorial assay (Appendix Figure A6.7A) was a consequence of inhibition of ciprofloxacin efflux in MRSA cells. To this end, ciprofloxacin accumulation in *S. aureus* 4s cells was measured by a previously reported fluorimetric method (Giraud et al. 2000). On the basis of a calibration plot (Appendix Figure A6.8A), it was evident that ciprofloxacin accumulation in MRSA cells in the absence of C1 or C1-PNC, increased gradually and attained a plateau level of around 3.6 µM per mg of cell,

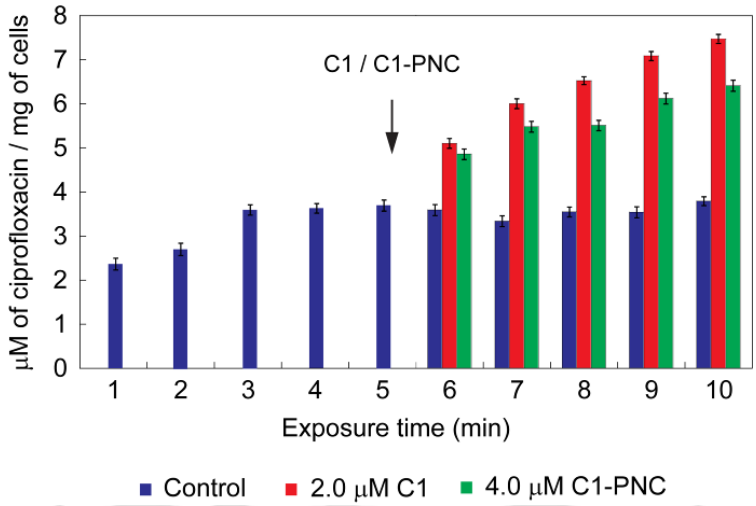

Figure 6.7. Measurement of *S. aureus* 4s cell-associated ciprofloxacin. Cells were incubated in 50 mM phosphate buffer (pH 7.0) with 32 μM ciprofloxacin for the first five minutes. Following addition of either C1 or C1-PNC (indicated by an arrow) in separate sets, the cells were incubated for another five minutes. Subsequently the cells were washed with ice cold phosphate buffer and incubated in 0.1 M glycine buffer (pH 3.0) for 15 h and then the cells were pelleted and ciprofloxacin in the supernatant was measured.

following 3.0 min of exposure to the antibiotic (Figure 6.7). Interestingly, soon after addition of 4.0 μM C1-PNC, a rapid and notable increase in the accumulation of ciprofloxacin in MRSA cells was recorded, with the final ciprofloxacin levels reaching around 6.4 μM per mg of cell (Figure 6.7). A similar trend in the increase of ciprofloxacin accumulation in MRSA cells was evident for combinatorial treatment with C1 and the antibiotic, albeit of a slightly higher magnitude (Figure 6.7). The notion that C1-PNC could counter the active efflux process, which limits accumulation of ciprofloxacin in MRSA cells was further substantiated as a similar pattern of ciprofloxacin accumulation in MRSA cells was observed when the EPIs CCCP and reserpine were employed in combination with ciprofloxacin in control experiments (Appendix Figure A6.8B).

6.3.7. Plausible Mode of Efflux Inhibition in MRSA Cells

In clinical MRSA strains, a key efflux pump involved in the extrusion of EtBr and ciprofloxacin is the NorA protein, which belongs to the major facilitator superfamily

(MFS) type of pump (Jang 2016). Hence, it is expected that the clinical MRSA strain *S. aureus* 4s, which exhibited potent efflux of both EtBr and ciprofloxacin is likely to possess a NorA protein. The possibility of this notion is supported by the fact that a known NorA pump inhibitor such as reserpine could potentiate the action of ciprofloxacin against *S. aureus* 4s cells (Appendix Figure A6.7C), which is consistent with the results reported for NorA expressing *S. aureus* strains in an earlier study (Sabatini et al. 2008). Notwithstanding the high likelihood of the presence of NorA in *S. aureus* 4s, the presence of other efflux pump proteins known to be involved in the efflux of EtBr and ciprofloxacin (Jang 2016) cannot be completely ruled out. It has been shown in previous studies that in *S. aureus*, the NorA protein uses the proton motive force to support transport of substrates and is thus inhibited by CCCP, which is known to dissipate the membrane proton gradient (Kaatz et al. 2002). The amphiphile C1 can disrupt the transmembrane potential in bacterial cells (Chapter 2, Figure 2.13). Hence, akin to CCCP, it is expected that C1-loaded PNP is likely to inhibit NorA efflux activity in *S. aureus* 4s cells by dispelling the transmembrane potential in the target cells.

In order to probe the plausible interaction between the amphiphile C1 and the NorA efflux pump present in MRSA, the subsequent goal was to pursue molecular docking studies with C1 and the *S. aureus* NorA protein. Given that the crystal structure of NorA is yet to be determined, a model of the target protein was first generated by homology modelling. The *S. aureus* NorA structure was modelled based on close homologues (PDB ID: 1PW4, 3WDO and 4LDS) and the generated model was validated using standard methods (Appendix Figure A6.9-A6.12, Table A6.2-A6.3). Molecular docking studies indicated that the binding energy for the interaction between C1 and the modelled NorA protein was -10.02 Kcal/mol, while that obtained with the known EPIs CCCP and reserpine were -4.69 Kcal/mol and -6.42 Kcal/mol, respectively. Interaction of C1 with the NorA model was primarily mediated by hydrophobic interactions, wherein 15 amino acid residues of the NorA protein were involved (Appendix Figure A6.13A, Table A6.4). In addition, one hydrogen bond and a π-cation interaction were also implicated in the interaction between C1 and the NorA protein (Appendix Figure A6.13A, Table A6.4). Likewise, the predominant role of the hydrophobic interaction was also captured in the docking studies with the known EPIs reserpine and CCCP (Appendix Figure A6.13B-

A6.13C, Table A6.4). Collectively, the docking studies with C1 and the EPIs suggested that the NorA binding pocket was primarily hydrophobic in nature. Hydrophobic as well as H-bonding interactions are thought to be involved in the interaction of ciprofloxacin with NorA pump (Joshi et al. 2014). It thus seems probable that binding of C1 with NorA through hydrophobic interactions and H-bond may hinder interaction of ciprofloxacin with NorA protein and thereby reduce efflux of the antibiotic from the target cell.

6.3.8. Cytotoxic Potential of Combinatorial Therapy

Aminoglycosides and fluoroquinolones are considered as important therapeutic agents for mitigation of staphylococcal infections (LaPlante and Woodmansee 2009; Houlihan et al. 1997; Tsuji and Rybak 2005). However, antibiotics belonging to these categories are known to have toxic implications (Cosgrove et al. 2009; Owens and Ambrose 2005) and hence their therapeutic application warrants circumspection. In order to circumvent this problem, a viable alternative is combination therapy, wherein the effective therapeutic dose

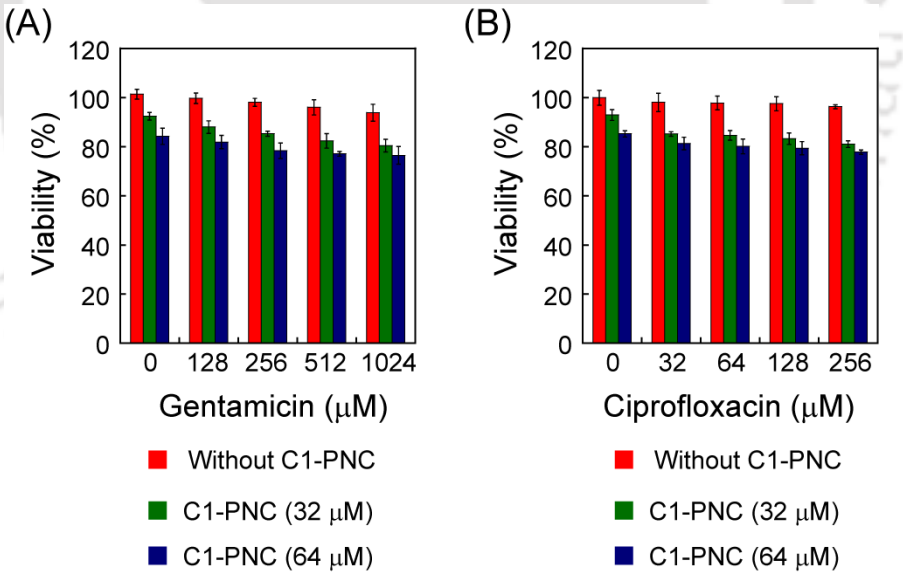

Figure 6.8. MTT assay to ascertain the effect of C1-PLNC in combination with gentamicin and ciprofloxacin on HEK 293 cells. Each data point represents mean ± standard deviation from six samples.

of the antibiotic is decreased and thus there is a reduction in the adverse effect imparted on host cells. In the present study, it was apparent that deployment of C1-PNC as an adjuvant was beneficial as it could significantly reduce the effective dose of the antibiotics gentamicin and ciprofloxacin against the MRSA strain *S. aureus* 4s (Table 6.2-6.3, Appendix Table A6.1). However, to assess the merit of this combination, it was pertinent to ascertain the cytotoxic potential of the combination regime. To this end, an MTT assay indicated that at the tested concentrations of C1-PNC and the antibiotics in combination, viability of HEK 293 cells was nearly 80% (Figure 6.8). It may also be mentioned here that in the context of host-directed toxicity, loading of the amphiphile C1 onto PNPs yielded significant benefit as the toxicity of C1-PNC on HEK 293 cells was manifold less as compared to C1 alone at an equivalent concentration (Appendix Figure A6.14). The low level of payload release at physiological pH from C1-PNC (Figure 6.3B) presumably leads to a reduction in cell-directed toxicity. In the cytotoxicity assay, the highest tested concentration of gentamicin and ciprofloxacin was 1024 µM and 256 µM, respectively, which corresponded to the $MBEC_{90}$ values of the respective antibiotics against the MRSA strain *S. aureus* 4s, when used in combination with 64 µM C1-PNC (Table 6.3). It was also noteworthy that the viability of HEK 293 cells was high following treatment with either 1024 µM gentamicin or 256 µM ciprofloxacin singularly (Figure 6.8). Clearly, the synergistic combination of C1-PNC and the antibiotics not only enhanced the anti-MRSA efficacy of the antibiotics but also provided significant therapeutic leverage by reducing the risk of antibiotic-associated host cell toxicity.

6.4. Significant Findings

The salient findings of this chapter are as follows:

1. The amphiphile-loaded nanomaterial (C1-PNC) could restore antibiotic sensitivity of a clinical MRSA strain, reduce the minimum effective dose of therapeutic antibiotics such as gentamicin and ciprofloxacin.

2. The membrane-directed activity of the amphiphilic C1 could be leveraged as the use of C1-PNC as an adjuvant resulted in higher cellular uptake of gentamicin and superior elimination of MRSA cells, likely caused by a compromise in the membrane barrier, which in turn, predispose the MRSA cells to the action of gentamicin.

3. The ability of C1-PNC to inhibit efflux pump and potentiate the activity of ciprofloxacin against an MRSA strain in a combinatorial assay is a significant lead and a promising intervention.

4. The present study also highlighted that the developed adjuvant nanomaterial not only countered the fundamental resistance mechanism in MRSA, reduce the effective dose and enhance the efficacy of therapeutic antibiotics, but also rendered the generation of a non-toxic combination regime, which can have prospect in mitigation of MRSA-mediated infection.

In the constant endeavour to overcome the scarcity of therapeutic approaches against life-threatening MRSA infections, the present study, which describes an amphiphile-based adjuvant nanomaterial, presents a promising approach to generate an anti-MRSA therapeutic. In future, it will be interesting to validate the adjuvant potential of the developed nanomaterial against a broader set of MRSA strains and in *in-vivo* infection models.

SUMMARY AND FUTURE PERSPECTIVE

SUMMARY AND FUTURE PERSPECTIVE

The ominous rise of drug-resistant bacteria in conjunction with a diminishing antibiotic armory demands a new paradigm in the discovery of antibacterials. Given this predicament, it is imperative to develop antibacterials, that act on compelling targets and are not compromised by resistance development. In this context, the present investigation, which reports the bactericidal activity and therapeutic potential of a dual-target pyridinium-based synthetic amphiphile augers well in addressing a contemporary global healthcare problem. The salient advancements of the study and the future prospect is discussed in the following section:

(1) The design principle of the synthetic amphiphile C1 was realized through a judicious tethering of chemical descriptors, that enabled spectroscopic probing of interactions and rendered a membrane-disrupting and DNA cleavage activity to the molecule. Bestowed with an ability to cleave cellular plasmid DNA, which is likely to harbor and disseminate resistance traits, the dual-target amphiphile C1 emerges as an antibacterial that can disarm the resistance mechanism and possibly curb the spread of drug-resistance encoding genes in pathogenic bacteria. The unique design principle of the synthetic amphiphile may serve as a prototype and inspire the development of analogous synthetic antibacterials in future for combating the menace of drug-resistant bacteria.

(2) The significant membrane-directed activity of the amphiphile C1 is likely to reduce the probability of resistance development in target pathogens and thus holds interesting prospect in antibacterial therapy. Further, the membrane-directed activity of the amphiphile could be leveraged to render the target bacteria susceptible to therapeutic antibiotics in combination, as vindicated by the encouraging results obtained in the present study. In future, it would be important to ascertain the adjuvant potential of the amphiphile in an *in vivo* model.

(3) The significant healthcare burden imposed by *Staphylococcus aureus* biofilm-associated infections coupled with their resistance to therapeutic antibiotics demands

potent antibiofilm agents. The present investigation addresses this important issue by presenting a potentially therapeutic nanomaterial loaded with the dual-target amphiphile C1, which targets *S. aureus* biofilm extracellular DNA (eDNA), breaches the matrix barrier, concurrently gains access and eliminates matrix-encased cells, resulting in dramatic abolition of biofilm. In an age when the efficacy of therapeutic antibiotics is diminishing, the developed nanomaterial renders an immutable effect, akin to 'killing two birds with a single stone' and provides a unique therapeutic platform for abolition of biofilm.

(4) The prevalence of life threatening infections caused by methicillin-resistant *S. aureus* (MRSA) underscores an urgent need for an effective anti-MRSA intervention. In the present investigation, this important issue is addressed by presenting a nanomaterial loaded with the amphiphile C1 as an adjuvant, that could enhance the activity of therapeutic antibiotics in a combinatorial regime and restore susceptibility of MRSA biofilm to antibiotics. Studies undertaken to probe the mechanism revealed higher cellular uptake of gentamicin and superior elimination of MRSA cells, while the ability of the developed nanomaterial to impede efflux pump activity in MRSA is a promising lead towards rejuvenating an effective ciprofloxacin-mediated therapy against MRSA. A significant highlight of the investigation is that the developed adjuvant nanomaterial not only countered the fundamental resistance mechanism in MRSA, but also reduced the effective dose of therapeutic antibiotics and thereby rendered the generation of a non-toxic combination regime, which could have prospect in mitigation of MRSA-mediated clinical infection. In the constant endeavour to overcome MRSA infections, it will be interesting in future to validate the adjuvant potential of the developed nanomaterial against a broader set of clinical MRSA strains and in *in vivo* infection models.

(5) The amphiphile C1 exhibited significant membrane-targeting activity against target bacteria. Hence, it would be interesting in future to explore the amphiphile as a surface-active antibacterial agent and inhibit the formation of biofilms, which constitute a significant menace in the treatment of device-related infections. The ability of the amphiphile-loaded nanomaterial (C1-HNC) to annihilate pre-grown biofilm from a model

catheter vindicates the prospect of the generated payload nanomaterial in device-associated antibiofilm therapy. In future, it would be interesting to use the amphiphile-loaded nanocarrier in conjunction with a rational materials chemistry principle and develop a surface active coating for catheters and other medical devices that supports a controlled-release of the active amphiphile and prevents invasion by biofilms.

The present investigation essentially provides a fundamental guideline to the research community working at the intersection of chemistry, biology and materials science and striving to develop synthetic molecules that display potent bactericidal activity, are non-toxic and hold therapeutic potential against life-threatening antibiotic-resistant bacteria. A graphical representation of the significant findings emerging from the present investigation is indicated in in **Scheme 1**.

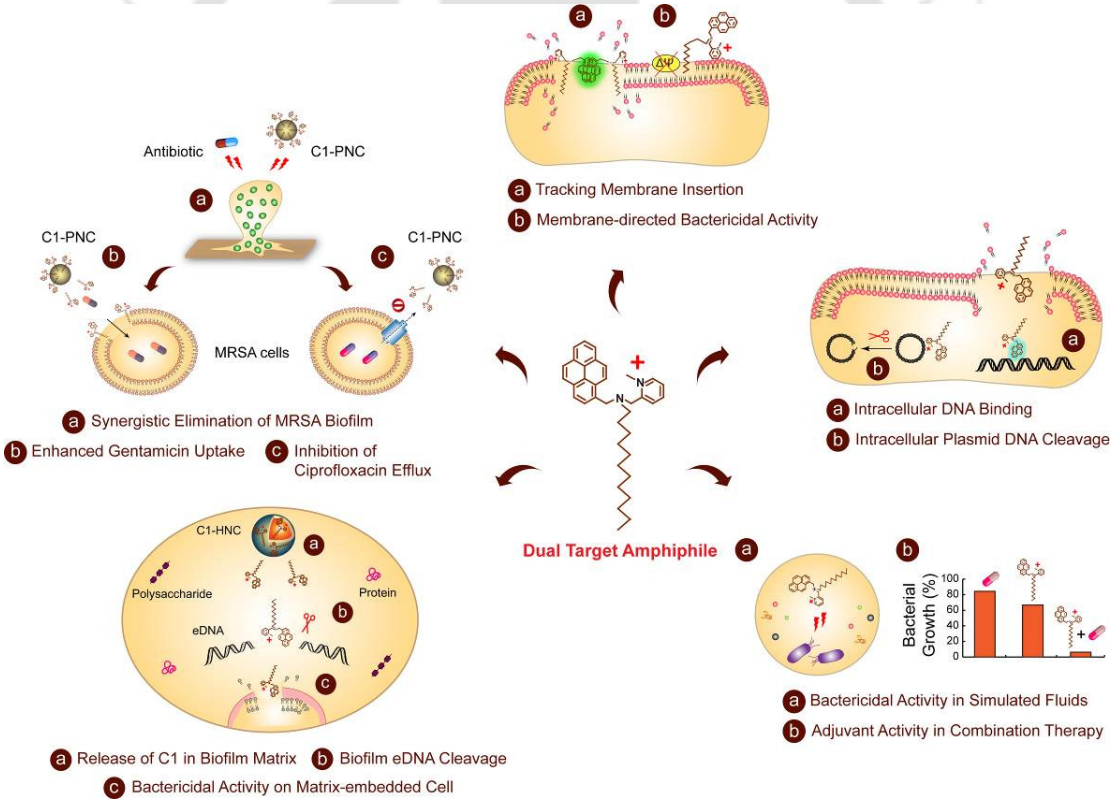

Scheme 1. Graphical representation of the significant findings of the present investigationn.

BIBLIOGRAPHY

Bibliography

1. Adhikari, M. D.; Das, G.; Ramesh, A. Retention of nisin activity at elevated pH in an organic acid complex and gold nanoparticle composite. *Chem. Commun*. **2012**, *48*, 8928-8930.
2. Adhikari, M. D.; Goswami, S.; Panda, B. R.; Chattopadhyay, A.; Ramesh, A. Membrane-directed high bactericidal activity of gold nanoparticle-polythiophene composite for niche applications against pathogenic bacteria, *Adv. Healthcare Mater*. **2013**, *2*, 599-606.
3. Alekshun, M. N.; Levy, S. B. Molecular mechanisms of antibacterial multidrug resistance. *Cell*. **2007**, *128*, 1037-1050.
4. Allesen-Holm, M.; Barken, K. B.; Yang, L.; Klausen, M.; Webb, J. S.; Kjelleberg, S.; Molin, S.; Givskov, M.; Tolker-Nielsen, T. A characterization of DNA release in *Pseudomonas aeruginosa* cultures and biofilms. *Mol Microbiol*. **2006**, *59*, 1114-1128.
5. Almeida Da Silva, P. E.; Palomino, J. C. Molecular basis and mechanisms of drug resistance in *Mycobacterium tuberculosis*: classical and new drugs. *J Antimicrob Chemother*. **2011**, *66*, 1417-1430.
6. Archer, N. K.; Mazaitis, M. J.; Costerton, W.; Leid, J. G.; Powers, M. E.; Shirtliff, M. E. *Staphylococcus aureus* biofilms: properties, regulation and roles in human disease. *Virulence* **2011**, *2*, 445-459.
7. Arciola, C. R.; Campoccia, D.; Speziale, P.; Montanaro, L.; Costerton, J. W. Biofilm formation in Staphylococcus implant infections. A review of molecular mechanisms and implications for biofilm-resistant materials. *Biomaterials*. **2012**, *33*, 5967-5982.
8. Arpin, C.; Noury, P.; Boraud, D.; Coulange, L.; Manetti, A.; Andre, C.; M'Zali, F.; Quentin, C. NDM-1-producing *Klebsiella pneumoniae* resistant to colistin in a French community patient without history of foreign travel, *Antimicrob. Agents Chemother.* **2012,** *56*, 3432-3434.
9. Atkins, J. L.; Patel, M. B.; Cusumano, Z.; Gokel, G. W. Enhancement of antimicrobial activity by synthetic ion channel synergy. *Chem. Commun*. **2010**, *46*, 8166-8167.

10. Banerjee, R.; Das, P. K.; Srilakshmi, G. V.; Chaudhuri A.; Rao, N. M. Novel series of non-glycerol-based cationic transfection lipids for use in liposomal gene delivery. *J. Med. Chem.* **1999**, *42*, 4292-4299.
11. Barantsevich, E. P.; Churkina, I. V.; Barantsevich, N. E.; Pelkonen, J.; Schlyakhto, E. V.; Woodford, N. Emergence of *Klebsiella pneumoniae* producing NDM-1 carbapenemase in Saint Petersburg, Russia. *J. Antimicrob. Chemother.* **2013,** *68*, 1204-1206.
12. Barber, K. E.; Werth, B. J.; Ireland, C. E.; Stone, N. E.; Nonejuie, P.; Sakoulas, G.; Pogliano, J.; Rybak, M. J. Potent synergy of ceftobiprole plus daptomycin against multiple strains of *Staphylococcus aureus* with various resistance phenotypes, *J. Antimicrob. Chemother.* **2014,** *69*, 3006-3010.
13. Basu, A.; Thiyagarajan, D.; Kar, C.; Ramesh, A.; Das, G. Synthesis, crystal structure and biomolecular interaction studies of pyridine-based thiosemicarbazone and its Ni (II) and Cu (II) complexes. *RSC Adv*. **2013**, *3*, 14088-14098.
14. Baussanne, I.; Bussiere, A.; Halder, S.; Ganem-Elbaz, C.; Ouberai, M.; Riou, M.; Paris, J. M.; Ennifar, E.; Mingeot-Leclercq, M.P.; Decout, J. L. Synthesis and antimicrobial evaluation of amphiphilic neamine derivatives, *J. Med. Chem*. **2010**, *53*, 119-127.
15. Bavaro, M. F. *Escherichia coli* O157: what every internist and gastroenterologist should know. *Curr. Gastroenterol. Rep*. **2009**, *11*, 301-306.
16. Bera, S.; Zhanel, G. G.; Schweizer, F. Antibacterial activities of aminoglycoside antibiotics-derived cationic amphiphiles. Polyol-modified neomycin B-, kanamycin A-, amikacin-, and neamine-based amphiphiles with potent broad spectrum antibacterial activity. *J. Med. Chem*. **2010**, *53*, 3626-3631.
17. Blair, J. M.; Webber, M. A.; Baylay, A. J.; Ogbolu, D. O.; Piddock, L. J. Molecular mechanisms of antibiotic resistance. *Nat. Rev. Microbiol*. **2015**, *13*, 42-51.
18. Bolla, J. M.; Alibert-Franco, S.; Handzlik, J.; Chevalier, J.; Mahamoud, A.; Boyer, G.; Kiec-Kononowicz, K.; Pages, J. M. Strategies for bypassing the membrane barrier in multidrug resistant Gram-negative bacteria. *FEBS Lett*. **2011**, *585*, 1682-1690.

19. Bordi, C.; de Bentzmann, S. Hacking into bacterial biofilms: a new therapeutic challenge. *Ann. Intensive Care*. **2011**, *1*, 19.
20. Bowdish, D. M.; Davidson, D. J.; Lau, Y. E.; Lee, K.; Scott, M. G.; Hancock, R. E. Impact of LL-37 on anti-infective immunity. *J. Leukoc. Biol*. **2005**, *77*, 451-459.
21. Brahmachari, S.; Debnath, S.; Dutta, S.; Das, P. K. Pyridinium based amphiphilic hydrogelators as potential antibacterial agents. *Beilstein J. Org. Chem*. **2010**, *6*, 859-868.
22. Brincat, J. P.; Broccatelli, F.; Sabatini, S.; Frosini, M.; Neri, A.; Kaatz, G. W.; Cruciani, G.; Carosati, E. Ligand promiscuity between the efflux pumps human p-glycoprotein and *S. aureus* NorA. *ACS Med. Chem. Lett.* **2012**, *3*, 248-251.
23. Brink, A. J.; Coetzee, J.; Clay, C. G.; Sithole, S.; Richards, G. A.; Poirel, L.; Nordmann, P. Emergence of New Delhi Metallo-Beta-Lactamase (NDM-1) and *Klebsiella pneumoniae* Carbapenemase (KPC-2) in South Africa, *J. Clin. Microbiol.* **2012,** *50*, 525-527.
24. Brogden, K. A. Antimicrobial peptides: pore formers or metabolic inhibitors in bacteria? *Nat. Rev. Microbiol*. **2005**, *3*, 238-250.
25. Brown, E. D.; Wright, G. D. Antibacterial drug discovery in the resistance era. *Nature*. **2016**, *529*, 336-343.
26. Burli, R. W.; Ge, Y.; White, S.; Baird, E. E.; Touami, S. M.; Taylor, M.; Kaizerman J. A.; Moser, H. E. DNA binding ligands with excellent antibiotic potency against drug-resistant Gram-positive bacteria. *Bioorg. Med. Chem. Lett*. **2002**, *12*, 2591-2594.
27. Burli, R. W.; McMinn, D.; Kaizerman, J. A.; Hu, W.; Ge, Y.; Pack, Q.; Jiang, V.; Gross, M.; Garcia, M.; Tanaka, R.; Moser, H. E. DNA binding ligands targeting drug-resistant Gram-positive bacteria. Part 1: Internal benzimidazole derivatives. *Bioorg. Med. Chem. Lett*. **2004**, *14*, 1253-1257.
28. Burton, E.; Gawande, P. V.; Yakandawala, N.; LoVetri, K.; Zhanel, G. G.; Romeo, T.; Friesen, A. D.; Madhyastha, S. Antibiofilm activity of GlmU enzyme inhibitors against catheter-associated uropathogens. *Antimicrob. Agents Chemother*. **2006**, *50*, 1835-1840.

29. Bush, K.; Courvalin, P.; Dantas, G.; Davies, J.; Eisenstein, B.; Huovinen, P.; Jacoby, G. A.; Kishony, R.; Kreiswirth, B. N.; Kutter, E.; Lerner, S. A.; Levy, S.; Lewis, K.; Lomovskaya, O.; Miller, J. H.; Mobashery, S.; Piddock, L. J.; Projan, S.; Thomas, C. M.; Tomasz, A.; Tulkens, P. M.; Walsh, T. R.; Watson, J. D.; Witkowski, J.; Witte, W.; Wright, G.; Yeh, P.; Zgurskaya, H. I. Tackling antibiotic resistance. *Nat. Rev. Microbiol*. **2011**, *9*, 894-896.
30. Cartiera, M. S.; Ferreira, E. C.; Caputo, C.; Egan, M. E.; Caplan, M. J.; Saltzman, W. M. Partial correction of cystic fibrosis defects with PLGA nanoparticles encapsulating curcumin. *Mol. Pharmaceutics* **2009**, *7*, 86-93.
31. Centers for Disease Control and Prevention. (https://www.cdc.gov/drugresistance/threat-report-2013/)
32. Chambers, H. F., DeLeo, F. R. Waves of resistance: *Staphylococcus aureus* in the antibiotic era. *Nat. Rev. Microbiol.* **2009**, *7*, 629-641.
33. Chang, H. H.; Cohen, T.; Grad, Y. H.; Hanage, W. P.; O'Brien, T. F.; Lipsitch, M. Origin and proliferation of multiple-drug resistance in bacterial pathogens, *Microbiol. Mol. Biol. Rev.* **2015,** *79*, 101-116.
34. Charteris, W. P.; Kelly, P. M.; Morelli, L.; Collins, J. K. Development and application of an *in vitro* methodology to determine the transit tolerance of potentially probiotic Lactobacillus and Bifidobacterium species in the upper human gastrointestinal tract. *J. Appl. Microbiol*. **1998**, *84*, 759-768.
35. Chen, C.; Pan, F.; Zhang, S.; Hu, J.; Cao, M.; Wang, J.; Xu, H.; Zhao, X.; Lu, J. R. Antibacterial activities of short designer peptides: a link between propensity for nanostructuring and capacity for membrane destabilization. *Biomacromolecules*. **2010**, *11*, 402-411.
36. Chiang, W. C.; Nilsson, M.; Jensen, P. O.; Hoiby, N.; Nielsen, T. E.; Givskov, M.; Tolker-Nielsen, T. Extracellular DNA shields against aminoglycosides in *Pseudomonas aeruginosa* biofilms. *Antimicrob. Agents Chemother*. **2013**, *57*, 2352-2361.
37. Choi, H.; Lee, D. G. Antimicrobial peptide pleurocidin synergizes with antibiotics through hydroxyl radical formation and membrane damage, and exerts antibiofilm activity. *Biochim Biophys Acta*. **2012**, *1820*, 1831-1838.

38. Chung, C. T.; Niemela, S. L.; Miller, R. H. One-step preparation of competent *Escherichia coli*: Transformation and storage of bacterial cells in the same solution. *Proc. Natl. Acad. Sci*. **1989**, *86*, 2172-2175.
39. Clare L.K.; Patrick, H.V. Cell dispersal in biofilms: An extracellular DNA masks nature's strongest glue. *Mol. Microbiol.* **2010**, *77*, 801-804.
40. CLSI performance standards for antimicrobial susceptibility tests; seventeenth informational supplement. CLSI document M100-S17. Clinical and Laboratory Standards Institute, Wayne, PA, 2007.
41. Collin, F.; Karkare, S.; Maxwell, A. Exploiting bacterial DNA gyrase as a drug target: current state and perspectives. *Appl Microbiol Biotechnol*. **2011**, *92*, 479-497.
42. Cosgrove, S. E.; Vigliani, G. A.; Campion, M.; Fowler, V. G. Jr.; Abrutyn, E.; Corey, G. R.; Levine, D. P.; Rupp, M. E.; Chambers, H. F.; Karchmer, A. W.; Boucher, H. W. Initial low-dose gentamicin for *Staphylococcus aureus* bacteremia and endocarditis is nephrotoxic. *Clin. Infect. Dis.* **2009**, *48*, 713-721.
43. Costa, S. S.; Viveiros, M.; Rosato, A. E.; Melo-Cristino, J.; Couto, I. Impact of efflux in the development of multidrug resistance phenotypes in *Staphylococcus aureus*. *BMC Microbiol.* **2015**, *15*, 232.
44. Costerton, J. W.; Stewart, P. S.; Greenberg, E. P. Bacterial biofilms: A common cause of persistent infections. *Science* **1999**, *284*, 1318-1322.
45. Cotter, P. D.; Gahan, C. G.; Hill, C. Analysis of the role of the *Listeria monocytogenes* F0F1 -AtPase operon in the acid tolerance response. *Int. J. Food Microbiol*. **2000**, *60*, 137-146.
46. Couto, I.; Costa, S. S.; Viveiros, M.; Martins, M.; Amaral, L. Efflux-mediated response of *Staphylococcus aureus* exposed to ethidium bromide. *J. Antimicrob. Chemother.* **2008**, *62*, 504-513.
47. Craig, W. A. Basic pharmacodynamics of antibacterials with clinical applications to the use of beta-lactams, glycopeptides, and linezolid. *Infect. Dis. Clin. North Am*. **2003**, *17*, 479-501.
48. Craig, W. A. Pharmacokinetic/pharmacodynamic parameters: rationale for antibacterial dosing of mice and men. *Clin. Infect. Dis*. **1998**, *26*, 1-10.

49. Cue, D.; Lei, M. G.; Lee, C. Y. Genetic regulation of the intercellular adhesion locus in *Staphylococci*. *Front. Cell. Infect. Microbiol*. **2012**, *2*, 38.
50. Danhier, F.; Ansorena, E.; Silva, J. M.; Coco, R.; Le Breton, A.; Preat, V. PLGA-based nanoparticles: an overview of biomedical applications. *J. Control Release* **2012**, *161*, 505-522.
51. Danhorn, T.; Fuqua, C. Biofilm formation by plant-associated bacteria. *Annu. Rev. Microbiol*. **2007**, *61*, 401-422.
52. Das, T.; Krom, B.P.; van der Mei, H.C.; Busscher, H.J.; Sharma, P.K. DNA mediated bacterial aggregation is dictated by acid-base interactions. *Soft Matter* **2011**, *7*, 2927-2935.
53. Das, T.; Sharma, P.K.; Busscher, H. J.; van der Mei, H.C.; Krom, B.P. Role of extracellular DNA in initial bacterial adhesion and surface aggregation. *Appl. Environ. Microbiol*. **2010**, *76*, 3405-3408.
54. Davies, J.; Davies, D. Origins and evolution of antibiotic resistance. *Microbiol. Mol. Biol. Rev*. **2010**, *74*, 417-433.
55. de laFuente-Nunez, C.; Reffuveille, F.; Fernandez, L.; Hancock, R. E. Bacterial biofilm development as a multicellular adaptation: antibiotic resistance and new therapeutic strategies. *Curr. Opin. Microbiol*. **2013**, *16*, 580-589.
56. Debnath, S.; Shome, A.; Das, D.; Das, P. K. Hydrogelation through self-assembly of Fmoc-peptide functionalized cationic amphiphiles: potent antibacterial agent. *J. Phys. Chem. B* **2010**, *114*, 4407-4415.
57. Delcour, A. H. Outer membrane permeability and antibiotic resistance. *Biochim. Biophys. Acta*. **2009**, *1794*, 808-816.
58. Deresinski S. Methicillin-resistant *Staphylococcus aureus*: an evolutionary, epidemiologic, and therapeutic odyssey. *Clin. Infect. Dis*. **2005**, *40*, 562-573.
59. Deresinski S. Vancomycin heteroresistance and methicillin-resistant *Staphylococcus aureus*. *J. Infect. Dis*. **2009**, *199*, 605-609.
60. Donlan, R. M. Biofilms and device-associated infections. *Emerg. Infect. Dis*. **2001**, *7*, 277-281.

61. Duncan, B.; Li, X.; Landis, R. F.; Kim, S. T.; Gupta, A.; Wang, L. S.; Ramanathan, R.; Tang, R.; Boerth, J. A.; Rotello, V. M. Nanoparticle-stabilized capsules for the treatment of bacterial biofilms. *ACS Nano* **2015**, *9*, 7775-7782.
62. Dutta, S.; Shome, A.; Kar, T.; Das, P. K. Counterion-induced modulation in the antimicrobial activity and biocompatibility of amphiphilic hydrogelators: influence of in-situ-synthesized Ag-nanoparticle on the bactericidal property. *Langmuir*. **2011**, *27*, 5000-5008.
63. Dyatkina, N. B.; Roberts, C. D.; Keicher, J. D.; Dai, Y.; Nadherny, J. P.; Zhang, W.; Schmitz, U.; Kongpachith, A.; Fung, K.; Novikov, A. A.; Lou, L.; Velligan, M.; Khorlin, A. A.; Chen., M. S. Minor groove DNA binders as antimicrobial agents. 1. pyrrole tetraamides are potent antibacterials against vancomycin resistant enteroccoci and methicillin resistant *Staphylococcus aureus*. *J. Med. Chem*. **2002**, *45*, 805-817.
64. Dymond, M. K.; Attard, G. S. Cationic type I amphiphiles as modulators of membrane curvature elastic stress *in vivo*. *Langmuir*. **2008**, *24*, 11743-11751.
65. Ejim. L.; Farha. M. A.; Falconer, S. B.; Wildenhain, J.; Coombes, B. K.; Tyers, M.; Brown, E. D.; Wright, G. D. Combinations of antibiotics and nonantibiotic drugs enhance antimicrobial efficacy. *Nat. Chem. Biol*. **2011,** *7*, 348-350.
66. Elzoghby, A. O.; Samy, W. M.; Elgindy, N. A. Albumin-based nanoparticles as potential controlled release drug delivery systems. *J. Control. Release*, **2012**, *157*, 168-182.
67. Elzoghby, A. O.; Samy, W. M.; Elgindy, N. A. Protein-based nanocarriers as promising drug and gene delivery systems. *J. Control. Release*, **2012**, *161*, 38-49.
68. Faig, A.; Arthur, T. D.; Fitzgerald, P. O.; Chikindas, M.; Mintzer, E.; Uhrich, K. E. Biscationic tartaric acid-based amphiphiles: Charge location impacts antimicrobial activity. *Langmuir* **2015,** *31*, 11875-11885.
69. Fair, R. J.; Tor, Y. Antibiotics and bacterial resistance in the 21st century. *Perspect. Medicin. Chem*. **2014**, *6*, 25-64.
70. Fernandes, P. Antibacterial discovery and development--the failure of success? *Nat Biotechnol*. **2006**, *24*, 1497-1503.

71. Fernández Fuentes, M. Á.; Ortega Morente, E.; Abriouel, H.; Pérez Pulido, R.; Gálvez, A. Antimicrobial resistance determinants in antibiotic and biocide-resistant gram-negative bacteria from organic foods. *Food Control*. **2014**, *37*, 9-14.
72. Fernandez, L.; Hancock, R. E. Adaptive and mutational resistance: role of porins and efflux pumps in drug resistance. *Clin. Microbiol. Rev*. **2012**, *25*, 661-681.
73. Finch, R. G.; Eliopoulos, G. M. Safety and efficacy of glycopeptide antibiotics. *J. Antimicrob. Chemother.* **2005**, *55: Suppl. S2*, ii5-ii13.
74. Findlay, B.; Zhanel G. G.; Schweizer, F. Cationic amphiphiles, A new generation of antimicrobials inspired by the natural antimicrobial peptide scaffold, *Antimicrob. Agents Chemother*. **2010**, *54*, 4049-4058.
75. Fischbach, M. A.; Walsh, C. T. Antibiotics for emerging pathogens, *Science* **2009**, *325*, 1089-1093.
76. Fischbach, M. Combination therapies for combating antimicrobial resistance. *Curr. Opin. Microbiol*. **2011**, *14*, 519-523.
77. Fischer, D.; Li, Y.; Ahlemeyer, B.; Krieglstein, J.; Kissel, T. *In vitro* cytotoxicity testing of polycations: influence of polymer structure on cell viability and hemolysis. *Biomaterials*. **2003**, *24*, 1121-1131.
78. Flemming, H. C.; Wingender, J. The biofilm matrix. *Nat. Rev. Microbiol*. **2010**, *8*, 623-633.
79. Floyd, J. L.; Smith, K. P.; Kumar, S. H.; Floyd, J. T.; Varela, M. F. LmrS is a multidrug efflux pump of the major facilitator superfamily from *Staphylococcus aureus*. *Antimicrob. Agents Chemother.* **2010**, *54*, 5406-5412.
80. Forier, K.; Raemdonck, K.; Smedt, S. C. D.; Demeester, J.; Coenye, T.; Braeckmans, K. Lipid and polymer nanoparticles for drug delivery to bacterial biofilms. *J. Control. Release* **2014**, *190*, 607-623.
81. Foster, J. W. Escherichia coli acid resistance: tales of an amateur acidophile. *Nat. Rev. Microbiol*. **2004**, *2*, 898-907.
82. Foster, J. W. When protons attack: microbial strategies of acid adaptation. *Curr. Opin. Microbiol*. **1999**, *2*, 170-174.

83. Foster, T. J.; Geoghegan, J. A.; Ganesh, V. K.; Hook, M. Adhesion, invasion and evasion: The many functions of the surface proteins of *Staphylococcus aureus*. *Nat. Rev. Microbiol.* **2014**, *12*, 49-62.
84. Foulston, L.; Elsholz, A. K. W.; DeFrancesco, A. S.; Losick, R. The extracellular matrix of *Staphylococcus aureus* biofilms comprises cytoplasmic proteins that associate with the cell surface in response to decreasing pH. *mBio* **2014**, *5*, e01667-14.
85. Ganesan, A.; Christena, L. R.; Subbarao, H. M. V.; Venkatasubramanian, U.; Thiagarajan, R.; Sivaramakrishnan, V.; Kasilingam, K.; Saisubramanian, N.; Ganesan, S. S. Identification of benzochromene derivatives as a highly specific NorA efflux pump inhibitor to mitigate the drug resistant strains of *S. aureus*. *RSC Adv*. **2016**, *6*, 30258-30267.
86. Giacometti, A.; Cirioni, O.; Del Prete, M. S.; Paggi, A. M.; D'Errico, M. M.; Scalise, G. Combination studies between polycationic peptides and clinically used antibiotics against Gram-positive and Gram-negative bacteria. *Peptides*, **2000**, *21*, 1155-1160.
87. Gill, E. E.; Franco, O. L.; Hancock, R. E. Antibiotic adjuvants: diverse strategies for controlling drug-resistant pathogens. *Chem. Biol. Drug. Des*. **2015**, *85*, 56-78.
88. Giraud, E.; Cloeckaert, A.; Kerboeuf, D.; Chaslus-Dancla, E. Evidence for active efflux as the primary mechanism of resistance to ciprofloxacin in *Salmonella enterica* serovar *typhimurium*. *Antimicrob. Agents Chemother.* **2000**, *44*, 1223-1228.
89. Gloag, E. S.; Turnbull, L.; Huang, A.; Vallotton, P.; Wang, H.; Nolan, L. M.; Mililli, L.; Hunt, C.; Lu, J.; Osvath, S. R.; Monahan, L. G.; Cavaliere, R.; Charles, I. G.; Wand, M. P.; Gee, M. L.; Prabhakar, R.; Whitchurch, C. B. Self-organization of bacterial biofilms is facilitated by extracellular DNA. *Proc. Natl. Acad. Sci*. **2013**, *110*, 11541-11546.
90. Gokel, G. W.; Negin, S. Synthetic membrane active amphiphiles. *Adv. Drug Delivery Rev*. **2012**, *64*, 784-796.
91. Gootz, T. D. The global problem of antibiotic resistance. *Crit. Rev. Immun*. **2010**, *30*, 79-93.

92. Gorden, J.; Small, P. L. Acid resistance in enteric bacteria. *Infect. Immun*. **1993**, *61*, 364-367.
93. Goswami, S.; Adhikari, M. D.; Kar, C.; Thiyagarajan, D.; Das, G.; Ramesh, A. Synthetic amphiphiles as therapeutic antibacterials: Lessons on bactericidal efficacy and cytotoxicity and potential application as an adjuvant in antimicrobial chemotherapy, *J. Mater. Chem. B* **2013**, *1*, 2612-2623.
94. Goswami, S.; Thiyagarajan, D.; Das, G.; Ramesh, A. Biocompatible nanocarrier fortified with a dipyridinium-based amphiphile for eradication of biofilm. *ACS Appl. Mater. Interfaces* **2014**, *6*, 16384-16394.
95. Goswami, S.; Thiyagarajan, D.; Samanta, S.; Das, G.; Ramesh, A. A zinc complex of a neutral pyridine-based amphiphile: a highly efficient and potentially therapeutic bactericidal material. *J. Mater. Chem. B*, **2015**, *3*, 7068-7078.
96. Govan, J. R.; Deretic, V. Microbial pathogenesis in cystic fibrosis: mucoid *Pseudomonas aeruginosa* and *Burkholderia cepacia*. *Microbiol. Rev*. **1996**, *60*, 539-574.
97. Gubernator, J.; Drulis-Kawa, Z.; Kozubek, A. A simply and sensitive fluorometric method for determination of gentamicin in liposomal suspensions. *Int. J. Pharm*. **2006**, *327*, 104-109.
98. Gutsmann, T.; Seydel, U. Impact of the glycostructure of amphiphilic membrane components on the function of the outer membrane of Gram-negative bacteria as a matrix for incorporated channels and a target for antimicrobial peptides or proteins. *Eur. J. Cell Biol*. **2010**, *89*, 11-23.
99. Haldar, J.; Kondaiah, P.; Bhattacharya, S. Synthesis and antibacterial properties of novel hydrolyzable cationic amphiphiles. Incorporation of multiple head groups leads to impressive antibacterial activity. *J. Med. Chem.* **2005**, *48*, 3823-3831.
100. Hall-Stoodley, L.; Costerton, J. W.; Stoodley, P. Bacterial biofilms: from the natural environment to infectious diseases. *Nat. Rev. Microbiol*. **2004**, *2*, 95-108.
101. Hancock, R. E. W.; Chapple, D. S. Peptide antibiotics. *Antimicrob. Agents Chemother.* **1999**, *43*, 1317-1323.
102. Hancock, R. E.; Sahl, H. G. Antimicrobial and host-defense peptides as new anti-infective therapeutic strategies. *Nat. Biotechnol*. **2006**, *24*, 1551-1557.

103. Harris, T. L.; Worthington. R. J.; Melander, C. Potent small-molecule suppression of oxacillin resistance in methicillin-resistant *Staphylococcus aureus*. *Angew. Chem. Int. Ed.* **2012**, *51*, 11254-11257.

104. Hawkey, P. M.; Jones, A. M. The changing epidemiology of resistance. *J. Antimicrob. Chemother*. **2009**, *64 Suppl 1*, i3-10.

105. Hayden, M.K.; Rezai, K.; Hayes, R. A.; Lolans, K.; Quinn, J.P.; Weinstein, R.A. Development of daptomycin resistance *in vivo* in methicillin-resistant *Staphylococcus aureus*. *J. Clin. Microbiol.* **2005**, *43*, 5285-5287.

106. He, J.; Soderling, E.; Osterblad, M.; Vallittu, P. K.; Lassila, L. V. Synthesis of methacrylate monomers with antibacterial effects against *S. mutans*. *Molecules* **2011,** *16*, 9755-9763.

107. Hernandez-Gil, J.; Ferrer, S.; Salvador, E.; Calvo, J.; Garcia-Espana, E.; Mareque-Rivas, J. C. A dinucleating ligand which promotes DNA cleavage with one and without a transition metal ion. *Chem. Commun*. **2013**, *49*, 3655-3657.

108. Hess, D. J.; Henry-Stanley, M. J.; Wells, C. L. Antibacterial synergy of glycerol monolaurate and aminoglycosides in *Staphylococcus aureus* biofilms. *Antimicrob. Agents Chemother.* **2014**, *58*, 6970-6973.

109. Hetrick, E. M.; Schoenfisch, M. H. Reducing implant-related infections: active release strategies. *Chem. Soc. Rev*. **2006**, *35*, 780-789.

110. Hoefel, D.; Grooby, W. L.; Monis, P. T.; Andrews, S.; Saint, C. P. A comparative study of carboxyfluorescein diacetate and carboxyfluorescein diacetate succinimidyl ester as indicators of bacterial activity. *J. Microbiol. Methods*. **2003**, *52*, 379-388.

111. Hogan, D.; Kolter, R. Why are bacteria refractory to antimicrobials? *Curr. Opin. Microbiol*. **2002**, *5*, 472-477.

112. Holler, J. G.; Slotved, H. C.; Molgaard, P.; Olsen, C. E.; Christensen, S. B. Chalcone inhibitors of the NorA efflux pump in *Staphylococcus aureus* whole cells and enriched everted membrane vesicles. *Bioorg. Med. Chem.* **2012**, *20*, 4514-4521.

113. Hoque, J.; Akkapeddi, P.; Yarlagadda, V.; Uppu, D. S.; Kumar, P.; Haldar, J. Cleavable cationic antibacterial amphiphiles: synthesis, mechanism of action, and cytotoxicities, *Langmuir* **2012,** *28*, 12225-12234.

114. Houlihan, H.H.; Mercier, R. C.; Rybak, M. J. Pharmacodynamics of vancomycin alone and in combination with gentamicin at various dosing intervals against methicillin-resistant *Staphylococcus aureus*-infected fibrin-platelet clots in an *in vitro* infection model. *Antimicrob. Agents Chemother.* **1997**, *41*, 2497-2501.

115. Hu, X. L.; Li, D.; Shao, L.; Dong, X.; He, X. P.; Chen, G. R.; Chen, D. Triazole-linked glycolipids enhance the susceptibility of MRSA to β-lactam antibiotics. *ACS Med. Chem. Lett.* **2015**, *6*, 793-797.

116. Huh, A.J.; Kwon, Y. J. "Nanoantibiotics": A new paradigm for treating infectious diseases using nanomaterials in the antibiotics resistant era. *J. Control. Release* **2011**, *156*, 128-145.

117. Hurdle, J. G.; O'Neill, A. J.; Chopra, I.; Lee, R. E. Targeting bacterial membrane function: an underexploited mechanism for treating persistent infections. *Nat. Rev. Microbiol*. **2011**, *9*, 62-75.

118. Izano, E. A.; Amarante, M. A.; Kher, W. B.; Kaplan, J. B. Differential roles of poly-N-acetylglucosamine surface polysaccharide and extracellular DNA in *Staphylococcus aureus* and *Staphylococcus epidermidis* biofilms. *Appl. Environ. Microbiol*. **2008**, *74*, 470-476.

119. Izumrudov, V. A.; Zhiryakova, M. V.; Goulko, A. A. Ethidium bromide as a promising probe for studying DNA interaction with cationic amphiphiles and stability of the resulting complexes. *Langmuir* **2002**, *18*, 10348-10356.

120. Jaffe, R. I.; Lane, J. D.; Abury, S. V.; Niemeyerh, D. M. Rapid extraction from and direct identification in clinical samples of methicillin-resistant staphylococci using the PCR. *J. Clin. Microbiol*. **2000**, *38*, 3407-3412.

121. Jakubovics, N. S.; Shields, R. C.; Rajarajan, N.; Burgess, J. G. Life after death: The critical role of extracellular DNA in microbial biofilms. *Lett. Appl. Microbiol.* **2013**, *57*, 467-475.

122. Jang, S. Multidrug efflux pumps in *Staphylococcus aureus* and their clinical implications. *J. Microbiol*. **2016**, *54*, 1-8.

123. Jennings, M. C.; Ator, L. E.; Paniak, T. J.; Minbiole, K. P.; Wuest, W. M. Biofilm-eradicating properties of quaternary ammonium amphiphiles: simple mimics of antimicrobial peptides. *ChemBiochem*. **2014**, *15*, 2211-2215.

124. Jennings, M. C.; Buttaro, B. A.; Minbiole, K. P. C.; Wuest, W. M. Bioorganic investigation of multicationic antimicrobials to combat QAC-resistant *Staphylococcus aureus*. *ACS Infect. Dis.* **2015**, *1*, 304-309.

125. Jin, Y.; Shao, C.; Li, J.; Fan, H.; Bai, Y.; Wang, Y. Outbreak of multidrug resistant NDM-1-producing *Klebsiella pneumoniae* from a neonatal unit in Shandong Province, China, *PLoS One* **2015,** *10*, e0119571.

126. Johnston, C. W.; Skinnider, M. A.; Dejong, C. A.; Rees, P. N.; Chen, G. M.; Walker, C. G.; French, S.; Brown, E. D.; Berdy, J.; Liu, D. Y.; Magarvey, N. A. Assembly and clustering of natural antibiotics guides target identification, *Nat. Chem. Biol.***2016,** *12*, 233-239.

127. Jones, S. M.; Morgan, M.; Humphrey, T. J.; Lappin-Scott, H. Effect of vancomycin and rifampicin on meticillin-resistant *Staphylococcus aureus* biofilms. *Lancet*. **2001**, *357*, 40-41.

128. Joo, H.; Chan, J. L.; Cheung, G. Y. C.; Otto, M. Subinhibitory concentrations of protein synthesis-inhibiting antibiotics promote increased expression of the Agr virulence regulator and production of phenol-soluble modulin cytolysins in community-associated methicillin-resistant *Staphylococcus aureus*. *Antimicrob. Agents Chemother*. **2010**, *54*, 4942-4944.

129. Joshi. P.; Singh, S.; Wani, A.; Sharma, S.; Jain, S. K.; Singh, B.; Gupta, B. D.; Satti, N. K.; Koul, S.; Khan, I. A.; Kumar, A.; Bharate, S. B., Vishwakarma, R. A. Osthol and curcumin as inhibitors of human Pgp and multidrug efflux pumps of *Staphylococcus aureus*: reversing the resistance against frontline antibacterial drugs. *Med. Chem. Commun.* **2014**, *5*, 1540-1547.

130. Kaatz, G. W.; McAleese, F.; Seo, S. M. Multidrug resistance in *Staphylococcus aureus* due to overexpression of a novel multidrug and toxin extrusion (MATE) transport protein. *Antimicrob. Agents Chemother.* **2005**, *49*, 1857-1864.

131. Kaatz, G. W.; Seo, S. M.; Ruble, C. A. Efflux-mediated fluoroquinolone resistance in *Staphylococcus aureus*. *Antimicrob. Agents Chemother.* **1993**, *37*, 1086-1094.

132. Kaatz, G.W.; Moudgal, V. V.; Seo, S. M. Identification and characterization of a novel efflux-related multidrug resistance phenotype in *Staphylococcus aureus*. *J. Antimicrob. Chemother.* **2002**, *50*, 833-838.

133. Kaizerman, J. A.; Gross, M. I.; Ge, Y.; White, S.; Hu, W.; Duan, J.; Baird, E. E.; Johnson, K. W.; Tanaka, R. D.; Moser, H. E.; Burli, R. W. DNA binding ligands targeting drug-resistant bacteria: structure, activity, and pharmacology. *J. Med. Chem.* **2003**, *46*, 3914-3929.

134. Kang, Y.; Liu, K.; Zhang, X. Supra-amphiphiles: a new bridge between colloidal science and supramolecular chemistry. *Langmuir* **2014**, *30*, 5989-6001.

135. Kaplan, J. B.; Izano, E. A.; Gopal, P.; Karwacki, M. T.; Kim, S.; Bose, J. L.; Bayles, K. W.; Horswill, A. R. Low levels of β-lactam antibiotics induce extracellular DNA release and biofilm formation in *Staphylococcus aureus*. *mBio* **2012**, *3*, e00198-12.

136. Kaplan, J. B.; Lovetri, K.; Cardona, S. T.; Madhyastha, S.; Sadovskaya, I.; Jabbouri, S.; Izano, E. A. Recombinant human DNase I decreases biofilm and increases antimicrobial susceptibility in staphylococci. *J. Antibiot*. **2012**, *65*, 73-77.

137. Kaplan, J. B.; Velliyagounder, K.; Ragunath, C.; Rohde, H.; Mack, D.; Knobloch, J. K.; Ramasubbu, N. Genes involved in the synthesis and degradation of matrix polysaccharide in *Actinobacillus actinomycetemcomitans* and *Actinobacillus pleuropneumoniae* biofilms. *J Bacteriol*. **2004**, *186*, 8213-8220.

138. Kar, C.; Adhikari, M. D.; Ramesh, A.; Das, G. Selective sensing and effective separation of Hg^{2+} from aqueous medium with a pyrene based amphiphilic ligand. *RSC Adv*. **2012**, *2*, 9201-9206.

139. Kawade, V. A.; Kumbhar, A. A.; Kumbhar, A. S.; Nather, C.; Erxleben, A.; Sonawane U. B.; Joshi, R. R. Mixed ligand cobalt(II) picolinate complexes: synthesis, characterization, DNA binding and photocleavage. *Dalton Trans.* 2011, **40**, 639-650.

140. Kaye, K. S.; Kaye, D. Multidrug-resistant Pathogens: Mechanisms of resistance and epidemiology. *Curr. Infect. Dis. Rep*. **2000**, *2*, 391-398.
141. Khalaf, A. I.; Waigh, R. D.; Drummond, A. J.; Pringle, B.; McGroarty, I.; Skellern, G. G.; Suckling, C. J. Distamycin analogues with enhanced lipophilicity: synthesis and antimicrobial activity. *J. Med. Chem*. **2004**, *47*, 2133-2156.
142. Khameneh, B.; Iranshahy, M.; Ghandadi, M.; Ghoochi Atashbeyk, D.; Fazly Bazzaz, B. S.; Iranshahi, M. Investigation of the antibacterial activity and efflux pump inhibitory effect of co-loaded piperine and gentamicin nanoliposomes in methicillin-resistant *Staphylococcus aureus*, *Drug Dev. Ind. Pharm.* **2015,** *41*, 989-994.
143. Koch, C.; Hoiby, N. Pathogenesis of cystic fibrosis. *Lancet*. **1993**, *341*, 1065-1069.
144. Kohanski, M. A.; Dwyer, D. J.; Collins, J. J. How antibiotics kill bacteria: from targets to networks. *Nat. Rev. Microbiol*. **2010**, *8*, 423-435.
145. Kohler, T.; Weidenmaier, C.; Peschel, A. Wall teichoic acid protects *Staphylococcus aureus* against antimicrobial fatty acids from human skin. *J. Bacteriol*. **2009**, *191*, 4482-4484.
146. Kokubo, T.; Kushitani, H.; Sakka, S.; Kitsugi, T.; Yamamuro, T. Solutions able to reproduce *in vivo* surface-structure changes in bioactive glass–ceramic A-W. *J. Biomed. Mater. Res*. **1990**, *24*, 721-734.
147. Konai, M. M.; Haldar, J. Lysine-based small molecules that disrupt biofilms and kill both actively growing planktonic and nondividing stationary phase bacteria, *ACS. Infect. Dis.* **2015,** *1*, 469-478.
148. Kosikowska, P.; Lesner, A. Antimicrobial peptides (AMPs) as drug candidates: a patent review (2003-2015). *Expert. Opin. Ther. Pat.* **2016**, *26*,689–702.
149. Kostakioti, M.; Hadjifrangiskou, M.; Hultgren, S. J. Bacterial biofilms: development, dispersal, and therapeutic strategies in the dawn of the postantibiotic era. *Cold Spring Harb. Perspect. Med*. **2013**, *3*, a010306.
150. Kumar, S.; Varela, M. F. Molecular mechanisms of bacterial resistance to antimicrobial agents. *Chemotherapy*. **2013**, *14*, 18.

151. Kumar, S.; Xue, L.; Arya, D. P. Neomycin-neomycin dimer: an all-carbohydrate scaffold with high affinity for AT-rich DNA duplexes, *J. Am. Chem. Soc.* **2011,** *133*, 7361-7375.

152. Kuroda, K.; DeGrado, W. F. Amphiphilic polymethacrylate derivatives as antimicrobial agents. *J. Am. Chem. Soc*. **2005**, *127*, 4128-4129.

153. LaDow, J. E.; Warnock, D. C.; Hamill, K. M.; Simmons, K. L.; Davis, R. W.; Schwantes, C. R.; Flaherty, D. C.; Willcox, J. A.; Wilson-Henjum, K.; Caran, K. L.; Minbiole, K. P.; Seifert, K. Bicephalic amphiphile architecture affects antibacterial activity. *Eur J Med Chem*. **2011**, *46*, 4219-4226.

154. Lambert, P.A. Mechanisms of antibiotic resistance in *Pseudomonas aeruginosa*, *J. Roy. Soc. Med.* **2002**, *95 (suppl 41)*, 22-26.

155. Lamp, K. C.; Rybak, M. J.; Bailey, E. M.; Kaatz, G. W. *In vitro* pharmacodynamic effects of concentration, pH, and growth phase on serum bactericidal activities of daptomycin and vancomycin. *Antimicrob Agents Chemother*. **1992**, *36*, 2709-2714.

156. Lange, R. P.; Locher, H. H.; Wyss, P. C.; Then, R. L. The targets of currently used antibacterial agents: lessons for drug discovery. *Curr Pharm Des*. **2007**, *13*, 3140-3154.

157. Langer, K.; Balthasar, S.; Vogel, V.; Dinauer, N.; von Briesen, H.; Schubert, D. Optimization of the preparation process for human serum albumin (HSA) nanoparticles. *Int. J. Pharmaceutics* **2003**, *257*, 169-180.

158. LaPlante, K.L.; Woodmansee, S. Activities of daptomycin and vancomycin alone and in combination with rifampin and gentamicin against biofilm-forming methicillin-resistant *Staphylococcus aureus* isolates in an experimental model of endocarditis. *Antimicrob. Agents Chemother.* **2009**, *53*, 3880-3886.

159. Lavigne, J. P.; Sotto, A.; Nicolas-Chanoine, M. H.; Bouziges, N.; Bourg, G.; Davin-Regli, A.; Pages, J. M. Membrane permeability, a pivotal function involved in antibiotic resistance and virulence in *Enterobacter aerogenes* clinical isolates. *Clin. Microbiol. Infect*. **2012**, *18*, 539-545.

160. Leevy, W. M.; Gammon, S. T.; Levchenko, T.; Daranciang, D. D.; Murillo, O.; Torchilin, V.; Piwnica-Worms, D.; Huettner, J. E.; Gokel, G. W. Structure-activity

relationships, kinetics, selectivity, and mechanistic studies of synthetic hydraphile channels in bacterial and mammalian cells. *Org. Biomol. Chem*. **2005**, *3*, 3544-3550.

161. Lepri, S.; Buonerba, F.; Goracci, L.; Velilla, I.; Ruzziconi, R.; Schindler, B. D.; Seo, S. M.; Kaatz, G. W.; Cruciani, G. Indole based weapons to fight antibiotic resistance: a structure-activity relationship study. *J. Med. Chem.* **2016**, *59*, 867-891.
162. Lewis, K. Multidrug tolerance of biofilms and persister cells. *Curr. Top. Microbiol. Immunol*. **2008**, *322*, 107-131.
163. Lewis, K. Platforms for antibiotic discovery. *Nat. Rev. Drug. Discov*. **2013**, *12*, 371-387.
164. Li, X. Z.; Nikaido, H. Efflux-mediated drug resistance in bacteria: an update. *Drugs* **2009**, *69*, 1555-1623.
165. Liu, Z. C.; Wang, B. D.; Yang, Z. Y.; Li, Y.; Qin, D. D.; Li, T. R. Synthesis, crystal structure, DNA interaction and antioxidant activities of two novel water-soluble Cu($^{2+}$) complexes derivated from 2-oxo-quinoline-3-carbaldehyde Schiff-bases. *Eur. J. Med. Chem*. **2009**, *44*, 4477-4484.
166. Locher, H. H.; Caspers, P.; Bruyere, T.; Schroeder, S.; Pfaff, P.; Knezevic, A.; Keck, W.; Ritz, D. Investigations of the mode of action and resistance development of cadazolid, a new antibiotic for treatment of *Clostridium difficile* infections. *Antimicrob. Agents Chemother*. **2014**, *58*, 901-908.
167. Lombardi, L.; Maisetta, G.; Batoni, G.; Tavanti, A. Insights into the antimicrobial properties of hepcidins: advantages and drawbacks as potential therapeutic agents, *Molecules* **2015,** *20*, 6319-6341.
168. Lowy, F. D. Antimicrobial resistance: the example of *Staphylococcus aureus*. *J. Clin. Invest*. **2003**, *111*, 1265-1273.
169. Lowy, F.D. *Staphylococcus aureus* infections. *N. Engl. J. Med*., **1998**, *339*, 520-532.
170. Ma, T. K. W.; Chow, K. M.; Choy, A. S. M.; Kwan, B. C. H.; Szeto, C. C.; Li, P. K. T. Clinical manifestation of macrolide antibiotic toxicity in CKD and dialysis patients, *Clin. Kidney J.* **2014,** *7*, 507-512.

171. Ma, Z.; Yang, J.; Han, J.; Gao, L.; Liu, H.; Lu, Z.; Zhao, H.; Bie, X. Insights into the antimicrobial activity and cytotoxicity of engineered α-helical peptide amphiphiles, *J. Med. Chem.* **2016,** *59*, 10946-10962.

172. Madsen, J. S.; Burmolle, M.; Hansen, L. H.; Sorensen, S. J. The interconnection between biofilm formation and horizontal gene transfer. *FEMS Immunol. Med. Microbiol*. **2012**, *65*, 183-195.

173. Maheswari, P. U.; Lappalainen, K.; Sfregola, M.; Barends, S.; Gamez, P.; Turpeinen, U.; Mutikainen, I.; van Wezela, G. P.; Reedijk. Structure and DNA cleavage properties of two copper(II) complexes of the pyridine-pyrazole-containing ligands mbpzbpy and Hmpzbpya. *Dalton Trans*. **2007**, *33*, 3676-3683.

174. Mahlapuu, M.; Håkansson, J.; Ringstad, L.; Björn, C. Antimicrobial Peptides: An Emerging Category of Therapeutic Agents, *Front. Cell Infect. Microbiol.* **2016,** *6*, 194.

175. Mahon, K. P., Jr.; Ortiz-Meoz, R. F.; Prestwich, E. G.; Kelley, S. O. Photosensitized DNA cleavage promoted by amino acids, *Chem. Commun.* **2003,** *15*, 1956-1957.

176. Mann, E. E.; Rice, K. C.; Boles, B. R.; Endres, J. L.; Ranjit, D.; Chandramohan, L.; Tsang, L. H.; Smeltzer, M. S.; Horswill, A. R.; Bayles, K. W. Modulation of eDNA release and degradation affects *Staphylococcus aureus* biofilm maturation. *PLoS One* **2009**, *4*, e5822.

177. Marafino, J. N.; Gallagher, T. M.; Barragan, J.; Volkers, B. L.; LaDow, J. E.; Bonifer, K.; Fitzgerald, G.; Floyd, J. L.; McKenna, K.; Minahan, N. T.; Walsh, B.; Seifert, K.; Caran, K. L. Colloidal and antibacterial properties of novel triple-headed, double-tailed amphiphiles: exploring structure-activity relationships and synergistic mixtures, *Bioorg. Med. Chem.* **2015,** *23*, 3566-73.

178. Marini, N. J.; Baliga, R.; Taylor, M. J.; White, S.; Simpson, P.; Tsai, L.; Baird, E. E. DNA binding hairpin polyamides with antifungal activity, *Chem. Biol.* **2003,** *10*, 635-644.

179. Marr, A. K.; Gooderham, W. J.; Hancock, R. E. Antibacterial peptides for therapeutic use: obstacles and realistic outlook. *Curr. Opin. Pharmacol*. **2006**, *6*, 468-472.

180. Marty, F.M.; Yeh, W. W.; Wennersten, C.B.; Venkataraman, L.; Albano, E.; Alyea, E.P.; Gold, H. S.; Baden, L. R.; Pillai, S. K. Emergence of a clinical daptomycin-resistant *Staphylococcus aureus* isolate during treatment of methicillin-resistant *Staphylococcus aureus* bacteremia and osteomyelitis. *J. Clin. Microbiol.* **2006**, *44*, 595-597.

181. Mather, A. E.; Reid, S. W.; Maskell, D. J.; Parkhill, J.; Fookes, M. C.; Harris, S. R.; Brown, D. J.; Coia, J. E.; Mulvey, M. R.; Gilmour, M. W.; Petrovska, L.; de Pinna, E.; Kuroda, M.; Akiba, M.; Izumiya, H.; Connor, T. R.; Suchard, M. A.; Lemey, P.; Mellor, D. J.; Haydon, D. T.; Thomson, N. R. Distinguishable epidemics of multidrug-resistant *Salmonella Typhimurium* DT104 in different hosts. *Science*. **2013**, *341*, 1514-1517.

182. Matsuzaki, K.; Mitani, Y.; Akada, K. Y.; Murase, O.; Yoneyama, S.; Zasloff, M.; Miyajima, K. Mechanism of synergism between antimicrobial peptides magainin 2 and PGLa. *Biochemistry*. **1998**, *37*, 15144-15153.

183. McCarthy, H.; Rudkin, J. K.; Black, N. S.; Gallagher, L.; O'Neill, E.; O'Gara, J. P. Methicillin resistance and the biofilm phenotype in *Staphylococcus aureus*. *Front. Cell. Infect. Microbiol*. **2015**, *5*, 1-9.

184. McCoy, L. S.; Xie, Y.; Tor, Y. Antibiotics that target protein synthesis. *Wiley Interdiscip. Rev. RNA*. **2011**, *2*, 209-232.

185. Mercier, R. C.; Stumpo, C.; Rybak, M. J. Effect of growth phase and pH on the *in vitro* activity of a new glycopeptide, oritavancin (LY333328), against *Staphylococcus aureus* and *Enterococcus faecium*. *J Antimicrob Chemother*. **2002**, *50*, 19-24.

186. Merrell, D. S.; Camilli, A. Acid tolerance of gastrointestinal pathogens. *Curr. Opin. Microbiol.***2002**, *5*, 51-55.

187. Meyers, S. R.; Juhn, F. S.; Griset, A. P.; Luman, N. R.; Grinstaff, M. W. Anionic amphiphilic dendrimers as antibacterial agents. *J. Am. Chem. Soc*. **2008**, *130*, 14444-14445.

188. Mitra, R. N.; Shome, A.; Paul, P.; Das, P. K. Antimicrobial activity, biocompatibility and hydrogelation ability of dipeptide-based amphiphiles. *Org. Biomol. Chem*. **2009**, *7*, 94-102.

189. Molin, S.; Tolker-Nielsen, T. Gene transfer occurs with enhanced efficiency in biofilms and induces enhanced stabilisation of the biofilm structure. *Curr. Opin. Biotechnol*. **2003**, *14*, 255-261.

190. Morar, M.; Wright, G. D. The genetic enzymology of antibiotic resistance, *Ann. Rev. Genet*. **2010**, *44*, 25-51.

191. Mowery, B. P.; Lee, S. E.; Kissounko, D. A.; Epand, R. F.; Epand, R. M.; Weisblum, B.; Stahl, S. S.; Gellman, S. H. Mimicry of antimicrobial host-defense peptides by random copolymers. *J. Am. Chem. Soc*. **2007**, *129*, 15474-15476.

192. Muder, R. R.; Brennen, C.; Rihs, J. D.; Wagener, M. M.; Obman, A.; Stout, J. E.; Yu, V. L. Isolation of *Staphylococcus aureus* from the urinary tract: association of isolation with symptomatic urinary tract infection and subsequent staphylococcal bacteremia. *Clin. Infect. Dis.* **2006**, *42*, 46-50.

193. Mueller, M.; de la Pena, A.; Derendorf, H. Issues in pharmacokinetics and pharmacodynamics of anti-infective agents: kill curves versus MIC. *Antimicrob. Agents Chemother*. **2004**, *48*, 369-377.

194. Mukherjee, S.; Singh, A. K.; Adhikari, M. D.; Ramesh, A. Quantitative appraisal of the probiotic attributes and in vitro adhesion potential of anti-listerial bacteriocin-producing lactic acid bacteria. *Prob. Antimicro. Prot.* **2013**, *5*, 99-109.

195. Mulcahy, H.; Charron-Mazenod, L.; Lewenza, S. Extracellular DNA chelates cations and induces antibiotic resistance in *Pseudomonas aeruginosa* biofilms. *PLoS Pathog*. **2009**, *4*, e1000213.

196. Murima, P.; McKinney, J. D.; Pethe, K. Targeting bacterial central metabolism for drug development, *Chem. Biol.* **2014,** *21*, 1423-1432.

197. Naber C. K. *Staphylococcus aureus* bacteremia: epidemiology, pathophysiology, and management strategies. *Clin. Infect. Dis*. **2009**, *48*, S231-S237.

198. Naghmouchi, K.; Drider, D.; Baah, J.; Teather, R. Nisin A and Polymyxin B as Synergistic Inhibitors of Gram-positive and Gram-negative Bacteria. *Prob. Antimicro. Prot*. **2010**, *2*, 98-103.

199. Nikaido, H. Molecular basis of bacterial outer membrane permeability revisited. *Microbiol. Mol. Biol. Rev*. **2003**, *67*, 593-656.

200. Nikaido, H. Multidrug resistance in bacteria. *Ann. Rev. Biochem.* **2009**, 78, 119-146.

201. Noimark, S.; Dunnill, C. W.; Wilson, M.; Parkin, I. P. The role of surfaces in catheter-associated infections. *Chem. Soc. Rev*. **2009**, *38*, 3435-3448.

202. Nolte, O. Antimicrobial resistance in the 21st century: a multifaceted challenge. *Protein Pept. Lett*. **2014**, *21*, 330-335.

203. Nordmann, P.; Poirel, L.; Walsh, T. R.; Livermore, D. M. The emerging NDM carbapenemases. *Trends Microbiol.* **2011**, *19*, 588-595.

204. O'Connell, K. M. G.; Hodgkinson, J. T.; Sore, H. F.; Welch, M.; Salmond, G. P. C.; Spring, D. R. Combating multidrug-resistant bacteria: current strategies for the discovery of novel antibacterials. *Angew. Chem.* **2013**, *125*, 10904-10932.

205. Oda, Y.; Kanaoka, S.; Sato, T.; Aoshima, S.; Kuroda, K. Block versus random amphiphilic copolymers as antibacterial agents, *Biomacromolecules* **2011,** *12*, 3581-3591.

206. Okamoto, A.; Tainaka, K.; Nishiza, K.; Saito, I. Monitoring DNA structures by dual fluorescence of pyrene derivatives, *J. Am. Chem. Soc.* **2005,** *127*, 13128-13129.

207. Okshevsky, M.; Regina, V. R.; Meyer, R. L. Extracellular DNA as a target for biofilm control. *Curr. Opin. Biotechnol*. **2015**, *33*, 73-80.

208. Olson, K. M.; Starks, C. M.; Williams, R. B.; O'Neil-Johnson, M.; Huang, Z.; Ellis, M.; Reilly, J. E.; Eldridge, G. R. Novel pentadecenyl tetrazole enhances susceptibility of methicillin-resistant Staphylococcus aureus biofilms to gentamicin, *Antimicrob. Agents Chemother.* **2011,** *55*, 3691-3695.

209. Onufrak, N. J.; Forrest, A.; Gonzalez, D. Pharmacokinetic and Pharmacodynamic Principles of Anti-infective Dosing, *Clin. Ther.* **2016,** *38*, 1930-1947.

210. Otto, M. Staphylococcal biofilms. *Curr. Top. Microbiol. Immunol*. **2008**, *322*, 207-228.

211. Otto, M. *Staphylococcus epidermidis* - the 'accidental' pathogen. *Nat. Rev. Microbiol*. **2009**, *7*, 555-567.

212. Owens, R. C. Jr.; Ambrose, P. G. Antimicrobial safety: focus on fluoroquinolones. *Clin. Infect. Dis.* **2005**, *41*, S144-S157.

213. Palermo, E. F.; Kuroda, K. Chemical structure of cationic groups in amphiphilic polymethacrylates modulates the antimicrobial and hemolytic activities. *Biomacromolecules*. **2009**, *10*, 1416-1428.

214. Palermo, E. F.; Sovadinova, I.; Kuroda, K. Structural determinants of antimicrobial activity and biocompatibility in membrane-disrupting methacrylamide random copolymers. *Biomacromolecules*. **2009**, *10*, 3098-3107.

215. Palmer, A. C.; Kishony, R. Opposing effects of target overexpression reveal drug mechanisms. *Nat. Commun*. **2014**, *5*, 4296.

216. Paniak, T. J.; Jennings, M. C.; Shanahan, P. C.; Joyce, M. D.; Santiago, C. N.; Wuest, W. M.; Minbiole, K. P. The antimicrobial activity of mono-, bis-, tris-, and tetracationic amphiphiles derived from simple polyamine platforms, *Bioorg. Med. Chem. Lett.* **2014,** *24*, 5824-5828.

217. Parsek, M. R.; Tolker-Nielsen, T. Pattern formation in *Pseudomonas aeruginosa* biofilms. *Curr. Opin. Microbiol*. **2008**, *11*, 560-566.

218. Patel, D.; Kosmidis, C.; Seo, S. M.; Kaatz, G. W. Ethidium bromide MIC screening for enhanced efflux pump gene expression or efflux activity in *Staphylococcus aureus*. *Antimicrob. Agents Chemother.* **2010**, *54*, 5070-5073.

219. Pieroni, M.; Dimovska, M.; Brincat, J. P,; Sabatini, S.; Carosati, E.; Massari, S.; Kaatz, G. W.; Fravolini, A. From 6-aminoquinolone antibacterials to 6-amino-7-thiopyranopyridinylquinolone ethyl esters as inhibitors of *Staphylococcus aureus* multidrug efflux pumps. *J. Med. Chem.* **2010**, *53*, 4466-4480.

220. Podoll, J. D.; Liu, Y.; Chang, L.; Walls, S.; Wang, W.; Wang, X. Bio-inspired synthesis yields a tricyclic indoline that selectively resensitizes methicillin-resistant *Staphylococcus aureus* (MRSA) to beta-lactam antibiotics, *Proc. Natl. Acad. Sci.* **2013,** *110*, 15573-15578.

221. Poole, K. Efflux-mediated antimicrobial resistance. *J. Antimicrob. Chemother.* **2005**, *56*, 20-51.

222. Purdy Drew, K. R.; Sanders, L. K.; Culumber, Z. W.; Zribi, O.; Wong, G. C. Cationic amphiphiles increase activity of aminoglycoside antibiotic tobramycin in the presence of airway polyelectrolytes. *J Am Chem Soc*. **2009**, *131*, 486-493.

223. Qian, J.; Wang, L.; Gu, W.; Liu, X.; Tian, J.; Yan, S. Efficient double-strand cleavage of DNA mediated by Zn(II)-based artificial nucleases, *Dalton Trans.* **2011,** *40*, 5617-5624.

224. Raja, D.S.; Bhuvanesh, N. S. P.; Natarajan, K. Effect of N(4)-phenyl substitution in 2-oxo-1,2-dihydroquinoline-3-carbaldehyde semicarbazones on the structure, DNA/protein interaction, and antioxidative and cytotoxic activity of Cu(II) complexes. *Inorg. Chem.* **2011**, *50*, 12852-12866.

225. Ramakrishnan, S.; Shakthipriya, D.; Suresh, E, Periasamy, V. S.; Akbarsha M. A.; Palaniandavar, M. Ternary dinuclear copper(ii) complexes of a hydroxybenzamide ligand with diimine coligands: The 5,6-dmp ligand enhances DNA binding and cleavage and induces apoptosis. *Inorg. Chem.* 2011, **50**, 6458–6471.

226. Ramanathan, M.; Shrestha, L. K.; Mori, T.; Ji, Q.; Hill, J. P.; Ariga, K. Amphiphile nanoarchitectonics: from basic physical chemistry to advanced applications. *Phys. Chem. Chem. Phys.* **2013**, 15, 10580-10611.

227. Rawlinson, L. A.; Ryan, S. M.; Mantovani, G.; Syrett, J. A.; Haddleton, D. M.; Brayden, D. J. Antibacterial effects of poly(2-(dimethylamino ethyl)methacrylate) against selected gram-positive and gram-negative bacteria. *Biomacromolecules*. **2010**, *11*, 443-453.

228. Rehm, S.J.; Tice A. *Staphylococcus aureus*: methicillin-susceptible *S. aureus* to methicillin-resistant *S. aureus* and vancomycin-resistant *S. aureus*. *Clin. Infect. Dis*. **2010**, *51*, S176-S182.

229. Repakova, J.; Holopainen, J. M.; Karttunen, M.; Vattulainen, I. Influence of pyrene-labeling on fluid lipid membranes. *J. Phys. Chem. B*, **2006**, *110*, 15403-15410.

230. Rice, K. C.; Mann, E. E.; Endres, J. L.; Weiss, E. C.; Cassat, J. E.; Smeltzer, M. S.; Bayles, K. W. The cidA murein hydrolase regulator contributes to DNA release and biofilm development in *Staphylococcus aureus*. *Proc. Natl. Acad. Sci.* **2007**, *104*, 8113-8118.

231. Richard, H.; Foster, J. W. Escherichia coli glutamate- and arginine-dependent acid resistance systems increase internal pH and reverse transmembrane potential. *J. Bacteriol*. **2004**, *186*, 6032-6041.

232. Sabatini, S.; Gosetto, F.; Iraci, N.; Barreca, M. L.; Massari, S.; Sancineto, L.; Manfroni, G.; Tabarrini, O.; Dimovska, M.; Kaatz, G. W.; Cecchetti, W. Re-evolution of the 2-phenylquinolines: ligand-based design, synthesis, and biological evaluation of a potent new class of *Staphylococcus aureus* NorA efflux pump inhibitors to combat antimicrobial resistance. *J. Med. Chem.* **2013**, *56*, 4975-4989.

233. Sabatini, S.; Gosetto, F.; Manfroni, G.; Tabarrini, O.; Kaatz, G. W.; Patel, D.; Cecchetti, V. Evolution from a natural flavones nucleus to obtain 2-(4 propoxyphenyl) quinoline derivatives as potent inhibitors of the *S. aureus* NorA efflux pump. *J. Med. Chem.* **2011**, *54*, 5722-5736.

234. Sabatini, S.; Gosetto, F.; Serritella, S.; Manfroni, G.; Tabarrini, O.; Iraci, N.; Brincat, J. P.; Carosati, E.; Villarini, M.; Kaatz, G. W.; Cecchetti, V. Pyrazolo[4,3-*c*][1,2]benzothiazines 5,5-dioxide: a promising new class of *Staphylococcus aureus* NorA efflux pump inhibitors. *J. Med. Chem.* **2012**, *55*, 3568-3572.

235. Sabatini, S.; Kaatz, G. W.; Rossolini, G. M.; Brandini, D.; Fravolini, A. From phenothiazine to 3-phenyl-1,4-benzothiazine derivatives as inhibitors of the *Staphylococcus aureus* NorA multidrug efflux pump. *J. Med. Chem.* **2008**, *51*, 4321-4330.

236. Saha, S.; Savage, P. B.; Bal, M. Enhancement of the efficacy of erythromycin in multiple antibiotic-resistant gram-negative bacterial pathogens. *J. Appl. Microbiol.* **2008**, *105*, 822-828.

237. Scheffer, U.; Strick, A.; Ludwig, V.; Peter, S.; Kalden, E.; Gobel, M. W. Metal-free catalysts for the hydrolysis of RNA derived from guanidines, 2-aminopyridines, and 2-aminobenzimidazoles. *J. Am. Chem. Soc.* **2005**, *127*, 2211-2217.

238. Scherr, T. D.; Heim, C. E.; Morrison, J. M.; Kielian, T. Hiding in plain sight: Interplay between staphylococcal biofilms and host immunity. *Front. Immunol.* **2014**, *5*, 37.

239. Shai, Y. Mode of action of membrane active antimicrobial peptides. *Biopolymers*. **2002**, *66*, 236-248.

240. Shimanovich, U.; Bernardes, G. J. L.; Knowles, T. P. J.; Cavaco-Paulo, A. Protein micro- and nano-capsules for biomedical applications. *Chem. Soc. Rev*. **2014**, *43*, 1361-1371.

241. Silver, L. L. Challenges of antibacterial discovery. *Clin Microbiol Rev*. **2011**, *24*, 71-109.

242. Singh, A. K. Ramesh, A. Evaluation of a facile method of template DNA preparation for PCR-based detection and typing of lactic acid bacteria. *Food Microbiol*. **2009**, *26*, 504-513.

243. Singh, A. K.; Mukherjee, S.; Adhikari, M. D.; Ramesh, A. Fluorescence-based comparative evaluation of bactericidal potency and food application potential of anti-listerial bacteriocin produced by lactic acid bacteria isolated from indigenous samples. *Prob. Antimicrob. Proteins*. **2012**, *4*, 122-132.

244. Singh, P. K.; Schaefer, A. L.; Parsek, M. R.; Moninger, T. O.; Welsh, M. J.; Greenberg, E. P. Quorum-sensing signals indicate that cystic fibrosis lungs are infected with bacterial biofilms. *Nature*. **2000**, *407*, 762-764.

245. Singh, R.; Ray, P.; Das, A.; Sharma, M. Penetration of antibiotics through *Staphylococcus aureus* and *Staphylococcus epidermidis* biofilms. *J. Antimicrob. Chemother*. **2010**, *65*, 1955-1958.

246. Singh, V.; Arora, V.; Alam, M. J.; Garey, K. W. Inhibition of biofilm formation by esomeprazole in *Pseudomonas aeruginosa* and *Staphylococcus aureus*. *Antimicrob. Agents Chemother*. **2012**, *56*, 4360-4364.

247. Slomberg, D. L.; Lu, Y.; Broadnax, A. D.; Hunter, R. A.; Carpenter, A. W.; Schoenfisch, M. H. Role of size and shape on biofilm eradication for nitric oxide-releasing silica nanoparticles. *ACS Appl. Mater. Interfaces* **2013**, *5*, 9322-9329.

248. Song, A.; Walker, S. G.; Parker, K. A.; Sampson, N. S. Antibacterial studies of cationic polymers with alternating, random, and uniform backbones, *ACS chem biol.* **2011,** *6*, 590-599.

249. Sook, K. E.; Jeong, S. I.; Kim, J. H.; Park, C.; Kim, S. M.; Kim, J. K.; Lee, K. M.; Lee, S. H.; So, H.; Park, R. Synergistic effects of the combination of 20-

hydroxyecdysone with ampicillin and gentamicin against methicillin-resistant *Staphylococcus aureus*. *J. Microbiol. Biotechnol*. **2009**, *19*, 1576–1581.

250. Sorrenti, A.; Illa, W. O.; Ortuño. R, M. Amphiphiles in aqueous solution: well beyond a soap bubble. *Chem. Soc. Rev.* **2013,** *42*, 8200-8219.
251. Speziale, P.; Pietrocola, G.; Foster, T. J.; Geoghegan, J. A. Protein-based biofilm matrices in staphylococci. *Front. Cell. Infect. Microbiol*. **2014**, *4*, 171.
252. Speziale, P.; Pietrocola, G.; Rindi, S.; Provenzano, M.; Provenza, G.; Di Poto, A.; Visai, L.; Arciola, C. R. Structural and functional role of *Staphylococcus aureus* surface components recognizing adhesive matrix molecules of the host. *Future Microbiol*. **2009**, *4*, 1337-1352.
253. Stewart, P. S.; Costerton, J. W. Antibiotic resistance of bacteria in biofilms. *Lancet*. **2001**, *358*, 135-138.
254. Stone, P. W. Economic burden of healthcare-associated infections: an American perspective. *Expert. Rev. Pharmacoecon. Outcomes Res*. **2009**, *9*, 417-422.
255. Stryjewski, M. E., Corey, G. R. Methicillin-resistant *Staphylococcus aureus*: An evolving pathogen. *Clin. Infect. Dis*. **2014**, *58*, S10-S19.
256. Sugandhi, E. W.; Macri, R. V.; Williams, A. A.; Kite, B. L.; Slebodnick, C.; Falkinham, J. O.; Esker, A. R.; Gandour, R. D. Synthesis, critical micelle concentrations, and antimycobacterial properties of homologous, dendritic amphiphiles. Probing intrinsic activity and the "cutoff" effect. *J. Med. Chem*. **2007**, *50*, 1645-1650.
257. Sun, J.; Deng, Z.; Yan, A. Bacterial multidrug efflux pumps: mechanisms, physiology and pharmacological exploitations. *Biochem. Biophys. Res. Commun*. **2014**, *453*, 254-267.
258. Tamma, P. D.; Cosgrove, S. E.; Maragakis, L. L. Combination therapy for treatment of infections with Gram-negative bacteria. *Clin. Microbiol. Rev*. **2012**, *25*, 450-470.
259. Tamplin, M. L. Inactivation of Escherichia coli O157:H7 in simulated human gastric fluid. *Appl Environ Microbiol*. **2005**, *71*, 320-325.
260. Thangamani, S.; Mohammad, H.; Abushahba, M. F. N.; Sobreira, T. J. P.; Hedrick, V. E.; Paul, L. N.; Seleem, M. N. Antibacterial activity and mechanism of

action of auranofin against multi-drug resistant bacterial pathogens. *Sci. Rep.* **2016,** *6*, 22571.

261. Thangamani, S.; Younis, W.; Seleem, M. N. Repurposing ebselen for treatment of multidrug-resistant staphylococcal infections, *Sci. Rep.* **2015,** *5*, 11596.
262. Toprak, E.; Veres, A.; Michel, J. B.; Chait, R.; Hartl, D. L.; Kishony, R. Evolutionary paths to antibiotic resistance under dynamically sustained drug selection. *Nat. Genet*. **2012**, *44*, 101-105.
263. Tseng, B. S.; Zhang, W.; Harrison, J. J.; Quach, T. P.; Song, J. L.; Penterman, J.; Singh, P. K.; Chopp, D. L.; Packman, A. I.; Parsek, M. R. The extracellular matrix protects *Pseudomonas aeruginosa* biofilms by limiting the penetration of tobramycin. *Environ. Microbiol*. **2013**, *15*, 2865-2878.
264. Tsuji, B.T.; Rybak, M. J. Short-course gentamicin in combination with daptomycin or vancomycin against *Staphylococcus aureus* in an in vitro pharmacodynamic model with simulated endocardial vegetations. *Antimicrob. Agents Chemother.* **2005**, *49*, 2735-2745.
265. Uday, P. S.; Thiyagarajan, D.; Goswami, S.; Adhikari, M. D.; Das, G.; Ramesh, A. Amphiphile-mediated enhanced antibiotic efficacy and development of a payload nanocarrier for effective killing of pathogenic bacteria. *J. Mater. Chem. B* **2014**, *2*, 5818-5827.
266. Ulvatne, H.; Karoliussen, S.; Stiberg, T.; Rekdal, O.; Svendsen, J. S. Short antibacterial peptides and erythromycin act synergically against *Escherichia coli*. *J. Antimicrob., Chemother*. **2001**, *48*, 203-208.
267. Van Bambeke, F.; Mingeot-Leclercq, M. P.; Struelens, M. J.; Tulkens, P. M. The bacterial envelope as a target for novel anti-MRSA antibiotics. *Trends Pharmacol. Sci*. **2008**, *29*, 124-134.
268. van den Berg, T. A.; Feringa, B. L.; Roelfes, G. Double strand DNA cleavage with a binuclear iron complex, *Chem. Commun.* **2007,** *2*, 180-182.
269. van Meer, G.; de Kroon, A. I. Lipid map of the mammalian cell. *J. Cell. Sci*. **2011**, *124*, 5-8.

270. Vekhoff, P.; Duca, M.; Guianvarc'h, D.; Benhida, R.; Arimondo, P. B. Sequence-specific base pair mimics are efficient topoisomerase IB inhibitors, *Biochemistry* **2012,** *51*, 43-51.

271. Virto, R.; Manas, P.; Alvarez, I.; Condon, S.; Raso, J. Membrane damage and microbial inactivation by chlorine in the absence and presence of a chlorine-demanding substrate. *Appl. Environ. Microbiol*. **2005**, *71*, 5022-5028.

272. Viveiros, M.; Martins, A.; Paixao, L.; Rodrigues, L.; Martins, M.; Couto, I.; Fahnrich, E.; Kern, W. V.; Amaral, L. Demonstration of intrinsic efflux activity of *Escherichia coli* K-12 AG100 by an automated ethidium bromide method. *Int. J. Antimicrob. Agents.* **2008**, *31*, 458-462.

273. Vooturi, S. K.; Cheung, C. M.; Rybak, M. J.; Firestine, S. M. Design, synthesis, and structure-activity relationships of benzophenone-based tetraamides as novel antibacterial agents. *J. Med. Chem*. **2009**, *52*, 5020-5031.

274. Vudumula, U.; Adhikari, M. D.; Ojha, B.; Goswami, S.; Das, G.; Ramesh, A. Tuning the bactericidal repertoire and potency of quinoline-based amphiphiles for enhanced killing of pathogenic bacteria, *RSC Adv*. **2012**, *2*, 3864-3871.

275. Walker, S.; Sofia, M. J.; Axelrod, H. R. Chemistry and cellular aspects of cationic facial amphiphiles. *Adv. Drug Deliv. Rev*. **1998**, *30*, 61-71.

276. Wang, L. S.; Gupta, A.; Rotello, V. M. Nanomaterials for the treatment of bacterial biofilms. *ACS Infect. Dis*. **2016**, *2*, 3-4.

277. Wang, L.; Chen, Y. P.; Miller, K. P.; Cash, B. M.; Jones, S.; Glenn, S.; Benicewicz, B. C.; Decho, A. W. Functionalised nanoparticles complexed with antibiotic efficiently kill MRSA and other bacteria. *Chem. Commun.* **2014**, *50*, 12030-12033.

278. Wassenaar, T. M.; Ussery, D.; Nielsen, L. N.; Ingmer, H. Review and phylogenetic analysis of qac genes that reduce susceptibility to quaternary ammonium compounds in Staphylococcus species. *Eur. J. Microbiol. Immunol. (Bp)*. **2015**, *5*, 44-61.

279. Weidenmaier, C.; Peschel, A. Teichoic acids and related cell-wall glycopolymers in Gram-positive physiology and host interactions. *Nat. Rev. Microbiol*. **2008**, *6*, 276-287.

280. Westerhoff, H. V.; Zasloff, M.; Rosner, J. L.; Hendler, R. W.; De Waal, A.; Vaz Gomes, A.; Jongsma, P. M.; Riethorst, A.; Juretic, D. Functional synergism of the magainins PGLa and magainin-2 in *Escherichia coli*, tumor cells and liposomes. *Eur. J. Biochem*. **1995**, *228*, 257-264.

281. Whitchurch, C. B.; Tolker-Nielsen, T.; Ragas, P. C.; Mattick, J. S. Extracellular DNA required for bacterial biofilm formation. *Science*. **2002**, *295*, 1487.

282. Wilson, D. N. Ribosome-targeting antibiotics and mechanisms of bacterial resistance. *Nat. Rev. Microbiol*. **2014**, *12*, 35-48.

283. Wimley, W. C. Describing the mechanism of antimicrobial peptide action with the interfacial activity model. *ACS Chem. Biol*. **2010**, *5*, 905-917.

284. Wimley, W. C.; Hristova, K. Antimicrobial peptides: successes, challenges and unanswered questions. *J. Membrane Biol*. **2011**, *239*, 27-34.

285. Winnik, F. M. Photophysics of preassociated pyrenes in aqueous polymer solutions and in other organized media, *Chem. Rev*. **1993**, *93*, 587-614.

286. Wispelwey, B. Clinical implications of pharmacokinetics and pharmacodynamics of fluoroquinolones. *Clin. Infect. Dis*. **2005**, *41 Suppl 2*, S127-135.

287. World Health Organization. (http://www.who.int/drugresistance/documents/surveillancereport/en/)

288. Worthington, R.; Melander, C. Combination approaches to combat multidrug-resistant bacteria. *Trends Biotechnol.* **2013**, *31*, 177-184.

289. Wright, G. D. Bacterial resistance to antibiotics: enzymatic degradation and modification. *Adv Drug Deliv. Rev*. **2005**, *57*, 1451-1470.

290. Wright, G. D. Molecular mechanisms of antibiotic resistance. *Chem Commun*. **2011**, *47*, 4055-4061.

291. Xu, D.; Jiang, L.; Singh, A.; Dustin, D.; Yang, M.; Liu, L.; Lund, R.; Sellati, T. J.; Dong, H. Designed supramolecular filamentous peptides: Balance of nanostructure, cytotoxicity and antimicrobial activity, *Chem. Commun.* **2015,** *51*, 1289-1292.

292. Xu, Y.; Suzuki, Y.; Ito, K.; Komiyama, M. Telomeric repeat-containing RNA structure in living cells, *Proc. Natl. Acad. Sci*. **2010**, *107*, 14579-14584.

293. Xue, L.; Ranjan, N.; Arya, D. P. Synthesis and spectroscopic studies of the aminoglycoside (neomycin)-perylene conjugate binding to human telomeric DNA, *Biochemistry* **2011,** *50*, 2838-2849.

294. Yang, L.; Gordon, V. D.; Mishra, A.; Som, A.; Purdy, K. R.; Davis, M. A.; Tew, G. N.; Wong, G. C. Synthetic antimicrobial oligomers induce a composition-dependent topological transition in membranes. *J. Am. Chem. Soc*. **2007**, *129*, 12141-12147.

295. Yeaman, M. R.; Yount, N. Y. Mechanisms of antimicrobial peptide action and resistance. *Pharmacol Rev*. **2003**, *55*, 27-55.

296. Yeh, P. J.; Hegreness, M. J.; Aiden, A. P.; Kishony, R. Drug interactions and the evolution of antibiotic resistance. *Nat. Rev. Microbiol*. **2009**, *7*, 460-466.

297. Zasloff, M. Antimicrobial peptides of multicellular organisms. *Nature* **2002**, *415*, 389-395.

298. Zhang, L. J.; Gallo, R. L. Antimicrobial peptides, *Curr. Biol.* **2016,** *26*, R14-R19.

299. Zimmermann, L.; Das, I.; Desire, J.; Sautrey, G.; Barros, R. S. V.; El Khoury, M.; Mingeot-Leclercq, M. P.; Decout, J. L. New broad-spectrum antibacterial amphiphilic aminoglycosides active against resistant bacteria: from neamine derivatives to smaller neosamine analogues, *J. Med. Chem.* **2016,** *59*, 9350-9369.

APPENDIX

APPENDIX

A 2.1. Synthesis of Amphiphiles

A 2.1.1. Compound 1 (C1)

The synthesis route of C1 is indicated in Scheme A2.1. The precursor molecule **I^2** was synthesized following the reported procedure (Kar et al. 2012). 100 mg of 1-pyrenealdehyde was refluxed with 88 mg (1.1 eqv.) of dodecylamine in methanol to afford the desired Schiff base N-((pyren-6-yl) methylene) dodecan-1-amine in 70 % yield. The Schiff base was reduced by gradual addition of $NaBH_4$ in its methanolic solution to obtain N-((pyren-6-yl) methyl) dodecan-1-amine (**I^1**). The intermediate **I^2** was directly synthesized from N-((pyren-6-yl) methyl) dodecan-1-amine by refluxing it with 1-chloromethyl (pyridine hydrochloride) in the presence of K_2CO_3 in CH_3CN for 72 hours. Crude product was purified by column chromatography with 55% yield. C1 was synthesized by reacting **I^2** with CH_3I in MeCN solvent.

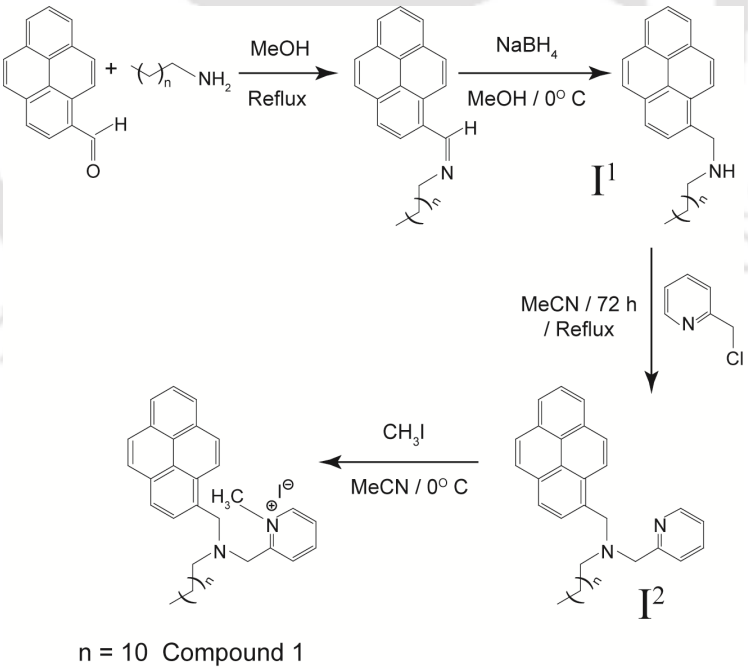

Scheme A 2.1. Synthesis route of C1.

A 2.1.2. Compound 2 (C2)

The synthesis route of C2 is indicated in Scheme A2.2. 230.26 mg of 1-pyrenealdehyde was refluxed with 80.44 mg (1.1 eqv.) of butylamine in methanol to afford the desired Schiff base N-((pyren-6-yl) methylene) butane-1-amine in 80% yield. The Schiff base was reduced by gradual addition of $NaBH_4$ in its methanolic solution to obtain N-((pyren-6-yl) methyl) butane-1-amine. C2 was directly synthesized from N-((pyren-6-yl) methyl) butane-1-amine by refluxing it with 1-chloromethyl (pyridine hydrochloride) in the presence of K_2CO_3 in CH_3CN for 48 hours. Crude product was purified by column chromatography with 68% yield.

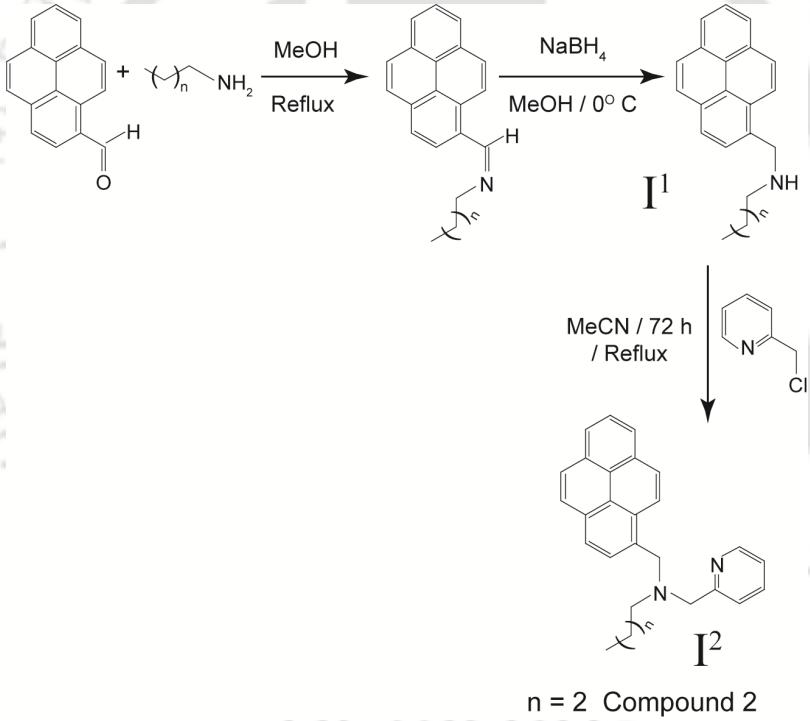

Scheme A 2.2. Synthesis route of C2.

A 2.2. Characterization of C1:

^{1}H NMR ($CDCl_3$, 400 MHz): 0.87ppm (t, 3H); 1.25ppm (m, 18H); 1.69 ppm (broad multiplate, 2H); 2.73 ppm (t, 2H); 3.95 ppm (s, 2H); 4.12 ppm (s, 3H); 4.33 ppm (s, 2H); 6.96 ppm (t,1H); 7.38 ppm (t, 1H); 7.47 ppm (t, 1H); 7.86-8.27 ppm (m, 9H); 8.45 ppm (d, 1H); ^{13}C NMR ($CDCl_3$, 100 MHz): 155.58 ppm, 146.09 ppm, 143.19 ppm, 131.10 ppm, 130.45 ppm, 129.66 ppm, 128.58 ppm, 127.80 ppm, 127.23 ppm, 126.41 ppm, 125.68 ppm, 125.07 ppm, 124.71 ppm, 123.24 ppm, 96.98 ppm, 58.23 ppm, 57.30 ppm, 56.69 ppm, 46.44 ppm, 31.99 ppm, 29.73 ppm, 29.44 ppm, 27.60 ppm, 26.90 ppm, 22.77 ppm, 14.22 ppm, 1.086 ppm; MS (positive mode, *m/*z): Calcd. for C1**:** 505.357. Found 505.357.

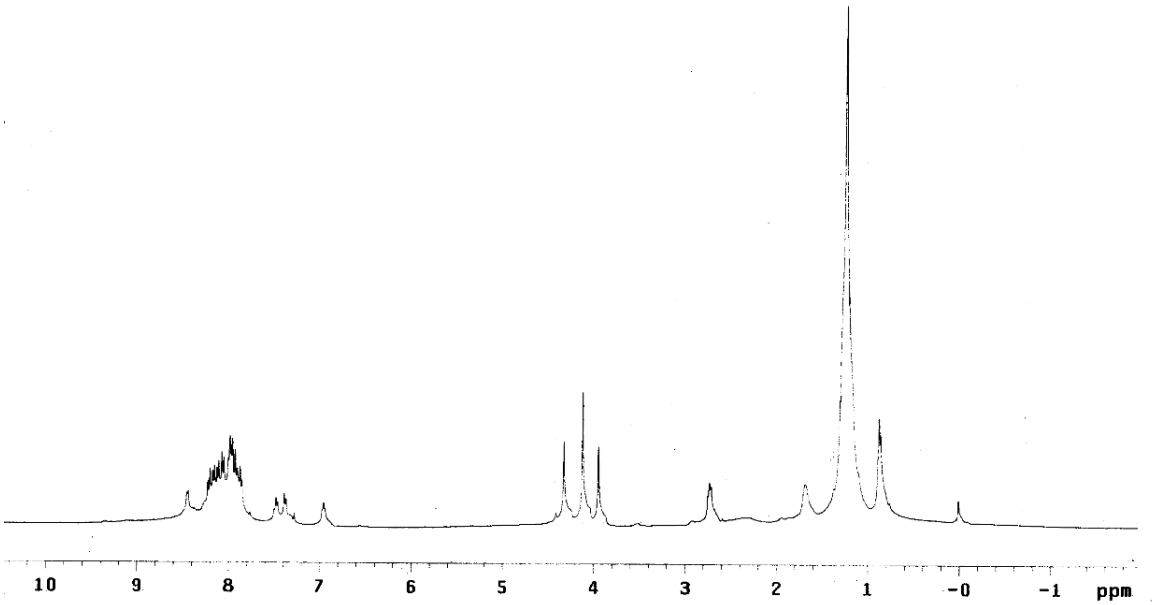

Figure A 2.1. ^{1}H NMR spectra of C1 in $CDCl_3$ solution.

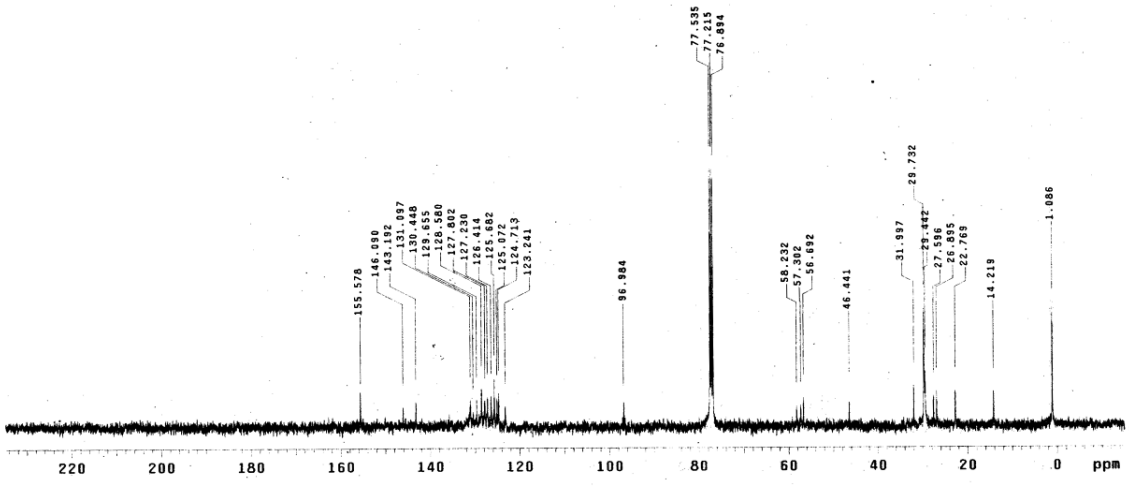

Figure A 2.2. ^{13}C NMR spectra of C1 in $CDCl_3$ solution.

A 2.3. Characterization of C2:

^{1}H NMR ($CDCl_3$, 400 MHz): 0.83 ppm (t, 3H); 1.28 ppm (m, 2H); 1.64 ppm (m, 2H); 2.61ppm (t, 2H); 3.81 ppm (s, 2H); 4.32 ppm (s, 2H); 7.06 ppm (t, 1H); 7.43 ppm (d, 1H); 7.53 ppm (t, 1H); 7.90-8.19 ppm (m, 8H); 8.45 ppm (d, 1H);8.53 ppm (d, 1H); ^{13}C NMR ($CDCl_3$, 100 MHz): 160.69 ppm, 148.57 ppm, 136.45 ppm, 133.31 ppm, 131.43 ppm, 131.02 ppm, 130.76 ppm, 129.91 ppm, 128.32 ppm, 127.59 ppm, 127.12 ppm, 127.08 ppm, 125.93 ppm, 125.12 ppm, 125.06 ppm, 124.92 ppm, 124.58 ppm, 124.28 ppm, 123.25 ppm, 121.88 ppm, 60.52 ppm, 57.62 ppm, 54.81 ppm, 29.30 ppm, 20.80 ppm, 14.18 ppm, 1.21 ppm, MS (positive mode, *m/*z): Calcd. for C2+H: 379.217. Found 378.218.

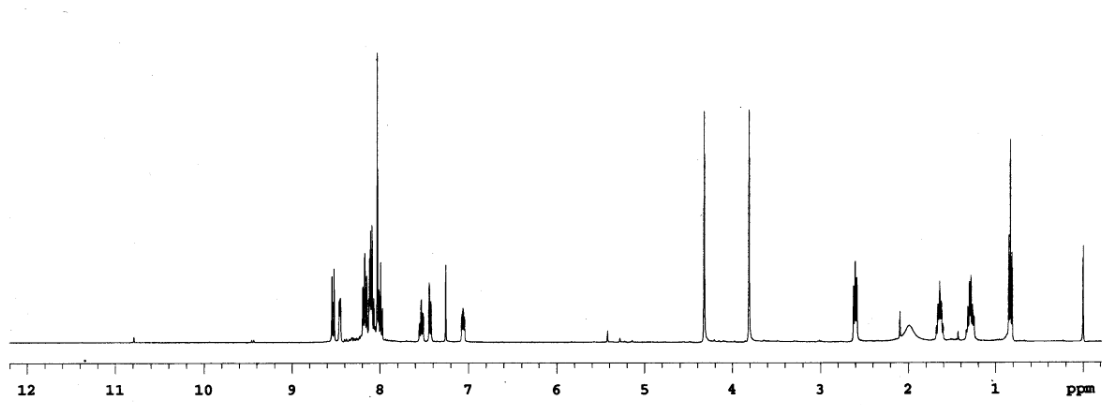

Figure A 2.3. ^{1}H NMR spectra of C2 in $CDCl_3$ solution.

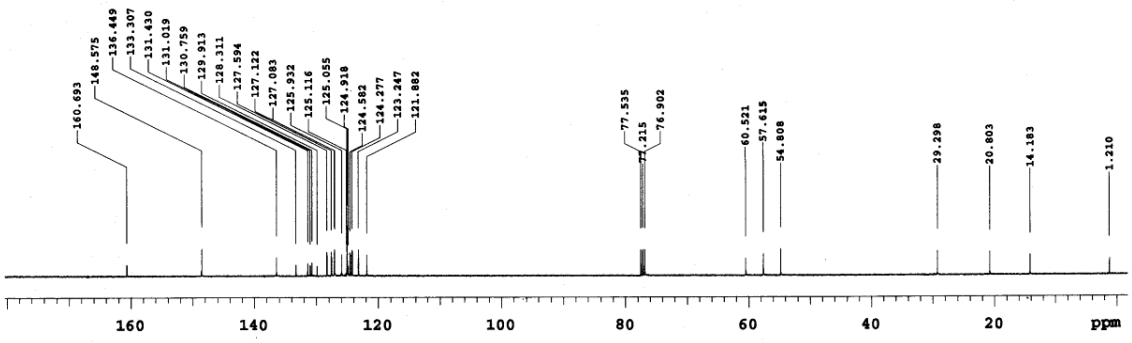

Figure A 2.4. ^{13}C NMR spectra of C2 in $CDCl_3$ solution.

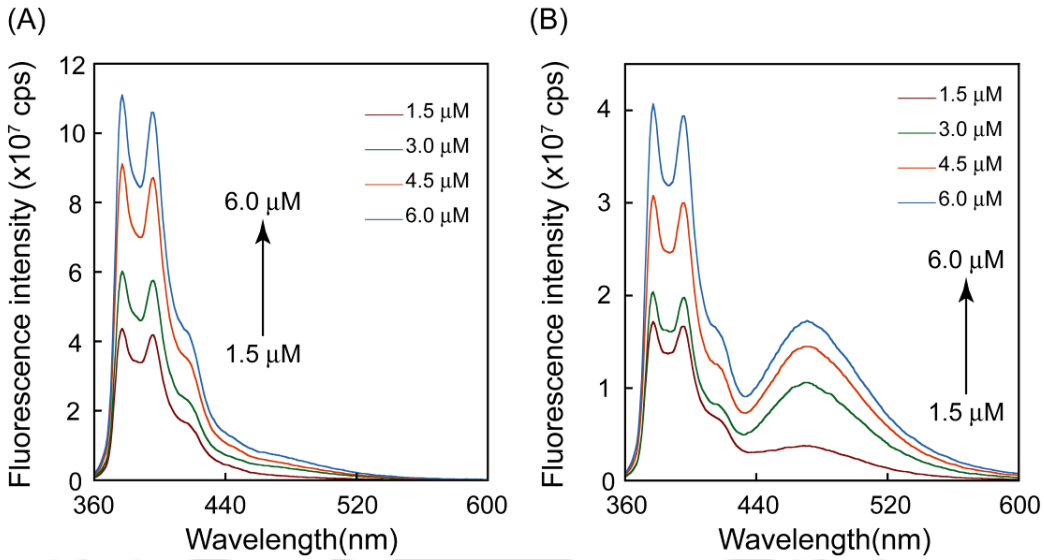

Figure A 2.5. Fluorescence emission spectra of (A) C1 and (B) *S. aureus* MTCC 96 bound-C1.

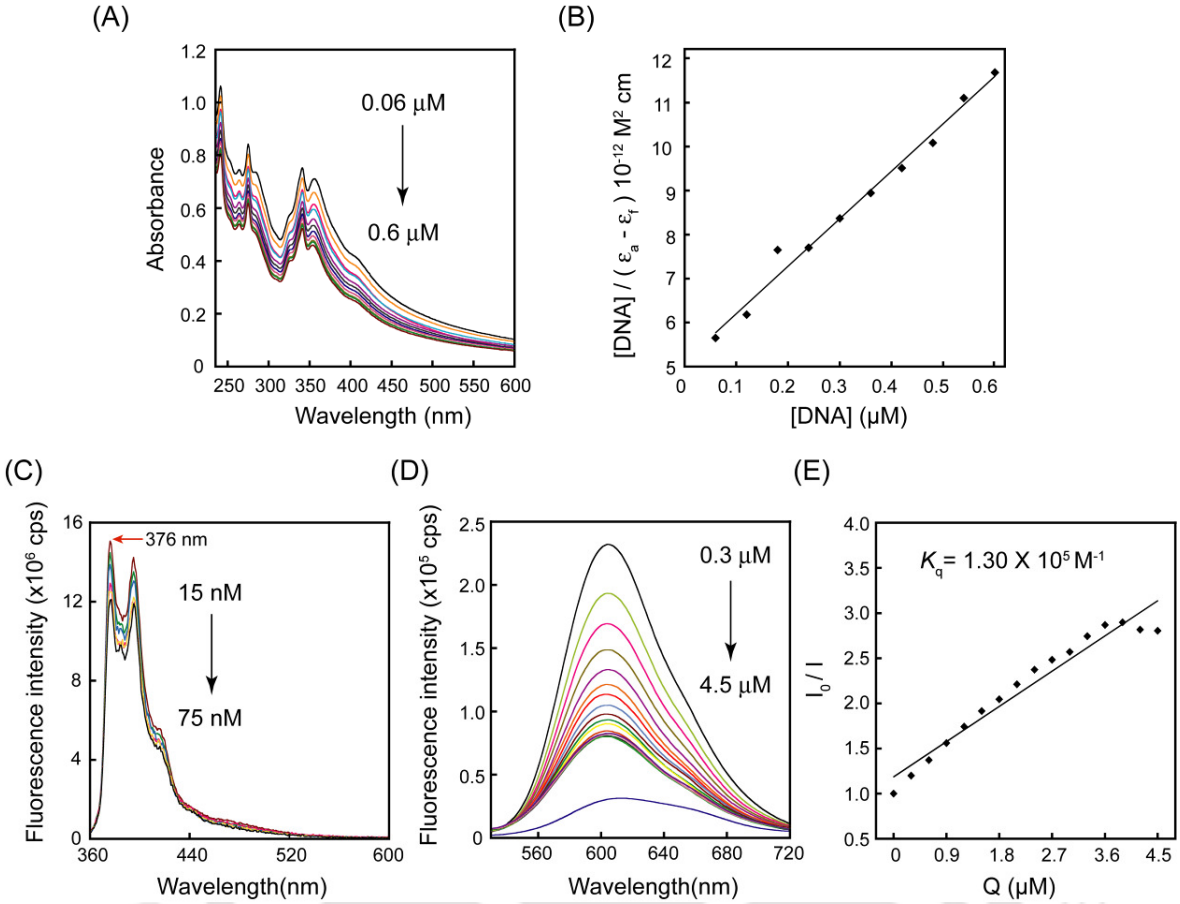

Figure A 3.1. (A) UV-visible absorbance spectroscopy of C2 (5.0 µM) upon addition of calf thymus DNA (0.06 µM - 0.6 µM). (B) Binding isotherm of C2 with calf thymus DNA determined by UV-visible absorbance titration spectroscopy. (C) Fluorescence emission spectroscopy of C2 (150 nM) upon interaction with calf thymus DNA (15 nM – 75 nM). (D) Ethidium bromide displacement assay with C2 (0.3 µM - 4.5 µM). (E) Stern-Volmer plot for ethidium bromide displacement assay with C2.

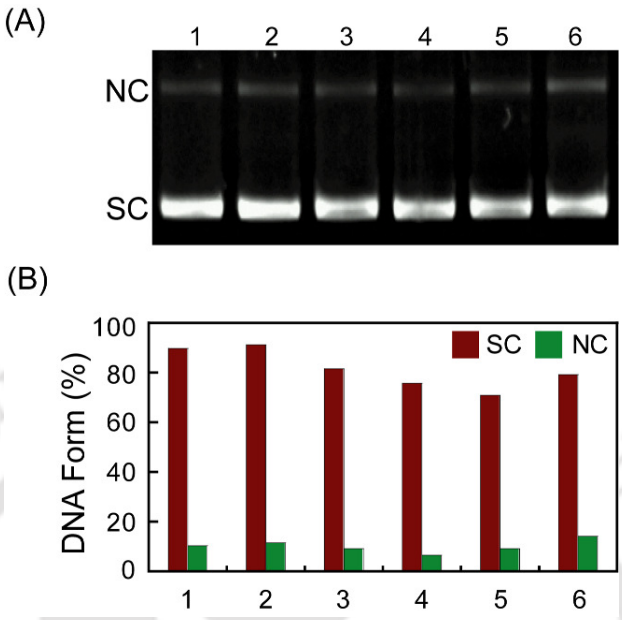

Figure A 3.2. (A) Agarose gel electrophoresis of pUC18 plasmid DNA treated with C2. Lanes 1: control (untreated plasmid DNA); 2-6: plasmid DNA treated with 6.0 µM, 12 µM, 18 µM, 24 µM and 30 µM of C2, respectively. (B) Quantification of band intensity of various topological forms of plasmid DNA obtained in (A) using ImageJ analysis software.

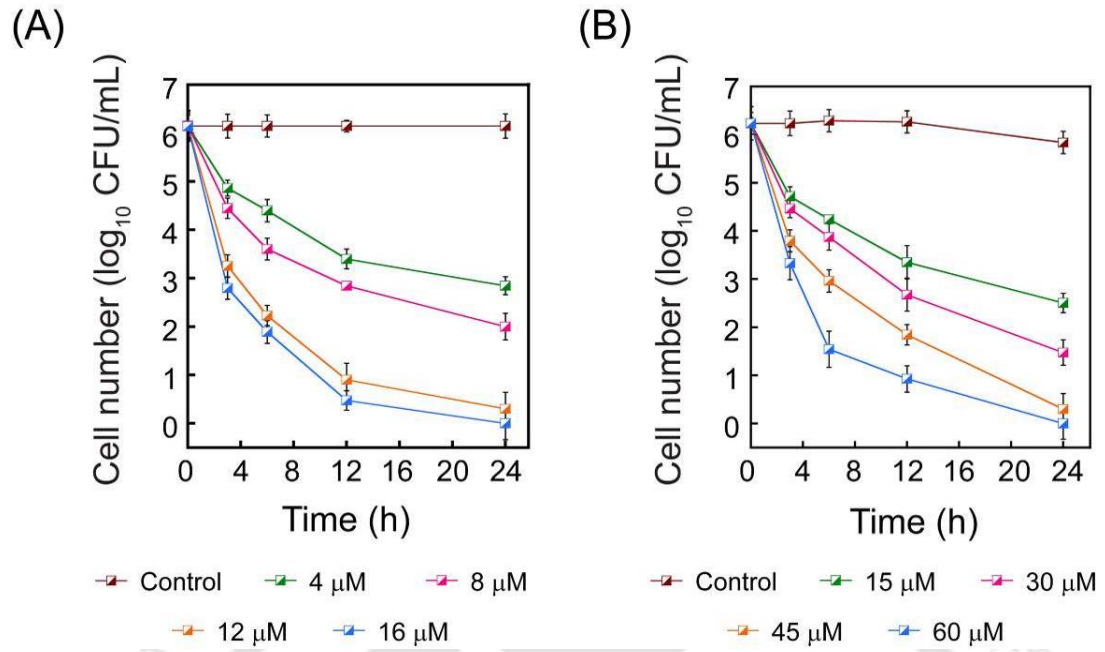

Figure A 4.1. Antibacterial activity of C1 against (A) *S. aureus* MTCC 96 and (B) *E. coli* MTCC 433 cells incubated in simulated body fluid.

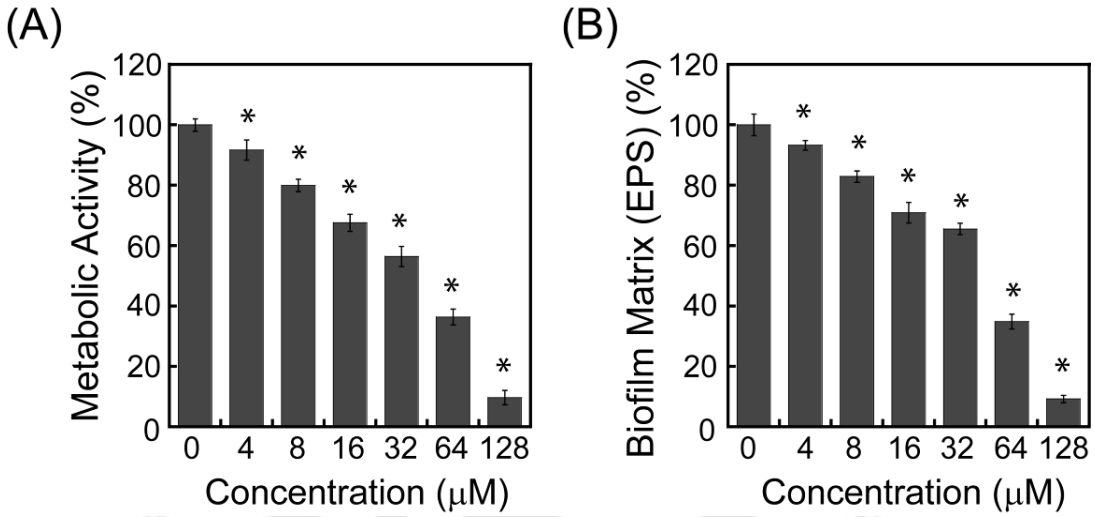

Figure A 5.1. Effect of C1 on *S. aureus* MTCC 96 biofilm measured by (A) MTT assay and (B) Congo red assay. * indicates *p* value < 0.001 in ANOVA.

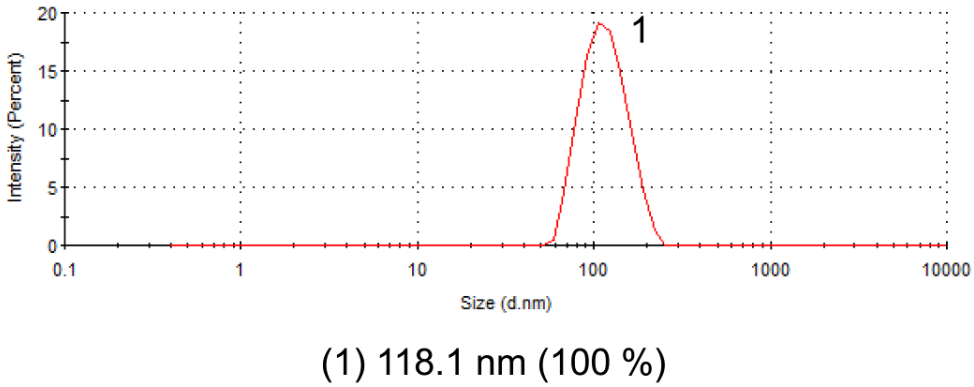

Figure A 5.2. Particle size distributions of C1 estimated by dynamic light scattering. The particle size and percentage of the aggregated species (in parenthesis) of C1 (peak 1) is indicated below the plot.

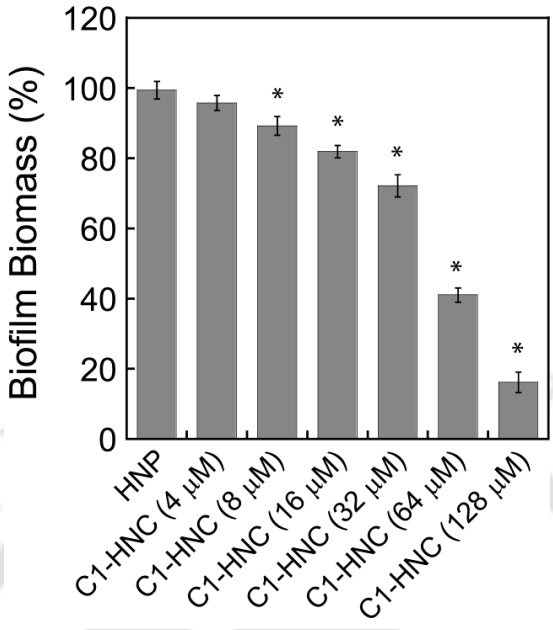

Figure A 5.3. Eradication of *S. aureus* MTCC 96 biofilm by C1-HNC determined by crystal violet assay. * indicates p value < 0.001 in ANOVA.

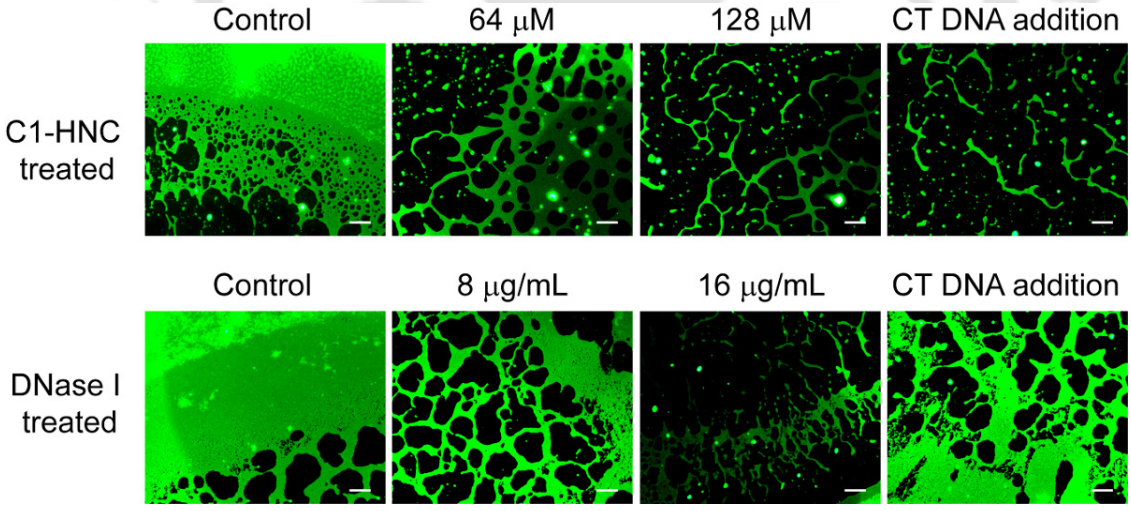

Figure A 5.4. Fluorescence microscope analysis to study the effect of CT-DNA supplementation on C1-HNC and DNase I-treated *S. aureus* MTCC 96 biofilm. The biofilm was stained with cFDA-SE. Scale bar for the images is 100 μm. Based on cFDA-SE staining the panels representing CT-DNA supplementation indicate irreversible eradication of *S. aureus* biofilm in case of treatment with C1-HNC as opposed to treatment with DNase I.

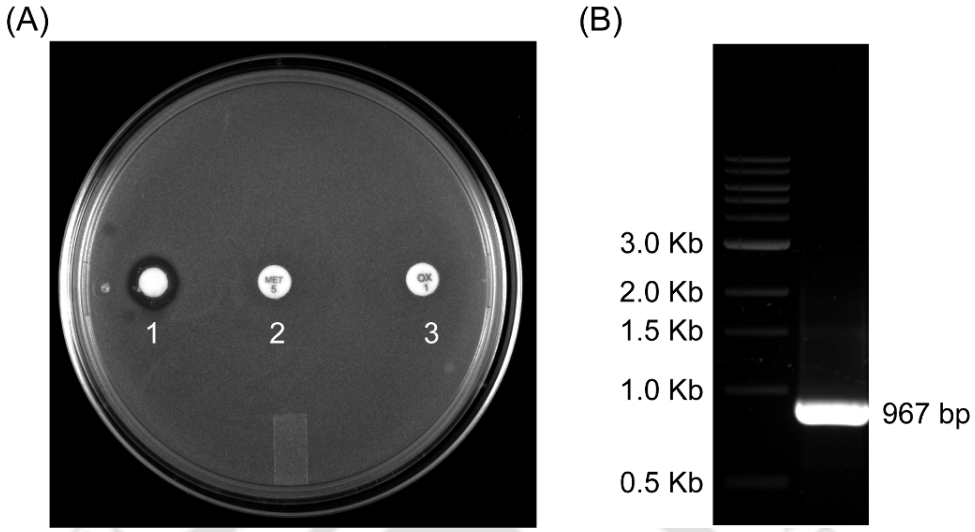

Figure A 6.1. (A) Disc diffusion assay to ascertain the susceptibility of *S. aureus* 4s. Disc 1 was impregnated with 24 µM of C1. Discs 2 and 3 are ready to use discs of methicillin (5.0 µg) and oxacillin (1.0 µg), respectively. (B) PCR-based detection of *mecA* gene in *S. aureus* 4s. The *mecA* amplicon was 967 bp in length.

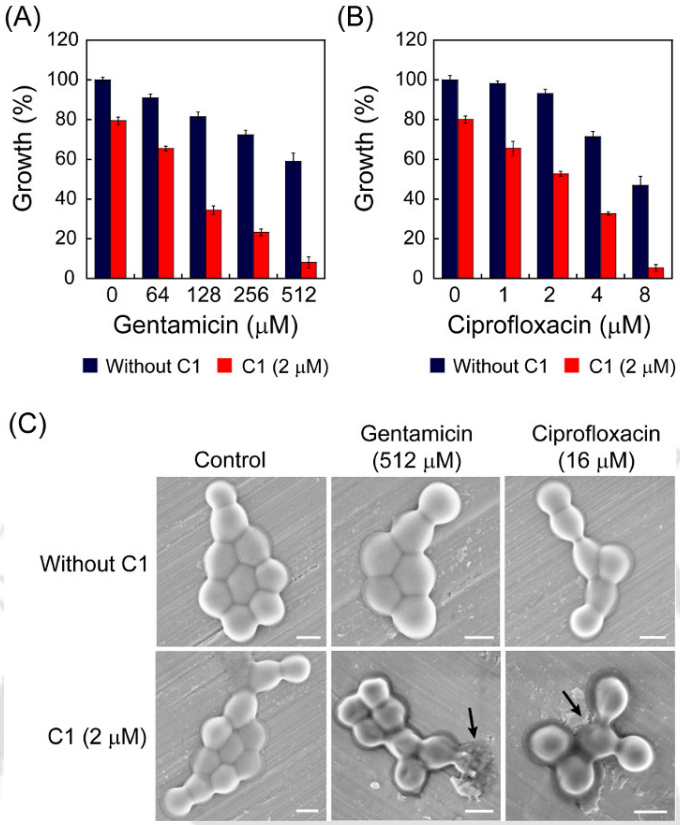

Figure A6.2. Combination effect of (A) C1 and gentamicin and (B) C1 and ciprofloxacin on *S. aureus* 4s cells. (C) FESEM analysis of *S. aureus* 4s cells treated with C1 in combination with either gentamicin or ciprofloxacin. Scale bar for the images is 0.5 μm.

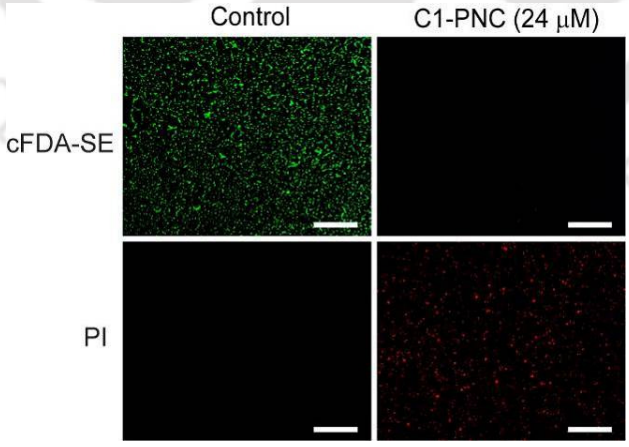

Figure A6.3. cFDA-SE and PI-based fluorescence microscopic analysis of C1-PNC treated *S. aureus* 4s cells. Scale bar for the images is 100 μm.

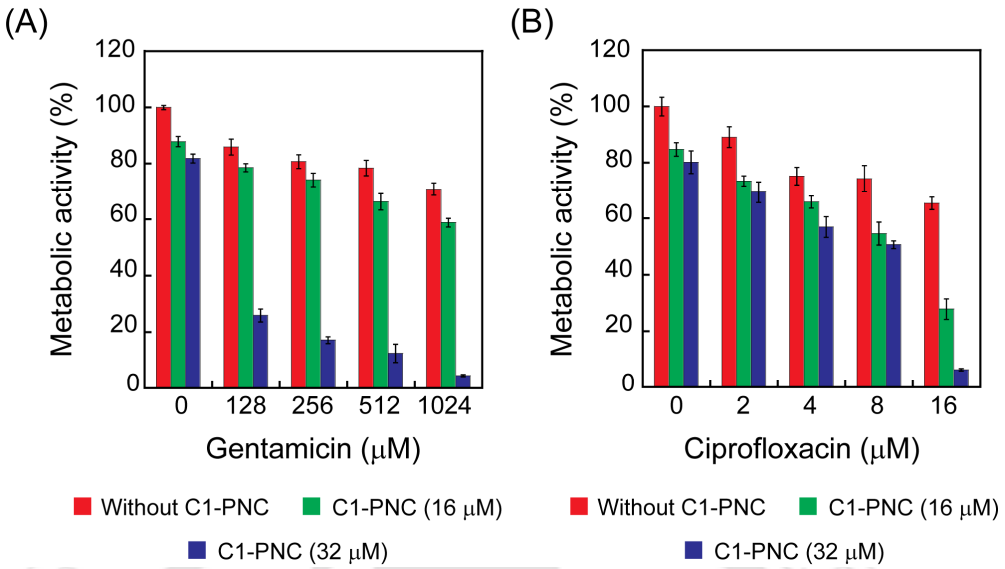

Figure A6.4. Effect of C1-PNC in combination with antibiotics on *S. aureus* 4s biofilm formation.

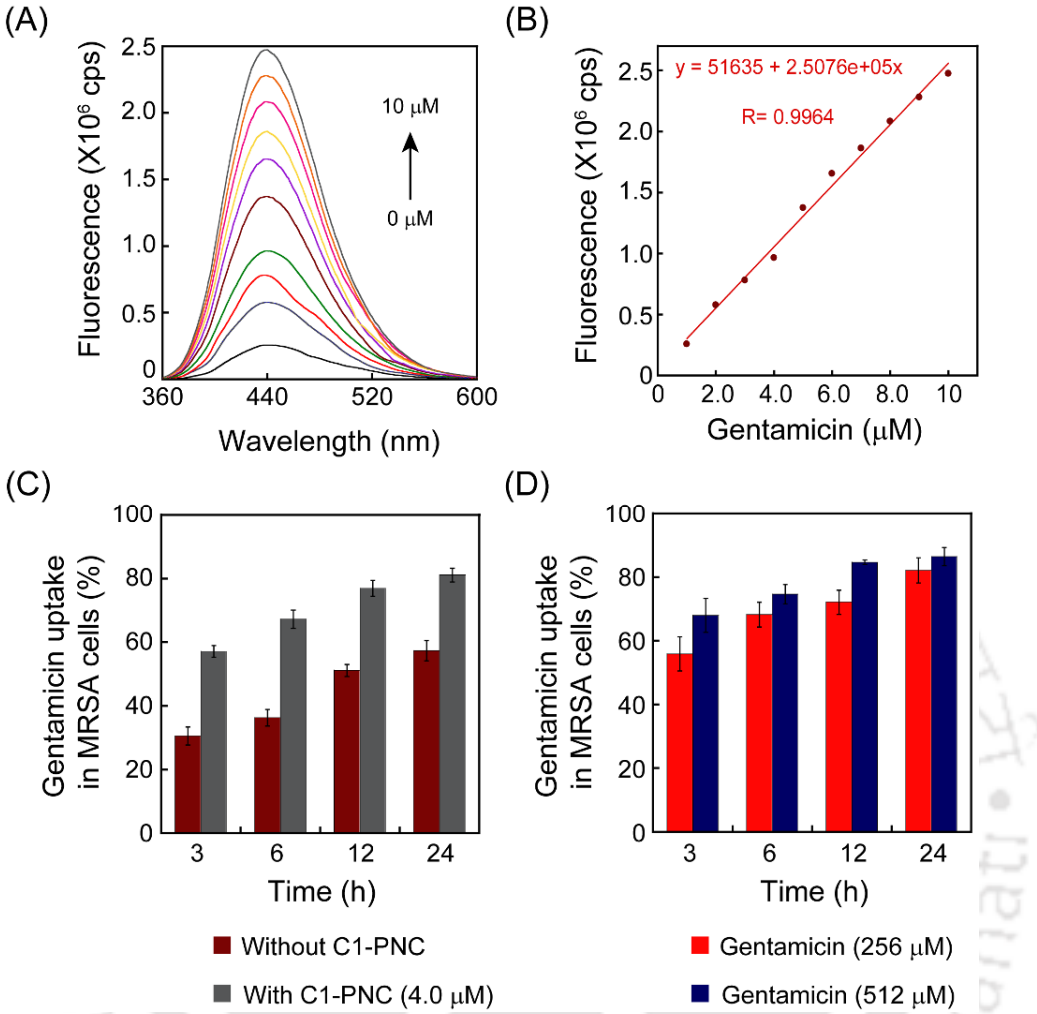

Figure A6.5. (A) Fluorescence spectra of OPA-gentamicin complex generated with various concentrations of gentamicin. (B) Calibration plot for samples in (A). (C) Uptake of gentamicin in C1-PNC-treated MRSA cells. The concentration of gentamicin was 512 μM. (D) Uptake of gentamicin in C1-treated MRSA cells. The concentration of C1 was 2.0 μM.

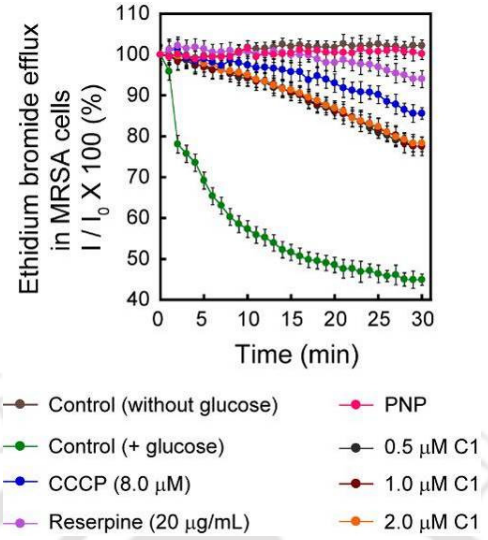

Figure A6.6. Effect of PLGA nanoparticles (PNPs) and C1 on EtBr efflux in *S. aureus* 4s cells.

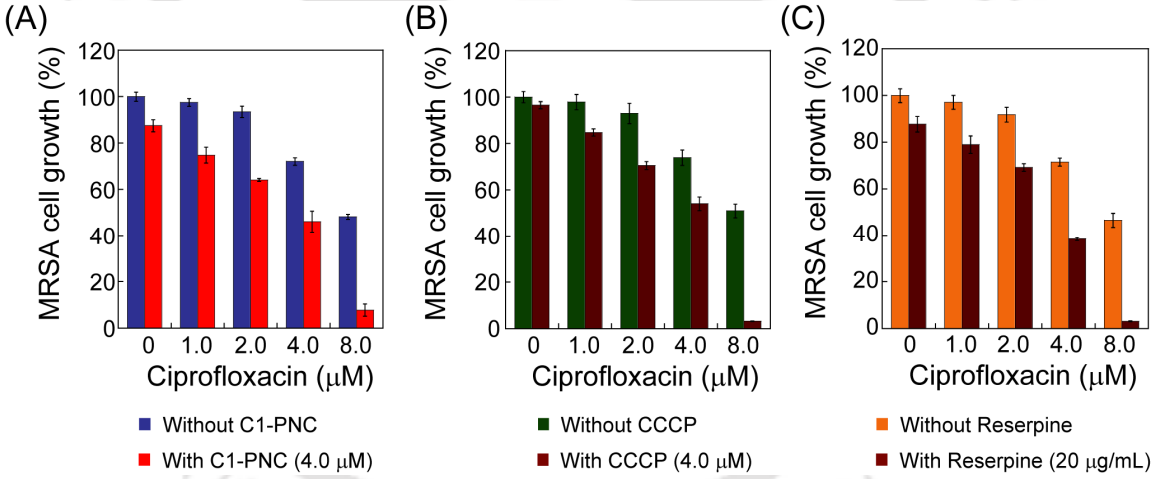

Figure A6.7. Effect of ciprofloxacin in combination with (A) C1-PNC, (B) CCCP and (C) reserpine on the growth of *S. aureus* 4s cells.

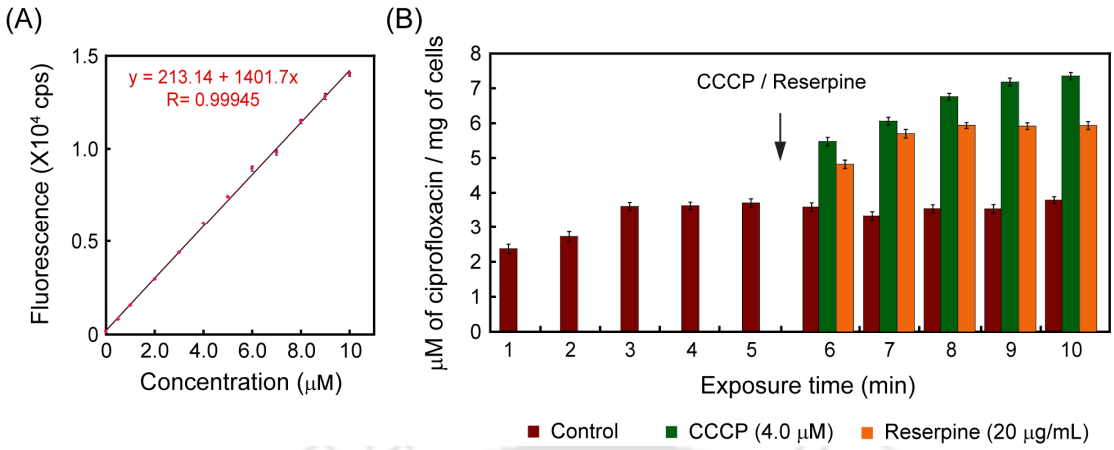

Figure A6.8. (A) Calibration plot generated by using various concentrations of ciprofloxacin (0.5 μM-10 μM) in a fluorescence-based assay. (B) Measurement of *S. aureus* 4s cell-associated ciprofloxacin. Cells were incubated in 50 mM phosphate buffer (pH 7.0) with 32 μM ciprofloxacin for the first five minutes. Following addition of either CCCP or reserpine (indicated by an arrow) in separate sets, the cells were incubated for another five minutes. Subsequently the cells were washed with ice cold phosphate buffer and incubated in 0.1 M glycine buffer (pH 3.0) for 15 h and then the cells were pelleted and ciprofloxacin in the supernatant was measured.

A6.1. Homology Modelling and Molecular Docking Studies

Homology modelling of *S. aureus* NorA protein and molecular docking studies to predict interaction of C1 with the modelled NorA protein was pursued. The NorA protein sequence of *Staphylococcus aureus* subsp. *aureus* NCTC 8325 (Accession No: AAB31949.1) was retrieved from the NCBI protein database (http://www.ncbi.nlm.nih.gov/protein/). For developing the model of the NorA protein, three template proteins were chosen whose crystal structures are available. The PDB ID of the template proteins were 1PW4, 3WDO and 4LDS having a resolution of 3.3 Å, 3.15 Å and 3.2 Å, respectively (http://www.rcsb.org/pdb/home/home.do). All three proteins essentially belong to the transporter family. Subsequently, the 3D model of the NorA protein of *S. aureus* subsp. *aureus* NCTC 8325 was built by using the program MODELLER Version 9.14 in conjunction with EasyModeller version 4.0. (Marti-Renom et al. 2000; Sali and Blundell 1993; Fiser et al 2000; Kuntal et al. 2010) The quality of the generated model was verified using the SAVES server (http://nihserver.mbi.ucla.edu/SAVES/). The environment profile was developed using Verify3D and ERRAT (Luthy et al. 1992; Bowie et al. 1991; Colovos and Yeates 1993). Calculations for Ramachandran plot were performed by PROCHECK by using swiss model verifying interface (Laskowski et al. 1993; Guex and Peitsch 1997). The Ramachandran plot was analyzed using WHATCHECK (Hooft et al. 1996). The structure of the target protein and the template were studied by super imposing using PyMOL version 1.7.4.5 from Schrodinger (www.pymol.org).

Docking of C1, reserpine and CCCP with the generated NorA model was accomplished using AutoDock 4.2.5.1 (http://autodock.scripps.edu/) The energy minimization of the modeled NorA protein structure was done using Swiss Pdb Viewer 4.10. (Guex and Peitsch 1997). The energy minimized structure was saved in .pdb format. Further this structure was subjected to addition of hydrogens, addition of Kollman United Atom charges and non-polar hydrogens were merged using Autodock 4.0. C1, reserpine and CCCP were drawn using ChemDraw Ultra 8.0 and the energy minimization of the molecules was achieved using Chem3D Ultra 8.0. Further the ligands were subjected to addition of Gastegier charges and non-polar hydrogens were merged using Autodock 4.0. For the docking studies, initially the grid was set to the binding pocket of NorA at

X=-23.192, Y=62.168, Z=11.805; dimensions (Å) at X=60.000, Y=50.000, Z=50.000; spacing 0.375 Å. At this conformation the central hydrophobic pocket of the NorA protein was covered. Docking was performed between the target protein and prepared ligands by applying Lamarckian genetic algorithm 50 in Autodock 4.0 with 25 GA runs and other parameters were set as follows: the number of individuals in the population was 150, maximum number of energy evaluations was 2500000, maximum number of generations was 27,000, top individual to survive to next generation was 1, gene mutation rate was 0.02, crossover rate was 0.8, Cauchy beta was 1.0, and genetic algorithm window size was 10.0. The bound conformation was chosen based on the least binding energy (kcal/ mol) and the .pdb file was generated and then analyzed using Protein-Ligand Interaction Profiler (PLIP). The docked conformations were represented using PyMOL. (https://www.pymol.org/).

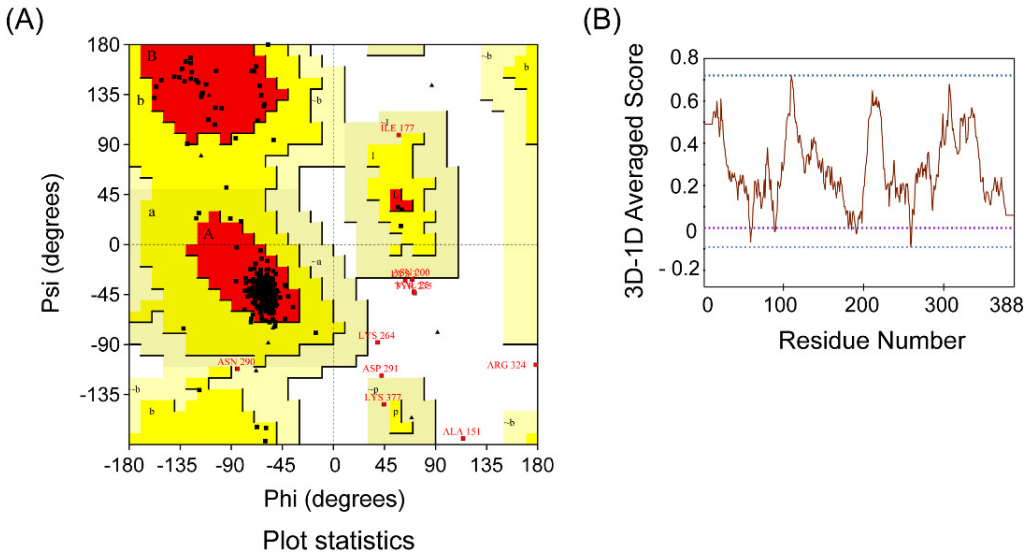

Plot statistics

Residues in most favoured regions [A,B,L]	305	91.6%
Residues in additional allowed regions [a,b,l,p]	17	5.1%
Residues in generously allowed regions [~a,~b,~l,~p]	3	0.9%
Residues in disallowed regions	8	2.4%
Number of non-glycine and non-proline residues	333	100.0%
Number of end-residues (excl. Gly and Pro)	2	
Number of glycine residues (shown as triangles)	39	
Number of proline residues	14	
Total number of residues	388	

Based on an analysis of 118 structures of resolution of at least 2.0 Angstroms and R-factor no greater than 20%, a good quality model would be expected to have over 90% in the most favoured regions.

Figure A6.9. (A) Calculations for Ramachandran plot of modelled NorA protein of *S. aureus*. (B) Compatibility check of atomic 3D model with respect to amino acid residues (1D) using SAVES.

Program: ERRAT2
File: /var/www/SAVES/Jobs/30549238//errat.pdb
Chain#:1
Overall quality factor: 78.100**

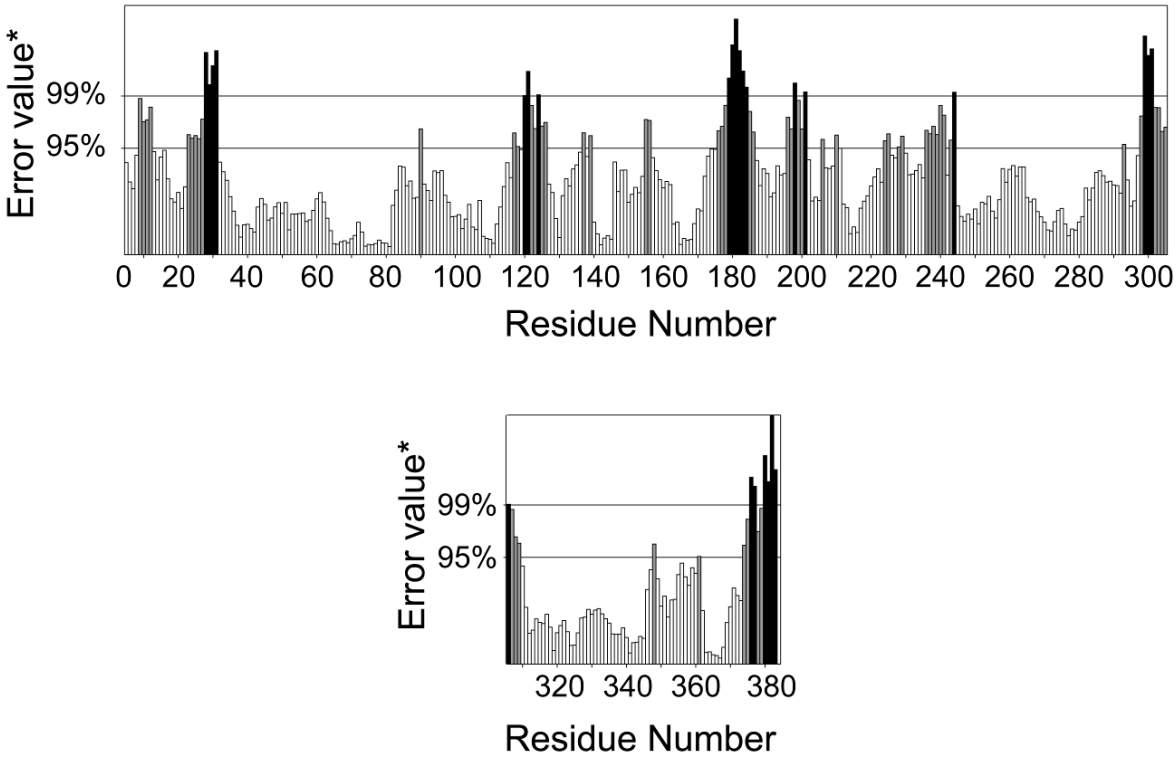

*On the error axis, two lines are drawn to indicate the confidence with which it is possible to reject regions that exceed that error value.

**Expressed as the % of the protein for which the calculated error value falls below the 95% rejection limit. Good high resolution structures generally produce values around 95% or higher. For lower resolutions (2.5-3 Å) the average overall quality factor is around 91%.

Figure A6.10. Verification of 3D profiles of generated NorA model using ERRAT program.

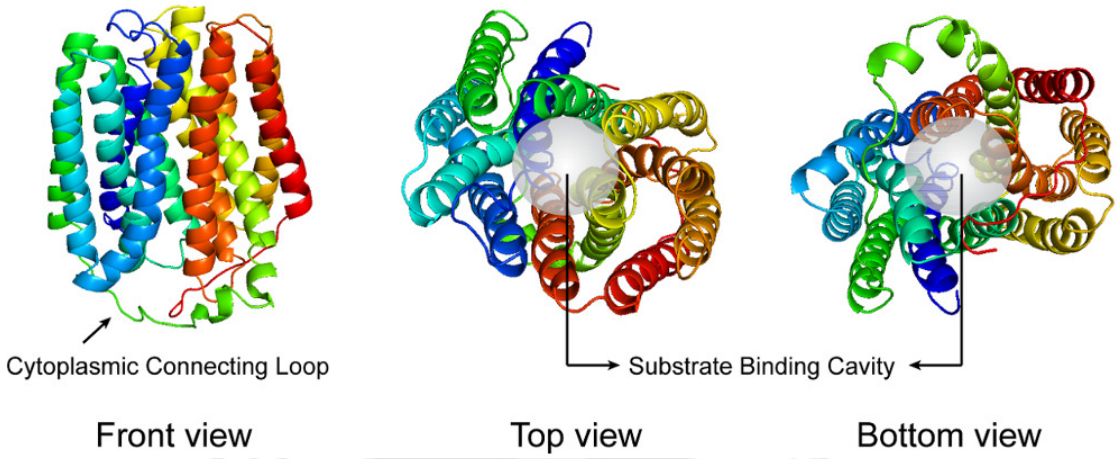

Figure A6.11. 3D model of *S. aureus* NorA protein generated by homology modelling. The substrate binding cavity is indicated by a gray circle.

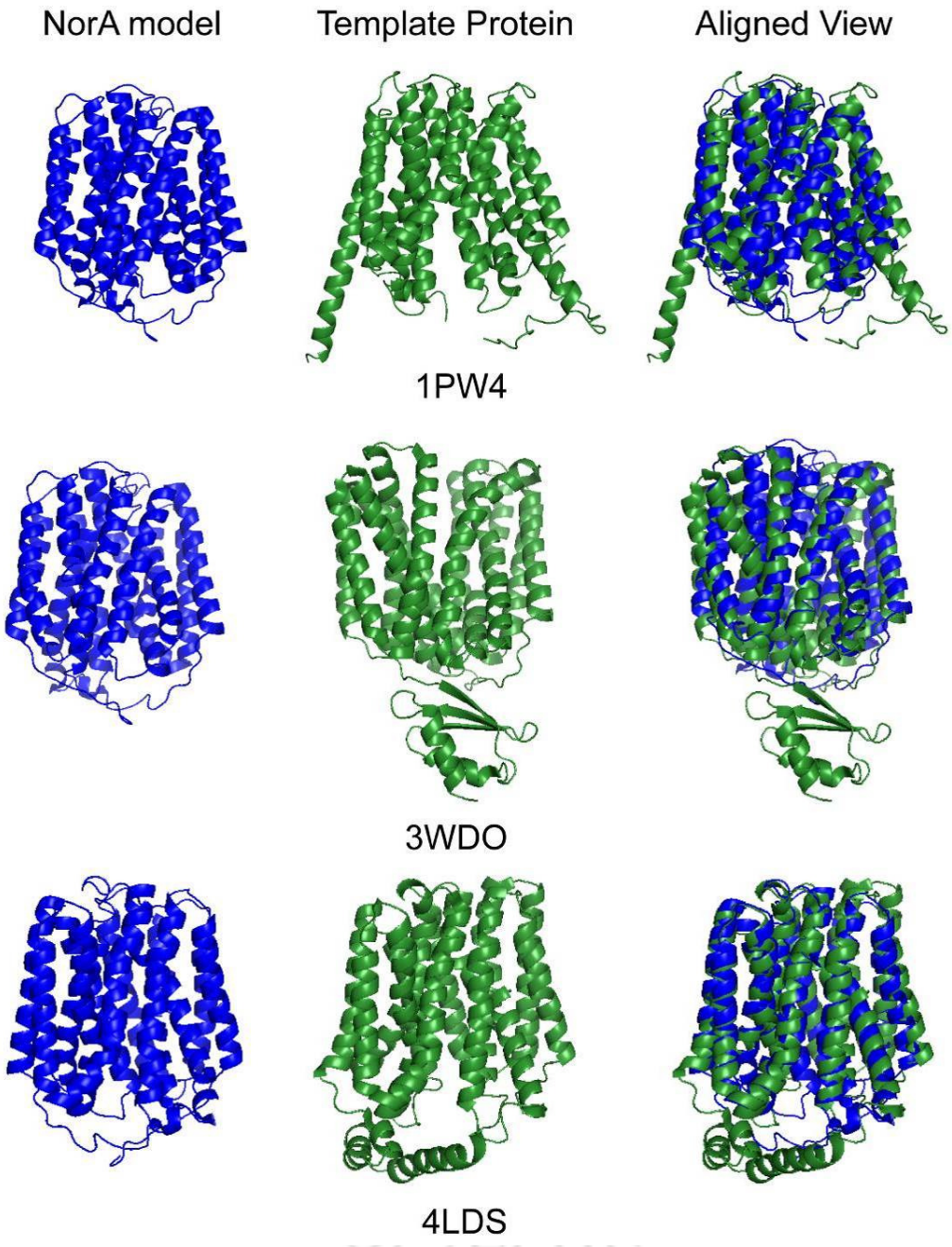

Figure A6.12. Superimposition of modelled S. aureus NorA protein and the template proteins. The PDB ID of the template proteins are indicated below the respective proteins.

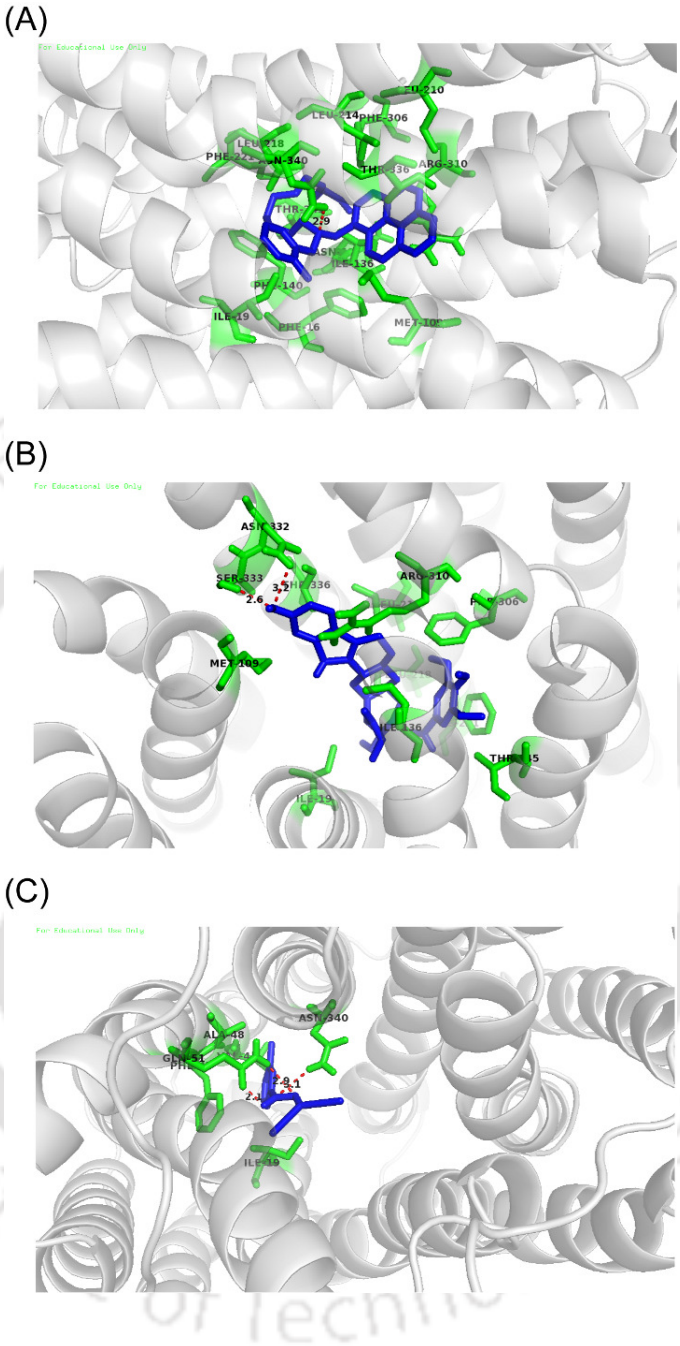

Figure A6.13. Docked structure of (A) C1, (B) reserpine and (C) CCCP and modelled *S. aureus* NorA protein. The figures indicate the putative binding sites and interaction pattern of the molecules with the modelled NorA protein. The stick model of C1, reserpine, CCCP and the interacting amino acid residues of NorA protein are shown in blue and green, respectively. Hydrogen bond interaction between the molecules and the protein is represented by a red dotted line.

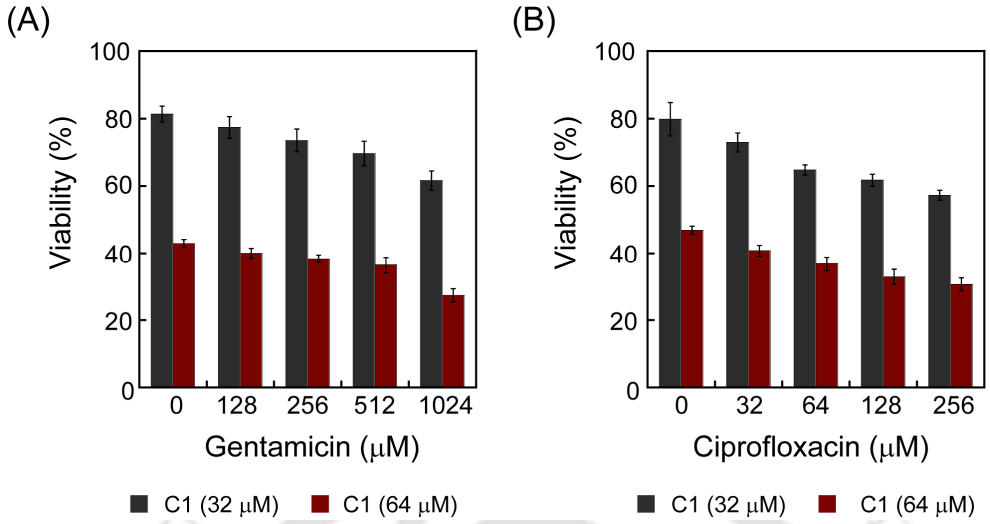

Figure A6.14. MTT assay to ascertain the effect of C1 in combination with gentamicin and ciprofloxacin on HEK 293 cell line. Each data point represents mean ± standard deviation from six samples.

Table A6.1. Fold reduction in MIC of therapeutic antibiotics against planktonic cells of the MRSA strain *S. aureus* 4s in combination with C1-PNC and determination of the nature of interaction based on FIC index.

Antibiotic (μM)	C1-PNC (μM)	Fold reduction in MIC of antibiotic	FIC index	Effect
Gentamicin (512 μM)	4.0	4.0	0.45	Synergy
Ciprofloxacin (8.0 μM)	2.0	8.0	0.2917	Synergy

Table A6.2. Structure Z-scores for NorA model.

Parameter	Structure Z-score
Resolution read from PDB file	-1.000
1st generation packing quality	-1.384
2nd generation packing quality	-2.249
Ramachandran plot appearance	1.003
chi-1/chi-2 rotamer normality	-2.718
Backbone conformation	-1.697
Inside/Outside distribution	1.235 (unusual)

Table A6.3. RMSZ-scores for NorA model.

Parameter	Structure Z-score
Bond lengths	0.936
Bond angles	1.293
Omega angle restraints	0.707 (tight)
Side chain planarity	0.301 (tight)
Improper dihedral distribution	1.176
B-factor distribution	0.304

Table A6.4. Binding interactions and binding energies of C1, reserpine and CCCP with the amino acid residues of *S. aureus* NorA efflux pump.

Molecule	Nature of Interaction*			Binding energy (kcal/ mol)
	Hydrophobic interaction	**Hydrogen bonds**	**Other interactions**	
C1	16 PHE, 19 ILE, 109 MET, 136 ILE, 137 ASN, 140 PHE, 210 LEU, 214 LEU, 218 LEU, 221 PHE, 245 THR, 306 PHE, 310 ARG, 336 THR, 340 ASN	1) 340 ASN, Donor 3122 [Nam]- Acceptor 3583 [N3], Donor angle- 122.31°, Distance H-A 2.95Å D-A 3.58Å	π - cation interactions 310 ARG	-10.02
Reserpine	19 ILE, 109 MET, 136 ILE, 214 LEU, 218 LEU, 221 PHE, 245 THR, 306 PHE, 310 ARG, 336 THR	1) 332 ASN, Donor 3051 [Nam]- Acceptor 3594 [O3], Donor angle- 103.90°, Distance H-A 3.16Å D-A 3.53Å 2) 333 SER, Donor 3060 [O3]- Acceptor 3594 [O3], Donor angle- 171.65°, Distance H-A 2.63Å D-A 3.63Å	π - stacking 221 PHE	-4.69
CCCP	19 ILE, 44 VAL, 47 PHE, 48 ALA	1) 51 GLN, Donor 3573 [Npl]- Acceptor 460 [O2], Donor angle- 112.44°, Distance H-A 2.08Å D-A 2.65Å 2) 51 GLN, Donor 461 [Nam]- Acceptor 3575 [N2], Donor angle- 141.90°, Distance H-A 2.90Å D-A 3.74Å 3) 340 ASN, Donor 3122 [Nam]- Acceptor 3573 [Npl], Donor angle- 160.48°, Distance H-A 3.09Å D-A 4.04Å	Nil	-6.42

* The amino acid residues of NorA protein involved in various kinds of interactions are indicated

.

References

1. Marti-Renom, M. A.; Stuart, A.; Fiser, A.; Sanchez, R.; Melo, F.; Sali, A. Comparative protein structure modeling of genes and genomes. *Annu. Rev. Biophys. Biomol. Struct*., 2000, **29**, 291.
2. Sali, A.; Blundell, T. L.; Comparative protein modelling by satisfaction of spatial restraints. *J. Mol. Biol*., 1993, **234**, 779.
3. Fiser, A.; Do, R. K.; Sali, A. Modeling of loops in protein structures. *Prot. Sci.,* 2000, **9**, 1753.
4. Kuntal, B. K.; Aparoy, P.; Reddanna, P. EasyModeller: A graphical interface to MODELLER. *BMC Res. Notes*, 2010, **3**, 226.
5. Luthy, R.; Bowie, J. U.; Eisenberg, D. Assessment of protein models with three-dimensional profiles. *Nature*, 1992, **356**, 83.
6. Bowie, J. U.; Luthy, R.; Eisenberg, D. A method to identify protein sequences that fold into a known three-dimensional structure. *Science*, 1991, **253**, 164.
7. Colovos, C.; Yeates, T. O. Verification of protein structures: patterns of nonbonded atomic interactions. *Prot. Sci*., 1993, **2**, 1511.
8. Laskowski, R. A.; MacArthur, M. W.; Moss, D.; Thornton, J. M.; PROCHECK: a program to check the stereochemical quality of protein structures. *J. Appl. Cryst*., 1993, **26**, 283.
9. Guex, N.; Peitsch, M. C. SWISS-MODEL and the Swiss-PdbViewer: an environment for comparative protein modeling. *Electrophoresis*, 1997, **18**, 2714.
10. Hooft, R.W.W.; Vriend, G.; Sander, C.; Abola, E. E. Errors in protein structures. *Nature*, 1996, **381**, 272.
11. https://www.pymol.org/
12. http://autodock.scripps.edu/downloads/autodock-registration/autodock-4-2-download-page/
13. Salentin, S.; Schreiber, S.; Haupt, V. J.; Adasme, M. F.; Schroeder, M. PLIP: fully automated protein-ligand interaction profiler. *Nucl. Acids Res*., 2015, **43**, W443.

LIST OF PUBLICATIONS

List of Publications

Publications from Ph.D. Thesis Work:

(A) Journal Publications:

1. **Thiyagarajan, D.**, Goswami, S., Kar, C., Das, G. and Ramesh, A. (2014) A prospective antibacterial for drug-resistant pathogens: A dual warhead amphiphile designed to track interactions and kill pathogenic bacteria by membrane damage and cellular DNA cleavage. *Chemical Communications* **50**, 7434-7436.
2. **Thiyagarajan, D.**, Das, G. and Ramesh, A. (2016) Extracellular DNA-targeting nanomaterial for effective elimination of biofilm. *ChemNanoMat* **2**, 879-887.
3. **Thiyagarajan, D.**, Das, G. and Ramesh, A. (2017). Amphiphilic cargo-loaded nanomaterial enhances antibiotic uptake and perturbs efflux: effective synergy for mitigation of methicillin-resistant *Staphylococcus aureus*. *ChemMedChem* **12**, 1125-1132.

(B) Conference Presentations:

1. **Thiyagarajan, D.**, Adhikari, M. D., Goswami, S., Kar, C., Das, G. and Ramesh, A. (2012). Membrane-targeting bactericidal activity of a Janus amphiphile. Abstract PD2-624 (MVM). Presented in 53rd Annual Conference of Association of Microbiologists of India (AMI), Bhubaneswar, 22-25 November 2012.

2. **Thiyagarajan, D.**, Goswami, S., Kar, C., Das, G. and Ramesh, A. (2013). Anti-biofilm activity of a bactericidal amphiphile. Presented in 54th Annual Conference of Association of Microbiologists of India (AMI), Rohtak, 17-20 November 2013.

List of Publications

Publications from Other Research Projects:

1. Goswami, S., Adhikari, M. D., Kar, C., **Thiyagarajan, D**., Das, G. and Ramesh, A. (2013) Synthetic amphiphiles as therapeutic antibacterials: lessons on bactericidal efficacy and cytotoxicity and potential application as an adjuvant in antimicrobial chemotherapy. *Journal of Materials Chemistry B* **1**, 2612-2623.
2. Basu, A., **Thiyagarajan, D.**, Kar, C., Ramesh, A. and Das, G. (2013) Synthesis, crystal structure and bio-macromolecular interaction studies of pyridine-based thiosemicarbazone and its Ni(II) and Cu(II) complexes. *RSC Advances* **3**, 14088-14098.
3. Datta, B. K., **Thiyagarajan, D**., Samanta, S., Ramesh, A. and Das, G. (2014) A novel chemosensor with visible light excitability for sensing Zn^{2+} in physiological medium and in HeLa cells. *Organic and Biomolecular Chemistry* **12**, 4975-4982.
4. Uday, S. P., **Thiyagarajan, D**., Goswami, S., Adhikari, M. D., Das, G. and Ramesh, A. (2014) Amphiphile-mediated enhanced antibiotic efficacy and development of a payload nanocarrier for effective killing of pathogenic bacteria, *Journal of Materials Chemistry B* **2**, 5818-5827.
5. Goswami, S., **Thiyagarajan, D**., Das, G. and Ramesh, A. (2014) Biocompatible nanocarrier fortified with a dipyridinium-based amphiphile for eradication of biofilm. *ACS Applied Materials & Interfaces* **6**, 16384-16394
6. Datta, B. K., **Thiyagarajan, D**., Kar, C., Ramesh, A. and Das, G. (2015). A near-infrared emissive Al^{3+} sensing platform for specific detection in solution, cells and probing DNase activity. *Analytica Chimica Acta* **882**, 76-82.
7. Datta, B. K., **Thiyagarajan, D.**, Ramesh, A. and Das, G. (2015). A Sole Multi-Analyte receptor responds with three distinct fluorescence signals: Traffic signal like sensing of Al^{3+}, Zn^{2+} and F^{-}. *Dalton Transactions* **44**, 13093-13099.
8. Goswami, S., **Thiyagarajan, D**., Samanta, S., Das, G. and Ramesh, A. (2015). A zinc complex of a neutral pyridine-based amphiphile: a highly efficient and potentially therapeutic bactericidal material. *Journal of Materials Chemistry B* **3**, 7068-7078.
9. Kapoor, V., Rai, R., **Thiyagarajan, D.,** Mukherjee, S., Das, G. and Ramesh, A. (2017). A nonbactericidal zinc-complexing ligand as a biofilm inhibitor: structure-guided contrasting effects on *Staphylococcus aureus* biofilm. *ChemBioChem*, **18**, 1502-1509.